Universität Rostock
Traditio et Innovatio

INSTITUT FÜR PHYSIK

# Non-Hermitian dynamics in lossy photonic waveguide systems

**Dissertation**
zur Erlangung des Grades
doctor rerum naturalium (Dr. rer. nat.)
am Institut für Physik
der Mathematisch-Naturwissenschaftlichen Fakultät
der Universität Rostock

vorgelegt von

Lucas Teuber, geb. am 10.8.1992 in Bremen
aus Rostock

Rostock, Februar 2021

https://doi.org/10.18453/rosdok_id00003110

**Gutachter:**
Prof. Dr. Stefan Scheel, Universität Rostock, Institut für Physik
Prof. Dr. Jan Wiersig, Universität Magdeburg, Institut für Physik

**Datum der Abgabe:**
08.02.2021

**Datum der Verteidigung:**
21.05.2021

# Zusammenfassung

Diese Arbeit befasst sich mit der theoretischen Beschreibung von integrierten photonischen Wellenleitern zur Simulation nicht-abelscher Eichfelder sowie der Untersuchung nicht-hermitescher Systeme.

Die künstlichen nicht-abelschen Eichfelder entstehen durch eine geschlossene, adiabatische Variation der Kopplungsparameter eines entarteten Wellenleitersystems. Eine detaillierte Studie der zugrundeliegenden Theorie führt zu einer Optimierungsvorschrift, die es erlaubt ideale Parametervariationen für experimentelle Realisierungen zu finden.

Die Untersuchung nicht-hermitescher Systeme, insbesondere solcher mit Parität-Zeit-Symmetrie, basiert auf Lösungen der Quantenmastergleichung eines beliebigen Wellenleitersystems mit Verlusten. Zwei verschiedene Lösungsansätze werden hergeleitet, die auf verschiedenen Lie-Algebra-Methoden basieren. Mithilfe dieser Lösungsansätze wird ein verlustbehaftetes Wellenleitersystem aus zwei gekoppelten Wellenleitern genauer untersucht. Dazu werden verschiedene Observablen berechnet. Insbesondere der Phasenübergang eines parität-zeit-symmetrischen Wellenleitersystems zur gebrochenen Symmetrie wird illustriert. Eine periodische Modulation der Verlustrate erlaubt es, die dafür nötige Verluststärke drastisch zu verringern.

# Summary

This thesis deals with the theoretical description of integrated photonic waveguides for the simulation of non-Abelian gauge fields as well as the study of non-Hermitian systems.

The artifical non-Abelian gauge fields emerge from a closed, adiabatic curve in the parameter manifold of a coupled waveguide system with degeneracies. Based on the underlying theory, an optimisation process is devised that was used to find ideal parameter variations of an experimental implementation.

Additionally, two Lie-algebraic methods that solve the quantum master equation of an arbitrary, lossy waveguide system are developed, which allow to study non-Hermitian systems, e.g. with parity-time-symmetry. Both methods are showcased at the hand of a lossy two-waveguide system. Various observables are calculated and especially the breaking of the parity-time-symmetry is shown. A periodic modulation of the loss rate leads to a drastically reduced threshold to reach this phase transition.

# Contents

**1. Introduction** **1**

**2. Integrated photonic waveguides** **5**
- 2.1. Classical description of photonic waveguides . . . . . . . . . . . . . . . . . . 5
- 2.2. The quantised coupled-mode equation . . . . . . . . . . . . . . . . . . . . . . . . 9

**3. Implementation of geometric phases and non-Abelian gaugefields** **13**
- 3.1. Differential geometry and geometric phases . . . . . . . . . . . . . . . . . . . 13
- 3.2. Fundamentals of gauge field theories . . . . . . . . . . . . . . . . . . . . . . . . 15
- 3.3. Geometric phases and holonomies in Hermitian systems . . . . . . . . . . . 18
- 3.4. Adiabatic evolution and the quantum metric . . . . . . . . . . . . . . . . . . 21
- 3.5. Implementation in photonic waveguides . . . . . . . . . . . . . . . . . . . . . . 23
  - 3.5.1. Details on couplings and optimised design . . . . . . . . . . . . . . . 26
  - 3.5.2. Experimental results . . . . . . . . . . . . . . . . . . . . . . . . . . . . . . 29
- 3.6. Increasing dimensionality using multiple photons . . . . . . . . . . . . . . . 33
- 3.7. Holonomic quantum computing in non-Hermitian systems . . . . . . . . . 36

**4. The quantum master equation of lossy waveguides and its Lie algebraic solutions** **39**
- 4.1. Open quantum systems . . . . . . . . . . . . . . . . . . . . . . . . . . . . . . . . . 39
  - 4.1.1. The quantum master equation in Born-Markov approximation . . . 41
  - 4.1.2. Applicability of the Born-Markov approximation to laser-written photonic waveguides . . . . . . . . . . . . . . . . . . . . . . . . . . . . . 42
  - 4.1.3. Liouville space formulation . . . . . . . . . . . . . . . . . . . . . . . . . . 43
- 4.2. Lie algebras induced by the Liouvillian of lossy waveguide systems . . . . . 45
- 4.3. Eigendecomposition of the Liouvillian . . . . . . . . . . . . . . . . . . . . . . . 48
  - 4.3.1. Liouville space ladder operators . . . . . . . . . . . . . . . . . . . . . . 51
  - 4.3.2. Eigendecomposition solution of the quantum master equation . . . 54
- 4.4. Wei-Norman expansion . . . . . . . . . . . . . . . . . . . . . . . . . . . . . . . . . 58

**5. The $\mathcal{PT}$-symmetric coupler** **63**
- 5.1. Solution via eigendecomposition . . . . . . . . . . . . . . . . . . . . . . . . . . . 63
- 5.2. Wei-Norman solution for the lossy waveguide coupler . . . . . . . . . . . . 71
  - 5.2.1. Exceptional points of arbitrary order in the $\mathcal{PT}$ coupler . . . . . . . 80

**6. The $\mathcal{PT}$-symmetric Floquet coupler** **85**
- 6.1. Elements of Floquet theory . . . . . . . . . . . . . . . . . . . . . . . . . . . . . . 85

6.2. The $\mathcal{PT}$-symmetric coupler with periodic loss . . . . . . . . . . . . . . . . 88
    6.2.1. Breaking of $\mathcal{PT}$ symmetry in the periodic coupler and the $\mathcal{PT}$ phase diagram . . . . . . . . . . . . . . . . . . . . . . . . . . . . . 88
    6.2.2. Exceptional points with reduced threshold . . . . . . . . . . . . . . 90

**7. Conclusion 93**

**A. Geometric interpretation of adiabatic transport in degenerate subspaces 97**

**B. Non-Abelian gauge fields from a detuned waveguide tripod 103**

**C. Detailed eigendecomposition of the $|1,1\rangle\langle 1,1|$-state in Liouville space 107**

**D. Regular representations at the exceptional point 111**

**E. Ideal propagation in lossy waveguides for two-photon states 115**

# 1. Introduction

Over a hundred years after its initial conception [1; 2] quantum physics revolutionised our understanding of the microcosmos and established itself as one pillar of modern science. Although many of its concepts seem counterintuitive, ground-breaking technological advancements like lasers or transistors were only possible due to quantum effects and their understanding. In the last few decades, the transfer of fundamental theory into technology with commercial application accelerated, which ushers in a "second quantum revolution" [3]. These prospective applications will impact all facets of our life. Interesting examples range from quantum imaging [4] over quantum sensing [5] to quantum computation or information processing [6] each with considerable enhancements compared to their classical counterparts.

Many physical implementations exist for these applications, ranging from single atoms and ions over molecules to semiconductors. Especially promising are optical systems relying on the fundamental quantum of light – the photon. Because it is arguably the first described quantum particle [1; 2], quantum optics has always been a vivid research field with the current state-of-the-art allowing not only to describe the quantised electromagnetic field itself but also its detailed interaction with matter [7; 8; 9]. With this knowledge an astonishing amount of experimental expertise and capabilities developed. The early building blocks were bulk-optical components like beam splitters and phase shifters for linear operations as well as nonlinear materials especially important for the creation of entangled photons [10; 11]. These components already allowed fundamental tests of quantum physics [12; 13] and linear optics alone was shown to be sufficient for applications like quantum computation processing [14; 15].

With the shift to real world applications, the experimental techniques matured and nowadays bulk-optical components are replaced by integrated photonic platforms [16]. Of special interest are designs based on laser-written waveguides with evanescent couplings that provide all necessary optical components [17; 18; 19; 20]. They are combined on a single, integrated chip resulting in high interferometric stability which leads to the notion of a "pocket quantum optics lab" [19]. Depending on the base material, the optical chip can include nonlinearities, e.g. in case of Lithium niobate [21]. As an experimental platform, laser-written waveguides are especially interesting because they allow to simulate complex quantum effects [22; 23]. This is because the paraxial Helmholtz equation that describes the light's propagation in such waveguide systems is mathematically equivalent to the Schrödinger equation [24]. Therefore, one can simulate first-quantisation problems using only classical light, see e.g. Refs. [25; 26]. When nonclassical light is used, a plethora of quantum optical effects can be studied: From creation of quantum states [27; 28; 29], over implementation of quantum gates [30; 31; 20; 32] to simulation of complex quantum walks [33; 34; 35; 36], to name just a few.

An interesting use of the simulation capabilities available in integrated photonic waveguides are implementations of geometric phases. These phases act as artificial gauge fields that allow to study the physical gauge fields which are the back bone of modern physics [37; 38; 39]. Additionally, geometric phases are the key ingredient for holonomic quantum computation (HQC) [40]. In this setting, holonomies are quantum gates that arise from cyclic variations of the system parameters. Consequently, they only depend on the geometric properties of the path through the manifold of parameters. As a result of this geometric nature, holonomic gates are inherently resilient against path fluctuations [41].

The emergence of a geometric phase in cyclic, adiabatic evolutions is well known for single states, which is often called the Berry-Pancharatnam phase [42; 43]. These scalar phases result in Abelian operations. However, non-Abelian generalisations where multiple degenerate states follow a cyclic, adiabatic evolution are equally valid [44]. These non-Abelian geometric phases, or gauge fields, result in nontrivial unitary operations acting on the subspace of the degenerate states. The resulting matrix-valued holonomies are the basic building blocks to perform HQC and pose an interesting alternative for quantum information processing [45; 46].

Geometric phases are typically implemented with atoms in optical lattices [47; 48; 49] or trapped ions [50]. Recent experiments showed the viability of photonic implementations using polarisation degrees-of-freedom [51]. However, this approach is limited to $2 \times 2$ unitary gates in the two-dimensional space of polarisations. One part of the present thesis shows how these limitations are lifted by using photonic waveguides which paves the road to efficient photonic HQC.

The other main part of this thesis deals with losses in photonic waveguide systems. Generally speaking, losses and decoherence are the largest adversaries when trying to conduct quantum experiments and scaling quantum devices for potential commercial applications. As a quantum system becomes larger and more elaborate, undesired and uncontrolled interactions with its environment become unavoidable [52]. Consequently, fundamental quantum properties like quantum interference and entanglement are destroyed, nullifying any expected advantage over classical systems. Due to the detrimental effects of losses a considerable amount of research is dedicated to them, resulting in an established and comprehensive theory of open quantum systems [53].

Techniques were developed that aim to avoid or correct the impact of losses. Examples include loss avoidance techniques via decoherence-free subspaces [54; 55; 56; 57] which are closely related to efforts which use tailored system-environment interactions that allow not only to avoid losses but can also be used to deliberately create quantum states [58; 59; 60]. In this example loss is not seen as a hindrance but as a resource of interesting physics in itself.

This change in perspective also manifests in current research regarding non-Hermitian quantum physics that generalises the usual quantum theories centred around Hermitian Hamiltonians. Such non-Hermitian extensions of quantum physics entail many intriguing concepts not found in conventional Hermitian physics due to their potentially complex spectra and biorthogonal eigenbases [61; 62]. They allow for degeneracies in the complex spectra that simultaneously result in a coalescence of the eigenvectors. Such degeneracies are aptly called exceptional points (EPs) [63] as they themselves and their surroundings give rise to exceptional behaviours. These often counterintuitive effects range from unidirectional mode-switching when encircling an EP [64; 65; 66] over self-orthogonal eigenmodes [67] and loss-induced revival of lasing [68] to increased sensitivity in the vicinity of an EP [69; 70; 71; 72].

An important subset of non-Hermitian systems are those with parity-time ($\mathcal{PT}$) symmetry. In their seminal paper, Bender and Boettcher [73] showed that non-Hermitian Hamiltonians can still possess purely real spectra as long as they and their eigenvectors are $\mathcal{PT}$-symmetric. Such a $\mathcal{PT}$-symmetric phase is embedded in the complex spectrum and the transition to the $\mathcal{PT}$-broken phase is marked by an EP. Commonly, such a $\mathcal{PT}$ symmetry is implemented via symmetric gain-loss distributions whilst passive implementations with an asymmetric distribution of only loss are also often used to avoid the need of a finely tuned balance between gain and loss [74]. The physics of such $\mathcal{PT}$-symmetric systems is well tested for classical implementations like microwave cavities [65], LRC circuits [75], pendulums [76], or optical couplers [77]. These open systems are correctly described by effective non-Hermitian Hamiltonians whose active and passive forms are related by shifts along the complex energy axis.

On the other hand, experiments with quantum systems have also been reported, e.g. for single photons [78], ultra-cold atoms [79], single NV centers in diamond [80], or single superconducting qubits [81]. Although these implementations use quantum systems, they are still based on single-particle descriptions limiting their observables to first-quantisation effects which are essentially covered by classical wave mechanics. However, the first second-quantisation effect in a $\mathcal{PT}$ system was recently measured with the two-photon correlation in a lossy waveguide coupler [82]. The emergence of quantum $\mathcal{PT}$ systems gives rise to many new questions regarding their difference to the classical $\mathcal{PT}$ systems. For example, there is an ongoing debate whether the expected increase in sensitivity at the EP also occurs at the quantum level or if it is always counteracted by quantum noise [83]. Quantum optical setups with active $\mathcal{PT}$ symmetry were ruled out because the gain leads to thermal broadening [84]. In addition, certain setups like coherent input states in coupled cavities [85] or Brillouin ring laser gyroscopes [86] showed an exact compensation of the increased sensitivity by an excess-noise factor due to the self-orthogonal eigenmodes [87]. However, a final judgement is still pending and requires a deeper understanding of quantum $\mathcal{PT}$ systems.

In this thesis we develop a full quantum description of lossy waveguide systems as a tool to possibly shine light on this and other questions and to allow the design of future experiments. The retrieved solutions give insight into when it is valid to use an effective non-Hermitian Hamiltonian, like in the classical case, and open the way to describe arbitrary quantum observables. Additionally, our analysis extends on a recently suggested scheme to implement higher-order EPs [88] in waveguide $\mathcal{PT}$ couplers using more than two photons. These higher-order EPs are expected to further enrich the intriguing effects of complex degeneracies [89; 90; 83].

## Outline

The outline of this thesis is as follows. Chapter 2 introduces the theoretical foundations of integrated photonic waveguides. This entails the derivations of their description in classical as well as quantum optics. The classical description centres around the paraxial Helmholtz equation culminating in a coupled-mode theory following with an outlined derivation of its quantised form.

In Chapter 3 we discuss the implementation of holonomies in integrated photonic waveguides. We begin by recapitulating how certain dynamics result in geometrical phases and how these features emerge in waveguides. Interestingly, purely geometric dynamics generally emerge from first-order differential equations such as the Schrödinger equation or, in our case, the paraxial Helmholtz equation. Thus, at this point no quantisation is necessary. A classical experiment conducted in joint work with the group of Professor Alexander Szameit showcases the emergence of these geometric dynamics. However, certain benefits can only be obtained if one advances to the fully quantised description. For example, we discuss how the use of second-quantised Fock states allows to drastically increase the dimensionality [91]. In addition, the Hermitian theory of holonomies can be extended to non-Hermitian systems [92]. This results in larger sets of control parameters, e.g. by adding loss rates, facilitating the creation of universal holonomic quantum gates.

In Chapter 4 we focus on the description of open quantum systems with emphasis on applying it to waveguide arrays. For that purpose we recapitulate fundamentals on the theory of open quantum system and discuss which approximations are applicable to the photonic waveguides. The result is a quantum master equation of Lindblad type in the coupled-mode picture where individual waveguides can experience single-photon losses. In order to prepare our following main work, we will introduce the concept of the Liouville space, an open-systems generalisation of the common Hilbert space. Building on this, we present problem solving strategies based on a Lie algebraic interpretation of the Lindblad master equation. First, we show how to utilise eigendecompositions of the algebra induced by the master equation. This yields analytical solutions for waveguide arrays with constant parameters, e.g. coupling strength and loss rates. Second, we present a Wei-Norman expansion that solves the master equation for arbitrarily varying parameters.

In the following Chapter 5, the previously obtained solutions to the quantum master equation of lossy waveguide arrays are applied to the instructive example of a $\mathcal{PT}$-symmetric coupler. We derive observables like the two-photon correlation. Our result has been experimentally validated in a recent experiment conducted in joint work with the group of Professor Alexander Szameit [82]. In addition, we will discuss the case of an arbitrary number of photons which results in higher-order EPs.

In Chapter 6 the $\mathcal{PT}$-symmetric coupler is studied in case of periodically modulated losses. This Floquet coupler is analysed with respect to its $\mathcal{PT}$-phase diagram. The key result is that the threshold for broken $\mathcal{PT}$ symmetry can be greatly reduced which should facilitate tests of EPs and the general behaviour at the phase transition.

Finally, Chapter 7 sees the concluding remarks and a discussion of possible future research.

# 2. Integrated photonic waveguides

The integrated photonic waveguides, which serve as the experimental platform for the present theoretical contribution, are manufactured in silica glass using the direct-laser-writing technique [30]. For that, a femtosecond-pulsed high-intensity laser is tightly focussed inside the amorphous glass, see Fig. 2.1. The large energy deposited in the small laser focus results in a violent reorganisation of the silica bounds which subsequently results in a permanent increase of the refractive index [30]. These light-guiding lines are not limited to one plain but can be written in any three-dimensional configuration. This opens up various geometries like 3D couplers [17] or whole waveguide arrays, see for example Ref. [25].

Additionally, the index contrast is relatively small, usually of order $10^{-7}$ [30; 93], and thus the waveguiding itself is only weak and any changes in the system happen gradually. Therefore, the whole system is more stretched out along the propagation direction leading to a paraxial propagation. For example, the transversal extend of the waveguide system is usually on the scale of micrometres whereas the propagation length is often a few centimetres. Thus, the theoretical description of the light propagation in such structures is well described in a slowly-varying envelope approximation [10].

The main feature of such a waveguide system, the coupling of modes, is introduced by varying the distance of the waveguides which results in weak, distance-dependent coupling due to the evanescent overlap of the guided modes. This small overlap ideally does not affect the individual transverse mode fields of the waveguides and thus the setup is well approximated by a coupled-mode theory [94]. The paraxial approximation and the resulting coupled-mode theory is the basis for the classical as well as the quantum optical description of the waveguides which we will now discuss in more depth.

## 2.1. Classical description of photonic waveguides

Our starting point of the classical description are the macroscopic Maxwell equations without free charges,

$$\boldsymbol{\nabla}\cdot\boldsymbol{D} = 0\,, \tag{2.1}$$

$$\boldsymbol{\nabla}\times\boldsymbol{H} = \partial_t\boldsymbol{D}\,, \tag{2.2}$$

$$\boldsymbol{\nabla}\cdot\boldsymbol{B} = 0\,, \tag{2.3}$$

$$\boldsymbol{\nabla}\times\boldsymbol{E} = -\partial_t\boldsymbol{B}\,, \tag{2.4}$$

with constitutive equations $\boldsymbol{D} = \varepsilon\boldsymbol{E}$ and $\boldsymbol{B} = \mu\boldsymbol{H}$ for isotropic materials. The silica glass interacts only with the electric field, hence we can set $\mu = \mu_0$ and $\varepsilon = \varepsilon_{\mathrm{r}}\varepsilon_0$ for

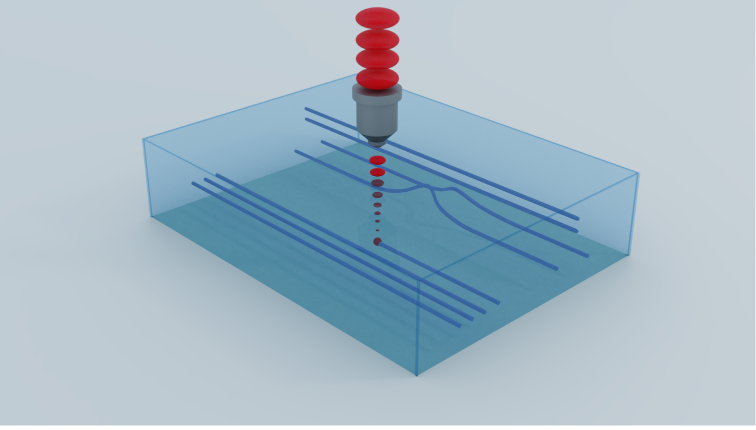

Fig. 2.1.: Laser-writing of an evanescently coupled waveguide system. The pulsed laser creates a permanent index-increase along which light is guided.

the permeability and permittivity. The relative permittivity is now a position-dependent function, $\varepsilon_{\mathrm{r}}(\boldsymbol{r})$, because of the index contrast of the laser-written waveguides compared to the ambient glass.

In order to study the evolution of the electric field, we derive its governing equation inside the glassy material and we start by calculating $\boldsymbol{\nabla} \times (\boldsymbol{\nabla} \times \boldsymbol{E})$. Comparing the differential geometric result with the result from inserting Eqs. (2.4) and (2.2) leads to the wave equation of the electric field,

$$\nabla^2 \boldsymbol{E} - \boldsymbol{\nabla} \left( \boldsymbol{\nabla} \cdot \boldsymbol{E} \right) = \frac{\varepsilon_{\mathrm{r}}(\boldsymbol{r})}{c^2} \partial_t^2 \boldsymbol{E} \, , \tag{2.5}$$

with the speed of light $c = 1/\sqrt{\mu_0 \varepsilon_0}$. Because the index contrast of the waveguides is supposed to be small, we can approximate that $\boldsymbol{\nabla} \cdot \boldsymbol{E} \approx \varepsilon^{-1} \boldsymbol{\nabla} \cdot \boldsymbol{D} = 0$, where we used Eq. (2.1). Furthermore, we do not consider any polarisation effects and assume the field to be of a single frequency $\omega$, i.e. $\boldsymbol{E}(\boldsymbol{r}, t) = E(\boldsymbol{r}) \exp(-\mathrm{i}\omega t) \boldsymbol{v}$ with some constant polarisation vector $\boldsymbol{v}$. The wave equation (2.5) thus becomes the Helmholtz equation for the amplitude $E(\boldsymbol{r})$,

$$\left( \Delta + \frac{n^2(\boldsymbol{r})\, \omega^2}{c^2} \right) E(\boldsymbol{r}) = 0 \, , \tag{2.6}$$

where we used the definition $n(\boldsymbol{r})^2 = \varepsilon_{\mathrm{r}}(\boldsymbol{r})$ of the refractive index of the medium. The refractive index is assumed to be of the form $n(\boldsymbol{r}) = n_0 + \delta n(\boldsymbol{r})$ with variations $\delta n(\boldsymbol{r}) \ll n_0$ at the laser-written waveguides.

In general, the propagation of this field through the waveguide architecture is paraxial and we designate this preferred axis as the $z$-axis. Decomposing the field as envelope amplitude and plane wave along $z$-direction, i.e. $E(\boldsymbol{r}) = \boldsymbol{\mathcal{E}}(\boldsymbol{r}) \mathrm{e}^{\mathrm{i}kz}$, allows to rewrite the Helmholtz equation as

$$\left( 2\mathrm{i}\, k\, \partial_z + \partial_z^2 - k^2 + \Delta_{\mathrm{t}} + \frac{n^2(\boldsymbol{r})\, \omega^2}{c^2} \right) \mathcal{E}(\boldsymbol{r}) = 0 \, , \tag{2.7}$$

where $k = n_0\,\omega/c$ is the wave vector amplitude in the ambient medium and $\Delta_{\mathrm{t}} = \partial_x^2 + \partial_y^2$ the transverse Laplace operator.

We now approximate that $n^2(\boldsymbol{r}) \approx n_0^2 + 2n_0\delta n(\boldsymbol{r})$ using the fact that $\delta n(\boldsymbol{r}) \ll n_0$. Next, we apply the paraxial wave approximation stating that the change of the amplitude $\mathcal{E}$ over one wavelength is negligible. This translates to $\partial_z^2\mathcal{E} \ll k^2\mathcal{E}$ and $\partial_z^2\mathcal{E} \ll k\partial_z\mathcal{E}$ which yields the paraxial Helmholtz equation [10]

$$\left(\mathrm{i}\frac{1}{k}\,\partial_z + \frac{1}{2\,k^2}\Delta_{\mathrm{t}} + \frac{\delta n(\boldsymbol{r})}{n_0}\right)\mathcal{E}(\boldsymbol{r}) = 0\,. \tag{2.8}$$

The structure of the paraxial Helmholtz equation is the same as for the Schrödinger equation of quantum mechanics. In fact, when defining $k = n_0\,2\pi/\lambda = n_0/\lambda\!\!\!{}^-$, we find

$$\left(\mathrm{i}\lambda\!\!\!{}^-\,\partial_z + \frac{\lambda\!\!\!{}^{-2}}{2\,n_0}\Delta_{\mathrm{t}} + \delta n(\boldsymbol{r})\right)\mathcal{E}(\boldsymbol{r}) = 0\,, \tag{2.9}$$

which is analogous to the Schrödinger equation,

$$\left(\mathrm{i}\hbar\,\partial_t + \frac{\hbar^2}{2\,m}\Delta - V(\boldsymbol{r})\right)\Psi(\boldsymbol{r},t) = 0\,, \tag{2.10}$$

of a nonrelativistic particle of mass $m$ in the potential $V(\boldsymbol{r})$. Classical waves propagating in a waveguide system along the $z$-direction can thus simulate the time evolution of nonrelativistic particles. This comes to no surprise because first quantisation is just the act of describing particles via wavefunctions. Nonetheless, this simulation allows to research the behaviour of complicated quantum systems with relatively simple photonic setups [24; 18].

An especially beneficial approach is to discretise the paraxial propagation in Eq. (2.9) with respect to the fundamental waveguide modes, leading to a coupled mode description. With this aim in mind, we write the refractive index difference $\delta n(\boldsymbol{r})$ of a system of $M$ waveguides as the sum

$$\delta n(\boldsymbol{r}) = \sum_{j=1}^{M} \delta n_j(\boldsymbol{r})\,. \tag{2.11}$$

If the waveguides are sufficiently far apart, one can expect that the total field is approximately comprised of the individual waveguide eigenmodes. Hence, we decompose the envelope amplitude $\mathcal{E}$ into individual modes localised at the $j$th waveguide, i.e.

$$\mathcal{E}(\boldsymbol{r}) = \sum_{j=1}^{M} A_j(z)\,T_j(x,y)\,\mathrm{e}^{\mathrm{i}k_j z}\,. \tag{2.12}$$

The different modes consist of a $z$-dependent amplitude $A_j$, a transverse mode profile $T_j(x, y)$, and a plain wave complex phase determined by the wave vector amplitude $k_j$ relative to the overall plain wave.

Inserting this ansatz into Eq. (2.9) leads to

$$\sum_{j=1}^{M}\left(\mathrm{i}ƛ\, T_j\,\partial_z A_j - ƛ k_j\, T_j A_j + \frac{ƛ^2}{2n_0} A_j\,\Delta_{\mathrm{t}} T_j + \sum_{i=1}^{M}\delta n_i\, A_j\, T_j\right) = 0\,. \tag{2.13}$$

Note that we assumed the tranverse mode profiles $T_j$ to not depend on $z$. However, when changing the position of the waveguides they could potentially have a dependence $T_j(x - x_0(z), y - y_0(z))$, i.e. following the waveguides but otherwise keeping their shape. This does not pose a problem, because the waveguides only gradually change their position as required for the paraxial approximation. Therefore, $\partial_z x_0 \approx \partial_z y_0 \approx 0$ meaning those contributions can be neglected. For ease of notation we thus still omit any $z$-dependence. However, keep in mind that the waveguide positions can still change facilitating $z$-dependent couplings.

The transverse mode profiles $T_j(x, y)$, by definition, fulfil the Helmholtz equations,

$$\left(\frac{ƛ^2}{2n_0}\Delta_{\mathrm{t}} + \delta n_j(\boldsymbol{r})\right) T_j = 0\,, \tag{2.14}$$

of the individual waveguides. This means that the individual $T_j(x, y)$ are eigenfunctions of the Hermitian operator $\Delta_{\mathrm{t}}$ for different eigenvalues. Consequently, these eigenmodes are orthogonal to each other,

$$\iint \mathrm{d}x\mathrm{d}y\, T_l^*\, T_j = \delta_{lj}\,. \tag{2.15}$$

Note that this approximation hinges on sufficient distances between the waveguides. Otherwise their unperturbed, individual eigenmodes without any surrounding waveguides would not be an adequate assumption. In this case the expansion in Eq. (2.12) should either be performed using the supermodes [95] of the total waveguide system or one sticks with the individual, unperturbed modes and takes their non-orthogonality into account, see for example Ref. [96].

With the orthogonality in Eq. (2.14) in mind we now integrate Eq. (2.13) with $\iint \mathrm{d}x\mathrm{d}y\, T_l^*$. The result reads

$$\mathrm{i}ƛ\,\partial_z A_l - ƛ\, k_l\, A_l + \sum_{j=1}^{M} A_j \sum_{\substack{i=1\\ i\neq j}}^{M} \iint \mathrm{d}x\mathrm{d}y\,\delta n_i\, T_l^*\, T_j = 0\,. \tag{2.16}$$

where the complicated summation terms can be simplified by introducing the coupling constants

$$\kappa_{jl} = \frac{1}{ƛ}\sum_{\substack{i=1\\ i\neq j}}^{M} \iint \mathrm{d}x\mathrm{d}y\,\delta n_i\, T_l^*\, T_j\,. \tag{2.17}$$

For cases $j \neq l$ these constants quantify the overlap between modes $j$ and $l$ mediated by the index profiles. Because of the large distances, this overlap is only located at the tail of

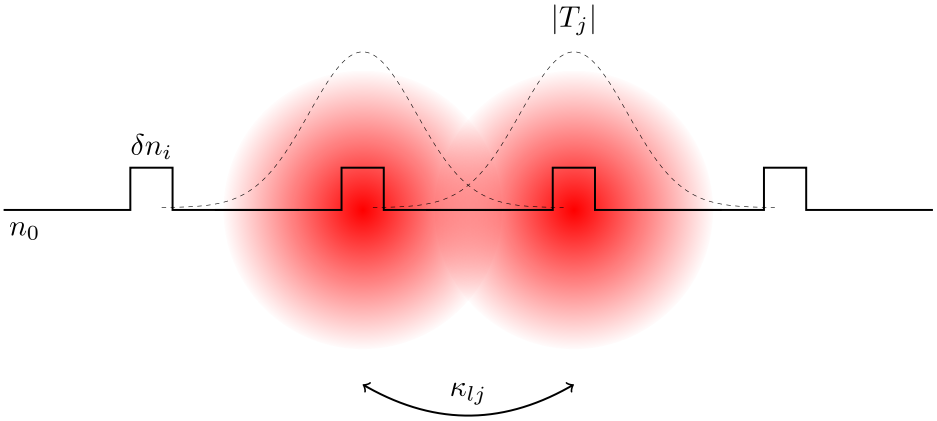

Fig. 2.2.: Sketch of evanescent overlaps. The different modes centred around the waveguides couple via overlap mediated by the index $\delta n_i$, cf. Eq. (2.17).

the mode profiles and the couplings are thus aptly coined as evanescent, cf. Fig. 2.2. In the case $j = l$ the coupling constant describes a self-coupling mediated by the index profiles of other waveguides. This contribution is, however, often negligible due to the large distances that are already assumed. Nevertheless, we can simply add it to the already appearing wave vector amplitude $k_l$ by defining the propagation constant $\sigma_l = \kappa_{ll} - k_l$. The result

$$\mathrm{i}\,\partial_z A_l + \sigma_l\, A_l + \sum_{\substack{j=1\\ j\neq l}}^{M} \kappa_{jl}\, A_j = 0 \tag{2.18}$$

is the coupled-mode propagation equation for the amplitudes $A_j(z)$.

## 2.2. The quantised coupled-mode equation

The process of quantisation of a classical theory, e.g. represented here by the coupled-mode equation (2.18), is generally well understood [97]. This is especially true in quantum optics where this transition entails the use of photons as the fundamental energy quanta [7]. The key step here is to elevate the amplitudes $A_l(z)$ to bosonic operators $\hat{a}_l(z)$ and postulate equal-space commutator relations for them, i.e.

$$[\hat{a}_l(z), \hat{a}_k^\dagger(z)] = \delta_{lk}\,. \tag{2.19}$$

Replacing all the amplitudes in Eq. (2.18) with their operator counterparts, its quantised version reads

$$\mathrm{i}\,\partial_z \hat{a}_l + \sigma_l\, \hat{a}_l + \sum_{\substack{j=1\\ j\neq l}}^{M} \kappa_{jl}\, \hat{a}_j = 0\,. \tag{2.20}$$

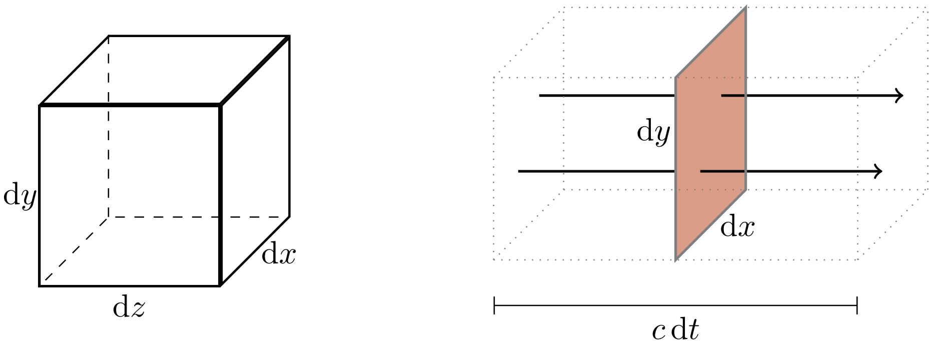

Fig. 2.3.: Quantisation geometries. (Left panel) Volume integration over d$x$d$y$d$z$ leading to equal-time commutator relations. (Right panel) Flux integration over d$x$d$y$$c$d$t$ leading to equal-space commutator relations in $z$.

Based on this coupled-mode equation, a Hamiltonian operator can be deduced for such waveguides systems by comparing Eq. (2.20) with the Heisenberg equation ($\hbar = 1$)

$$\partial_z \hat{f} = \mathrm{i}\left[\hat{f}, \hat{H}\right] \tag{2.21}$$

and utilising the commutator in Eq. (2.19). The Hamiltonian consistent with the coupled-mode equation (2.20) is then

$$\hat{H} = \sum_{i=1}^{M} \sigma_i\, \hat{a}_i^\dagger \hat{a}_i + \sum_{\substack{i,j=1\\ i\neq j}}^{M} \kappa_{ij}\, \hat{a}_i^\dagger \hat{a}_j + \mathrm{H.\,c.} \tag{2.22}$$

The observant reader might have spotted an oddity in this derivation. To be precise, the Heisenberg equation (2.21) has the wrong sign. The reason for this is that the dynamical variable is not, as usual, the time $t$ but the propagation distance $z$. Obviously, this also means that the dimensions of the Hamiltonian are per length instead of per time ($\hbar = 1$) and it thus does not describe the energy. This results in subtle differences in the details of the quantisation of the propagating fields.

The remedy for these discrepancies is to base the quantisation not on a decomposition of spatial modes in a quantisation volume $V$ but instead replace the decomposition in $z$-direction with a temporal mode decomposition [98; 99; 100]. The new quantisation geometry is then the flux in a given time $T$ through a unit area perpendicular to $z$, see Fig. 2.3. Thus, the integration is over the hyperplane d$x$d$y$$c$d$t$ instead of d$x$d$y$d$z$.

The bosonic operator $\hat{a}_l(z)$ and $\hat{a}_l^\dagger(z)$ are then interpreted as to describe the creation or annihiliation of a photon in the waveguide mode with index $l$ that passes the area at $z$ in the time $T$ [101]. It can be proven that the equal-space commutator relations, Eq. (2.19), are consistent with their equal-time counterparts [101]. Additionally, the important quantity that governs the dynamics is no longer the Hamiltonian, i.e. the energy, but technically the momentum. Physically, this means that no longer the energy over a certain volume is the basis for the quantisation but the flux through an area over a certain time. For this momentum operator the Heisenberg-like equation (2.21) is then correct [100].

Despite these slight differences the resulting equations are analogous to the familiar quantisation, Heisenberg equation, and resulting Hamiltonian. In fact, detailed calculations of the momentum operator [102; 103] show that in case of waveguide propagation the result in Eq. (2.22) is the same and the two approaches are connected via the simple relation $z = c\,t$ [100]. For this reason, we will still use the notion of a Hamiltonian throughout this thesis but keep the clear connection of the physical interpretation as a flux to the propagation through the waveguide array as well as the directly resulting $z$-dependent equation of motion.

### Summary

In this chapter, we introduced the coupled-mode theory that describes the paraxial propagation in photonic waveguides along the $z$-axis. The coupled-mode equations are formulated for classical field amplitudes in Eq. (2.18) as well as for the corresponding bosonic mode operators in Eq. (2.20). From the quantised coupled-mode equation a Hamiltonian was derived, Eq. (2.22), that is the basis for the rest of the thesis. In the next chapter, we discuss how geometric phases and artificial non-Abelian gauge fields emerge from the evolution under a specific form of this Hamiltonian.

# 3. Implementation of geometric phases and non-Abelian gaugefields

The previous chapter introduced the basic theoretical description of light propagation through a system of coupled waveguides. In this chapter we provide a first example of an application of said description by showing how one can implement geometric phases in such waveguide systems. These phases arise naturally in systems that are subject to adiabatic evolutions and solely depend on the geometry of their parameter space. Consequently, they have a deep connection to the mathematical theory of differential geometry. Additionally, these geometric phases share great similarity with gauge fields which lie at the heart of modern physics [97; 39].

In order to see these interconnections and to understand how they emerge in our waveguide systems, we begin with a prelude of the basic notions of differential geometry. Subsequently, we recapitulate the fundamentals of gauge field theories and illustrate their ties with geometric phases. Afterwards we discuss how these concepts resurface when describing the evolution of physical systems, particularly our coupled waveguides. Finally, we show how geometric phases or gauge fields can be implemented in an experiment with waveguides and close with some notions on how their uses can be expanded upon with multiple-photon states and non-Hermiticity.

## 3.1. Differential geometry and geometric phases

The first concept of differential geometry we need, is the covariant derivative of a vector $\boldsymbol{V} = V^\nu \boldsymbol{e}_\nu$ (written in Einstein's sum convention for Greek indices) with components $V^\nu$ and basis vectors $\boldsymbol{e}_\nu$. Along the coordinate $x^\mu$, the covariant derivative is defined as [104]

$$\nabla_\mu \boldsymbol{V} = \left(\partial_\mu V^\nu + V^\epsilon \Gamma^\nu_{\mu\epsilon}\right) \boldsymbol{e}_\nu = 0 \tag{3.1}$$

with the definition of the Christoffel symbols $\Gamma^\nu_{\mu\epsilon}$ being

$$\partial_\mu \boldsymbol{e}_\epsilon = \Gamma^\nu_{\mu\epsilon} \boldsymbol{e}_\nu \, . \tag{3.2}$$

The covariant derivative encapsulates not only the change of the components along the coordinate $x^\mu$ but also carries the information of how the basis $\boldsymbol{e}_\nu$ itself changes along the way. In flat coordinate spaces, like Euclidean space, this is of course irrelevant as the basis is invariant and thus the Christoffel symbols evaluate to zero. However, in general,

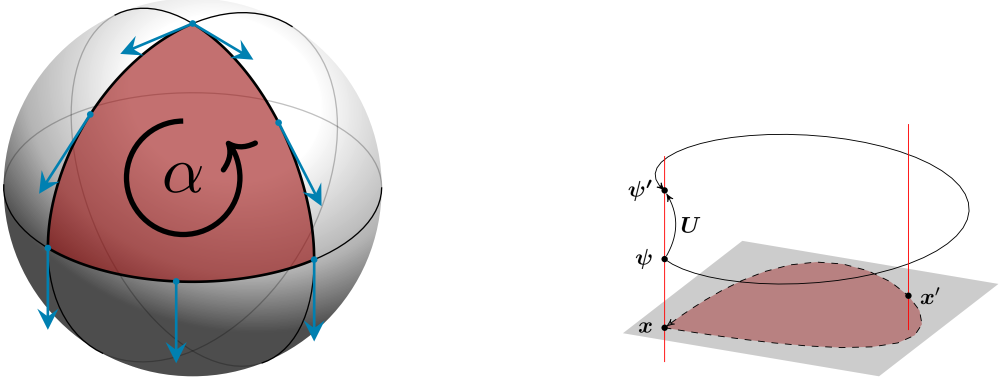

(a) Parallel transport of a vector on a sphere (b) Abstract parallel transport with fibres.

Fig. 3.1.: Geometric concepts of parallel transport and holonomies. The closed parallel transport of a vector or state over a curved manifold creates a geometric phase/holonomy.

curved spaces their contribution is nontrivial and provides the necessary information to connect the fields at different points in space. For this reason, the additional term in the covariant derivative is also called the *connection*. In case of coordinate spaces this is the Christoffel symbol.

Using the covariant derivative (3.1), a special case of traversing the coordinate space can be defined and that is the notion of parallel transport. The vector $\boldsymbol{V}$ is said to be parallel transported along a curve with coordinates $x^\nu(\xi)$ parametrised by $\xi$ if [104]

$$\mathrm{D}_\xi V^\nu \equiv \partial_\xi V^\nu + \Gamma^\nu_{\mu\epsilon}\,\partial_\xi x^\mu(\xi)\,V^\epsilon = 0\,. \tag{3.3}$$

This concept is visualised in Fig. 3.1a where a vector is parallel transported on a globe. Starting at the north pole, the vector is first shifted south along a meridian which is followed by a shift along the equator and finally a back propagation to the north pole. The vector is held parallel along the entire way according to Eq. (3.3). This is most easily imagined when holding the vector fixed, i.e. parallel to itself, and instead moving the globe beneath. Regardless of the way one thinks about it, the vector changed its direction during the transport due to the curvature of the globe. This angle $\alpha$ between initial and final state of the vector is the geometric phase and it is directly linked to the area on the curved globe enclosed by the parallel transport.

In this simple example, rooted in basic geometry and thus easily visualised, the geometric phase is a scalar value because a single vector or state is parallel transported. From the perspective of quantum physics this would be described as a single state $\psi$ acquiring a phase $\alpha$ when traversing a closed loop in the space comprised of the experimental parameters controlling the system, i.e.

$$\psi \to \psi' = \mathrm{e}^{\mathrm{i}\alpha}\psi\,. \tag{3.4}$$

The phase $\alpha$ is then the geometric phase. When multiple states or vectors are involved, the geometric phase becomes matrix-valued and the final state is given by the vector-valued initial state times the unitary matrix $\boldsymbol{U} = \exp(\mathrm{i}\boldsymbol{\alpha})$,

$$\boldsymbol{\psi} \to \boldsymbol{\psi}' = \boldsymbol{U}\boldsymbol{\psi} \,. \tag{3.5}$$

The operation $\boldsymbol{U}$ that results from the closed-loop parallel transport is called a *holonomy.*

In Fig. 3.1b this generalised sense of parallel transport can be seen in the context of fibre bundles. The fundamental mathematical theory of fibre bundles is the basis of modern differential geometry which comes with a host of own conventions, notations, and concepts [105; 106; 107]. Although it goes beyond the scope of this thesis it does provide helpful images to visualise the theory of holonomies in the abstract, matrix-valued case. Starting point is the vector-valued state $\boldsymbol{\psi}$ at the initial system parameters $\boldsymbol{x}$, e.g. couplings and propagation constants of our waveguides. This parameter space is represented by the underlying sheet in Fig. 3.1b and is the base manifold on which each point is associated with a fibre. These fibres form vector spaces of states that are transformed into each other by the holonomies. For example, the collection of arrows in the plain tangent to the north pole in Fig. 3.1a constitute a fibre where all states are connected by simple rotations determined by the scalar geometric phase $\alpha$. A different point of the sphere is then associated with another fibre, i.e. vectors in a tangent plane at this point.

In the more abstract sense of Fig. 3.1b the holonomy $\boldsymbol{U} = \exp(\mathrm{i}\boldsymbol{\alpha})$ might be more complicated in detail but follows the same scheme. The state $\boldsymbol{\psi}$ is still parallel transported following a closed loop in the parameter manifold and thus picks up a geometric phase $\boldsymbol{\alpha}$ which is determined by the size and curvature of the area of the parameter space enclosed by the loop. Thus, although the system returns to the initial configuration the state vector is changed which is visualised as a shift along the fibre.

Under a few conditions, holonomies resurface in gauge field theories and the evolution of generic physical systems like our coupled waveguides. In fact, differential geometry with its roots in fibre bundle theory is the mathematical language of gauge field theories as well as the evolution of physical systems [108]. The key is to identify the condition of closed parallel transport in the different settings. Later we will see that this means that accessible physical systems, like the photonic waveguides, can be used to implement artificial gauge fields and holonomies. On the one hand, the artificial gauge fields could then be used to simulate the building blocks of the fundamental gauge field theories [109; 48; 110]. On the other hand, the holonomies are general unitary transformations around which a whole theory of quantum computation is established - holonomic quantum computation (HQC) [40; 46].

## 3.2. Fundamentals of gauge field theories

Gauge field theories are ubiquitous in modern theoretical physics as they are able to describe the behaviour of elementary particles ranging from photons in electrodynamics to the whole particle zoo (quarks, gluons, etc.) in the standard model [39; 111]. Their basis are Lagrangians $\mathscr{L}$ that encapsulate the theory's symmetries and from which equations of motions are derived via Euler-Lagrange equations. The defining property of gauge field theories is their invariance or symmetry with regard to Lie group transformations, e.g. (special) unitary groups for Yang-Mills theories. Such symmetries are physically motivated, e.g. one would expect the Schrödinger equation to be invariant under U(1) group transformations of the wavefunction because a global complex phase factor should not change any observable.

The basic idea of gauge field theories is captured by considering, for example, the Lagrangian

$$\mathscr{L} = \frac{1}{2}(\partial_\mu \boldsymbol{\phi})^\dagger \partial^\mu \boldsymbol{\phi} - \frac{1}{2} m^2 \boldsymbol{\phi}^\dagger \boldsymbol{\phi} \tag{3.6}$$

for a free particle field $\boldsymbol{\phi}$ of mass $m$ which in general is vector-valued. The Lagrangian $\mathscr{L}$, and with it the derived theory, is invariant under unitary transformations

$$\boldsymbol{\phi} \rightarrow \boldsymbol{\phi}' = \boldsymbol{U}\boldsymbol{\phi}\,, \tag{3.7}$$

with a constant matrix

$$\boldsymbol{U} = \mathrm{e}^{\mathrm{i}\boldsymbol{\alpha}}\,, \tag{3.8}$$

where $\boldsymbol{\alpha}$ is a real matrix, i.e. similar to the holonomic transformations in Eq. (3.4) and (3.5).

The invariance in Eq. (3.7) amounts to a global symmetry when $\boldsymbol{U}$ is constant. But what if we demand the symmetry to be local, i.e. $\boldsymbol{\alpha}$ and thus $\boldsymbol{U}$ to depend on the coordinates $x^\mu$? In this case, the derivative in the Lagrangian produces additional terms in accordance with the product rule,

$$\partial_\mu \boldsymbol{\phi}' = (\partial_\mu \boldsymbol{U})\,\boldsymbol{\phi} + \boldsymbol{U}\,\partial_\mu \boldsymbol{\phi}\,. \tag{3.9}$$

These additional terms cause the original Lagrangian (3.6) to vary under the transformation (3.7).

This problem can be remedied by introducing a modified derivative

$$D_\mu = \partial_\mu + \boldsymbol{A}_\mu\,, \tag{3.10}$$

with the gauge field $\boldsymbol{A}_\mu$, which is similar to the covariant derivative introduced in Eq. (3.1). This is the first of many hints towards the importance of differential geometry as the mathematical language of gauge fields. In fact, the gauge field $\boldsymbol{A}_\mu$ takes on the role of a connection that keeps track of the local symmetry. This is ensured by demanding that the gauge field itself transforms as

$$\boldsymbol{A}_\mu \rightarrow \boldsymbol{A}'_\mu = \boldsymbol{U}\boldsymbol{A}_\mu\boldsymbol{U}^{-1} + (\partial_\mu \boldsymbol{U})\,\boldsymbol{U}^{-1}\,. \tag{3.11}$$

With this property, the transformed covariant derivative is simply

$$D_\mu \boldsymbol{\phi} \rightarrow (D_\mu \boldsymbol{\phi})' = \partial_\mu \boldsymbol{\phi}' + \boldsymbol{A}'_\mu\,\boldsymbol{\phi}' = \boldsymbol{U} D_\mu \boldsymbol{\phi}\,, \tag{3.12}$$

which is the same as for the global symmetry where $\boldsymbol{U}$ directly commutes with the derivative. Hence, when defining a Lagrangian with the new covariant derivative, i.e.

$$\mathscr{L} = \frac{1}{2}(D_\mu \boldsymbol{\phi})^\dagger D^\mu \boldsymbol{\phi} - \frac{1}{2} m^2 \boldsymbol{\phi}^\dagger \boldsymbol{\phi}\,, \tag{3.13}$$

it is again invariant and follows now the local symmetry.

A special kind of symmetry is connected to the special unitary groups SU($n$) that result in Yang-Mills theories which cover the standard model and thus the fundamentals of modern physics. In these theories the gauge field itself is considered as a dynamical variable by adding a term

$$\mathscr{L}_{\mathrm{F}} = -\frac{1}{4}\mathrm{Tr}\left(\boldsymbol{F}_{\mu\nu}\boldsymbol{F}^{\mu\nu}\right) \tag{3.14}$$

to the Lagrangian (3.13), where $\boldsymbol{F}_{\mu\nu}$ is a field strength tensor defined as

$$\boldsymbol{F}_{\mu\nu} = [D_\mu, D_\nu] = \partial_\mu \boldsymbol{A}_\nu - \partial_\nu \boldsymbol{A}_\mu + [\boldsymbol{A}_\mu, \boldsymbol{A}_\nu]\,. \tag{3.15}$$

In electrodynamics, for which the symmetry group is U(1), this tensor directly contains the electric and magnetic field components. In fact, when only considering $\mathscr{L}_{\mathrm{F}}$ for the theory and inserting it into the Euler-Lagrange equations one recovers the vacuum Maxwell equations [97]. Note that for the U(1) gauge theory all the above quantities become scalar and the theory is Abelian, i.e. commutative. However, for other symmetry groups like SU(2) for the weak and SU(3) for the strong interaction the theories are non-Abelian and the full matrix-valued equations need to be considered.

As we have just seen, the gauge field takes the role of a connection that preserves the symmetry of a Lagrangian by modifying the partial derivative to a covariant derivative. Now, just as in abstract differential geometry, one can define a parallel transport along a curve $\mathcal{C}$ based on the gauge field connection $\boldsymbol{A}_\mu$ which would equate to $D_\mu \boldsymbol{\phi} = \boldsymbol{0}$ as in Eq. (3.3). This results in a differential equation

$$\partial_\mu \boldsymbol{\phi} = -\boldsymbol{A}_\mu\, \boldsymbol{\phi}\,. \tag{3.16}$$

The transformation $\boldsymbol{U}_{\mathcal{C}}$ that propagates the state along the curve is then the path-ordered integral

$$\boldsymbol{U}_{\mathcal{C}} = \mathcal{P}\mathrm{e}^{-\int_{\mathcal{C}} \boldsymbol{A}_\mu \mathrm{d}x^\mu}\,. \tag{3.17}$$

This transformation is identical to the parallel transport from abstract differential geometry. The integral over the gauge field connection thus becomes a geometric phase that now intricately links geometric properties to the symmetry associated with the gauge field transformation.

For a closed curve $\mathcal{C}$ the matrix $\boldsymbol{U}_{\mathcal{C}}$ again becomes a holonomy, meaning we have now come full circle. The holonomy transformation (3.4) or (3.5) is then identified with the symmetry under the gauge field transformation (3.7). Consequently, the invariance under the gauge transformation graphically means the invariance under shift along the fibre as seen in Fig. 3.1b. A fibre structure is thus uniquely identified with a symmetry cementing the fact that fibre bundle theory and differential geometry are merely the mathematical language of gauge field theories. We close this section by noting that the line integral in Eq. (3.17) of the gauge field connection $\boldsymbol{A}_\mu$, which tracks the local symmetry, can be recast as a surface integral over the enclosed area $\square_{\mathcal{C}}$

$$\boldsymbol{U}_{\mathcal{C}} = \mathcal{P}\,\mathrm{e}^{-\int_{\square_{\mathcal{C}}} \boldsymbol{F}_{\mu\nu} \mathrm{d}x^\mu \wedge \mathrm{d}x^\nu}\,, \tag{3.18}$$

where $\wedge$ is the wedge product [112; 113]. This gives the field strength tensor of Yang-Mills theories the role of a curvature which then defines the geometric phase. What is now left, is to see how such geometric phases or gauge fields emerge in the cyclic evolution of physical systems.

## 3.3. Geometric phases and holonomies in Hermitian systems

The emergence of geometric phases in the evolution of physical systems was first discovered in the scalar case by Pancharatnam [42] and independently by Berry [43]. This Pancharatnam–Berry phase explains the famous Aharonov–Bohm effect [37] where a charged particle accumulates a geometric phase from the vector gauge field of an isolated solenoidal magnetic field. It was shown later by Wilczek and Zee [44] that a similar effect occurs generally in degenerate subspaces of a system that follows a closed adiabatic dynamic resulting in matrix-valued geometric phases. Due to their matrix-valued nature these geometric phases and their associated holonomies are non-Abelian.

The two main ingredients in implementing such non-Abelian geometric phases are the degenerate subspaces and an adiabatic, cyclic evolution. We start with a Schrödinger equation

$$\mathrm{i}\,\partial_z|\psi(z)\rangle = \hat{H}(z)\,|\psi(z)\rangle\,, \tag{3.19}$$

where the Hamiltonian possesses a degenerate spectrum. Because we can always shift the scale of the Hamiltonian it is possible to chose one subspace to eigenvalue 0 which is often called a *dark* subspace in contrast to *bright* subspaces with nonzero eigenvalues. The latter acquire a dynamic phase from their nonzero eigenvalue which is why we focus for simplicity on the degenerate dark subspace spanned by $N_{\mathcal{D}}$ *dark* states $\{|\mathcal{D}_i(z)\rangle\}$.

Note that we already used $z$ as the dynamical variable in Eq. (3.19) in anticipation of the later use for waveguide propagation. Additionally, the starting point of the Schrödinger equation does not mean only quantum systems are considered. As we have already seen in Chapter 2, the classical paraxial propagation in the waveguides is mathematically identical to the Schrödinger equation.

Now the adiabaticity becomes important because the evolution has to be confined to the degenerate subspace and thus no level crossings are allowed. Later we will discuss how to ensure the adiabaticity in experiments but for now we simply demand that the evolution is adiabatic and can thus decompose the initial state at $z = 0$ in the basis of dark states, i.e.

$$|\psi(0)\rangle = \sum_{i=1}^{N_{\mathcal{D}}} c_i\,|\mathcal{D}_i(0)\rangle\,. \tag{3.20}$$

Formally, we write the evolved state using the evolution operator,

$$|\psi(z)\rangle = \hat{U}(z)\,|\psi(0)\rangle = \sum_{i,j=1}^{N_{\mathcal{D}}} U_{ij}\,c_j\,|\mathcal{D}_i(z)\rangle\,, \tag{3.21}$$

where

$$\hat{U}(z) = \sum_{i,j=1}^{N_{\mathcal{D}}} U_{ij} \, |\mathcal{D}_i(z)\rangle\langle\mathcal{D}_j(0)| \,. \tag{3.22}$$

If the evolution is adiabatic and thus confined to the zero-eigenvalue dark subspace, the Schrödinger equation leads to $\mathrm{i}\,\partial_z|\psi(z)\rangle = 0$. Subsequently, when inserting Eq. (3.21) one finds

$$\partial_z|\psi(z)\rangle = \sum_{i,j=1}^{N_{\mathcal{D}}} c_j \left(\partial_z U_{ij} \, |\mathcal{D}_i(z)\rangle + U_{ij} \, \partial_z|\mathcal{D}_i(z)\rangle\right) = 0 \,. \tag{3.23}$$

This is the central equation that links the physical evolution with the preceding geometric notion of parallel transport, cf. Eq. (3.3). The first term of the summand is the derivative of the components, here given by $U_{ij}$, whereas the second term covers the derivative of the basis $|\mathcal{D}_i(z)\rangle$. Note that the changing experimental parameters of the system, e.g. coupling and propagation constant, take on the role of the coordinates $\{x^\mu(z)\}$ now parametrised by $z$. Varying these parameters such that they return to their initial configuration creates a closed curve. The derivative $\partial_z|\mathcal{D}_i(z)\rangle$ of the changing basis is then the derivative along this curve and reads

$$\partial_z|\mathcal{D}_i(z)\rangle = \sum_{k=1}^{N_{\mathcal{D}}} \partial_z x^\mu \left(\boldsymbol{A}_\mu\right)_{ki} |\mathcal{D}_k(z)\rangle \,. \tag{3.24}$$

The matrix $\boldsymbol{A}_\mu$ with components

$$\left(\boldsymbol{A}_\mu\right)_{ki} = \langle\mathcal{D}_k(x^\mu(z))|\partial_\mu|\mathcal{D}_i(x^\mu(z))\rangle \tag{3.25}$$

takes on the role of the connection, telling us how to stitch together the evolution along the curve under the varying basis. The Eq. (3.23) then exactly matches the definition of the parallel transport in Eq. (3.3). Therefore, it is clear that an adiabatic evolution within a degenerate subspace is just a parallel transport [114]. This is intuitive because an adiabatic process means that the evolution is infinitely slow so that the state can perfectly follow without changing to other levels in the spectrum - the state stays parallel to itself along the way.

A few things have to be noted here. First, the sum notation in Eq. (3.24) is peculiar because the index $k$ runs over $\{1, \ldots, N_{\mathcal{D}}\}$ whereas $\mu$ indicates the experimental parameters, i.e. the coordinates. Second, the index $\mu$ is still written with the Einstein sum convention. These peculiarities are due to the fact that the sets of indices encountered in Eq. (3.24) are qualitatively different. On the one hand, the Greek index $\mu$ labels the experimental parameters which are full geometric quantities, i.e. the coordinates of the underlying space of parameters. In Fig. 3.1b this space is represented by the underlying sheet. On the other hand, the Latin index $k$ does not refer to coordinate basis vectors of the parameter space but instead labels the dark subspace basis vectors, which corresponds to the fibre in Fig. 3.1b.

As a result the Latin indices are not geometrically linked to the Greek indices of the coordinates $x^\mu$. This problem did not occur for the Christoffel symbol $\Gamma^\nu_{\mu\epsilon}$ because there the fibres are the tangential spaces spanned by basis vectors created from derivatives along the coordinates $x^\mu$ itself. In contrast, the fibres for the connection $(\boldsymbol{A}_\mu)_{ik}$ are the dark subspaces that lack this direct relation to the parameter space but depend on the structure of the Hamiltonian. Therefore, although the quantities $(\boldsymbol{A}_\mu)_{ik}$ are connections they are not exactly identical to the geometric Christoffel symbols defined in Eq. (3.2). This subtle difference ties in with the general geometric interpretation of (quantum) physics and has some interesting effects that are discussed in more detail in the Appendix A.

Nonetheless, the $N_\mathcal{D} \times N_\mathcal{D}$-matrix $\boldsymbol{A}_\mu$ acts as a general connection and we have seen in the preceding sections that it thus should be a gauge field connection. In order to check whether this is true, we simply have to tests its behaviour under a unitary basis transformation

$$|\mathcal{D}'_i\rangle = \sum_j M_{ij}\, |\mathcal{D}_j\rangle\,, \tag{3.26}$$

with a unitary matrix $\boldsymbol{M}$. Using the definition (3.25), the new gauge field is

$$\left(\boldsymbol{A}'_\mu\right)_{ki} = \sum_{nj} \left(\boldsymbol{A}_\mu\right)_{nj} M^*_{kn}\, M_{ij} + \sum_n M^*_{kn}\, \partial_\mu M_{in}\,, \tag{3.27}$$

or in matrix notation

$$\boldsymbol{A}'_\mu = \boldsymbol{M}\boldsymbol{A}_\mu\boldsymbol{M}^{-1} + (\partial_\mu \boldsymbol{M})\boldsymbol{M}^{-1}\,, \tag{3.28}$$

which is the same as the defining Eq. (3.11) for a properly transformed gauge field under change of basis. Hence, the $\boldsymbol{A}'_\mu$ emerging from an evolving physical system as occurring in Eq. (3.23) is a gauge field connection.

This already opens the way to implement gauge fields via geometric phases. But with this relation established, we can go even further by returning to the constraint of the cyclic adiabatic evolution. Because Eq. (3.23) has to hold for arbitrary input states, i.e. $\forall\, c_j$, each bracketed expression has to evaluate to zero. When applying $\langle \mathcal{D}_k(z)|$ from the left and using the chain rule $\partial_z = \partial_z x^\mu\, \partial_{x^\mu}$ this results in

$$\partial_\mu U_{kj} = -\sum_{i=1}^{N_\mathcal{D}} \left(\boldsymbol{A}_\mu\right)_{ki} U_{ij}\,. \tag{3.29}$$

A general solution to this equation for the closed curve $\mathcal{C}$ in parameter space is the path-ordered integral

$$\boldsymbol{U}_\mathcal{C} = \mathcal{P}\exp\left(-\oint_\mathcal{C} \boldsymbol{A}_\mu \mathrm{d}x^\mu\right). \tag{3.30}$$

This unitary evolution operator is again a holonomy and it is determined by the cyclic integral over the gauge field connection $\boldsymbol{A}_\mu$.

When interpreting the holonomies as unitary transformations, it is clear that these can be seen as computational gates, e.g. transforming an input in some computational code into a desired output. This is the general idea of HQC where the required quantum gates are constructed from carefully chosen loops in the parameter space of a degenerate

Hamiltonian. Due to the geometric nature, these gates are especially robust against fluctuations along the path [54; 41]. This is easily seen from Eq. (3.18) where the geometric phase is recast as a surface integral. Random fluctuations along the path that average out over the whole loop give the same enclosed area and thus the same geometric phase leading to a stable holonomy. Additionally, most quantum gates operate on just two qubits because larger operations can also be constructed from consecutive two-qubit gates. In contrast, the dimension of a holonomy is given by the dimension of the chosen degenerate space of the Hamiltonian and can therefore create larger gates in only one cyclic evolution of the system.

The last part does, however, pose some questions regarding the completeness of the holonomies, i.e. how many different gates can be created with loops in the parameter space of a given Hamiltonian? Generally speaking, a complete $\mathrm{U}(N_{\mathcal{D}})$ group can be created from an $N_{\mathcal{D}}$-dimensional subspace when the resulting gauge fields $\boldsymbol{A}_\mu$ span the whole group algebra. However, in detail this is a delicate question which is not the main focus of this thesis but which is covered in Ref. [45]. We merely focus on the most important point and that the completeness is usually fulfilled when the dimension of the parameter space is large enough. At the example of photonic waveguides we will shortly see that already a few parameters allow for the creation of specific but not all possible gates. Adding more parameters like the propagation constants can solve this problem. At the end of this chapter we will discuss how to increase the number of parameters even further using non-Hermitian systems.

We close this section with a final note on the gauge field connection. It was already mentioned that because the geometric phase is calculated from a gauge field connection it allows in principle to simulate non-Abelian gauge field theories in such degenerate systems. However, the gauge field itself is not an observable because it is not gauge or basis invariant. This can be seen by its transformation in Eq. (3.28) which contains an additional term $(\partial_\mu \boldsymbol{M})\boldsymbol{M}^{-1}$. Therefore, we instead use the so called Wilson loop [38]

$$W_{\mathcal{C}} = \mathrm{Tr}\, \boldsymbol{U}_{\mathcal{C}} \,, \tag{3.31}$$

as it is measurable and can be used to reconstruct the gauge field connection in a chosen basis [115]. It is an important quantity in gauge field theories because it is linked to the question of quark confinement [38] and in that capacity often used in numerical analyses of discrete gauge field theories [110]. We will use it later on to evaluate experimental implementations of a gauge field in photonic waveguides [116].

## 3.4. Adiabatic evolution and the quantum metric

Up to this point we assumed perfect adiabaticity. However, deviation from this idealisation has to be taken into account when preparing an experiment. In the present case, an interesting approach borrowed from geometry can be used to find curves $\mathcal{C}$ through the parameter space that minimise the nonadiabatic, or diabatic, error. This approach is based on the formulation of a metric on the parameter space spanned by the experimental parameters or coordinates $x^\mu$. With the metric as a measure of length, a shortest path

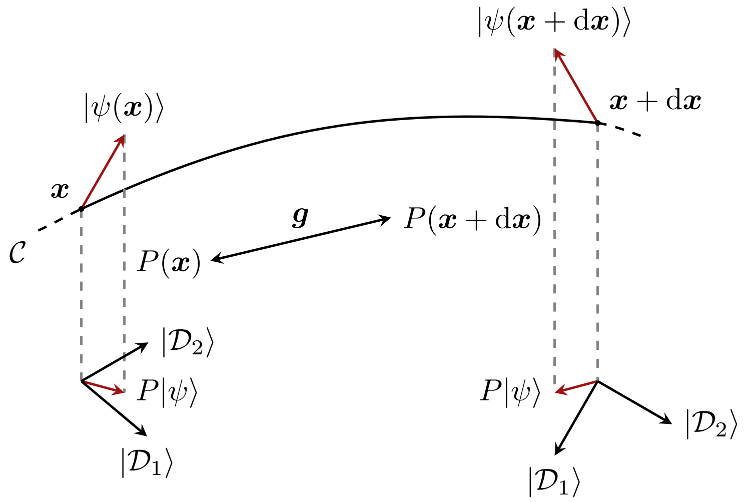
$|\psi(\boldsymbol{x}+\mathrm{d}\boldsymbol{x})\rangle$
$|\psi(\boldsymbol{x})\rangle$
$\boldsymbol{x}+\mathrm{d}\boldsymbol{x}$
$\boldsymbol{x}$
$\boldsymbol{g}$
$P(\boldsymbol{x}+\mathrm{d}\boldsymbol{x})$
$\mathcal{C}$
$P(\boldsymbol{x})$
$|\mathcal{D}_2\rangle$
$P|\psi\rangle$
$P|\psi\rangle$
$|\mathcal{D}_1\rangle$
$|\mathcal{D}_2\rangle$
$|\mathcal{D}_1\rangle$

Fig. 3.2.: Schematic concept of the quantum metric: Following a small displacement $\mathrm{d}\boldsymbol{x}$ along the curve $\mathcal{C}$, the projection operator $\hat{P}$ onto the dark subspace changes. This change is described by the quantum metric $\boldsymbol{g}$. Adapted from Ref. [116].

under experimental constraints can be found which minimises the diabatic error that results from the geometry [117].

The link between this geometric approach and the physics of the cyclic evolution can be understood as follows. The parallel or adiabatic transport of a physical state entails that the state remains exclusively in the subspace over which the gauge field connection (3.25) is defined. Consequently, no transitions to other subspaces occur and the state should always project unto the subspace, which can be tested using the subspace projector $\hat{P}(x^\mu) = \sum_i |\mathcal{D}_i(x^\mu)\rangle\langle\mathcal{D}_i(x^\mu)|$. This projection is sketched in Fig. 3.2. Along the path $\mathcal{C}$, i.e. for different configurations of the parameters $x^\mu$, the state $|\psi(\boldsymbol{x})\rangle$ is projected by $\hat{P}$ unto the degenerate subspace. Over an infinitesimal change $\boldsymbol{x} \to \boldsymbol{x} + \mathrm{d}\boldsymbol{x}$ the change $\mathrm{d}\hat{P}$ of the projection operator can be calculated using the trace norm [108; 117]

$$||\mathrm{d}\hat{P}||^2 = \mathrm{Tr}\left(\partial_\mu \hat{P}\,\partial_\nu \hat{P}\right)\mathrm{d}x^\mu\mathrm{d}x^\nu = g_{\mu\nu}\,\mathrm{d}x^\mu\mathrm{d}x^\nu\,. \tag{3.32}$$

Here, the quantum metric $g_{\mu\nu} = \mathrm{Tr}\left(\partial_\mu \hat{P}\,\partial_\nu P\right)$ was defined which describes how the projection operator changes along a curve. It is the trace of the real part of the so-called quantum geometric tensor [118; 108; 117; 114], whose imaginary part is the field strength tensor $\mathbf{F}_{\mu\nu}$ of the (non-Abelian) gauge field, see Eq. (3.15). Details on this and further relations to the general geometric interpretation of the physical evolution along the curve $\mathcal{C}$ can be found in the Appendix A.

Based on the notion of a metric tensor one can define a path length $L$ in the parameter space as

$$L = \int_{z_\mathrm{i}}^{z_\mathrm{f}} \sqrt{g_{\mu\nu}\,\partial_z x^\mu\,\partial_z x^\nu}\,\mathrm{d}z\,, \tag{3.33}$$

integrated from the initial variable $z_\mathrm{i}$ to the final variable $z_\mathrm{f}$. This implies that one can find a shortest path from $z_\mathrm{i}$ to $z_\mathrm{f}$ through the geometry of the parameter space defined by $g_{\mu\nu}$. Known in physics from the principle of least action, these shortest paths are the geodesic. Because the quantum metric carries the information on how much the projection operator $\hat{P}$ changes, the shortest paths are those with the minimal change in $\hat{P}$. For the evolution of the state this means that it minimises the chances to not be projected onto the dark subspace. Hence, in the present setting such a geodesic describes the evolution with the least diabatic error when traversing the parameter space [117].

However, a given implementation might place certain experimental constraints on the possible range of values for the parameters $x^\mu$ and thus on the achievable curves $\mathcal{C}$. For example the photonic waveguides require weak couplings and are also restricted by the length of the glass chip they are written in. Nevertheless, although perfect geodesics might not be obtainable one can still minimise $L$ under the additional constraints using (3.33). Thus, it is possible to find parameter variations that comply with the constraints and still provide the most adiabatic evolution. Such an optimisation ensures that the previously discussed geometric phase does emerge from the evolution in a realistic system.

## 3.5. Implementation in photonic waveguides

In the following section we will outline the physical implementation of an artificial non-Abelian gauge field or holonomy in integrated photonic waveguides. This work was jointly published with Mark Kremer from the Experimental Solid-State Optics group under Professor Alexander Szameit [116]. While the experiment itself was conducted by Mark Kremer the waveguide structure, especially its optimisation using the quantum metric, was designed by the author.

The first main ingredient is the degenerate (dark) subspace which is generally achieved adopting an $N$-pod structure known from atomic physics [48], cf. Fig. 3.3a. There, $N$ ground states $|g_i\rangle$ are coupled to one excited state $|e\rangle$. Such a system has $N_\mathcal{D} = N-1$ dark states with zero eigenvalue and two *bright* states with nonzero eigenvalues. This is the generalised case of the STIRAP (**STI**mulated **R**aman **A**diabatic **P**assage) protocol [119; 120] for which $N = 2$.

The atomic $N$-pod is now transferred to the photonic waveguide setting by coupling $N$ waveguides to a single central one, meaning $M = N + 1$ waveguides in total, see Fig. 3.3b. Interestingly, it suffices to use classical light in the waveguide setup which exemplifies how the paraxial Helmholtz equation simulates the Schrödinger equation – the evolution in quantised atomic energy levels is mapped to a dynamic in coupled discrete waveguide modes. A simple STIRAP process ($N = 2$) in waveguides was already done in Refs. [121; 122] but focussed on the full adiabatic passage from one outer waveguide to the other via the central waveguide. However, with our generalised approach it is possible to study non-Abelian geometric phases and gauge fields that result in arbitrary outputs.

Note that the different ground state energies in Fig. 3.3a relate to different propagation constants in the waveguide $N$-pod, Fig. 3.3b. However, these are not required to obtain the degenerate dark subspace which only requires the coupling structure. In fact, one would probably chose the same propagation constant for easier calculations and experimental

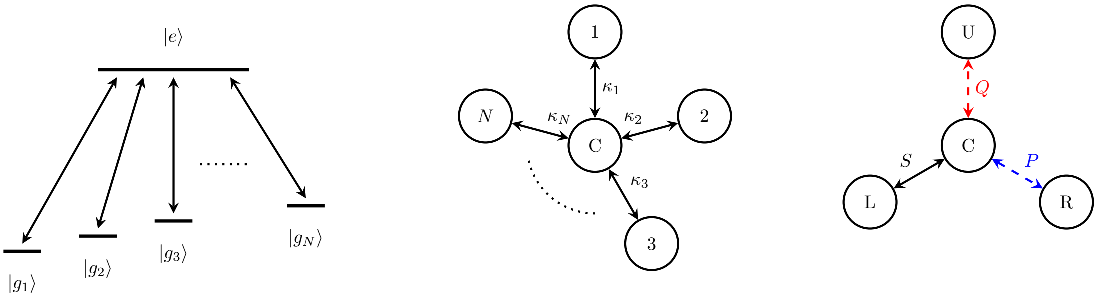

(a) **Atomic $N$-pod.** (b) **Waveguide $N$-pod.** (c) **Waveguide tripod.**

Fig. 3.3.: Realisations of $N$-pods in atomic systems and waveguide arrays.

implementation. This would not be possible in an atomic setup as one would hardly find a system with enough ground states of same energy.

Furthermore, adding more waveguides is conceptually easier than finding new atomic systems with the required level structure. Such an increase in the number of modes $N$ coupled to the central mode has, however, its limits even for waveguides. More waveguides would mean smaller distances between the outer waveguides which, depending on the specific distance variations, inevitably results in significant evanescent couplings that lift the symmetry needed for the degenerate subspace structure. In Section 3.6, we will discuss how to overcome this obstacle using multiple-photon states.

In our experimental implementation, we chose a tripod ($N = 3$) with four waveguides labelled L, R, U, and C coupled via real, $z$-dependent coupling parameters $\{x^\mu\} = \{S, P, Q\}$, see Fig. 3.3c. The paraxial Helmholtz equation for the classical field amplitudes $a_\mathrm{L}, a_\mathrm{R}, a_\mathrm{U}, a_\mathrm{C}$ in the individual waveguides reads,

$$\mathrm{i}\,\partial_z \begin{pmatrix} a_\mathrm{L} \\ a_\mathrm{R} \\ a_\mathrm{U} \\ a_\mathrm{C} \end{pmatrix} = \begin{pmatrix} 0 & 0 & 0 & S \\ 0 & 0 & 0 & P \\ 0 & 0 & 0 & Q \\ S & P & Q & 0 \end{pmatrix} \cdot \begin{pmatrix} a_\mathrm{L} \\ a_\mathrm{R} \\ a_\mathrm{U} \\ a_\mathrm{C} \end{pmatrix} . \tag{3.34}$$

The tripod Hamiltonian supports two dark states with zero eigenvalue,

$$|\mathcal{D}_1\rangle = \sin\theta\,|w_\mathrm{L}\rangle - \cos\theta\,|w_\mathrm{R}\rangle\,, \tag{3.35}$$

$$|\mathcal{D}_2\rangle = \cos\theta\sin\phi\,|w_\mathrm{L}\rangle + \sin\theta\sin\phi\,|w_\mathrm{R}\rangle - \cos\phi\,|w_\mathrm{U}\rangle\,, \tag{3.36}$$

where $|w_\mathrm{L,R,U}\rangle$ are the orthogonal eigenmodes of the respective waveguides with the angle parametrisations

$$\theta = \arctan\left(\frac{P}{S}\right)\,, \tag{3.37}$$

$$\phi = \arctan\left(\frac{Q}{\sqrt{S^2+P^2}}\right)\,. \tag{3.38}$$

Notably, they do not involve the eigenstate $|w_{\mathrm{C}}\rangle$ to which all other states are originally coupled to. In addition, the system possesses two *bright* states $|\mathcal{B}_{\pm}\rangle$ with eigenvalues $\zeta_{\pm} = \pm\sqrt{S^2 + P^2 + Q^2}$ that read

$$|\mathcal{B}_{\pm}\rangle = \frac{1}{\sqrt{2}} \left( \frac{S}{\zeta_{\pm}} |w_{\mathrm{L}}\rangle + \frac{P}{\zeta_{\pm}} |w_{\mathrm{R}}\rangle + \frac{Q}{\zeta_{\pm}} |w_{\mathrm{U}}\rangle + |w_{\mathrm{C}}\rangle \right) . \tag{3.39}$$

In contrast to the dark states, the bright states do contain the central waveguide providing a simple distinction later in the experiment.

With the degenerate dark subspace known, we can calculate the $\mathbf{A}_{\mu}$ from Eq. (3.25) which yields

$$\mathbf{A}_S = \frac{\mathrm{i}\, P\, Q}{(S^2 + P^2)\, \zeta_+} \sigma_y \, , \tag{3.40}$$

$$\mathbf{A}_P = \frac{\mathrm{i}\, S\, Q}{(S^2 + P^2)\, \zeta_-} \sigma_y \, . \tag{3.41}$$

Apparently, the simple tripod setup with real couplings results in matrix-valued, yet commutative geometric phases. Subsequently, the holonomy is readily calculated from Eq. (3.30) as we can ignore the path ordering, resulting in [120]

$$\boldsymbol{U} = \begin{pmatrix} \cos\gamma & \sin\gamma \\ -\sin\gamma & \cos\gamma \end{pmatrix} , \tag{3.42}$$

with

$$\gamma = \int_{z_{\mathrm{i}}}^{z_{\mathrm{f}}} \frac{Q\, (S\, \partial_z P - P\, \partial_z S)}{(S^2 + P^2)\, \zeta_+} \, \mathrm{d}z \, . \tag{3.43}$$

Because we have a two-dimensional dark subspace the resulting holonomy is an element of the unitary group U(2).

Although the noncommutative case is more general and desirable, our proof-of-concept experiment shows all necessary features to construct such arbitrary noncommutating geometric phases, most notably the optimisation via the quantum metric to ensure adiabaticity. Therefore, the expressions for the gauge field connections in Eqs. (3.40) and (3.41) as well as the derived holonomy in Eq. (3.42) allow us, in principle, to implement and study non-Abelian gauge fields. This leads to the side note that one effectively uses the *gauge bosons* of an Abelian gauge field theory, i.e. the photon, to simulate more complex non-Abelian gauge fields. Truly noncommutative gauge fields, and thus holonomies in all of U(2), can already be achieved by including propagation constants on the main diagonal of the Hamiltonian (3.34). A detailed investigation of this is done in the Appendix B.

Despite the fact that the holonomy (3.42) is an element of the Abelian group SO(2)<U(2) it is not decomposable into separate Abelian subsystems. In order to verify this claim, one can evaluate the Wilson loop [38] as defined in Eq. (3.31), which yields

$$W_{\mathcal{C}} = 2\cos\gamma \, . \tag{3.44}$$

A Wilson loop that evaluates to ±2 means that no evolution took place ($\gamma = 0$) and thus the holonomy is simply the unit matrix. This case would indicate a trivial system that could be written as isolated Abelian subsystems [47].

### 3.5.1. Details on couplings and optimised design

The second main ingredient for the implementation of non–Abelian gauge fields is the adiabaticity of the evolution. As outlined in the theoretical preliminary in Section 3.4 this can be achieved by optimising the parameter variation using the quantum metric $\boldsymbol{g}$. Using its definition in Eq. (3.32) together with the dark states as in Eq. (3.35) the quantum metric reads

$$\mathbf{g} = 2\,\mathrm{diag}\left(1, \cos^2(\phi)\right) . \tag{3.45}$$

This metric is two-dimensional despite having originally three couplings $S$, $P$, and $Q$. One degree of freedom is removed due to the normalisation and thus the mixing angles $\theta$ and $\phi$ are the relevant parameters. Plugging this result for $g_{\mu\nu}$ into the definition of the path length $L$, see Eq. (3.33), one only needs the functional form of the parameters or coordinates $\{x^\mu\} = \{\theta, \phi\}$ in dependence of the $z$-dependent couplings $S$, $P$, and $Q$.

In order to sensibly minimise $L$ we fixed the general functional form of the couplings with a small set of parameters. We choose Gaussian pulses for $S$ and $P$ and held $Q = \Omega_Q$ constant. The Gaussian pulse sequences are parametrised by

$$S(z) = \Omega \exp\left(-\frac{(z - \bar{z} + \tau)^2}{T^2}\right) , \tag{3.46}$$

$$P(z) = \Omega \exp\left(-\frac{(z - \bar{z} - \tau)^2}{T^2}\right) , \tag{3.47}$$

where $\bar{z}$ is half the total propagation length $(z_\mathrm{f} - z_\mathrm{i})$, set in our experiments to 15 cm, $\Omega$ is the amplitude, $T$ the width parameter, and $\tau$ the separation of the two Gaussian pulses from the center at $\bar{z}$.

Experimental constraints limit the range of values for the parameters $\bar{z}$, $\Omega$, $T$, and $\tau$ and thus the range of obtainable holonomies $\boldsymbol{U}$ that can be realised. For example, it has to be ensured that the coupled-mode approximation is valid and thus the total amplitude of the couplings where limited to values below $2\,\mathrm{cm}^{-1}$. This is a major limitation as adiabaticity can theoretically be achieved by choosing very strong couplings as these lead to large gaps between the dark subspace and the bright states with eigenvalues $\pm\sqrt{S^2 + P^2 + Q^2}$. This larger gap would then translate to a lower transition probability.

Another sensible design choice is the demand that the initial and final dark states are simple. When setting $P(z_\mathrm{i})/S(z_\mathrm{i}) \approx 0$ and $S(z_\mathrm{f})/P(z_\mathrm{f}) \approx 0$ at the beginning and end of the propagation one finds that the dark states become

$$\begin{aligned} |\mathcal{D}_1(z_\mathrm{i})\rangle &= -|w_R\rangle \, , \qquad & |\mathcal{D}_1(z_\mathrm{i})\rangle &= |w_L\rangle \, , \\ |\mathcal{D}_2(z_\mathrm{i})\rangle &= |w_L\rangle \, , \qquad & |\mathcal{D}_2(z_\mathrm{f})\rangle &= |w_R\rangle \, , \end{aligned} \tag{3.48}$$

which considerably simplifies the initiation and measurement in the experiment. However, this additional demand places further constraints on the couplings as they have to be effectively zero at the initial and final points which we deemed fulfilled in our numerical calculations when the strengths of the Gaussian pulses were less than 5 % of the peak amplitude $\Omega$.

Based on the quantum metric and its resulting path length $L$, see Eq. (3.33), we searched for those parameter sets $\Omega_Q$, $\Omega$, $T$, and $\tau$ that comply with the above conditions and which minimised $L$. For that, we performed numerical calculations of $L$ with the coupling variations as defined via the parameters $\Omega_Q$, $\Omega$, $T$, and $\tau$. Each set also resulted in a different theoretical value for the Wilson loop when using Eqs. (3.43) and (3.44). Binning the results for $L$ according to their value of $W_\mathcal{C}$ we could choose those that minimise $L$ for a given loop. A collection of three experimentally tested parameters can be found in Tab. 3.1.

A suitable check whether the path length optimisation leads to an adiabatic evolution is to simulate (or later measure) the intensity in the central waveguide C. As seen from the definition of the dark states in Eqs. (3.35) and (3.35), the central waveguide is never excited in the dark subspace. Therefore, any excitation in waveguide C resulted from transitions to the bright states, Eq. (3.39), and thus a nonadiabatic evolution. Consequently, the deviation from the adiabatic evolution is measured by the population of the central waveguide, which we define as

$$\delta = \int\limits_{z_\mathrm{i}}^{z_\mathrm{f}} \left( |a_\mathrm{C}^{(1)}|^2 + |a_\mathrm{C}^{(2)}|^2 \right) \, \mathrm{d}z \,, \tag{3.49}$$

where $|a_\mathrm{C}^{(i)}|^2$ denotes the intensity in the central waveguide C for the initial excitation of the first ($i = 1$) or second ($i = 2$) dark state, respectively. In order to test the adiabaticity before the experimental realisation, extensive simulations of the amplitude dynamics were run based on Eq. (3.34). This was done alongside the path length optimisation itself.

In Fig. 3.4 the results for the deviation $\delta$ and the path length $L$ are shown as density plots for different sets of varied parameter pairs. The constant parameters are then set to $T, \tau = 1\,\mathrm{cm}$ or $\Omega, \Omega_Q = 1\,\mathrm{cm}^{-1}$ with the exception of the plots with $\tau$ and $\Omega_Q$ varied (center two lower plots) where $T = 2\,\mathrm{cm}$. For the case where the shift parameter $\tau$ and width $T$ are varied, see right lower two plots in Fig. 3.4, some configurations did not comply with the constraints that the couplings are effectively zero at beginning and end and are thus left blank.

The comparison of matching plots for $\delta$ and $L$ shows that both methods follow in general a similar trend, especially with respect to the position of the minimal deviation and minimal path length. The differences in both schemes may originate from interferences of the two bright states, which can lead to intensity fluctuations in the central waveguide C and thus an interference pattern in $\delta$. Such patterns are most prominent in the lower and upper right panels of Fig. 3.4.

Additionally, the deviation measure $\delta$ is defined with the two different initial conditions, first or second dark state, whereas the path length is purely a geometric measure only depending on the shape of the couplings. Different initial conditions have an additional impact on the adiabaticity of the state evolution, as is known from the original STIRAP process where one differentiates between intuitive and counter-intuitive pulse sequences, see for example Ref. [119]. Being more precise, the counter-intuitive pulse sequence results generally in a more adiabatic evolution compared to the intuitive sequence. The reason

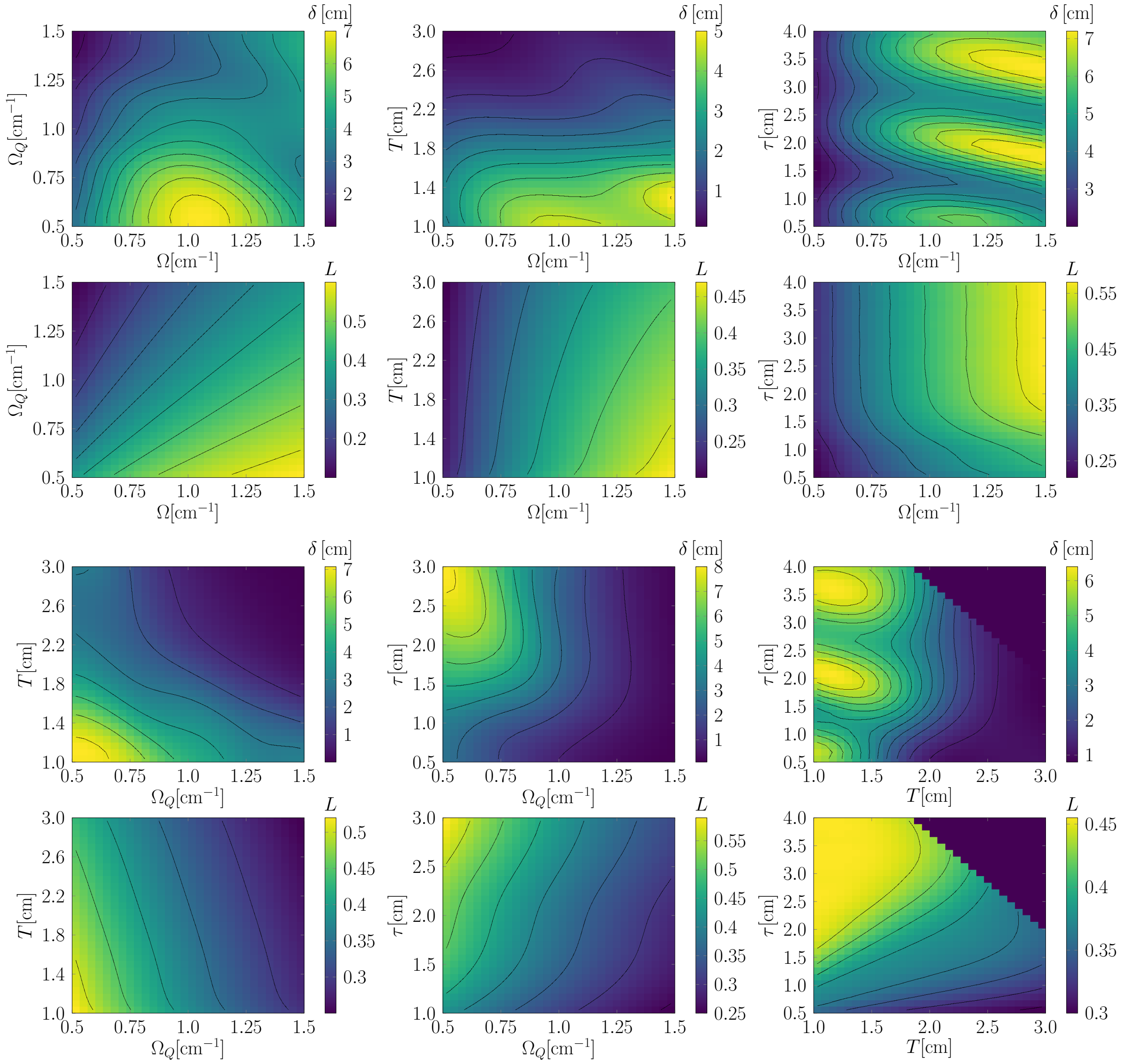

Fig. 3.4.: Plots for comparison between central waveguide population $\delta$ and path length $L$. In 2-by-1 blocks the results for $\delta$ and $L$ are depicted for two varied parameters. The other parameters are then held constant. Adapted from Ref. [116].

Table 3.1.: Coupling pulse parameters for the experimental realisation of different pulse shapes and the resulting Wilson loop values together with theoretical predictions.

| $\Omega_Q$ (cm$^{-1}$) | $\Omega$ (cm$^{-1}$) | $T$ (cm) | $\tau$ (cm) | $\lvert W_{\mathcal{C}}^{\text{theo}}\rvert$ | $\lvert W_{\mathcal{C}}^{\text{exp}}\rvert$ |
|---|---|---|---|---:|---:|
| 1.42 | 1.23 | 3 | 1.5 | 0.88 | 0.87 |
| 1.53 | 1.46 | 3 | 1.5 | 0.97 | 1.00 |
| 1.60 | 1.8 | 3 | 1.5 | 1.07 | 1.13 |

for this is that in the counter-intuitive sequence the waveguide with the initial excitation is coupled to the central waveguide after the other waveguide. Therefore, the energy separation $\sqrt{S^2 + P^2 + Q^2}$ of the bright states from the dark states is already increased. Consequently, the adiabaticity condition is easier fulfilled as transitions over large gaps are less likely. However, this cannot be seen in the quantum metric as it is symmetric with respect to $S$ and $P$. As a result the path length $L$ for the optimisation is symmetric under exchange of $S$ and $P$. This change of sequence is equivalent to a change of initial condition. Launching the light into the left waveguide with coupling $S$ and in intuitive and counter-intuitive coupling sequence is therefore equal to fixing the sequence and launching the light once in the left and once in the right waveguide. The missing sensitivity of the quantum metric bases optimisation can thus be explained with the fact that the initial condition does not influence it. This reliance on the abstract geometry of the coupling variations is, however, an advantage because any implementation of a gauge field or holonomic quantum gate $\boldsymbol{U}$ should not be tailored to a specific input in contrast to the specialised STIRAP process.

As a result, the optimisation of the path length $L$ is yielding the expected results of a minimised nonadiabatic error and does so independently of the initial state. Moreover, the path length $L$ is, as a function of the system parameters, much smoother than the deviation $\delta$, which is beneficial for the calculation of the optimal parameters. In addition, one only has to solve a one-dimensional integral (Eq. (3.33)) to calculate $L$, while for the extraction of the deviation $\delta$ one needs to simulate the entire propagation dynamics for every set of parameters. This might especially be challenging for larger system sizes or networks. The reduced computational effort thus clearly favours the optimisation with the quantum metric. Improvements of this techniques might be found by more elaborate optimisation algorithms applied to the measure $L$. Additionally, one can soften some of these constraints, e.g. use other functional forms for the couplings or make the measurement and initiation more complex.

### 3.5.2. Experimental results

With the suitable parameters for the couplings found, the waveguides can be fabricated. The chosen parameter values are listed in the first four columns of Tab. 3.1. A visualisation of such a waveguide design can be seen in Fig. 3.5a. The corresponding $z$-dependent couplings and the resulting closed curve in parameter space are seen in Figs. 3.5b and 3.5c.

State initiation now amounts to coupling laser light into either the waveguide R or L for the dark state $|\mathcal{D}_1\rangle$ or $|\mathcal{D}_2\rangle$, cf. Eq. (3.48). In order to measure the evolution dynamics along the $z$-direction a fluorescence microscopy technique is used that collects light scattered from colour centers in the waveguides [18]. One example where the waveguide L (second dark state) is excited can be seen in Fig. 3.6a with the corresponding theoretical prediction from the coupled mode equations (3.34) in Fig. 3.6b. Clearly, the evolution is adiabatic because the central waveguide (between white dashed lines in Fig. 3.6a) is only marginally excited. The intensity originally concentrated in waveguide L is thus solely distributed between the three outer waveguides. The odd looking spread at the end of the propagation length is attributed to the out-of-focus position of the waveguides L and R due to them being led away from the waveguide C and thus from the central focus plane spanned by C and U. In conclusion, the experiment generally aligns well with the simulation and confirms the optimisation using the quantum metric.

However, in order to test whether the geometric description based on the holonomy is truly correct, one has to specifically measure the output intensities leaving the glass chip. Such a measurement of the end facet can be seen in Fig. 3.7a, again for the case where the second dark state is initially excited. The results from this intensity measurement are marked as red dots at the end ($z = 15\,\mathrm{cm}$) in Fig. 3.6a and they align with the prediction from the simulation. Because the experimental results (red dots) align very well with the simulation result, we can conclude that the geometric description is fitting. As a final sanity test it was checked whether all waveguides do, in fact, couple with each other because otherwise the assumed adiabaticity could just be attributed to the fact that the central waveguide is not excited because it is decoupled from the outer waveguides. For this, light was launched into the central waveguide and in Fig. 3.7b the resulting end facet can be seen. Clearly, the whole system does couple as all waveguides are visibly excited.

With this reassurance the original experiment for the dark subspace evolution can be repeated but this time initiating the first dark state instead. This allows to retrieve all the absolute values of the components of the holonomy $\boldsymbol{U}$. The restriction to the absolute values stems from the fact that only intensities are measured and thus any phase information lost. Nonetheless, as we only consider real couplings in a classical optics experiment it is sufficient to measure the intensities allowing to calculated the absolute value of the Wilson loop $|W_{\mathcal{C}}|$. The results for the chosen parameters can be found in the last column of Tab. 3.1 with the theoretical predictions in the second-to-last column.

Note that the criterion $|W_{\mathcal{C}}| = 2$ for a trivial system of two uncoupled Abelian subsystems is changed in our specific implementations to $|W_{\mathcal{C}}| = 0$ because of the switch of the dark state basis, see Eqs. (3.48). This switch of basis means that the case of no evolution, e.g. $|w_{\mathrm{L}}\rangle \to |w_{\mathrm{L}}\rangle$ corresponds in the dark state basis to $|\mathcal{D}_2(z_{\mathrm{i}})\rangle \to |\mathcal{D}_1(z_{\mathrm{f}})\rangle$ and therefore the anti-diagonal unit matrix instead of the unit matrix. Besides the change in the criterion in $|W_{\mathcal{C}}|$, this basis change has no repercussion.

The results in Tab. 3.1 clearly show that the system is of nontrivial nature ($|W_{\mathcal{C}}| \neq 0$) and thus cannot be decomposed in separate Abelian subsystems. Therefore, the presented waveguide design and its adiabatic optimisation did implement the non-Abelian geometric phase and its resulting holonomy as intended.

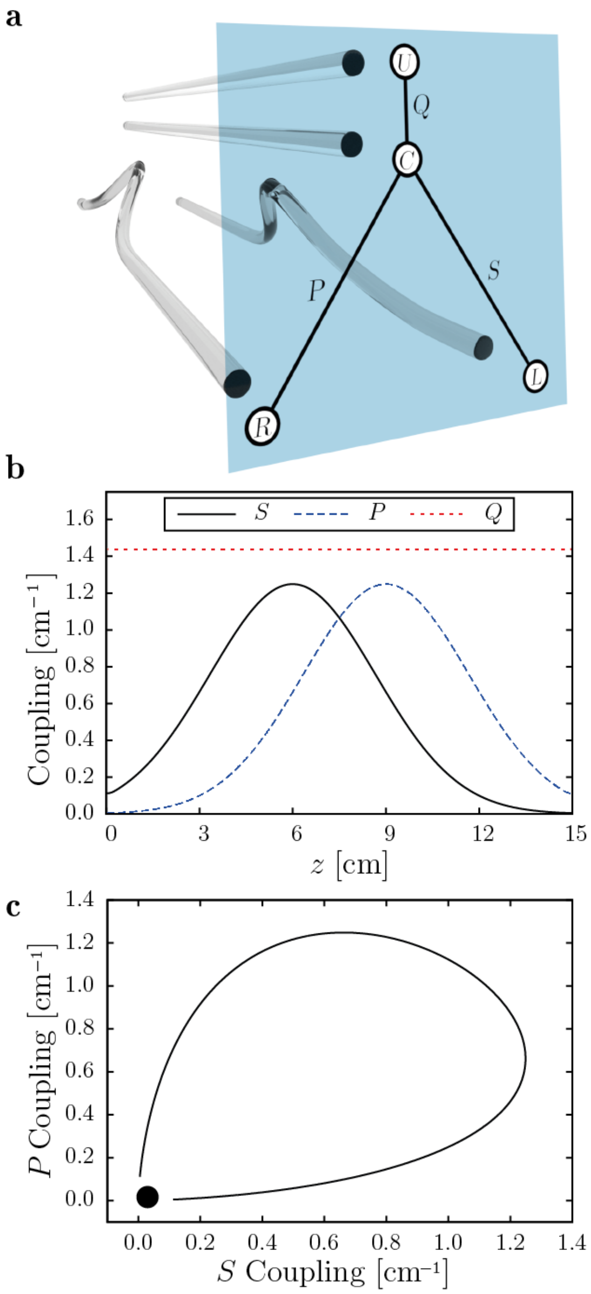

Fig. 3.5.: (a) 3D-rendering of the waveguides for one realisation. (b) Coupling variation along propagating distance $z$. (c) Curve in the parameter manifold $\{S, P, Q\}$ ($Q = \text{const}$). Taken from Ref. [116].

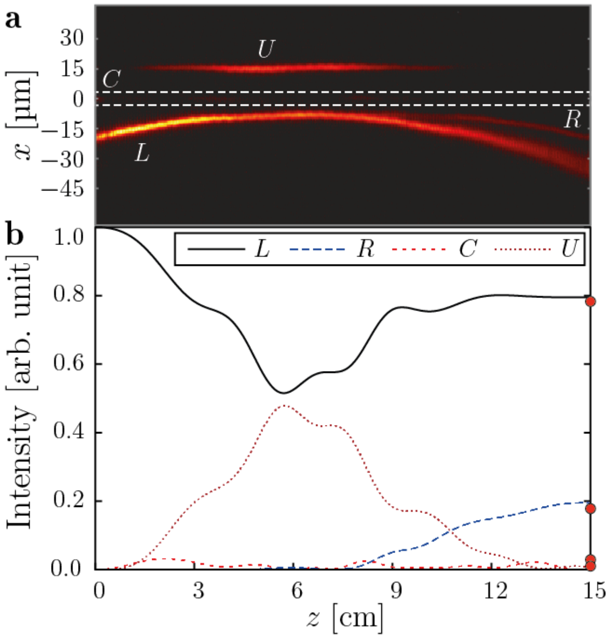

Fig. 3.6.: Intensity distribution in the four waveguides along the propagation distance. (a) Experimentally measured fluorescence signal which is proportional to the intensity in the waveguides. The waveguide L was excited, thus the second dark state. The central waveguide C is located between the dashed lines, highlighting the almost vanishing intensity. (b) Theoretically predicted intensity from the coupled-mode theory using Eq. (3.34). Red dots at the end facet are the experimentally measured intensities. Taken from Ref. [116].

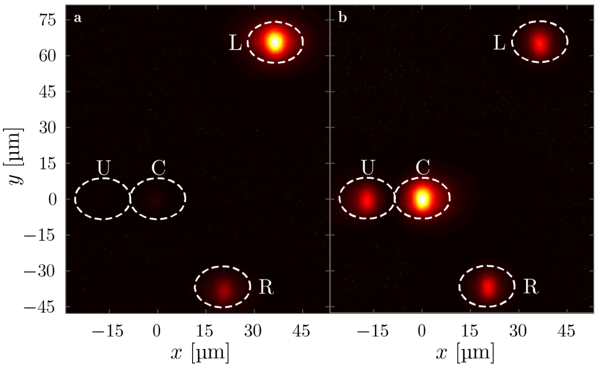

Fig. 3.7.: Measured intensities at the end facet. (a) Intensity distribution for dark-state excitation. This is for the same set of parameters as seen in Fig. 3. The result is clearly restricted to the dark subspace. (b) Intensity distribution for bright-state distribution. The waveguide C and U, and with that the bright states, are dominantly excited. Taken from Ref. [116].

The outlined scheme to implement a non-Abelian geometric phase has some limitations. Most notably the possible dimension $N_{\mathcal{D}}$ of the degenerate subspace, which for the $N$-pod was $N-1$, is limited in our waveguide setup due to the fact that only couplings to the central waveguide are allowed, cf. Fig. 3.3b. Couplings between the outer waveguides break the required symmetry of the system and lift the degeneracy of the dark subspace. Because the evanescent coupling is distance-dependent, more waveguides physically mean less distance between them when they are arranged around the central waveguide.

Additionally, one needs a *sufficiently* large set of variable parameters to ensure that the implemented holonomies cover the whole of their respective unitary groups $\mathrm{U}(N_{\mathcal{D}})$. This was discussed in Ref. [45] with the result that the number of required parameters has to scale rapidly for larger quantum codes. For specific holonomies the limited set of parameters provided by couplings and propagation constants might be sufficient. However, to fully utilise the whole range of possible holonomies and gates one has to provide more parameters.

In the closing sections of this chapter we will show a possible solution to each of these problems. The first can be remedied by *going quantum*, i.e. using Fock states of more than one photon, which we investigated in detail in Ref. [91]. The second problem is approached by introducing non-Hermiticity to the theory of holonomies which we did in Ref. [92]. This provides additional parameters like losses, which are the focus of the rest of this thesis.

## 3.6. Increasing dimensionality using multiple photons

In this section we show how the use of multiple-photon Fock states leads to an increase of the dimensionality of the subspaces of an $N$-pod. In turn this leads to higher dimensional gauge fields and holonomies for more advanced applications.

Up to this point only classical light was considered and equation (3.34) governed the evolution of classical waveguide amplitudes $a_i$. As discussed in the preceding chapter this equation can be quantised allowing to calculate the dynamics of bosonic mode operators $\hat{a}_i$. The Hamiltonian corresponding to the $N$-pod, see Fig. 3.3b, then reads

$$\hat{H} = \sum_{i=1}^{N} \kappa_i \left( \hat{a}_i^\dagger \hat{a}_\mathrm{C} + \hat{a}_\mathrm{C} \hat{a}_i^\dagger \right) . \tag{3.50}$$

In the following, we restrict the dynamic under this Hamiltonian to a subspace $\mathcal{H}_{N_\mathrm{p}}$ spanned by the $N_\mathrm{p}$-photon Fock states over the $M = N+1$ waveguide modes

$$\mathcal{F}_{N_\mathrm{p}} = \left\{ |n_1, \dots, n_{N+1}\rangle \,\middle|\, \sum_{j=1}^{N+1} n_j = N_\mathrm{p} \right\} . \tag{3.51}$$

When represented in this basis, the Hamiltonian $\hat{H}$ defines an operator on the reduced Hilbert space $\mathcal{H}_{N_\mathrm{p}}$ with dimensions $k = (N_\mathrm{p}+N)!/(N_\mathrm{p}!N!)$. Here, $k$ is the number of possibilities to distribute $N_\mathrm{p}$ identical photons on $N+1$ labelled waveguides.

With the $k$ Fock states of $\mathcal{F}_{N_\mathrm{p}}$, a $k{\times}k$-dimensional matrix representation $\boldsymbol{H} = (H_{ij})_{i,j=1}^{k}$ can be calculated. When $\boldsymbol{H}$ is diagonalised one finds for all $k$ a decomposition of the Hilbert space $\mathcal{H}$ into orthogonal eigenspaces

$$\mathcal{H} = \mathcal{H}_{\mathcal{D}} \oplus \mathcal{H}_{\mathcal{B}_+}^{(1)} \oplus \mathcal{H}_{\mathcal{B}_-}^{(1)} \oplus \cdots \oplus \mathcal{H}_{\mathcal{B}_+}^{(N_\mathrm{p})} \oplus \mathcal{H}_{\mathcal{B}_-}^{(N_\mathrm{p})}\,, \tag{3.52}$$

where $\mathcal{H}_{\mathcal{D}}$ is a dark subspace, and $\mathcal{H}_{\mathcal{B}_\pm}^{(n)}$ is the eigenspace corresponding to the energy $\pm n\,\varepsilon = \pm n\,\sqrt{|\kappa_1|^2 + \cdots + |\kappa_N|^2}$ $(n = 1, \ldots, N_\mathrm{p})$. The reason for this systematic decomposition is that the coupling structure is still the same compared to the classical case, meaning the fundamental symmetry of the waveguide system and thus the underlying subspace structure remains.

In order to prove this, one can directly diagonalise the Hamiltonian in its operator form (3.50) instead of using possibly numerical calculations to diagonalise the $k{\times}k$ matrix representation $\boldsymbol{H}$. This leads to new bosonic mode operators $\hat{b}_-, \hat{d}_1, \ldots, \hat{d}_{N-1}, \hat{b}_+$ that are linear superpositions of the original waveguide mode operators $\hat{a}_j$. The new mode operators represent exactly the same modes as in the classical case, i.e. $N-1$ dark modes and two bright modes with energies $\pm\varepsilon$, respectively. In this diagonal basis, the Hamiltonian becomes

$$\hat{H} = -\varepsilon\,\hat{b}_-^\dagger\hat{b}_- + \varepsilon\,\hat{b}_+^\dagger\hat{b}_+\,, \tag{3.53}$$

which allows a simple use of new Fock states $|n_-, n_{\mathcal{D}}, n_+\rangle$ that count the number of excitations $n_\pm$ in the two bright modes and the number of excitations $n_{\mathcal{D}}$ in the $N-1$ dark modes. The eigenvalue equation of these Fock states is

$$\hat{H}|n_-, n_{\mathcal{D}}, n_+\rangle = \varepsilon\,(n_+ - n_-)\,|n_-, n_{\mathcal{D}}, n_+\rangle\,, \tag{3.54}$$

with $n_- + n_{\mathcal{D}} + n_+ = N_\mathrm{p}$. For $N_\mathrm{p}$ this creates $2N_\mathrm{p}+1$ different subspaces to the eigenvalues $-N_\mathrm{p}\,\varepsilon, -(N_\mathrm{p}-1)\,\varepsilon, \ldots, N_\mathrm{p}\,\varepsilon$ which are the subspaces in Eq. (3.52), thus proving our initial assessment.

Going further, we can use the new Fock basis to calculate the dimensions of these orthogonal subspaces. Starting with $\mathcal{H}_{\mathcal{D}}$, we have to determine the number of dark states when $N_\mathrm{p}$ photons are used in a setup with $(M = N+1)$ waveguides which then amounts to counting the number of possibilities to distribute the photons over the modes so that the eigenvalue $\varepsilon(n_+ - n_-)$ becomes zero. In the simplest case, this holds true if $n_+, n_- = 0$, i.e. when all $N_\mathrm{p}$ photons are distributed over the $N-1$ dark modes which has $\binom{N_\mathrm{p}+N-2}{N_\mathrm{p}}$ possibilities. Generally, however, this requires an equal number of photons in the positive and negative bright modes with the rest in the dark modes. For example, one can have one photon in each positive and negative bright mode, thus $\binom{N_\mathrm{p}-2+N-2}{N_\mathrm{p}-2}$ ways remain to distribute the rest of the photons over the dark modes. This continues until all photons are equally distributed over the positive and negative bright modes. However, there are two distinct cases, $N_\mathrm{p}$ odd or even, for which one finds two formulas for the total number of dark states, i.e.

$$d(N_\mathrm{p}, N) = \begin{cases} \sum_{n=1}^{N_\mathrm{p}/2} \binom{2n+N-2}{2n} & \text{if } N_\mathrm{p} \text{ even,} \\ \sum_{n=0}^{(N_\mathrm{p}-1)/2} \binom{2n+1+N-2}{2n+1} & \text{if } N_\mathrm{p} \text{ odd.} \end{cases} \tag{3.55}$$

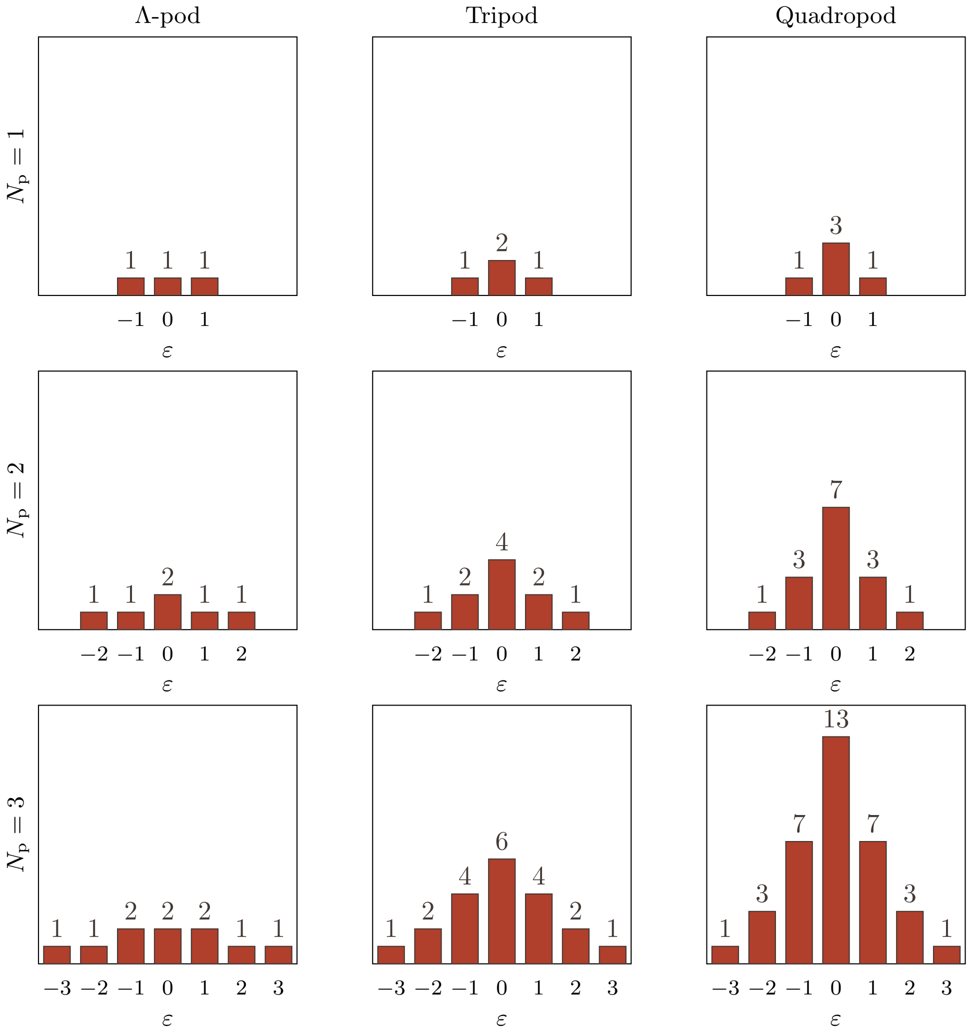

Fig. 3.8.: Spectrum of an $N$-pod system filled with $N_\mathrm{p}$ photons. The number of eigenstates $d(N_\mathrm{p}, N)$ is depicted over the eigenvalues (in multiples of $\varepsilon$) for $N, N_\mathrm{p} \in \{1, 2, 3\}$. In the simple case of one photon $N_\mathrm{p} = 1$ an increase of the number $N$ of coupled waveguides only increases the dark subspace dimension and does so linearly. In contrast, for more photons the dimension of the dark subspace increases nonlineary and additional degenerate bright subspaces emerge. Adapted from Ref. [91].

When counting the number of bright states with energy $\pm k\varepsilon$, one first has to put $k$ photons in either the negative or positive bright mode, and then distribute the rest as if to create a dark state. Thus, for bright states with energy $\pm k\varepsilon$ there are $d(N_\mathrm{p} - k, M)$ possibilities which is then the dimension of the subspace $\mathcal{H}_{\mathcal{B}_+}^{(k)}$. For some values of $N_\mathrm{p}$ and $N$ the degeneracies are graphically shown in Fig. 3.8.

The dramatic increase in dimensionality by using multiple photons instead of classical light opens the way to implement non-Abelian gauge fields and holonomies of higher dimensions while avoiding any detrimental effects from undesired couplings between the outer waveguides. This shows a clear advantage compared to other photonic implementations like such based on polarisation which are limited to only $2 \times 2$-dimensional gauge fields. Note also that this route of increasing the dimensionality via multi-photon states would not be possible in atomic setups as those are inherently first-quantised states with only a single occupancy.

In addition to the increased degeneracy of the dark subspace we emphasise that also the bright subspaces gain considerable degeneracies. Therefore, one could also implement holonomies in the now degenerate bright subspaces. The only difference to the original scheme in the dark subspace is the dynamic phase $\exp(\pm\mathrm{i}\,k\,\varepsilon\,z)$ that is additionally accumulated. However, because this phase is only a relative phase to the other subspaces, this poses no hindrance. In fact, a complete HQC computation can be performed in the bright subspaces as was discussed in great detail in our publication [91] which was jointly published with Julien Pinske of our group.

## 3.7. Holonomic quantum computing in non-Hermitian systems

The last point we make in this chapter is to discuss how certain non-Hermitian systems can increase the number of independent parameters allowing for more curves through parameter space and thus more and different non-Abelian geometric phases or holonomies. This is crucial to ensure that enough independent holonomic gates can be created in order to obtain complete unitary groups.

Usually, quantum mechanics is formulated based on Hermitian operator, e.g. an Hermitian Hamiltonian is used as the generator of the Schrödinger equation. Hermitian operators always have a real spectrum and thus observables, linking the theory to measurable quantities. However, it has been pointed out that certain non-Hermitian operators also have a real spectrum and are thus candidates to generalise conventional quantum mechanics [73; 61; 123; 62]. Systems with real spectra governed by such non-Hermitian Hamiltonians are said to be pseudo-Hermitian.

Consider a $z$-dependent $N$-dimensional non-Hermitian Hamiltonian $\hat{H}(z) \neq \hat{H}^\dagger(z)$. Due to its non-Hermiticity its right- and left eigenvectors $|\Phi_n\rangle$ and $\langle\tilde{\Phi}_n|$ differ, i.e. $|\Phi_n\rangle^\dagger =$

$\langle\Phi_n| \neq \langle\tilde{\Phi}_n|$. Thus, generally, one has two eigenvalue equations

$$\begin{aligned} \hat{H}(z)\,|\Phi_n(z)\rangle &= E_n\,|\Phi_n(z)\rangle\,, \\ \hat{H}^\dagger(z)\,|\tilde{\Phi}_n(z)\rangle &= E_n\,|\tilde{\Phi}_n(z)\rangle\,. \end{aligned} \tag{3.56}$$

The left and right eigenvectors form a biorthogonal basis $\{|\Phi_n\rangle, |\tilde{\Phi}_n\rangle\}$ with $\langle\tilde{\Phi}_n|\Phi_m\rangle = \delta_{nm}$ [124]. The special case of a pseudo-Hermitian system is found when demanding that there exists a positive-definite and Hermitian operator $\hat{\eta}(z)$ for which

$$\hat{H}^\dagger(z) = \hat{\eta}(z)\,\hat{H}(z)\,\hat{\eta}^{-1}(z)\,. \tag{3.57}$$

It is then said that $\hat{H}$ is Hermitian with respect to $\hat{\eta}$ or $\hat{\eta}$-Hermitian. The operator $\hat{\eta}$ is itself a Hilbert-space metric [125; 63] because it induces a new inner product

$$\langle\Phi,\Psi\rangle_{\hat{\eta}} = \langle\Phi|\,\hat{\eta}\,|\Psi\rangle\,, \tag{3.58}$$

for all vectors $\Phi,\Psi$ in the new Hilbert space $\mathscr{H}_{\hat{\eta}(z)}$. Regarding this inner product, the biorthogonal basis $\{|\Phi_n\rangle, |\tilde{\Phi}_n\rangle\}$ can again be written as an orthogonal basis with $|\tilde{\Phi}_n\rangle = \hat{\eta}\,|\Phi_n\rangle$. Following this relation of the left and right eigenvectors, the metric $\hat{\eta}$ can be defined as [126; 62]

$$\hat{\eta} = \sum_n |\tilde{\Phi}_n\rangle\langle\tilde{\Phi}_n|\,. \tag{3.59}$$

Based on this concept of $\hat{\eta}$-Hermiticity many familiar aspects of conventional quantum mechanics can be transferred to pseudo- or $\hat{\eta}$-Hermitian systems. The basic idea is here to replace any inner products of conventional quantum mechanics with the $\hat{\eta}$-inner product from Eq. (3.58) in consistent manner. For example, the evolution operator $\hat{U}$ of such a pseudo-Hermitian system is no longer unitary. However, one can formulate a generalised unitarity condition [126] by consistently inserting the $\hat{\eta}$-inner product. This entails that instead of demanding

$$\partial_z\langle\phi(z)|\psi(z)\rangle = 0\,, \tag{3.60}$$

for states $|\psi(z)\rangle$ and $|\phi(z)\rangle$ of an Hermitian system which is fulfilled when $\hat{U}^\dagger\hat{U} = \hat{1}$, one demands for states $|\Psi(z)\rangle$ and $|\Phi(z)\rangle$ of an $\hat{\eta}$-Hermitian system

$$\partial_z\langle\Phi(z),\Psi(z)\rangle_{\hat{\eta}} = \partial_z\langle\Phi|\,\hat{\eta}\,|\Psi\rangle = 0\,. \tag{3.61}$$

Consistency then demands that the evolution is governed by a modified Schrödinger equation [126; 124]

$$\mathrm{i}\,\partial_z|\Psi(z)\rangle = \hat{\Lambda}(z)\,|\Psi(z)\rangle\,, \tag{3.62}$$

where $\Lambda(z)$ is the generator of $z$-displacement and is given by

$$\hat{\Lambda}(z) = \hat{H}(z) + \mathrm{i}\hat{K}(z)\,, \tag{3.63}$$

with $\hat{K}(z) = -\hat{\eta}^{-1}(z)\,\partial_z\hat{\eta}(z)/2$. Introducing the covariant derivative $\mathrm{D}_z = \partial_z - \hat{K}(z)$ the modified Schrödinger equation takes on the more familiar form

$$\mathrm{i}\,\mathrm{D}_z|\Psi(z)\rangle = \hat{H}(z)\,|\Psi(z)\rangle\,. \tag{3.64}$$

Based on Eq. (3.64) one can again investigate closed parameter variations that then lead to modified geometric phases and holonomies [92]. However, the geometric phases are then non-(anti)-Hermitian and subsequently the holonomies only pseudo-unitary. Nevertheless, the very same calculations can be performed as in the unitary case as long as one makes consistent use of the $\hat{\eta}$-inner product. Besides opening the way to a plethora of new exciting effects due to its non-Hermiticity that generalise conventional quantum mechanics, pragmatically this introduces a host of new parameters to manipulate allowing for more complex curves and thus holonomies. For example, one could introduce losses to the system which one could naively describe via an effective non-Hermitian Hamiltonian $\hat{H}_{\text{eff}}$. A waveguide system with loss rates $\gamma_i$ in its $M$ waveguides would then simulate the effective Hamiltonian

$$\hat{H}_{\text{eff}} = \sum_{i=1}^{M} (\sigma_i - \mathrm{i}\gamma_i)\, \hat{a}_i^\dagger \hat{a}_i + \sum_{\substack{i,j=1 \\ i\neq j}}^{M} \kappa_{ij}\, \hat{a}_i^\dagger \hat{a}_j + \text{H. c.} \tag{3.65}$$

clearly increasing the number of available parameters from the original propagation constants $\sigma_i$ and couplings $\kappa_{ij}$. A thorough investigation of non-Hermitian HQC in lossy waveguides can be found in Ref. [92].

## Summary

This chapter focussed on the implementation of artificial gauge fields and holonomies in photonic waveguides. It explained the fundamental link between differential geometry and gauge field theories: A gauge field is a connection that contains the information of how a Hilbert space basis changes along parameter variations. This information is vital for the definition of parallel transport, cf. Eq. (3.3). These concepts reemerge in the adiabatic evolution under a degenerate Hamiltonian. An adiabatic transport, cf. Eq. (3.23), in the degenerate subspace is then just a parallel transport under a gauge field connection. Especially interesting cases of adiabatic transports occur for closed parameter variations, for which the total evolution is a holonomy – the basic building block of HQC.

The necessary adiabaticity is achieved by an optimisation with the quantum metric, i.e. path length minimisation under experimental constraints. This optimisation was used for the design of a tripod waveguide system that was realised in a proof-of-principle experiment, see Section 3.5. The result was the successful implementation of an artificial $2\times 2$ gauge field and holonomy.

In addition, we showed how the dimension of such gauge fields and holonomies can be increased with the use of multiple-photon Fock states, cf. Eq. (3.55). Finally, we discussed how a non-Hermitian extension of the theory provides a larger set of parameters, e.g. by adding loss rates. This allows more distinct curves in parameter space, which is crucial for completeness of the holonomies. In the next chapter, we answer the question how such effective non-Hermitian Hamiltonians emerge from a full quantum treatment of lossy photonic waveguides in the first place.

# 4. The quantum master equation of lossy waveguides and its Lie algebraic solutions

In the last chapter we saw from the example of holonomies that non-Hermiticities like losses can be beneficial by providing interesting resources in their own right. This leads to the question how lossy, and thus non-Hermitian, dynamics in waveguides can be described in a full quantum treatment. Although the general theory of open systems is well understood and documented in textbooks [53], solutions for specific problems are often complicated to find once one deviates from prototypical scenarios. Therefore, in this chapter, we demonstrate some approaches that permit to find solutions for the quantum dynamics of lossy waveguides [127].

## 4.1. Open quantum systems

Consider a collection of waveguides inside a glass chip. The coupled waveguide modes constitute the system of interest and everything else is its environment, cf. Fig. 4.1. This separation is the basis of the usual approach in describing open quantum systems [53]. A system of interest with a manageable size, i.e. dimensionality of its Hilbert space, is separated from a large, possibly infinite bath. The total evolution is again assumed to be governed by a Hermitian Hamiltonian

$$\hat{H} = \hat{H}_{\mathrm{S}} + \hat{H}_{\mathrm{I}} + \hat{H}_{\mathrm{B}} \tag{4.1}$$

that is decomposed into the system $\hat{H}_{\mathrm{S}}$, the bath $\hat{H}_{\mathrm{B}}$, and the interaction $\hat{H}_{\mathrm{I}}$ between both of them.

At this stage we transition from a description of the quantum states based on Hilbert space vectors $|\psi\rangle$ to one based on the density operators $\hat{\rho}$. This allows to cover general mixed quantum states of the waveguide subsystem, which will result from the lossy dynamics and their resulting decoherence. The quantum state $\hat{\rho}$ of the total compound of system and bath follows the unitary evolution

$$\hat{\rho}(z) = \hat{U}(z)\,\hat{\rho}(0)\,\hat{U}^{\dagger}(z)\,, \tag{4.2}$$

where the evolution operator $\hat{U}(z)$ obeys

$$\partial_z \hat{U} = \hat{H}\,\hat{U}\,, \tag{4.3}$$

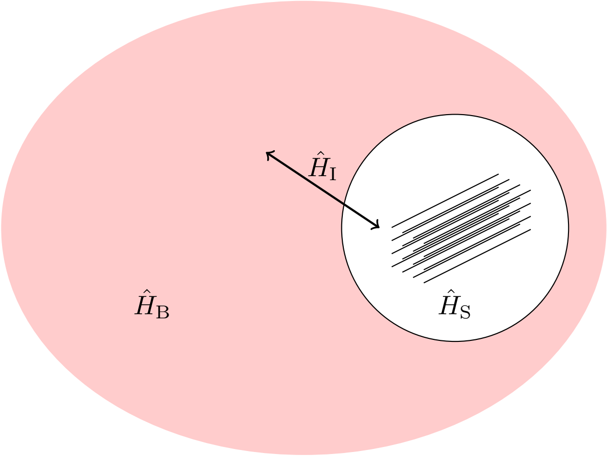

Fig. 4.1.: System-bath model of open quantum systems. The system of coupled photonic waveguides interacts with its surrounding environment. Energy transferred from the system to its bath is lost.

with the initial condition $\hat{U}(0) = \mathbb{1}_\mathcal{H}$, i.e. the Hilbert space unity. Note that we already used $z$ as the dynamical variable anticipating the use for waveguide systems, but this is only for notational consistency.

The full evolution of the system and bath is, however, not explicitly calculable in most cases. In addition, the system is usually defined as containing all interesting aspects and is thus the main focus of interest. Therefore, it is beneficial to define an evolution just for the state of the system $\hat{\rho}_\mathrm{S}$, which is extracted from the total quantum state $\hat{\rho}$ by taking the partial trace over the bath's degrees-of-freedom,

$$\hat{\rho}_\mathrm{S}(z) = \mathrm{Tr}_\mathrm{B}\,\hat{\rho}(z) = \mathcal{U}(z)\,\hat{\rho}_\mathrm{S}(0)\,. \tag{4.4}$$

Here, we introduced the dynamical map $\mathcal{U}$ that maps $\hat{\rho}(0)$ to $\hat{\rho}(z)$. This map plays a central role in the dynamics of open quantum systems and is a generalisation of the familiar evolution operator in Hilbert space. In fact, for an isolated system ($\hat{H}_\mathrm{I} = 0$) the dynamical map becomes

$$\mathcal{U}(z)\,\hat{\rho}_\mathrm{S}(0) = \hat{U}_\mathrm{S}(z)\,\hat{\rho}_\mathrm{S}(0)\,\hat{U}_\mathrm{S}^\dagger(z)\,, \tag{4.5}$$

with $\hat{U}_\mathrm{S}(z)$ being a unitary evolution operator acting solely in the system's Hilbert space. Notice that the dynamical map $\mathcal{U}$ is not an operator of the system's Hilbert space and thus not indicated with a caret. Instead it acts on the operators of the Hilbert space itself which leads to it being called a *superoperator*. The notion of such superoperators will be expanded upon during the discussion of the theory of Liouville spaces later in this chapter.

### 4.1.1. The quantum master equation in Born-Markov approximation

As we can see from Eq. (4.4), the role of the dynamical map is to directly describe the evolution of the system in consistency with the collective evolution of the whole system-bath compound. However, the complicated system-bath interactions together with the nonlinear trace operation implies that generally no closed expressions for the dynamical map can be found. This can be alleviated under certain assumptions that allow (in some cases) to deduce fundamental properties of the dynamical map. The two assumptions that are important in our setting are the Born and Markov approximations. The Born approximation assumes that the effect of the system on the surrounding bath is negligible. This effectively means that the bath approximately remains in its initial state $\hat{\rho}_{\mathrm{B}}(0)$. The total state is then approximated as a direct product of the system state at time $t$ and the initial bath state [53],

$$\hat{\rho}(t) = \hat{\rho}_{\mathrm{S}}(t) \otimes \hat{\rho}_{\mathrm{B}}(0)\,. \tag{4.6}$$

In addition, the Markov approximation means that the future evolution of $\hat{\rho}$ is only determined by its present state and thus not affected by its past. This approximations is often described as discarding any "memory" effects which holds true when the system dynamics' predominant time scale is much larger than any correlation time of the bath. Effectively, this means that the Markov approximation considers the evolution to be coarse-grained [53]. Excitations of the system that are transferred to the bath are immediately dissipated and its coherence lost. Any energy transfer from the bath to the system is then incoherent and only determined by the current state without any dependence on the past evolution.

In conjunction, the Born and Markov approximations together with a rotating-wave approximation lead to the semigroup property for the dynamical map, which can be expressed as [53]

$$\mathcal{U}(z_1 + z_2) = \mathcal{U}(z_2)\mathcal{U}(z_1)\,, \quad z_1, z_2 \geq 0\,. \tag{4.7}$$

The generator of this semigroup is a linear map $\mathcal{L}$ that determines the evolution of the density operator via the von-Neumann equation [128]

$$\partial_z \hat{\rho}_{\mathrm{S}}(z) = \mathcal{L}\, \hat{\rho}_{\mathrm{S}}(z)\,. \tag{4.8}$$

which, by definition of $\mathcal{L}$ as the generator, has the formal solution

$$\mathcal{U}(z) = \mathrm{e}^{\mathcal{L}\, z}\,. \tag{4.9}$$

As a result, the generator $\mathcal{L}$ is, like the dynamical map $\mathcal{U}(z)$, a superoperator acting on Hilbert space operators like $\hat{\rho}_{\mathrm{S}}$.

Additional requirements for the dynamical map are that it is completely positive and trace-preserving. This ensures that the evolved density operator does, in fact, describe a physical state. In conjunction with the Born-Markov approximation a general form of the Liouvillian can be derived as [128; 53]

$$\mathcal{L}(\hat{\rho}) = -\mathrm{i}[\hat{H}_{\mathrm{S}}, \hat{\rho}] + \sum_{k=1}^{N^2-1} \gamma_k \left( \hat{A}_k\, \hat{\rho}\, \hat{A}_k^{\dagger} - \frac{1}{2}\hat{A}_k^{\dagger}\hat{A}_k\, \hat{\rho} - \frac{1}{2}\hat{\rho}\, \hat{A}_k^{\dagger}\hat{A}_k \right) = \partial_z \hat{\rho}\,, \tag{4.10}$$

with so-called Lindblad or jump operators $\hat{A}_k$ and jump rates $\gamma_k$ for a $N$ state system. The terms of the summand in Eq. (4.10) that modify the common von-Neumann equation are often called *dissipators*. The specific forms of the dissipators can in certain cases be rigorously derived from microscopic theories of the system-bath interaction or be given in a phenomenological way when the system under study approximately follow the assumptions of those microscopic theories [53]. In the former case the jump rates $\gamma_k$ can be deduced from first principles and in the latter case those describe model parameters retrieved from experiments.

As a final note, we add that the outlined theory is derived for $z$-independent systems but can easily be extended to cover $z$-dependent Liouvillians $\mathcal{L}(z)$. In this case the dynamical map is formally written as [53; 129]

$$\mathcal{U}(z, z_0) = \mathcal{P}\mathrm{e}^{\int_{z_0}^{z} \mathcal{L}(z')\,\mathrm{d}z'} . \tag{4.11}$$

with the path-ordering $\mathcal{P}$. Because $\mathcal{U}(z, z_0)$ is then a function of two variables it no longer satisfies a semigroup property but instead the softened condition of divisibility [53; 129]

$$\mathcal{U}(z_1 + z_2, 0) = \mathcal{U}(z_1 + z_2, z_1)\mathcal{U}(z_1, 0) , \quad z_1, z_2 \geq 0 . \tag{4.12}$$

Despite this small technical difference, the same Lindblad form of the dissipator can be derived where the Hamiltonian $\hat{H}_{\mathrm{S}}(z)$, rates $\gamma_k(z)$ and jump operators $\hat{A}_k(z)$ are now $z$-dependent. For this to be a good approximate description, the system has to be Markovian at any given value of $z$ which effectively requires all changes in $\hat{H}(z)$, $\gamma_k(z)$, or $\hat{A}_k(z)$ to be slow in comparison with the system-bath interaction and the bath correlation time.

### 4.1.2. Applicability of the Born-Markov approximation to laser-written photonic waveguides

The predictive quality of the above theory hinges on the Born-Markov approximation and thus places demanding requirements on the specific system under study. Therefore, we first have to evaluate if in our case of the lossy integrated photonic waveguides these approximations are indeed valid. Note that we only consider losses as the effect from the coupling to the bath because the photonic waveguides usually operate at or near optical frequencies. The surrounding environment then acts as a thermal bath at zero temperature.

For the laser-written waveguides considered in this thesis there are two proven methods to introduce losses in a controlled manner. First, one can periodically modulate a waveguide in the micrometer range which results in bending losses [130; 131]. Changing the frequency and amplitude of the modulations allows to tune the losses. The second technique is based on creating scattering centres via a deliberate start-stop modulation during the writing process [132]. Dwelling with the laser focus at certain points in the glass, effectively creates barriers in the index profile on which the photons can scatter. Because the writing laser can be precisely positioned and moved, this technique allows a finely tuned loss. For both approaches the scattered photons are irrevocably lost, which allows to treat the setup as an unmodulated waveguide that experiences Markovian loss of a rate $\gamma$.

In addition, the loss rates considered here are very small with only a few photons lost per centimetre on average. These single photons thus do not alter the ambient medium, i.e. the bath, in any perceptible way. Therefore, both techniques also fulfil the assumption of the Born approximation and we can write down the quantum master equation for a system of $M$ lossy photonic waveguides as

$$\partial_z \hat{\rho} = -\mathrm{i}\left[\hat{H}_\mathrm{S}, \hat{\rho}\right] + \sum_{k=1}^{M} \gamma_k \left(2\,\hat{a}_k\,\hat{\rho}\,\hat{a}_k^\dagger - \hat{a}_k^\dagger \hat{a}_k\,\hat{\rho} - \hat{\rho}\,\hat{a}_k^\dagger \hat{a}_k\right). \tag{4.13}$$

Here, the system Hamiltonian $\hat{H}_\mathrm{S}$ is the Hamiltonian of a waveguide system incorporating coupling and propagation constants as introduced in Eq. (2.22). The dissipator models the Markovian losses of rate $\gamma_k$ by removing photons using the bosonic mode operators $\hat{a}_k$.

The master equation (4.13) also holds true for $z$-dependent parameters, i.e. couplings $\kappa_{kl}(z)$, propagation constants $\sigma_k(z)$, and losses $\gamma_k(z)$, as long as they are slowly varying. This requires that the changes are limited to take place over the range of centimetres because the scattering is determined by modulations in the range of micrometres [130; 131; 132]. Additionally, when considering a parametric $z$-dependence, we assume that the modes, and thus the bosonic operators $\hat{a}_k$, remain the same. These requirements amount to the assumption that the system is static with regard to the system-bath interactions, i.e. the system is Markovian at any given value of $z$. Fortunately, these condition are automatically fulfilled for our paraxial propagations.

### 4.1.3. Liouville space formulation

With the quantum master equation (4.13) for a system of lossy waveguides at hand, we now set the stage for solving it by introducing the notion of the Liouville space $\mathfrak{L}$ [133]. This amounts to a vectorisation of the current Hilbert space operators, like the density operator, upon which now act the *superoperators* mentioned earlier, e.g. the Liouvillian $\mathcal{L}$. As a result, the cumbersome looking master equation (4.13) is reformulated into a more familiar, Schrödinger-like equation allowing to use well-known strategies for its solution.

A Liouville space $\mathfrak{L}$ is defined as the tensor product $\mathfrak{L} = \mathcal{H} \otimes \mathcal{H}'$ of two Hilbert spaces. When used to describe open quantum systems, $\mathcal{H}$ is often the Hilbert space of states $|\psi\rangle$ of the closed system one is interested in. The second Hilbert space is then the dual space $\mathcal{H}'$ spanned by the bras $\langle\psi|$. Therefore, the new elements of the Liouville space, i.e. the states or vectors of $\mathfrak{L}$, are the operators of the underlying Hilbert space. Hilbert space operators $\hat{A}$ as elements of $\mathfrak{L}$ are then written as double kets $|\hat{A}\rangle\rangle$. This elevates the description from the quantum states $|\psi\rangle \in \mathcal{H}$ to the density operators $|\hat{\rho}\rangle\rangle \in \mathfrak{L}$.

The Liouville space $\mathfrak{L}$ is itself a Hilbert space when equipped with the inner product

$$\langle\langle \hat{A} | \hat{B} \rangle\rangle = \mathrm{Tr}\left(\hat{A}^\dagger \hat{B}\right). \tag{4.14}$$

With this inner product on $\mathfrak{L}$, properties of the original Hilbert space carry over to $\mathfrak{L}$: In particular notions such as projections and completeness. However, attention has to be paid to some subtle details, especially regarding the dual elements $\langle\langle A|$. For non-Hermitian systems the dual space generally differs from the original space. See for example the effective non-Hermitian Hamiltonian used in Eq. (3.56), which had a biorthogonal basis of generalised left and right eigenvectors [62]. Likewise, we will later see that the Liouvillian $\mathcal{L}$ has a biorthogonal basis. Readers interested in the fundamental theory of spaces used in physics, especially those with a Dirac bra-ket notation, might take a look at Refs. [134; 135; 136] for an introduction into the underlying theory of rigged Hilbert spaces.

In the Liouville space formulation the von-Neumann equation (4.8) is written as

$$\partial_z|\hat{\rho}\rangle\rangle = \mathcal{L}\,|\hat{\rho}\rangle\rangle\,, \tag{4.15}$$

which then bears a strong resemblance to the Schrödinger equation where the state vectors are now given by $|\hat{\rho}\rangle\rangle$ and the right-acting superoperator $\mathcal{L}$ takes on the role of the Hamiltonian. An explicit form of right-acting superoperators in $\mathfrak{L}$ can be defined as left or right applications of Hilbert-space operators. For example, one can derive the two Liouville space superoperators $L[\hat{O}]$ and $R[\hat{O}]$ from the Hilbert space operator $\hat{O}$ as

$$\begin{aligned} L[\hat{O}]|\hat{A}\rangle\rangle &= \hat{O}\hat{A}\,, \\ R[\hat{O}]|\hat{A}\rangle\rangle &= \hat{A}\hat{O}\,. \end{aligned}$$

In case of the bosonic mode operators $\hat{a}_k$ of the individual waveguide modes we define a suitable set of superoperators as

$$L_k^-|\hat{A}\rangle\rangle = \hat{a}_k\hat{A}\,, \qquad L_k^+|\hat{A}\rangle\rangle = \hat{a}_k^\dagger\hat{A}\,, \tag{4.16}$$

$$R_k^-|\hat{A}\rangle\rangle = \hat{A}\hat{a}_k^\dagger\,, \qquad R_k^+|\hat{A}\rangle\rangle = \hat{A}\hat{a}_k\,. \tag{4.17}$$

These Liouville space operators inherit canonical commutator relations from the original Hilbert space operators, e.g. using the known commutator $\left[\hat{a}_i, \hat{a}_j^\dagger\right] = \delta_{ij}$ one finds

$$\left[L_i^-, L_j^+\right]|A\rangle\rangle = \left(\hat{a}_i\hat{a}_j^\dagger - \hat{a}_j^\dagger\hat{a}_i\right)\hat{A} = [\hat{a}_i, \hat{a}_j^\dagger]\hat{A} = \delta_{ij}\hat{A}. \tag{4.18}$$

Thus, the commutators are

$$[L_i^-, L_j^+] = \delta_{ij}\,, \quad [R_i^-, R_j^+] = \delta_{ij}\,, \quad [L_i^\pm, R_j^\pm] = 0\,. \tag{4.19}$$

Based on the superoperators $L_i^\pm$ and $R_i^\pm$, the dissipator from Eq. (4.13) can be defined as a right-action operator in $\mathfrak{L}$, i.e.

$$\sum_{k=1}^{M}\gamma_k\left(2\,\hat{a}_k\hat{\rho}\hat{a}_k^\dagger - \left\{\hat{a}_k^\dagger\hat{a}_k, \hat{\rho}\right\}\right) \quad\Rightarrow\quad \sum_{k=1}^{M}\gamma_k\left(2L_k^-R_k^- - L_k^+L_k^- - R_k^+R_k^-\right). \tag{4.20}$$

The same reformulation can be applied to the Hamiltonian of the coupled waveguide system in Eq. (2.22) which leads to the full Liouvillian

$$\begin{aligned}\mathcal{L} = \sum_{k=1}^{M} \Big[ (\mathrm{i}\sigma_k - \gamma_k)\, R_k^+ R_k^- - (\mathrm{i}\sigma_k + \gamma_k)\, L_k^+ L_k^- + 2\gamma_k L_k^- R_k^- \Big] \\ - \sum_{\substack{k,l=1 \\ k\neq l}}^{M} \mathrm{i}\,\kappa_{kl} \left( L_k^+ L_l^- + L_l^+ L_k^- - R_l^+ R_k^- - R_k^+ R_l^- \right). \qquad (4.21)\end{aligned}$$

As discussed in Sec. 4.1.1, the Liouvillian is the generator of the evolution superoperator $\mathcal{U}$. Transferred into the Liouville space it yields the formal solution $|\hat{\rho}(z)\rangle\rangle = \mathcal{U}(z,0)\,|\hat{\rho}(0)\rangle\rangle$ which now bears even stronger resemblance to the usual Hilbert space notation. Using this formal solution, the differential equation for the evolution superoperator $\mathcal{U}$ reads

$$\partial_z \mathcal{U}(z,0) = \mathcal{L}\,\mathcal{U}(z,0), \qquad \mathcal{U}(0,0) = \mathbb{1}_{\mathcal{L}} \qquad (4.22)$$

where $\mathbb{1}_{\mathcal{L}}$ is the unit operator in Liouville space. The question of how to solve this equation is the focus of the rest of this chapter and heavily relies on a Lie algebraic treatment of the involved right-acting superoperators.

## 4.2. Lie algebras induced by the Liouvillian of lossy waveguide systems

The superoperators $L_i^\pm$, $R_i^\pm$ and their composites like $L_i^+ L_j^-$ can be viewed as basis elements of Lie algebras with commutators derived from the fundamental commutators in Eq. (4.19). This allows the use of Lie algebraic techniques in order to find solutions for Eq. (4.22) with the Liouvillian (4.21).

We begin by introducing the *adjoint action* $\mathrm{ad}_X$ of an element $X$ of a Lie algebra as

$$\mathrm{ad}_X \bullet = [X, \bullet]\,. \qquad (4.23)$$

It allows operations such like concatenated commutators to be written as powers, e.g. $\mathrm{ad}_X^2 Y = [X,[X,Y]]$. In addition, it can be used to find a representation of the algebra often called adjoint representation or *regular representation*. The regular representation $\mathcal{R}(Z)$ of an element $Z$ of a Lie algebra spanned by $\{X_i\}$ is in its matrix form defined as [137]

$$\mathrm{ad}_Z X_i = [Z, X_i] = \mathcal{R}_{ij}(Z) X_j\,. \qquad (4.24)$$

The matrix representation $\mathcal{R}(Z)$ is a central part of Lie algebra theory because it encapsulates the fundamental structure constants of a Lie algebra by its definition via the commutator. In the upcoming section, a regular representation of the Liouvillian will be found which upon diagonalisation will allow the construction of ladder operators and states as a basis for the solution of Eq. (4.22).

Besides its direct use to find a solution via eigendecomposition, it also resurfaces in the definition of the *Cartan-Killing form* [137]

$$(X,Y)_{\mathrm{CK}} = \mathrm{Tr}\left(\mathcal{R}(X)\mathcal{R}(Y)\right), \tag{4.25}$$

which takes on the role of an inner product between two elements $X$, $Y$ of a Lie algebra. The importance of this inner product stems from its role in the structure analysis of a given algebra. The so called Levi decomposition theorem states that any Lie algebra can be decomposed into (semi)simple subalgebras and a maximally solvable subalgebra [137].

A solvable Lie algebra is an algebra $\mathfrak{g}$ with a finite chain of ideals $\mathfrak{i}_k$,

$$\mathfrak{g} \supseteq \mathfrak{i}_0 \supset \mathfrak{i}_1 \supset \cdots \supset \mathfrak{i}_r = 0, \tag{4.26}$$

which are themselves subalgebras that only project onto themselves under commutation with elements of larger algebras, e.g.

$$[\mathfrak{g}, \mathfrak{i}_k] \subseteq \mathfrak{i}_k \,. \tag{4.27}$$

In less abstract terms this simply means that any resulting matrix representation can be written as an upper diagonal matrix leading always to solvable systems of equations. An example of such a solvable algebra is a nilpotent algebra $\mathfrak{g}$ which has for each element $X$ an integer $n$ such that

$$\mathrm{ad}_X^n \, \mathfrak{g} = 0 \,. \tag{4.28}$$

In contrast, (semi)simple algebras are defined as containing exactly no ideal. This complementary definition is directly tied to the Levi decomposition.

In order to find this decomposition one takes a representative element $Z$ of the algebra and calculates its Cartan-Killing form $(Z,Z)_{\mathrm{CK}}$. The element $Z$ is representative as it encapsulates the whole algebra and usually one simply uses a superposition of all basis elements, $Z = \sum_i c_i X_i$. Other choices can be made in certain cases, see Ref. [137]. The Cartan-Killing form $(Z,Z)_{\mathrm{CK}}$ can then be positive, negative, or indefinite. All elements $X_i$ for which it is indefinite make up the nilpotent subalgebra. Removing these elements creates a new element $Z'$ for which again the Cartan-Killing form is calculated. This time, the indefinite part of the algebra creates the Abelian subalgebra which together with the nilpotent subalgebra give the maximally solvable subalgebra. In the picture of matrices and systems of equations, the nilpotent subalgebra yields the strictly upper diagonal parts and the Abelian subalgebra the diagonal components, i.e. simple scalar prefactors. The remaining elements for which the Cartan-Killing form $(Z',Z')_{\mathrm{CK}}$ is positive- or negative-definite create the (semi)simple subalgebra.

As an example consider the algebra created by the two-mode bosonic operators $\mathbb{1}_{\mathcal{H}}$, $\hat{a}_i$, $\hat{a}_i^\dagger$, $\hat{a}_i^\dagger \hat{a}_j$ $(i,j = 1,2)$. The Cartan-Killing product of the general element

$$Z = A\,\mathbb{1}_{\mathcal{H}} + B\,\hat{a}_1 + C\,\hat{a}_2 + D\,\hat{a}_1^\dagger + E\,\hat{a}_2^\dagger + F\,\hat{a}_1^\dagger\hat{a}_1 + G\,\hat{a}_1^\dagger\hat{a}_2 + H\,\hat{a}_2^\dagger\hat{a}_1 + I\,\hat{a}_2^\dagger\hat{a}_2 \tag{4.29}$$

is

$$(Z,Z)_{\mathrm{CK}} = 2\,F^2 + 2\,I^2 + 2\,(F-I)^2 + 12\,G\,H \,. \tag{4.30}$$

Because this form is independent from the coefficients $A$, $B$, $C$, $D$, and $E$, it is indefinite regarding the elements $\mathbb{1}_{\mathcal{H}}$, $\hat{a}_i$, and $\hat{a}_i^\dagger$ $(i = 1, 2)$. Therefore, these elements create the nilpotent subalgebra. This result can be verfied as one easily finds powers of their adjoint actions that evaluate to zero, for example

$$\mathrm{ad}^2_{\hat{a}_1}\, \hat{a}_1^\dagger \hat{a}_i = [\hat{a}_1, [\hat{a}_1, \hat{a}_1^\dagger \hat{a}_i]] = [\hat{a}_1, \hat{a}_i] = 0\,, \qquad i = 1, 2. \tag{4.31}$$

The reduced element $Z'$ without $\mathbb{1}_{\mathcal{H}}$, $\hat{a}_i$, and $\hat{a}_i^\dagger$ then yields the Cartan-Killing form

$$(Z', Z')_{\mathrm{CK}} = 2\,(F - I)^2 + 8\,G\,H\,. \tag{4.32}$$

The peculiar thing to notice is that only $G$, $H$, and $(F - I)$ occur. After a basis transformation $\{\hat{a}_1^\dagger\hat{a}_1, \hat{a}_2^\dagger\hat{a}_2, \hat{a}_1^\dagger\hat{a}_2, \hat{a}_2^\dagger\hat{a}_1\} \to \{\hat{a}_1^\dagger\hat{a}_1 + \hat{a}_2^\dagger\hat{a}_2, \hat{a}_1^\dagger\hat{a}_1 - \hat{a}_2^\dagger\hat{a}_2, \hat{a}_1^\dagger\hat{a}_2, \hat{a}_2^\dagger\hat{a}_1\}$, it is clear that the reduced Cartan-Killing form $(Z', Z')_{\mathrm{CK}}$ is indefinite regarding $\hat{a}_1^\dagger\hat{a}_1 + \hat{a}_2^\dagger\hat{a}_2$. Hence, this operator makes up the Abelian part, which together with the nipotent subalgebra yields the solvable subalgebra $\{\mathbb{1}_{\mathcal{H}}, \hat{a}_1, \hat{a}_1^\dagger, \hat{a}_2, \hat{a}_2^\dagger, \hat{a}_1^\dagger\hat{a}_1 + \hat{a}_2^\dagger\hat{a}_2\}$.

Subsequently, the remaining operators $\{\hat{a}_1^\dagger\hat{a}_1 - \hat{a}_1^\dagger\hat{a}_2, \hat{a}_2^\dagger\hat{a}_1, \hat{a}_2^\dagger\hat{a}_2\}$ constitute the semisimple subalgebra. In this special case this is even a simple algebra as it cannot be written as a direct sum of simple algebras and in fact it is the special linear algebra $\mathfrak{sl}(2, \mathbb{C})$ which is generally represented by operators

$$\mathcal{K}_0 = \hat{a}_1^\dagger\hat{a}_1 - \hat{a}_2^\dagger\hat{a}_2\,, \tag{4.33}$$

$$\mathcal{K}_+ = \hat{a}_1^\dagger\hat{a}_2\,, \tag{4.34}$$

$$\mathcal{K}_- = \hat{a}_2^\dagger\hat{a}_1\,, \tag{4.35}$$

with commutators

$$[\mathcal{K}_0, \mathcal{K}_\pm] = \pm 2\mathcal{K}_\pm, \quad [\mathcal{K}_+, \mathcal{K}_-] = \mathcal{K}_0. \tag{4.36}$$

This algebra will play an important role in Chapter 5 when we deal with the $\mathcal{PT}$-symmetric coupler. However, for now we return to the Liouville space operators of the lossy waveguide system.

From Eq. (4.21) it is obvious that a sensible choice for the whole algebra induced by the Liouvillian $\mathfrak{L}$ is spanned by

$$\{\mathbb{1}_{\mathfrak{L}}, L_i^\pm, R_i^\pm, L_i^+ L_j^-, R_i^+ R_j^-, L_i^- R_j^-\} \tag{4.37}$$

where we already added the Liouville-space identity $\mathbb{1}_{\mathfrak{L}}$ for closure. The indices $i, j$ range over all combinations of the $M$ waveguide modes. Note that even if not all modes couple, we still need to include all mode index combinations. This is due to the fact that commutators like $[L_i^+ L_{i+1}^-, L_{i+1}^+ L_{i+2}^-] = L_i^+ L_{i+2}^-$ occur. Therefore, all index combinations are possible under commutation and thus need to be included. Additionally, note that one only needs to include the loss operators $L_i^- R_j^-$ because we deal with a passive system where photons can be removed but not added.

As in the simple example of the two-mode Hilbert space operators above, the linear operators together with the unity operator can be split off to form a nilpotent subalgebra

$\{\mathbb{1}_{\mathfrak{L}}, L_i^{\pm}, R_i^{\pm}\}$. Evidently, when the Liouvillian $\mathcal{L}$ is interpreted not as a linear combination of the bilinear operators but as its own superoperator it can be added independently which results in a closed algebra spanned by

$$\{\mathbb{1}_{\mathfrak{L}}, L_i^{\pm}, R_i^{\pm}, \mathcal{L}\}\,. \tag{4.38}$$

The remaining bilinear superoperators,

$$\{L_i^{+}L_j^{-}, R_i^{+}R_j^{-}, L_i^{-}R_j^{-}\}\,, \tag{4.39}$$

then span their own algebra. In the following, we will use these two algebras as a basis to formulate solutions of Eq. (4.22). First, by using the algebra (4.38) in conjunction with the regular representation of the Liouvillian $\mathfrak{L}$, Second, by finding the Wei-Norman expansion of the evolution superoperator $\mathcal{U}$ based on the algebra (4.39).

## 4.3. Eigendecomposition of the Liouvillian

The first approach to solve Eq. (4.22) focusses on the $z$-independent case where $\mathcal{L} \neq \mathcal{L}(z)$. For this case the formal solution of the evolution superoperator reads $\mathcal{U} = \mathrm{e}^{\mathcal{L}z}$, cf. Eq. (4.9). Because $\mathcal{L}$ and $\mathcal{U}$ are connected via exponentiation both share the same eigenbasis. Thus, finding the eigendecomposition of $\mathcal{L}$ provides in turn an eigendecomposition of $\mathcal{U}$ and for that we diagonalise the regular representation $\mathcal{R}(\mathcal{L})$ in the algebra of linear operators, see Eq. (4.38).

This regular representation is generally a $(4M+2)\times(4M+2)$-matrix. However, because the commutator of $\mathcal{L}$ with the identity and $\mathcal{L}$ itself vanishes we can reduce our focus to the $4M\times 4M$-matrix $\mathcal{R}'(\mathcal{L})$ build up from the remaining superoperators $L_i^{\pm}$ and $R_i^{\pm}$. When arranging these linear operators as

$$\{L_1^{+}, \dots, L_M^{+}, R_1^{-}, \dots, R_M^{-}, R_1^{+}, \dots, R_M^{+}, L_1^{-}, \dots, L_M^{-}\}\,, \tag{4.40}$$

the regular representation becomes

$$\mathcal{R}'(\mathcal{L}) = \begin{pmatrix} -\mathrm{i}\boldsymbol{H}_{\text{eff}} & \boldsymbol{\Gamma} & \boldsymbol{0} & \boldsymbol{0} \\ \boldsymbol{0} & -\mathrm{i}\boldsymbol{H}_{\text{eff}}^{\dagger} & \boldsymbol{0} & \boldsymbol{0} \\ \boldsymbol{0} & \boldsymbol{0} & \mathrm{i}\boldsymbol{H}_{\text{eff}}^{\dagger} & \boldsymbol{\Gamma} \\ \boldsymbol{0} & \boldsymbol{0} & \boldsymbol{0} & \mathrm{i}\boldsymbol{H}_{\text{eff}} \end{pmatrix}. \tag{4.41}$$

Here we defined $\boldsymbol{\Gamma} = 2\,\mathrm{diag}(\gamma_1, \dots, \gamma_M)$ and the matrix representation

$$(\boldsymbol{H}_{\text{eff}})_{ij} = \delta_{ij}(\sigma_j - \mathrm{i}\gamma_j) + (1-\delta_{ij})\kappa_{ij} \tag{4.42}$$

of the effective non-Hermitian Hamiltonian $\hat{H}_{\text{eff}}$ which incorporates the loss rates $\gamma_k$ as complex propagation constants. This Hamiltonian was already introduced in Eq. (3.65) for the non-Hermitian holonomies and was adopted from classical physics. However, it does not lead to a physically meaningful, i.e. completely positive and trace-preserving dynamical map, when one derives the von-Neumann equation directly from the Schrödinger equation generated by $\hat{H}_{\text{eff}}$. The crucial difference is most clearly seen in the correct Liouvillian $\mathcal{L}$ in Eq. (4.21) where the additional terms $2\,\gamma_k\,L_k^- R_k^-$ occur. This quantum jump term is responsible for a correct, trace-preserving evolution of the density operator and it resurfaces in the regular representation $\mathcal{R}'(\mathcal{L})$ as the upper off-diagonal blocks $\mathbf{\Gamma}$. As a side note we remark that gain would create a similar contribution on the lower off-diagonal blocks when added via dissipators $2\,\gamma_k\,L_k^+ R_k^+$.

Utilising the block structure of the regular representation $\mathcal{R}'(\mathcal{L})$ in Eq. (4.41) leads to an efficient calculation of its eigenvalues and eigenvectors based on the diagonalisation of the effective non-Hermitian $\boldsymbol{H}_{\text{eff}}$. We begin by splitting the regular representation into two block matrices, i.e.

$$\mathcal{R}'(\mathcal{L}) = \begin{pmatrix} \mathbf{R} & \mathbf{0} \\ \mathbf{0} & \mathbf{R}^* \end{pmatrix}, \tag{4.43}$$

where

$$\mathbf{R} = \begin{pmatrix} -\mathrm{i}\boldsymbol{H}_{\text{eff}} & \mathbf{\Gamma} \\ \mathbf{0} & -\left(-\mathrm{i}\boldsymbol{H}_{\text{eff}}\right)^* \end{pmatrix}. \tag{4.44}$$

Note that $\mathbf{0}$ denotes, here and in the following, padding with zeros of appropriate dimensions. Clearly, when $\mathbf{v}$ is an eigenvector of $\mathbf{R}$ with eigenvalue $\zeta$ one finds that

$$\mathcal{R}'(\mathcal{L})\cdot\begin{pmatrix} \mathbf{v} \\ \mathbf{0} \end{pmatrix} = \begin{pmatrix} \mathbf{R}\cdot\mathbf{v} \\ \mathbf{0} \end{pmatrix} = \zeta\begin{pmatrix} \mathbf{v} \\ \mathbf{0} \end{pmatrix}. \tag{4.45}$$

Similarly, one finds

$$\mathcal{R}'(\mathcal{L})\cdot\begin{pmatrix} \mathbf{0} \\ \mathbf{v}^* \end{pmatrix} = \begin{pmatrix} \mathbf{0} \\ \mathbf{R}^*\cdot\mathbf{v}^* \end{pmatrix} = \zeta^*\begin{pmatrix} \mathbf{0} \\ \mathbf{v}^* \end{pmatrix}. \tag{4.46}$$

Hence, if the eigenvectors and eigenvalues of $\mathbf{R}$ are calculated, one has found the diagonalisation of the regular representation.

Taking a closer look at $\mathbf{R}$, it can be seen that its eigenvectors and eigenvalues are drawn from the eigensystem of $\boldsymbol{H}_{\text{eff}}$. In fact, when denoting the $M$ eigenvectors of $-\mathrm{i}\boldsymbol{H}_{\text{eff}}$ as $\boldsymbol{a}_j$, and their corresponding eigenvalues as $\lambda_j$, one finds that

$$\mathbf{R}\cdot\begin{pmatrix} \boldsymbol{a}_j \\ \mathbf{0} \end{pmatrix} = \lambda_j\begin{pmatrix} \boldsymbol{a}_j \\ \mathbf{0} \end{pmatrix}. \tag{4.47}$$

Noting the additional fact that $\mathrm{i}\boldsymbol{H}_{\text{eff}} - \mathbf{\Gamma} = (-\mathrm{i}\boldsymbol{H}_{\text{eff}})^*$, one also finds the eigenvalue equations

$$\mathbf{R}\cdot\begin{pmatrix} \boldsymbol{a}_j^* \\ \boldsymbol{a}_j^* \end{pmatrix} = (-\lambda_j^*)\begin{pmatrix} \boldsymbol{a}_j^* \\ \boldsymbol{a}_j^* \end{pmatrix}. \tag{4.48}$$

Because $\mathbf{R}$ is double the size of $-\mathrm{i}\boldsymbol{H}_{\text{eff}}$ these two equations are sufficient to construct the complete eigendecomposition. This means that the eigenvalues $\zeta$ of $\mathbf{R}$ are drawn from the $2M$ values $\{\lambda_j, -\lambda_j^*\}$ with eigenvectors $\boldsymbol{v} \in \{(\boldsymbol{a}_j, \mathbf{0})^T, (\boldsymbol{a}_j^*, \boldsymbol{a}_j^*)^T\}$.

From the two Eqs. (4.45) and (4.46) we recall that the eigenvalues of $\mathcal{R}'(\mathcal{L})$ are given by the eigenvalues of $\mathbf{R}$ and their complex conjugates, respectively. Therefore, it is straightforward that the diagonalisation of $\mathcal{R}'(\mathcal{L})$ yields $4M$ eigenvalues

$$\{\lambda_1, \ldots, \lambda_M, -\lambda_1^*, \ldots, -\lambda_M^*, \lambda_1^*, \ldots, \lambda_M^*, -\lambda_1, \ldots, -\lambda_M\}. \tag{4.49}$$

Analogously, the eigenvectors of $\mathcal{R}'(\mathcal{L})$ are determined by the eigenvectors of $\mathbf{R}$. Collected in a single matrix, these then take the form

$$\boldsymbol{T} = \begin{pmatrix} \boldsymbol{A} & \boldsymbol{A}^* & \boldsymbol{0} & \boldsymbol{0} \\ \boldsymbol{0} & \boldsymbol{A}^* & \boldsymbol{0} & \boldsymbol{0} \\ \boldsymbol{0} & \boldsymbol{0} & \boldsymbol{A}^* & \boldsymbol{A} \\ \boldsymbol{0} & \boldsymbol{0} & \boldsymbol{0} & \boldsymbol{A} \end{pmatrix}, \tag{4.50}$$

where

$$\boldsymbol{A} = (\mathbf{a}_1, \dots, \mathbf{a}_M) \tag{4.51}$$

is the matrix of normalised eigenvectors of $-\mathrm{i}\boldsymbol{H}_{\text{eff}}$. As a result, due to the block structure of the regular representation $\mathcal{R}'(\mathcal{L})$, its eigensystem can solely be constructed from the eigensystem of $-\mathrm{i}\boldsymbol{H}_{\text{eff}}$.

With the matrix of eigenvectors $\boldsymbol{T}$ we can now define a new diagonal basis of $\mathcal{R}'(\mathcal{L})$ by applying the inverse $\boldsymbol{T}^{-1}$ to the original basis as given in Eq. (4.40). A straightforward calculation shows that the inverse of $\boldsymbol{T}$ is

$$\boldsymbol{T}^{-1} = \begin{pmatrix} \boldsymbol{A}^{-1} & -\boldsymbol{A}^{-1} & \boldsymbol{0} & \boldsymbol{0} \\ \boldsymbol{0} & (\boldsymbol{A}^*)^{-1} & \boldsymbol{0} & \boldsymbol{0} \\ \boldsymbol{0} & \boldsymbol{0} & (\boldsymbol{A}^*)^{-1} & -(\boldsymbol{A}^*)^{-1} \\ \boldsymbol{0} & \boldsymbol{0} & \boldsymbol{0} & \boldsymbol{A}^{-1} \end{pmatrix}. \tag{4.52}$$

Subsequently, the diagonal basis of superoperators is given by

$$\begin{pmatrix} \boldsymbol{P}^+ \\ \boldsymbol{Q}^- \\ \boldsymbol{Q}^+ \\ \boldsymbol{P}^- \end{pmatrix} = \begin{pmatrix} \boldsymbol{A}^{-1} \cdot (\boldsymbol{L}^+ - \boldsymbol{R}^-) \\ (\boldsymbol{A}^*)^{-1} \cdot \boldsymbol{R}^- \\ (\boldsymbol{A}^*)^{-1} \cdot (\boldsymbol{R}^+ - \boldsymbol{L}^-) \\ \boldsymbol{A}^{-1} \cdot \boldsymbol{L}^- \end{pmatrix}, \tag{4.53}$$

where we used a vector notation for the superoperators, e.g. $\boldsymbol{P}^+ = (P_1^+, P_2^+, \dots, P_M^+)$. The components of $\boldsymbol{P}^\pm$ and $\boldsymbol{Q}^\pm$ are thus $4M$ superoperators that have the general form

$$P_i^+ = \sum_k c_{ik} (L_k^+ - R_k^-) \,, \quad P_i^- = \sum_k c_{ik} L_k^- \,, \tag{4.54}$$

$$Q_i^+ = \sum_k c_{ik}^* (R_k^+ - L_k^-) \,, \quad Q_i^- = \sum_k c_{ik}^* R_k^- \,, \tag{4.55}$$

where the $c_{ik}$ are the coefficients of the inverse eigenvector matrix $\boldsymbol{A}^{-1}$.

With the eigendecomposition of $\mathcal{R}'(\mathcal{L})$ at hand a few notes are in order: First, the above derivation showed that the eigensystem of $\mathcal{R}'(\mathcal{L})$ is directly derived from the eigensystem of the effective non-Hermitian Hamiltonian $\boldsymbol{H}_{\text{eff}}$. Consequently, the eigenvalues and eigenvectors have similar behaviours, e.g. when the eigenvalues $\lambda$ change from real to complex values the eigenvalues of $\mathcal{R}'(\mathcal{L})$ show the same changes, cf. Eq. (4.49). Because of this the Hamiltonian and the Liouvillian have their exceptional points at the same parameter values. This is intuitive but not generally the case [138]. However, for our system this allows to talk only of a single set of EPs without the immediate need of distinction.

Second, if gain is added to the system via a dissipator with jump operators $\hat{A}_k = \hat{a}_k^\dagger$, cf. Eq. (4.10), this adds a lower diagonal block of the gain rates in the matrices $\mathbf{R}$, see Eq. (4.44). This prevents the direct use of the eigenbasis of $\boldsymbol{H}_{\text{eff}}$ as shown above. Nonetheless, one can of course still find an eigendecomposition because $\mathcal{R}'(\mathcal{L})$ remains diagonalisable. However, this might require the use of more complicated eigenvectors or numerical approaches. For example Ref. [139] studied the case of a single bosonic mode coupled to a thermal bath resulting in different eigenvectors but with a similar connection between the eigenvalues.

Third, when the system is at the EP, the eigensystems of $\boldsymbol{H}_{\text{eff}}$ and $\mathcal{R}'(\mathcal{L})$ become defective and require a general Jordan decomposition with generalised eigenvectors. In turn, the direct link between the eigensystems of $\boldsymbol{H}_{\text{eff}}$ and $\mathcal{R}'(\mathcal{L})$ can no longer be established. However, in this case one can still attempt to directly find a Jordan decomposition of $\mathcal{R}'(\mathcal{L})$ itself allowing to formulate solutions at the EP. As in the case of gain, this might require numerical routines which might complicate the calculations but does not pose a fundamental problem.

Fourth, and most importantly for our following considerations, the specific naming and ordering convention for the superoperators $P_i^+$, $P_i^-$, $Q_i^+$, and $Q_i^-$ are by no means arbitrary. In fact, these superpositions of the original superoperators act as ladder operators creating and annihilating abstract excitations in Liouville space. Due to their importance we will invest some more time into them.

### 4.3.1. Liouville space ladder operators

The new superoperators $P_i^\pm$ and $Q_i^\pm$ show some interesting properties. They obey, after suitable normalisation, the commutator relations

$$[P_i^-, P_j^+] = \delta_{ij}, \quad [Q_i^-, Q_j^+] = \delta_{ij}\,, \tag{4.56}$$

with all other commutators vanishing. Furthermore, because they diagonalise the regular representation $\mathcal{R}'(\mathcal{L})$, they yield the eigenvalue commutator relations

$$\begin{aligned} \left[\mathcal{L}, P_i^+\right] &= \lambda_i P_i^+, \quad \left[\mathcal{L}, P_i^-\right] = -\lambda_i P_i^-, \\ \left[\mathcal{L}, Q_i^+\right] &= \lambda_i^* Q_i^+, \quad \left[\mathcal{L}, Q_i^-\right] = -\lambda_i^* Q_i^-. \end{aligned} \tag{4.57}$$

These two properties are reminiscent of the ladder operators of the usual harmonic oscillator Hamiltonian and in fact one can use the superoperators $P_i^\pm$ and $Q_i^\pm$ to construct the eigenstates of $\mathcal{L}$. In this picture, the superoperators $P_i^\pm$ and $Q_i^\pm$ create or annihilate excitations of $\pm\lambda_i$ or $\pm\lambda_i^*$ in Liouville space, respectively. However, these are abstract excitations in $\mathfrak{L}$ that are not identical to physical excitations from the original Hilbert space $\mathcal{H}$. For example, the annihilation superoperators $P_i^-$ and $Q_i^-$ actually remove photons from the system but do so by acting from the left or right on quantum states $\hat{\rho}$. Therefore, they not necessarily create just states of one photon less but also any off-diagonal terms between such states of different photon numbers. Also, the creation superoperators $P_i^+$ and $Q_i^+$ simultaneously contain superoperators that both add and subtract photons from left and right. Thus, a direct link between these excitations and the physical creation or annhihilation of photons in the waveguide system cannot be made.

Despite their abstract nature, the ladder superoperators $P_i^{\pm}$ and $Q_i^{\pm}$ can still be used to construct eigenvectors of the Liouvillian $\mathcal{L}$. The recipe is similar to the more familiar Hilbert space case and entails the calculation of a ground state $|0\rangle\rangle$ from which higher Fock-like states are created by application of the ladder superoperators. The ground state is as usual defined by the property that it evaluates to zero if an annihilation operator acts on it, which translates to

$$P_i^- |0\rangle\rangle = Q_i^- |0\rangle\rangle = 0\,, \qquad \forall i\,, \tag{4.58}$$

$$\langle\langle 0|P_i^+ = \langle\langle 0|Q_i^+ = 0\,, \qquad \forall i\,, \tag{4.59}$$

However, some care has to be exercised because $\mathcal{L}$ is non-Hermitian and, therefore, one has to calculate $|0\rangle\rangle$ and $\langle\langle 0|$ individually.

We begin with the right ground state $|0\rangle\rangle$ whose defining equation (4.58) is straightforwardly evaluated because the right action of the superoperators $P_i^{\pm}$, $Q_i^{\pm}$ are already known by the definitions of the underlying superoperators $L_i^{\pm}$, $R_i^{\pm}$. For this we insert a general state

$$|0\rangle\rangle = \sum_{\boldsymbol{n},\boldsymbol{m}} = \xi_{\boldsymbol{n},\boldsymbol{m}} |\boldsymbol{n}\rangle\langle\boldsymbol{m}| \tag{4.60}$$

as our ansatz, following similar considerations in Ref. [139] where it was used for the ground state of an harmonic oscillator coupled to a thermal bath. This translates to a single waveguide with specific gain and loss. In our generalised case of coupled waveguides, this approach results in a set of equations for the coefficients $\xi_{\boldsymbol{n},\boldsymbol{m}}$ once the conditions in Eq. (4.58) are calculated. Solving this set results in the unique solution

$$|0\rangle\rangle = |\mathbf{0}\rangle\langle\mathbf{0}|. \tag{4.61}$$

The reason for this simple result is that the annihilation superoperators $P_i^-$ or $Q_i^-$ only contain the Hilbert space annhihilation operators $\hat{a}$ acting from the left or right, respectively.

For the left ground state we can use a similar approach but we first need to know the left actions of the superoperators. These can be deduced from the definition of an adjoint superoperator via the Liouville space inner product as defined in Eq. (4.14). One example given for the superoperator $L^+$ reads:

$$\langle\langle \hat{A}|L^+|\hat{B}\rangle\rangle = \mathrm{Tr}\left[\hat{A}^\dagger \hat{a}^\dagger \hat{B}\right] = \mathrm{Tr}\left[(\hat{a}\hat{A})^\dagger \hat{B}\right] = \langle\langle \hat{a}\hat{A}|\hat{B}\rangle\rangle\,, \tag{4.62}$$

leading to the left action

$$\langle\langle \hat{A}|L^+ = \langle\langle \hat{a}\hat{A}| \tag{4.63}$$

and similarly for the other superoperators $L^-$ and $R^{\pm}$. The creation operators $P_i^+$ and $Q_i^+$ are superpositions of elements of the form $L_k^+ - R_k^-$ or $R_k^+ - L_k^-$ and thus the defining equations (4.59) become

$$\langle\langle \mathbf{0}|(L_k^+ - R_k^-) = \langle\langle \hat{a}\hat{A}| - \langle\langle \hat{A}\hat{a}| = 0\,, \tag{4.64}$$

$$\langle\langle \mathbf{0}|(R_k^+ - L_k^-) = \langle\langle \hat{A}\hat{a}^\dagger| - \langle\langle \hat{a}^\dagger\hat{A}| = 0\,. \tag{4.65}$$

These equations are only fulfilled by $\hat{A} \propto \mathbb{1}_{\mathcal{H}}$. In addition, we require a normalisation $\langle\langle \mathbf{0}|\mathbf{0}\rangle\rangle = 1$ and therefore we set

$$\langle\langle 0| = \mathbb{1}_{\mathcal{H}} \tag{4.66}$$

as the left ground state.

With the left and right ground state known, higher rungs of the metaphorical ladder are then obtained by applying the annihiliation superoperators $P_i^-$ and $Q_i^-$ to the left and the creation superoperator $P_i^+$ and $Q_i^+$ to the right, respectively. As with usual Fock states, these higher rungs are labelled with their number of excitations. However, with $P_i^\pm$ and $Q_i^\pm$ we have sets of two creation and annihilation superoperators and thus we also need two integers to label these. With these points in mind the higher-order states are then given by

$$|\boldsymbol{\alpha}, \boldsymbol{\beta}\rangle\rangle = \frac{1}{\sqrt{\boldsymbol{\alpha}!\,\boldsymbol{\beta}!}} \boldsymbol{P}^{+\,\boldsymbol{\alpha}} \boldsymbol{Q}^{+\,\boldsymbol{\beta}} |0\rangle\rangle\,, \tag{4.67}$$

$$\langle\langle \boldsymbol{\alpha}, \boldsymbol{\beta}| = \frac{1}{\sqrt{\boldsymbol{\alpha}!\,\boldsymbol{\beta}!}} \langle\langle 0| \boldsymbol{P}^{-\,\boldsymbol{\alpha}} \boldsymbol{Q}^{-\,\boldsymbol{\beta}}, \tag{4.68}$$

with multiindices $\boldsymbol{\alpha} = (\alpha_1, \ldots, \alpha_M)$ and with the superoperator expressions like $\boldsymbol{P}^{+\,\boldsymbol{\alpha}}$ defined as

$$\boldsymbol{P}^{+\,\boldsymbol{\alpha}} = \prod_{i=1}^{M} P_i^{+\,\alpha_i}. \tag{4.69}$$

With the commutation relations in Eq. (4.56) it is easily seen that the above bras and kets are biorthonormal, i.e.

$$\langle\langle \boldsymbol{\alpha}, \boldsymbol{\beta} | \boldsymbol{\alpha}', \boldsymbol{\beta}'\rangle\rangle = \delta_{\boldsymbol{\alpha},\boldsymbol{\alpha}'} \delta_{\boldsymbol{\beta},\boldsymbol{\beta}'}\,. \tag{4.70}$$

Now we prove that the ladder states $|\boldsymbol{\alpha}, \boldsymbol{\beta}\rangle\rangle$ and $\langle\langle \boldsymbol{\alpha}, \boldsymbol{\beta}|$ are indeed eigenstates of the Liouvillian $\mathcal{L}$. For this we use the identities

$$\left[\mathcal{L}, P_i^{+\,\alpha_i}\right] = \alpha_i\, \lambda_i\, P_i^{+\,\alpha_i}\,, \tag{4.71}$$

$$\left[\mathcal{L}, Q_i^{+\,\beta_i}\right] = \beta_i\, \lambda_i^*\, Q_i^{+\,\alpha_i}\,, \tag{4.72}$$

$$\left[\mathcal{L}, P_i^{-\,\alpha_i}\right] = -\alpha_i\, \lambda_i\, P_i^{-\,\alpha_i}\,, \tag{4.73}$$

$$\left[\mathcal{L}, Q_i^{-\,\beta_i}\right] = -\beta_i\, \lambda_i^*\, Q_i^{-\,\beta_i}\,, \tag{4.74}$$

which are easily proven by induction using the fundamental commutators in Eq. (4.57). In addition, we use the facts that $\mathcal{L}|0\rangle\rangle = 0$ and $\langle\langle 0|\mathcal{L} = 0$. The relation $\mathcal{L}|0\rangle\rangle = 0$ holds because in the Liouvillian $\mathcal{L}$ from Eq. (4.21) the superoperators acting first to the right on the vacuum $|0\rangle\rangle = |\mathbf{0}\rangle\langle\mathbf{0}|$ are all annhihilation operators. In order to understand why the relation $\langle\langle 0|\mathcal{L}| = 0$ holds, we have to use the left actions of the superoperators $L_i^\pm$ and $R_i^\pm$, cf. Eqs. (4.63)-(4.65). The left action of the Liouvillian from Eq. (4.21) on the left ground state $\langle\langle 0|$ is then

$$\begin{aligned}\langle\langle 0|\mathcal{L} = \sum_{k=1}^{M} \Big[ (\mathrm{i}\sigma_k - \gamma_k)\, \mathbb{1}_{\mathcal{H}}\, \hat{a}_k^\dagger \hat{a}_k - (\mathrm{i}\sigma_k + \gamma_k)\, \hat{a}_k^\dagger \hat{a}_k\, \mathbb{1}_{\mathcal{H}} + 2\gamma_k\, \hat{a}_k\, \mathbb{1}_{\mathcal{H}}\, \hat{a}_k^\dagger \Big] \\ - \sum_{\substack{k,l=1\\ k\neq l}}^{M} \mathrm{i}\,\kappa_{kl} \left( \hat{a}_k^\dagger \hat{a}_l \mathbb{1}_{\mathcal{H}} + \hat{a}_l^\dagger \hat{a}_k \mathbb{1}_{\mathcal{H}} - \mathbb{1}_{\mathcal{H}}\, \hat{a}_l^\dagger \hat{a}_k - \mathbb{1}_{\mathcal{H}}\, \hat{a}_k^\dagger \hat{a}_l \right) = 0\,. \end{aligned} \tag{4.75}$$

With both relations and the identities in Eqs. (4.71)-(4.74), the left and right eigenequations are straightforward calculations that yield

$$\mathcal{L}\,|\boldsymbol{\alpha},\boldsymbol{\beta}\rangle\rangle = (\boldsymbol{\alpha}\cdot\boldsymbol{\lambda} + \boldsymbol{\beta}\cdot\boldsymbol{\lambda}^*)\,|\boldsymbol{\alpha},\boldsymbol{\beta}\rangle\rangle = \mu_{\boldsymbol{\alpha},\boldsymbol{\beta}}\,|\boldsymbol{\alpha},\boldsymbol{\beta}\rangle\rangle, \tag{4.76}$$

$$\langle\langle\boldsymbol{\alpha},\boldsymbol{\beta}|\,\mathcal{L} = \langle\langle\boldsymbol{\alpha},\boldsymbol{\beta}|\,(\boldsymbol{\alpha}\cdot\boldsymbol{\lambda} + \boldsymbol{\beta}\cdot\boldsymbol{\lambda}^*) = \mu_{\boldsymbol{\alpha},\boldsymbol{\beta}}\,\langle\langle\boldsymbol{\alpha},\boldsymbol{\beta}|\,. \tag{4.77}$$

Here we defined the notations $\boldsymbol{\lambda} = (\lambda_1, \ldots, \lambda_M)^{\mathrm{T}}$ and $\boldsymbol{\alpha}\cdot\boldsymbol{\lambda} = \sum_i \alpha_i\,\lambda_i$. The eigenvalues $\mu_{\boldsymbol{\alpha},\boldsymbol{\beta}}$ of $\mathcal{L}$ are then directly determined by the eigenvalues $\lambda_i$ of $-\mathrm{i}\boldsymbol{H}_{\text{eff}}$ and the multiindices $\boldsymbol{\alpha}$ and $\boldsymbol{\beta}$. Consequently, the biorthogonal ladder states $|\boldsymbol{\alpha},\boldsymbol{\beta}\rangle\rangle$ and $\langle\langle\boldsymbol{\alpha},\boldsymbol{\beta}|$ are right and left eigenstates of the Liouvillian.

### 4.3.2. Eigendecomposition solution of the quantum master equation

Similarly to the eigenequation for the Liouvillian, we can find the action of the evolution operator $\mathcal{U} = \mathrm{e}^{\mathcal{L}\,z}$ on the states $|\boldsymbol{\alpha},\boldsymbol{\beta}\rangle\rangle$, which is elegantly calculated using the adjoint action $\mathrm{ad}_{\mathcal{L}}$, see Eq. (4.23) for its definition. Its advantage is in the formulation of the exponential operator expression [140]

$$\mathrm{e}^{X} Y \mathrm{e}^{-X} = \sum_n \frac{1}{n!}\mathrm{ad}_X^n Y = \mathrm{e}^{\mathrm{ad}_X} Y\,. \tag{4.78}$$

In case of the Liouvillian this implies that

$$\mathrm{e}^{\mathrm{ad}_{\mathcal{L}}} \boldsymbol{P}^{+\boldsymbol{\alpha}} = \mathrm{e}^{\boldsymbol{\alpha}\boldsymbol{\lambda}} \boldsymbol{P}^{+\boldsymbol{\alpha}}\,, \tag{4.79}$$

which can be derived with the help of the identity (4.71) and the Taylor series of the exponential function. As a result the evolution of a single eigenvector $|\boldsymbol{\alpha},\boldsymbol{\beta}\rangle\rangle$ is given by

$$\begin{aligned}\mathrm{e}^{\mathcal{L}\,z}|\boldsymbol{\alpha},\boldsymbol{\beta}\rangle\rangle &= \frac{1}{\sqrt{\boldsymbol{\alpha}!\,\boldsymbol{\beta}!}} \mathrm{e}^{\mathcal{L}\,z} \boldsymbol{P}^{+\boldsymbol{\alpha}} \boldsymbol{Q}^{+\boldsymbol{\beta}} \mathrm{e}^{-\mathcal{L}\,z}\, \mathrm{e}^{\mathcal{L}\,z}\,|0\rangle\rangle \\ &= \frac{1}{\sqrt{\boldsymbol{\alpha}!\,\boldsymbol{\beta}!}} \left(\mathrm{e}^{\mathrm{ad}_{\mathcal{L}}} \boldsymbol{P}^{+\boldsymbol{\alpha}} \boldsymbol{Q}^{+\boldsymbol{\beta}}\right) \mathrm{e}^{\mathcal{L}\,z}\,|0\rangle\rangle \\ &= \mathrm{e}^{\mu_{\boldsymbol{\alpha},\boldsymbol{\beta}}\,z}\,|\boldsymbol{\alpha},\boldsymbol{\beta}\rangle\rangle\,. \end{aligned} \tag{4.80}$$

Finally, using the completeness of the biorthogonal eigenstates, we can insert the relation

$$\sum_{\boldsymbol{\alpha},\boldsymbol{\beta}} |\boldsymbol{\alpha},\boldsymbol{\beta}\rangle\rangle\langle\langle\boldsymbol{\alpha},\boldsymbol{\beta}| = \mathbb{1}_{\mathfrak{L}} \tag{4.81}$$

into the formal solution $|\hat{\rho}(z)\rangle\rangle = \mathrm{e}^{\mathcal{L}\,z}|\hat{\rho}(0)\rangle\rangle$ of the quantum master equation. The result gives the evolved quantum state as

$$|\hat{\rho}(z)\rangle\rangle = \sum_{\boldsymbol{\alpha},\boldsymbol{\beta}} \mathrm{e}^{\mu_{\boldsymbol{\alpha},\boldsymbol{\beta}}\,z}|\boldsymbol{\alpha},\boldsymbol{\beta}\rangle\rangle\langle\langle\boldsymbol{\alpha},\boldsymbol{\beta}|\hat{\rho}(0)\rangle\rangle\,. \tag{4.82}$$

The sum runs over all possible combinations of multiindices $\boldsymbol{\alpha}$ and $\boldsymbol{\beta}$. However, the number of nonzero coefficients $\langle\langle\boldsymbol{\alpha},\boldsymbol{\beta}|\hat{\rho}(0)\rangle\rangle$ effectively limits the number of summands. More precisely, for an initial state $|\hat{\rho}(0)\rangle\rangle$ containing a maximum of $N_\mathrm{p}$ photons, the multiindices are restricted to $|\boldsymbol{\alpha}|, |\boldsymbol{\beta}| \leq N_\mathrm{p}$. This can easily seen from the coefficients

$$\langle\langle\boldsymbol{\alpha},\boldsymbol{\beta}|\hat{\rho}(0)\rangle\rangle = \frac{1}{\sqrt{\boldsymbol{\alpha}!\,\boldsymbol{\beta}!}}\langle\langle 0|\boldsymbol{P}^{-\,\boldsymbol{\alpha}}\boldsymbol{Q}^{-\,\boldsymbol{\beta}}|\hat{\rho}(0)\rangle\rangle \tag{4.83}$$

because all the $P_i^-$ and $Q_i^-$ only contain superoperators that represent annihilation operators $\hat{a}_i$ acting in the base Hilbert space. Therefore, the expression

$$\boldsymbol{P}^{-\,\boldsymbol{\alpha}}\boldsymbol{Q}^{-\,\boldsymbol{\beta}}|\hat{\rho}(0)\rangle\rangle \tag{4.84}$$

means that $|\boldsymbol{\alpha}|$ photons get subtracted from the left and $|\boldsymbol{\beta}|$ photons from the right of $\hat{\rho}(0)$ If more than the maximal number of photons $N_\mathrm{p}$ in the quantum state $|\hat{\rho}(0)\rangle\rangle$ is subtracted, the result is zero.

The eigendecomposition solution in Eq. (4.82) has the familiar form of eigenstates, overlaps, and eigenvalue exponentials as in Hilbert spaces known from closed systems. However, there is one major difference and that is that the eigenvectors $|\boldsymbol{\alpha},\boldsymbol{\beta}\rangle\rangle$ are not physical states themselves. This fact can be deduced from the general Liouville equation (4.15). The overall probability, and thus the trace $\mathrm{Tr}\,|\hat{\rho}\rangle\rangle = 1$, is a conserved quantity. Therefore, it must hold that

$$\partial_z \mathrm{Tr}\,|\hat{\rho}\rangle\rangle = \mathrm{Tr}\,\mathcal{L}|\hat{\rho}\rangle\rangle = 0\,, \tag{4.85}$$

for any quantum state $|\hat{\rho}\rangle\rangle$. Testing this for one of the eigenvectors $|\boldsymbol{\alpha},\boldsymbol{\beta}\rangle\rangle$, one finds that

$$\mathrm{Tr}\,\mathcal{L}|\boldsymbol{\alpha},\boldsymbol{\beta}\rangle\rangle = (\boldsymbol{\alpha}\cdot\boldsymbol{\lambda} + \boldsymbol{\beta}\cdot\boldsymbol{\lambda}^*)\,\mathrm{Tr}\,|\boldsymbol{\alpha},\boldsymbol{\beta}\rangle\rangle = \mu_{\boldsymbol{\alpha},\boldsymbol{\beta}}\,\mathrm{Tr}\,|\boldsymbol{\alpha},\boldsymbol{\beta}\rangle\rangle = 0\,, \tag{4.86}$$

which is only fulfilled when either $\mu_{\boldsymbol{\alpha},\boldsymbol{\beta}} = 0$ or $\mathrm{Tr}\,|\boldsymbol{\alpha},\boldsymbol{\beta}\rangle\rangle = 0$. Consequently, any eigenvector $|\boldsymbol{\alpha},\boldsymbol{\beta}\rangle\rangle$ with $\mu_{\boldsymbol{\alpha},\boldsymbol{\beta}} \neq 0$ cannot be a physical state. Only the vector $|\boldsymbol{0},\boldsymbol{0}\rangle\rangle = |0\rangle\rangle$ is itself a physical state, which in the present case of the passive waveguide system is the vacuum state, cf. Eq. (4.61).

Despite the fact that the eigenvectors $|\boldsymbol{\alpha},\boldsymbol{\beta}\rangle\rangle$ with $\mu_{\boldsymbol{\alpha},\boldsymbol{\beta}} \neq 0$ are not physical states themselves, the whole solution (4.82) is of course a physical state due to the completeness of the biorthogonal basis. Thus, under careful consideration of the vectors $|\boldsymbol{\alpha},\boldsymbol{\beta}\rangle\rangle$ and their weights $\langle\langle\boldsymbol{\alpha},\boldsymbol{\beta}|\hat{\rho}(0)\rangle\rangle$, one can still investigate the propagation properties of certain input states $|\hat{\rho}(0)\rangle\rangle$ by examining the eigenvalues $\mu_{\boldsymbol{\alpha},\boldsymbol{\beta}}$.

For example, one interesting question would be which kind of states lead to an ideal transport, i.e. which states experience the lowest losses when propagating through a given lossy waveguide system. The loss rates are of course given by the real parts $\mathrm{Re}(\mu_{\boldsymbol{\alpha},\boldsymbol{\beta}})$ of the Liouvillian eigenvalues. The question is thus, which states $|\hat{\rho}(0)\rangle\rangle$ maximise the overlaps $\langle\langle\boldsymbol{\alpha},\boldsymbol{\beta}|\hat{\rho}(0)\rangle\rangle$ with multiindices $\boldsymbol{\alpha}$ and $\boldsymbol{\beta}$ that create the lowest loss eigenvalues $\mu_{\boldsymbol{\alpha},\boldsymbol{\beta}} = \boldsymbol{\alpha}\cdot\boldsymbol{\lambda} + \boldsymbol{\beta}\cdot\boldsymbol{\lambda}^*$ of $\boldsymbol{\mathcal{L}}$.

For example, ordering the eigenvalues $\lambda_i$ from lowest to highest absolute value of the real part, i.e. loss,

$$\lambda_i, \lambda_k, \ldots, \lambda_t \tag{4.87}$$

means that

$$(\alpha_i, \beta_i), (\alpha_k, \beta_k), \ldots, (\alpha_t, \beta_t) \tag{4.88}$$

are the sets of most to least favourable indices. Choosing a state that predominantly or even exclusively overlaps with indices $\alpha_i$ and $\beta_i$ results in lower overall loss. An example of such a construction is discussed in the following chapter. In addition, one could of course raise different questions, e.g. tailored to specific observables, and analyse the state propagation under more elaborate constraints. But the fundamental procedure remains the same as in the familiar Hilbert space case, just with added complexity due to the state construction by the unphysical eigenvectors $|\boldsymbol{\alpha},\boldsymbol{\beta}\rangle\rangle$.

A closer look at these vectors $|\boldsymbol{\alpha},\boldsymbol{\beta}\rangle\rangle$ reveals an interesting property of the passive system. It can be shown that, under certain restrictions, the propagation is solely described by the effective Hamiltonian $\hat{H}_{\text{eff}}$. In order to understand this, we begin by rewriting the general form of the eigenvectors in Eq. (4.67) or, more specifically, of the creation superoperators $\boldsymbol{P}^{+\boldsymbol{\alpha}}\boldsymbol{Q}^{+\boldsymbol{\beta}}$. These take on the form

$$\boldsymbol{P}^{+\boldsymbol{\alpha}}\boldsymbol{Q}^{+\boldsymbol{\beta}} = \prod_{i=1}^{M}\left(\sum_{k=1}^{M} c_{ik}\left(L_k^+ - R_k^-\right)\right)^{\alpha_i}\prod_{j=1}^{M}\left(\sum_{m=1}^{M} c_{jm}^*\left(R_m^+ - L_m^-\right)\right)^{\beta_j} . \tag{4.89}$$

An elegant reformulation of such products based on permanents has been deduced in Refs. [141; 142] for bosonic modes and can directly be applied to the present case. The permanent of a square matrix $\boldsymbol{T}$ is hereby defined as [143]

$$\operatorname{per}\boldsymbol{T} = \sum_{\sigma\in S_n}\prod_{i=1}^{n} T_{i,\sigma(i)} \, , \tag{4.90}$$

where the summation runs over all index permutations $\sigma(i)$ that are part of the symmetric group $S_n$ of degree $n$. This is the symmetric variant of the determinant, in which the summands change sign depending on the then antisymmetric index permutation. The occurrence of permanents is because we only deal with bosonic mode operators resulting in symmetric terms in contrast to antisymmetric ones for fermions [144; 145].

Following the combinatoric arguments in Refs. [141; 142], the superoperator products in Eq. (4.89) can be written as

$$\begin{aligned}\boldsymbol{P}^{+\boldsymbol{\alpha}}\boldsymbol{Q}^{+\boldsymbol{\beta}} = &\sum_{\boldsymbol{p}\in R_{M,|\boldsymbol{\alpha}|}} \frac{1}{\boldsymbol{p}!}\operatorname{per}\left(\boldsymbol{A}^{-1}[\boldsymbol{p}|\boldsymbol{\alpha}]\right)\left(\boldsymbol{L}^+ - \boldsymbol{R}^-\right)^{\boldsymbol{p}} \\ &\times \sum_{\boldsymbol{q}\in R_{M,|\boldsymbol{\beta}|}} \frac{1}{\boldsymbol{q}!}\operatorname{per}\left(\left(\boldsymbol{A}^*\right)^{-1}[\boldsymbol{q}|\boldsymbol{\beta}]\right)\left(\boldsymbol{R}^+ - \boldsymbol{L}^-\right)^{\boldsymbol{q}} ,\end{aligned} \tag{4.91}$$

where the notation $\boldsymbol{M}[\boldsymbol{n}|\boldsymbol{m}]$ with multiindices $\boldsymbol{n}$, $\boldsymbol{m}$ of equal lengths designates a matrix built from $n_i{\times}m_j$ blocks of the components $M_{ij}$. In case of the inverse eigenvector matrix $\boldsymbol{A}^{-1}$ these are the coefficients $c_{ik}$, cf. Eq. (4.53) and discussion thereafter. The summations range over the sets $R_{M,|\boldsymbol{m}|}$ of all multiindices of length $M$ and absolute value $|\boldsymbol{m}|$.

The action of the superoperator terms $(\boldsymbol{L}^+ - \boldsymbol{R}^-)^{\boldsymbol{p}}$ and $(\boldsymbol{R}^+ - \boldsymbol{L}^-)^{\boldsymbol{q}}$ in Eq. (4.91) follow simple multinomial rules, e.g.

$$\left(\boldsymbol{L}^+ - \boldsymbol{R}^-\right)^{\boldsymbol{p}} = \prod_{s=1}^{M} \left(L_s^+ - R_s^-\right)^{p_s} = \prod_{s=1}^{M} \sum_{t=0}^{p_s} \binom{p_s}{t} L_s^{+\,p_s - t} (-R_s^-)^t \,, \tag{4.92}$$

$$\left(\boldsymbol{R}^+ - \boldsymbol{L}^-\right)^{\boldsymbol{q}} = \prod_{v=1}^{M} \left(R_v^+ - L_v^-\right)^{q_v} = \prod_{v=1}^{M} \sum_{w=0}^{q_v} \binom{p_v}{w} R_v^{+\,q_v - w} (-L_v^-)^w \,. \tag{4.93}$$

With these forms inserted into Eq. (4.91) the general construction principle of any eigenvector $|\boldsymbol{\alpha}, \boldsymbol{\beta}\rangle\rangle$ can be understood as follows: First, from $\boldsymbol{Q}^{+\boldsymbol{\beta}}$ the superoperator terms $R_v^{+\,q_v-w}(-L_v^-)^w$ are applied to $|0\rangle\rangle = |\boldsymbol{0}\rangle\langle\boldsymbol{0}|$. This effectively means that all terms with $w \neq 0$ vanish because they apply annihilation operators from the left to the vacuum. What remains are creation operators acting from the right, i.e. $R_v^{+\,q_v-w}|0\rangle\rangle = |\boldsymbol{0}\rangle\langle\boldsymbol{0}|\hat{a}^{q_v-w}$. On these terms the superoperators from $\boldsymbol{P}^{+\boldsymbol{\alpha}}$ are applied which, according to (4.92), are superoperators $L_s^{+\,p_s-t}(-R_s^-)^t$ that remove $t$ excitations from the right and add $p_s - t$ excitations from the left. This interplay of adding and removing excitations then results after evaluation of the summations and products in a general form

$$|\boldsymbol{\alpha}, \boldsymbol{\beta}\rangle\rangle = \hat{\varrho}_{|\boldsymbol{\alpha}|,|\boldsymbol{\beta}|} + \hat{\varrho}_{|\boldsymbol{\alpha}|-1,|\boldsymbol{\beta}|} + \hat{\varrho}_{|\boldsymbol{\alpha}|,|\boldsymbol{\beta}|-1} + \dots \tag{4.94}$$

of dyads $\hat{\varrho}_{|\boldsymbol{n}|,|\boldsymbol{m}|}$ consisting of bras with $|\boldsymbol{n}|$ photons and kets with $|\boldsymbol{m}|$ photons.

These expressions quickly become unwieldy for larger numbers of modes or photons. However, one special case is worth looking at and that is when an input state $|\hat{\rho}(0)\rangle\rangle$ contains $N_\mathrm{p}$ photons and we restrict any measurement to the $N_\mathrm{p}$-photon subspace. Then, any superoperator terms that remove photons, i.e. containing $L_i^-$ or $R_i^-$, do not contribute to expectation values. Thus we can rewrite the expression (4.91) as

$$\begin{aligned} \boldsymbol{P}^{+\boldsymbol{\alpha}} \boldsymbol{Q}^{+\boldsymbol{\beta}} |0\rangle\rangle \overset{|\boldsymbol{\alpha}|=|\boldsymbol{\beta}|=N_\mathrm{p}}{=} & \sum_{\boldsymbol{p}\in R_{M,N_\mathrm{p}}} \frac{1}{\boldsymbol{p}!} \mathrm{per}\left(\boldsymbol{A}^{-1}[\boldsymbol{p}|\boldsymbol{\alpha}]\right) \left(\hat{\boldsymbol{a}}^\dagger\right)^{\boldsymbol{p}} |\boldsymbol{0}\rangle \\ & \times \langle\boldsymbol{0}| \sum_{\boldsymbol{q}\in R_{M,N_\mathrm{p}}} \frac{1}{\boldsymbol{q}!} \mathrm{per}\left(\left(\boldsymbol{A}^*\right)^{-1}[\boldsymbol{q}|\boldsymbol{\beta}]\right) \left(\hat{\boldsymbol{a}}\right)^{\boldsymbol{q}} . \end{aligned} \tag{4.95}$$

The Hilbert space states constructed by

$$\sum_{\boldsymbol{p}\in R_{M,N_\mathrm{p}}} \frac{1}{\boldsymbol{p}!} \mathrm{per}\left(\boldsymbol{A}^{-1}[\boldsymbol{p}|\boldsymbol{\alpha}]\right) \left(\hat{\boldsymbol{a}}^\dagger\right)^{\boldsymbol{p}} |\boldsymbol{0}\rangle \,, \tag{4.96}$$

when summing over all multiindices $\boldsymbol{\alpha}$, are exactly the eigenstates of the effective Hamiltonian $\hat{H}_\mathrm{eff}$ with its eigenvector matrix $\boldsymbol{A}$. This shows that the passive system can be described by $\hat{H}_{\text{eff}}$ as long as the initial state has $N_{\text{p}}$ photons and all measurements are restricted to the $N_{\text{p}}$-photon subspace. A more thorough explanation as to why this is the case can be found when examining the algebraic structure of the system more closely. This will be done in the following section.

## 4.4. Wei-Norman expansion

The second approach to solve Eq. (4.22) is based on the Wei-Norman expansion [146], which is rooted in a thorough Lie algebraic analysis. It is a method to solve first-order differential equations such as Eq. (4.22) when the generator, in our case the Liouvillian, has the form

$$\mathcal{L}(z) = \sum_{k=1}^{m} c_k(z)\, X_k\,, \tag{4.97}$$

where the $X_k$ constitute a set of constant operators. If necessary this set of operators can be closed under commutation by addition of suitable operators resulting in a set $\{X_k\}_{k=1}^{n}$ with $n \geq m$. As we have already discussed in the beginning of Sec. 4.2 the relevant operators are in our case the set of bilinear superoperators, i.e.

$$\{X_k\}_{k=1}^{n} = \{L_i^+ L_j^-\,, R_i^+ R_j^-\,, L_i^- R_j^-\}_{i,j=1}^{M}\,, \tag{4.98}$$

see discussion leading to Eq. (4.39).

With a closed algebra spanning the generator $\mathcal{L}$ at hand, the evolution operator of the first-order differential equation under study is a product of individual exponentials [146]

$$\mathcal{U}(z) = \prod_{k=1}^{n} \mathcal{U}_k(z) = \prod_{k=1}^{n} \mathrm{e}^{g_k(z)\, X_k}\,, \tag{4.99}$$

with initial condition $\mathcal{U}(0) = \mathbb{1}_{\mathcal{L}}$. Differentiating the ansatz (4.99) leads to

$$\partial_z \mathcal{U}(z) = \partial_z \left( \prod_{k=1}^{n} \mathrm{e}^{g_k(z)\, X_k} \right) = \sum_{i=1}^{n} \partial_z g_i \prod_{p=1}^{i-1} \mathrm{e}^{g_p\, X_p} X_i \prod_{q=i}^{n} \mathrm{e}^{g_q\, X_q}\,. \tag{4.100}$$

In order to compare this to the original first-order differential equation, in our case Eq. (4.22), the operators $X_i$ have to be shifted to the left which can be accomplished with the help of the exponential operator expression (4.78) using the adjoint action. The result is a set of nonlinear differential equations for the functions $g_k(z)$

$$\boldsymbol{c} = \boldsymbol{M} \partial_z \boldsymbol{g}, \tag{4.101}$$

where $\boldsymbol{c}$ is the vector of expansion coefficents in Eq. (4.97). The matrix $\boldsymbol{M}$ generally depends on the functions $g_k(z)$ and also on the structure constants of the underlying algebra because of the use of the adjoint action in its derivation.

Similar to other, related schemes, like the Magnus expansion [147], the Wei-Norman method does not always yield a solution to any given problem . For general algebras one can check whether the matrix $\boldsymbol{M}$ is invertible. This yields solutions in at least a neighbourhood of the initial condition. However, due to the connection of the matrix $\boldsymbol{M}$ to the structure constants there is a direct link between the solvability of Eq. (4.101) and the algebraic structure of the operators $X_k$. For example, solvable Lie algebras, as their name suggests, always lead to an integrable set of nonlinear differential equations for the $g_k(z)$. This is because, for solvable algebras, there exists a chain of ideals resulting in a triangular form of $\boldsymbol{M}$ with nonvanishing diagonal [148]. In case that the algebra is not solvable one constructs its Levi decomposition into a solvable part and a remaining semisimple subalgebra [137; 146], see discussion at the beginning of Section 4.2. Following the Levi decomposition, the generator is also split as $\mathcal{L} = \mathcal{L}_{\mathrm{R}} + \mathcal{L}_{\mathrm{S}}$, i.e. in a part $\mathcal{L}_{\mathrm{R}}$ spanned by the operators of the solvable subalgebra (also called the radical) and a part $\mathcal{L}_{\mathrm{S}}$ spanned by the operators of the semisimple subalgebra. Accordingly, the evolution operator then becomes a product $\mathcal{U} = \mathcal{U}_{\mathrm{S}}\,\mathcal{U}_{\mathrm{R}}$ where each part obeys a separate differential equation

$$\partial_z \mathcal{U}_{\mathrm{S}} = \mathcal{L}_{\mathrm{S}}\,\mathcal{U}_{\mathrm{S}}\,, \tag{4.102}$$

$$\partial_z \mathcal{U}_{\mathrm{R}} = \big(\mathcal{U}_{\mathrm{S}}^{-1}\,\mathcal{L}_{\mathrm{R}}\,\mathcal{U}_{\mathrm{S}}\big)\,\mathcal{U}_{\mathrm{R}}\,. \tag{4.103}$$

The solvable part $\mathcal{U}_{\mathrm{R}}$ is easily integrated once the semisimple part is solved and $\mathcal{U}_{\mathrm{S}}^{-1}\,\mathcal{L}_{\mathrm{R}}\,\mathcal{U}_{\mathrm{S}}$ is calculated. Thus, the actual difficulty is usually to find the solution for the semisimple subalgebra. In the Section 5.2 we show such a solution for a lossy two-waveguide system.

From the above outline of the Wei-Norman expansion it is clear that the important task is the analysis of the Lie algebraic structure induced by $\mathcal{L}$. In case of the lossy oscillator system, the operators $X_k$ are drawn from the set $\{L_i^+ L_j^-, R_i^+ R_j^-, L_i^- R_j^-\}$ with $i, j = 1, \ldots, M$. Their decomposition can be found using the approach via the Cartan-Killing form (4.25) following the Hilbert space example, see Eqs. (4.29)-(4.32). The resulting decomposition reads

$$\begin{aligned}&\underbrace{\overbrace{\{L_i^- R_j^-\}}^{\text{nilpotent}} \oplus \overbrace{\{\textstyle\sum_k L_k^+ L_k^-\} \oplus \{\textstyle\sum_k R_k^+ R_k^-\}}^{\text{Abelian}}}_{\text{solvable (radical)}}\\ &\qquad \oplus \underbrace{\overbrace{\{L_k^+ L_k^- - L_{k+1}^+ L_{k+1}^-, L_i^+ L_{j\neq i}^-\}}^{\text{simple}} \oplus \overbrace{\{R_k^+ R_k^- - R_{k+1}^+ R_{k+1}^-, R_i^+ R_{j\neq i}^-\}}^{\text{simple}}}_{\text{semisimple}}\,.\end{aligned} \tag{4.104}$$

The nilpotent subalgebra $\{L_i^- R_j^-\}$ is to be understood as containing all combinations of indices $i, j = 1, \ldots, M$ and is responsible for removing excitations from the waveguide modes. The Abelian part contains the sum over all number operators, acting from the left and the right. Therefore, they indicate the total number of photons in the bra- or ket-states and are linked to the mean propagation constant and mean loss. Together, both parts form the solvable subalgebra. Note that we already split the Abelian subalgebra into subalgebras of the left and right actions as they always commute.

What is left are the difference operators, e.g. $L_k^+ L_k^- - L_{k+1}^+ L_{k+1}^-$, and the coupling operators $L_i^+ L_{j\neq i}^-$. These form two special linear Lie algebras $\mathfrak{sl}(M, \mathbb{C})$, one for the left and one for the right application, and together they create the semisimple subalgebra. Hence, this decomposition is very similar to the example of the two-mode bosonic operators. The main difference is that we now have duplicate Abelian and semisimple subalgebras for the left and right actions. This is because of the definition of the Liouville space as a product of Hilbert spaces.

An immediate result of this structure analysis is that the operators $L_i^- R_j^-$ of the nilpotent subalgebra are separated from the rest of the dynamics in the Wei-Norman expansion. In fact, the evolution superoperator $\mathcal{U} = \mathcal{U}_\mathrm{S}\mathcal{U}_\mathrm{R}$ can be written as

$$\mathcal{U}(z) = \underbrace{\overbrace{\prod_i \mathrm{e}^{g_i(z)\,X_i}}^{\text{semisimple}}}_{\mathcal{U}_\mathrm{S}} \underbrace{\overbrace{\prod_j \mathrm{e}^{g_j(z)\,X_j}}^{\text{Abelian}} \overbrace{\prod_k \mathrm{e}^{g_k(z)\,X_k}}^{\text{nilpotent}}}_{\mathcal{U}_\mathrm{R}} . \tag{4.105}$$

This is possible because the order of superoperators in $\mathcal{U}_\mathrm{R}$ is arbitrary as it always results in sets of equations that are integrable. When applied to an input state $|\hat{\rho}(0)\rangle\rangle$, the first action of $\mathcal{U}(z)$ in Eq. (4.105) is the removal of photons. Therefore, the quantum state upon which the rest of $\mathcal{U}(z)$ acts can be written as a sum of states with different photon numbers, i.e.

$$\overbrace{\prod_k \mathrm{e}^{g_k(z)\,X_k}}^{\text{nilpotent}} |\hat{\rho}(0)\rangle\rangle = \sum_{i=0}^{N_\mathrm{p}} w_i(z)\, |\hat{\rho}_{N_\mathrm{p}-i}\rangle\rangle\,, \tag{4.106}$$

where $N_\mathrm{p}$ is, again, the maximal photon number of the initial state and the $w_i(z)$ are norm-preserving weights. The remainder of $\mathcal{U}(z)$ contains the separate left and right applications of the Abelian and simple algebras $\mathfrak{sl}(M, \mathbb{C})$. Together these are simply left and right applications of the underlying effective non-Hermitian Hamiltonian. This is because the superoperators $L_i^- R_j^-$, which span the nilpotent subalgebra, represent all operations that stem from the quantum jump terms $\hat{a}_k\,\hat{\rho}\,\hat{a}_k^\dagger$ of the master equation (4.13). Removing these terms allows to rewrite the Lindblad master equation (4.13) as

$$\partial_z \hat{\rho} = -\mathrm{i}\,\hat{H}_\mathrm{eff}\,\hat{\rho} + \mathrm{i}\,\hat{\rho}\,\hat{H}_\mathrm{eff}^\dagger\,. \tag{4.107}$$

This is the von-Neumann equation one would derive from the non-Hermitian Schrödinger equation

$$\mathrm{i}\,\partial_z|\psi\rangle = \hat{H}_\mathrm{eff}\,|\psi\rangle\,. \tag{4.108}$$

Hence, when the dynamics is restricted to the $N_\mathrm{p}$-photon subspace, the same results for the observables are obtained when directly using the underlying effective Hamiltonian $\hat{H}_\mathrm{eff}$. Note that there are two conditions for this restriction to the highest-photon-number subspace: First, the initial state has to be an element of only this subspace and not of any subspaces with less photons. Second, all measurements have to be postselected to the highest photon number $N_\mathrm{p}$. This confirms the result from the end of Section 4.3.1, where

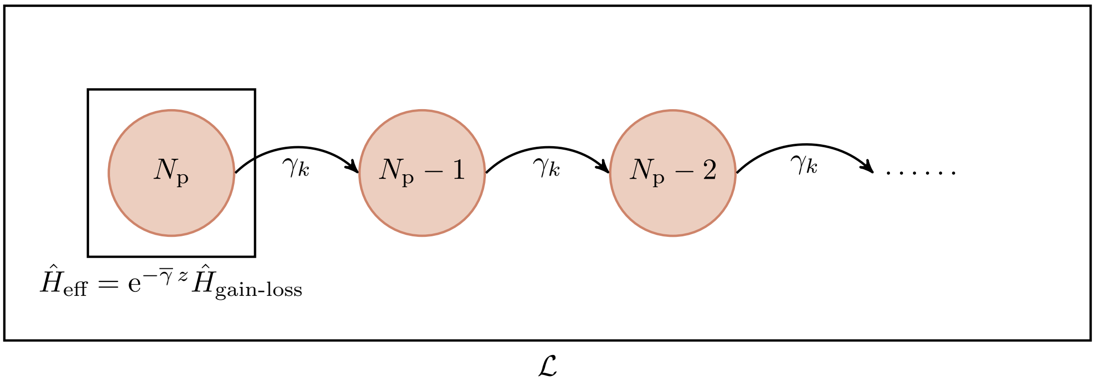

Fig. 4.2.: Illustration of a decomposed evolution under the Liouvillian of Eq. (4.21). The whole dynamic is determined by the Liouvillian $\mathcal{L}$ with loss-induced quantum jumps from higher to lower photon number subspaces and additional dynamics inside these subspaces. When the initial state and measurements are restricted to the highest-photon-number subspace the dynamic is solely described by $\hat{H}_\mathrm{eff}$. This effective non-Hermitian Hamiltonian can further be decomposed into a prefactor of the mean loss $\overline{\gamma}$ and a Hamiltonian $\hat{H}_\text{gain-loss}$ of an equivalent gain-loss profile.

we saw that the eigenvectors of the Liouvillian $\mathcal{L}$ contained the eigenstates of $\hat{H}_\mathrm{eff}$ under the restriction that the dynamics be confined to the $N_\mathrm{p}$-photon subspace.

In addition, another interesting fact of the algebraic structure in Eq. (4.104) is that the Abelian subalgebra is separated from the simple $\mathfrak{sl}(M, \mathbb{C})$ subalgebras. As a result, an overall exponential factor containing the mean propagation constant and, more importantly, the mean loss of the system can be separated from the underlying dynamics. Physically, this means that an active non-Hermitian system with loss and gain can be simulated by an all-loss passive system if the dynamics is restricted to the highest-photon-number subspace. The loss profile of the passive system then has to equal the desired gain-loss profile plus the mean loss, effectively amounting to a shift of the gain-loss scale. Therefore, one can study the dynamics of a gain-loss profile with effective non-Hermitian Hamiltonian $\hat{H}_\text{gain-loss}$ by implementing an equivalent passive system with postselected measurements. This is similar to the approach used in classical passive $\mathcal{PT}$ systems where the open system is correctly described by the effective non-Hermitian Hamiltonian alone, see e.g. Ref. [77]. However, we iterate that this requires for quantum measurements a postselection to the highest-photon-number subspace as was done in Refs. [81; 82].

A scheme of the decomposition can be seen in Fig. 4.2. The whole evolution is governed by the Liouvillian $\mathcal{L}$ of the lossy waveguide system, cf. Eq. (4.21). In this evolution, subspaces with higher photon numbers feed into subspaces with lower photon numbers via quantum jumps. These quantum jumps are one-photon losses in the individual waveguides with loss rates $\gamma_k$. When the initial state and all measurements are restricted to the subspace with highest photon number $N_\mathrm{p}$, the system can be described directly by the effective non-Hermitian Hamiltonian $\hat{H}_\mathrm{eff}$. This Hamiltonian can additionally be decomposed into an exponential decay factor with the mean loss $\overline{\gamma}$ and a Hamiltonian $\hat{H}_{\text{gain-loss}}$. This is the effective non-Hermitian Hamiltonian of an equivalent active $\mathcal{PT}$ system with a balanced gain-loss distribution.

### Summary

In this chapter, we applied the theory of open quantum systems to integrated photonic waveguides that experience losses. It was argued that the loss of photons scattered from the slowly varying waveguides during the paraxial propagation is well described in the Born-Markov approximations, see Section 4.1.2. This lead to the formulation of a Lindblad-type quantum master equation for the coupled waveguides, cf. Eq. (4.10). Two solution strategies were developed by elevating the problem to the Liouville space and closely inspecting the Lie algebras induced by the resulting Liouvillian superoperator in Eq. (4.21). First, an eigendecomposition of the evolution with abstract, Fock-like eigenvectors of the Liouvillian, cf. Eq. (4.82), which is valid for $z$-independent system parameters. The eigendecomposition is based on ladder operators derived from the regular representation of the Liouvillian in Eq. (4.41), see Section 4.3.1. Second, a Wei-Norman operator expansion of the evolution, cf. Eq. (4.105). It is applicable to waveguides with $z$-dependent parameters and fundamentally relies on the decomposition of the algebra as given in Eq. (4.104).

Both approaches consistently showed that the evolution under the quantum master equation can directly be described by an effective non-Hermitian Hamiltonian under the following constraints: The input state is only element of the highest-photon-number subspace and all measurements are postselected to this subspace. This result is most prominently seen in the structure analysis in Eq. (4.104) and the resulting Wei-Norman expansion in Eq. (4.105). Here, the photon-removing operations are clearly separated from the dynamics of the underlying effective non-Hermitian Hamiltonian. Furthermore, the mean propagation constant and mean loss can also be separated. This gives a thorough explanation as to why passive systems, like the lossy photonic waveguides, can be used to study active non-Hermitian Hamiltonians in the quantum regime. More importantly, it shows the limitations of this approach because it always requires a postselection to the highest-photon-number subspace.

Fortunately, both solutions, eigendecomposition and Wei-Norman expansion, allow the formulation of full quantum solutions of the quantum master equation. This enables the investigation of arbitrary quantum effects in lossy waveguide systems without the restriction to postselected measurements. In the following chapter, we will showcase these two approaches at the hands of the instructive two-waveguide $\mathcal{PT}$-symmetric coupler to elucidate details of the calculations.

# 5. The $\mathcal{PT}$-symmetric coupler

The solutions for the quantum master equation of a lossy waveguide system, as discussed in the last chapter, allow us to investigate non-Hermitian physics in a well-controlled environment. A simple yet intriguing example is the passive $\mathcal{PT}$-symmetric coupler consisting of two coupled waveguides where one experiences loss [82]. This is the passive version of a two-site system with balanced loss and gain, cf. left part of Fig. 5.1. It is invariant under exchange of both sites (parity transformation $\mathcal{P}$) and mutual exchange of gain and loss ($\mathrm{i} \to -\mathrm{i}$ or time-reversal transformation $\mathcal{T}$). Hamiltonians of such $\mathcal{PT}$-symmetric systems are quasi-Hermitian: Despite their non-Hermiticity they have a real spectrum, as shown by Bender and Boettcher in their seminal paper [73]. The same fundamental physics is present in the all-loss version where, instead of balanced gain and loss, one site has twice the loss rate, cf. right part of Fig. 5.1. When subtracting the mean loss the same gain-loss profile emerges which leads to the assumption that both systems are equal apart from the mean loss factor. In the last chapter this separation was confirmed from the algebraic decomposition of the Liouvillian $\mathcal{L}$ of the quantum master equation. In the following, we apply the solutions derived in Chapter 4 to the lossy, two-waveguide system in order to illustrate their explicit use.

## 5.1. Solution via eigendecomposition

As seen in the last chapter it is pivotal to find the eigendecomposition of the matrix representation $-\mathrm{i}\boldsymbol{H}_{\mathrm{eff}}$ of the the underlying effective non-Hermitian Hamiltonian $-\mathrm{i}\hat{H}_{\mathrm{eff}}$ in order to find the eigendecomposition of the Liouvillian $\mathcal{L}$. For two waveguides with

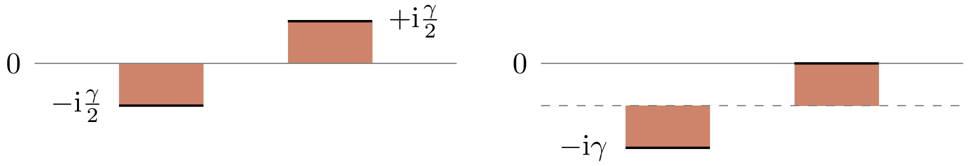

Fig. 5.1.: Comparison of active and passive $\mathcal{PT}$ couplers. (Left) The active coupler consisting of two sites with balanced gain and loss of $\pm\mathrm{i}\gamma/2$. (Right) The passive coupler with one lossless site and one with loss $-\mathrm{i}\gamma$. With respect to the mean loss $-\mathrm{i}\gamma/2$ (grey, dashed line), the passive coupler has the same profile as the active coupler.

mutual coupling $\kappa$ and where the first one experiences loss $\gamma$, the matrix $-\mathrm{i}\boldsymbol{H}_{\text{eff}}$ reads

$$-\mathrm{i}\boldsymbol{H}_{\text{eff}} = \begin{pmatrix} -\gamma & -\mathrm{i}\kappa \\ -\mathrm{i}\kappa & 0 \end{pmatrix} . \tag{5.1}$$

Because this is a non-Hermitian operator its eigensystem is, in general, biorthogonal [61; 62]. This means the right and left eigenvector can differ in contrast to the more familiar Hermitian case. The right eigenvectors $|v_i\rangle$ are given by the usual eigenequation

$$-\mathrm{i}\boldsymbol{H}_{\text{eff}}|v_i\rangle = \lambda_i|v_i\rangle \,, \tag{5.2}$$

whereas the left eigenvectors $\langle w_i|$ are derived from

$$\langle w_i|\,(-\mathrm{i}\boldsymbol{H}_{\text{eff}}) = \lambda_i\langle w_i| \,, \tag{5.3}$$

which can be reformulated for the kets $|w_i\rangle = \langle w_i|^\dagger$ as

$$(-\mathrm{i}\boldsymbol{H}_{\text{eff}})^\dagger\,|w_i\rangle = \lambda_i^*|w_i\rangle \,. \tag{5.4}$$

Solving these equations for the representation in Eq. (5.1), the eigenvalues of $-\mathrm{i}\boldsymbol{H}_{\text{eff}}$ are

$$\lambda_1 = \frac{1}{2}\,(-\gamma + \mathrm{i}\,\Omega) \,, \tag{5.5}$$

$$\lambda_2 = \frac{1}{2}\,(-\gamma - \mathrm{i}\,\Omega) \,, \tag{5.6}$$

where

$$\Omega = \sqrt{4\,\kappa^2 - \gamma^2} \,. \tag{5.7}$$

The respective unnormalised right and left eigenvectors are

$$|v_{1,2}\rangle = \left(\frac{\mathrm{i}\,\lambda_{1,2}}{\kappa}, 1\right)^{\mathrm{T}} \,, \tag{5.8}$$

$$\langle w_{1,2}| = \left(\frac{\mathrm{i}\,\lambda_{1,2}}{\kappa}, 1\right) . \tag{5.9}$$

At first glance these left and right eigenvectors seem equal but are, in fact, different due to the missing complex conjugation in $\langle w_{1,2}|$ leading to $\langle w_{1,2}|^\dagger = |w_{1,2}\rangle \neq |v_{1,2}\rangle$. Nonetheless, they still form a biorthogonal basis. As a test, it is straightforward to show that eigenvectors of different indices are indeed orthogonal, i.e.

$$\langle w_i|v_j\rangle = \begin{cases} 0 & \text{for } i \neq j \\ \frac{2\,\Omega\,(\Omega + \mathrm{i}\,\gamma)}{4\,\kappa^2} & \text{for } i = j = 1 \\ \frac{2\,\Omega\,(\Omega - \mathrm{i}\,\gamma)}{4\,\kappa^2} & \text{for } i = j = 2 \end{cases} . \tag{5.10}$$

Note that the complex conjugation (usually performed as an extra step in calculating the inner product) is already included in the bra-ket notation which satisfies the inner product relation $\langle w_i|v_j\rangle = \langle v_j|w_i\rangle^*$.

From Eq. (5.7) it is clear that $\Omega \in \mathbb{R}$ as long as $\gamma < 2\kappa$. Under this condition the eigenvalues of $-\mathrm{i}\boldsymbol{H}_{\text{eff}}$ are completely imaginary (apart from the overall mean loss $\gamma/2$), which translates to a real spectrum for the Hamiltonian $\hat{H}_{\text{eff}}$. This regime, where the Hamiltonian is quasi-Hermitian, is the $\mathcal{PT}$-symmetric phase of the system. Here, the system undergoes a coherent evolution, again apart from the mean loss. For $\gamma > 2\kappa$, however, the $\mathcal{PT}$ symmetry is broken and the system transitions to two modes decaying with rates $\frac{\gamma}{2} \pm |\Omega|$. The transition point $\gamma = 2\kappa$ from $\mathcal{PT}$ to $\mathcal{PT}$-broken symmetry is the exceptional point (EP). It earned its name due to its unconventional properties, which stem not only from the degeneracy of the spectrum but also from the simultaneous coalescence of the eigenvectors, cf. Eqs. (5.8) and (5.9). As seen from the eigenvalues in Eqs. (5.5) and (5.6), the degeneracy follows a square-root law in contrast to linear changes in Hermitian degeneracies [71]. The self-orthogonality at the EP, $\langle w_i|v_i\rangle_{\text{EP}} = 0$, is also a feature not present in Hermitian physics. It leads, for example, to an excess-noise factor known as the Petermann factor [87]. Therefore, probing non-Hermitian systems at or in the vicinity of their EPs promises insight into interesting effects not covered by conventional Hermitian physics.

When excluding the EP, $\Omega \neq 0$, we can derive the eigendecomposition of $\mathcal{R}'(\mathcal{L})$ from the eigensystem of $-\mathrm{i}\boldsymbol{H}_{\text{eff}}$ as outlined in Section 4.3. The exclusion of the EP avoids singular behaviour as the matrix $\boldsymbol{H}_{\text{eff}}$ becomes defective and thus cannot be diagonalised. In that case, one would need to revert to the general Jordan decomposition of $\mathcal{R}'(\mathcal{L})$ as noted in Section 4.3.

We start with the eigenvalues of $\mathcal{R}'(\mathcal{L})$ which are, according to Eq. (4.49), given by the set

$$\{\lambda_1, \lambda_2, -\lambda_1^*, -\lambda_2^*, \lambda_1^*, \lambda_2^*, -\lambda_1, -\lambda_2\}\,. \tag{5.11}$$

In addition, we need the matrix $\boldsymbol{A}$ of normalised right eigenvectors of $-\mathrm{i}\boldsymbol{H}_{\text{eff}}$ in order to calculate the eigenvectors of $\mathcal{R}'(\mathcal{L})$. After using Eq. (5.10) to normalise the biorthogonal basis, the matrix $\boldsymbol{A}$ reads

$$\boldsymbol{A} = \begin{pmatrix} \frac{-\Omega-\mathrm{i}\gamma}{\sqrt{2\,\Omega\,(\Omega+\mathrm{i}\gamma)}} & \frac{\Omega-\mathrm{i}\gamma}{\sqrt{2\,\Omega\,(\Omega-\mathrm{i}\gamma)}} \\ \frac{2\,\kappa}{\sqrt{2\,\Omega(\Omega+\mathrm{i}\gamma)}} & \frac{2\,\kappa}{\sqrt{2\,\Omega\,(\Omega-\mathrm{i}\gamma)}} \end{pmatrix}. \tag{5.12}$$

The inverse $\boldsymbol{A}^{-1}$ then yields the expansion coefficients of the eigenvectors of the regular representation $\mathcal{R}'(\mathcal{L})$ according to Eq. (4.53). These eigenvectors are the two sets of bosonic ladder superoperators, the first being ($i = 1, 2$)

$$P_i^+ = \epsilon_i \left(L_1^+ - R_1^-\right) + \tau_i \left(L_2^+ - R_2^-\right)\,, \tag{5.13}$$

$$P_i^- = \epsilon_i\, L_1^- + \tau_i\, L_2^-\,, \tag{5.14}$$

and the second

$$Q_i^+ = \epsilon_i^* \left(R_1^+ - L_1^-\right) + \tau_i^* \left(R_2^+ - L_2^-\right)\,, \tag{5.15}$$

$$Q_i^- = \epsilon_i^*\, R_1^- + \tau_i^*\, R_2^-\,, \tag{5.16}$$

where

$$\begin{aligned} \epsilon_1 &= -\frac{\Omega + \mathrm{i}\,\gamma}{\sqrt{2\,\Omega\,(\Omega + \mathrm{i}\,\gamma)}}\,, \quad \tau_1 = \frac{2\,\kappa}{\sqrt{2\,\Omega\,(\Omega + \mathrm{i}\,\gamma)}}\,, \\ \epsilon_2 &= \frac{\Omega - \mathrm{i}\,\gamma}{\sqrt{2\,\Omega\,(\Omega - \mathrm{i}\,\gamma)}}\,, \quad \tau_2 = \frac{2\,\kappa}{\sqrt{2\,\Omega\,(\Omega - \mathrm{i}\,\gamma)}}\,. \end{aligned} \tag{5.17}$$

Based on the ladder superoperators $P_i^{\pm}$ and $Q_i^{\pm}$, we can now calculate the overlaps $\langle\langle \boldsymbol{\alpha}, \boldsymbol{\beta} | \hat{\rho}(0) \rangle\rangle$ and eigenvectors $|\boldsymbol{\alpha}, \boldsymbol{\beta}\rangle\rangle$ of the Liouvillian as required for the eigendecomposition solution (4.82) for a given input state $|\hat{\rho}(0)\rangle\rangle$. The overlap can be calculated using the definition of the Liouville space inner product, cf. Eq. (4.14), and the construction rule for the left eigenvectors of $\mathcal{L}$ in Eq. (4.68). The general expression reads

$$\langle\langle \boldsymbol{\alpha}, \boldsymbol{\beta} | \hat{\rho}(0) \rangle\rangle = \frac{\mathrm{Tr}\left( P_1^{-\,\alpha_1}\, P_2^{-\,\alpha_2}\, Q_1^{-\,\beta_1}\, Q_2^{-\,\beta_2}\, |\hat{\rho}(0)\rangle\rangle \right)}{\sqrt{\alpha_1!\,\beta_1!\,\alpha_2!\,\beta_2!}}\,. \tag{5.18}$$

This expression depends on the input state $|\hat{\rho}(0)\rangle\rangle$ and determines which eigenvectors $|\boldsymbol{\alpha}, \boldsymbol{\beta}\rangle\rangle$ have to be considered. Together with the exponential function involving the eigenvalues $\mu_{\boldsymbol{\alpha},\boldsymbol{\beta}}$ of $\mathcal{L}$ one can then calculate the evolved state and thus any observable.

As an example we consider the two-photon correlation for a Hong-Ou-Mandel (HOM) experiment [149], as was done in Ref. [82]. For the HOM experiment the initial state is $|\hat{\rho}(0)\rangle\rangle = |1,1\rangle\langle 1,1|$. Because this is a two-photon state the multiindices are limited by $|\boldsymbol{\alpha}|, |\boldsymbol{\beta}| \leq 2$ as all other overlaps require the removal of three or more photons. Under this restriction one still has to find all overlaps with combinations of multiindices $(0,0)$, $(1,0)$, $(0,1)$, $(2,0)$, $(1,1)$, and $(0,2)$. Fortunately, this number of combinations is reduced due to the symmetry and the simple form of the initial state, i.e. all overlaps with $|\boldsymbol{\alpha}| \neq |\boldsymbol{\beta}|$ are zero. This is because, on the one hand, the multiindex $\boldsymbol{\alpha}$ gives the number of superoperators $P_i^-$ that only contain annihilation operators acting from the left, cf. Eq. (5.14). On the other hand, the multiindex $\boldsymbol{\beta}$ gives the number of superoperators $Q_i^-$ that only contain annihilation operators acting from the right, cf. Eq. (5.16). Any unbalanced combination of multiindices, $|\boldsymbol{\alpha}| \neq |\boldsymbol{\beta}|$, therefore results in different photon numbers in the bras and kets after application to $|\hat{\rho}(0)\rangle\rangle = |1,1\rangle\langle 1,1|$ which then evaluates to zero under the trace operation. Hence, only multiindex combinations with $|\boldsymbol{\alpha}| = |\boldsymbol{\beta}|$ result in nonzero overlaps. For example, this means we have

$$\langle\langle (1,0), (0,0) | \hat{\rho}(0) \rangle\rangle = 0\,, \tag{5.19}$$

$$\langle\langle (1,0), (1,0) | \hat{\rho}(0) \rangle\rangle = |\epsilon_1|^2 + |\tau_1|^2\,. \tag{5.20}$$

Once the nonzero overlaps are known the associated eigenvectors can be calculated with one example being

$$\begin{aligned} |(1,0),(1,0)\rangle\rangle &= \frac{1}{\sqrt{1!\,0!\,1!\,0!}} P_1^+ Q_1^+ |0\rangle\rangle \\ &= |\epsilon_1|^2 \Big( |10\rangle\langle 10| - |00\rangle\langle 00| \Big) + \epsilon_1\, \tau_1^*\, |10\rangle\langle 01| \\ &+ \epsilon_1^*\, \tau_1\, |01\rangle\langle 10| + |\tau_1|^2 \Big( |01\rangle\langle 01| - |00\rangle\langle 00| \Big)\,. \end{aligned} \tag{5.21}$$

This allows, in principle, to calculate the full quantum state $|\hat{\rho}(z)\rangle\rangle$ evolving from the initial state $|\hat{\rho}(0)\rangle\rangle = |1,1\rangle\langle 1,1|$. However, for a HOM experiment we are only interested in the two-photon coincidence rate $\Gamma = \langle \hat{a}_1^\dagger \hat{a}_2^\dagger \hat{a}_1 \hat{a}_2 \rangle$ [149] and so we can reduce the number of necessary eigenvectors even further. More precisely, we only need the $|1,1\rangle\langle 1,1|$-propability of the full quantum state, which can only emerge from the eigenvectors with $|\boldsymbol{\alpha}|, |\boldsymbol{\beta}| = 2$. These are nine eigenvectors with combinations of multiindices $\boldsymbol{\alpha}, \boldsymbol{\beta} \in \{(2,0),(1,1),(0,2)\}$ that are listed in the Appendix C together with their overlaps. The only missing pieces are then the respective eigenvalues $\mu_{\boldsymbol{\alpha},\boldsymbol{\beta}} = \boldsymbol{\alpha}\cdot\boldsymbol{\lambda} + \boldsymbol{\alpha}\cdot\boldsymbol{\lambda}^*$. Plugging everything into the solution in Eq. (4.82), the result can be interpreted as a Fourier series with frequencies $\exp(\pm n\,\mathrm{i}\,\Omega\, z)$ $(n = 0,1,2)$ and amplitudes as functions of the $\epsilon_i$ and $\tau_i$. The analytical result of this Fourier series for the two-photon coincidence rate is

$$\Gamma = \mathrm{e}^{-2\gamma z}\left(\frac{4\kappa^2\cos(\Omega z) - \gamma^2}{\Omega^2}\right)^2 . \tag{5.22}$$

In the original HOM experiment a 50:50 beam splitter made from a semitransparent mirror is used, resulting in bunching ($\Gamma = 0$) at the output ports [149]. For the waveguide coupler the splitting ratio depends on the total propagation length and in the lossless case, i.e. $\gamma = 0$, one can deduce from Eq. (5.22) that

$$\Gamma = \cos^2(2\,\kappa z) \tag{5.23}$$

with bunching first occuring at $\kappa z = \pi/4$. In the lossy case, this bunching point, where the two photons leave the system together from the same waveguide, is shifted due to the influence of the loss $\gamma$. In Fig. 5.2, the coincidence rates for two values of the loss $\gamma$ are plotted against the scaled propagation length $\kappa z$. In the Hermitian case $\gamma = 0$, the well-known result from the HOM experiment is reproduced. With increased non-Hermiticity, however, the bunching is shifted to shorter values of $\kappa z$ with one example $\gamma = \kappa$ shown. The red area indicates the maximal extend of the shift down to $\kappa z = 1/\sqrt{2}$, for which the system is in the $\mathcal{PT}$ phase ($\gamma < 2\kappa$). In Ref. [82], these predictions were experimentally confirmed.

The above example showcases the use of the solution (4.82) based on the eigendecomposition of the regular representation $\mathcal{R}'(\mathcal{L})$. It allows to calculate analytical expressions for the evolved quantum state for few photons and modes by hand. However, this is rather limited because the involved diagonalisation quickly becomes tedious for more than two modes. Also the Liouville space eigenstates $|\boldsymbol{\alpha},\boldsymbol{\beta}\rangle\rangle$ become hard to calculate by hand for larger photon numbers. Nevertheless, the outlined steps could easily be implemented numerically. For a waveguide system of constant parameters this allows the study of larger numbers of photons and modes [150].

Furthermore, we would like to reiterate that, although we excluded the case $\gamma = 2\kappa$ in the example above, the solution can generally be calculated at the EP using the eigendecomposition of the regular representation. When the eigenvectors coalesce at the EP the matrix $\mathcal{R}'(\mathcal{L})$ becomes defective and cannot be diagonalised. Instead one has to construct its Jordan normal form. For this form there exists a complete basis of generalised eigenvectors, which can be used for an eigendecomposition. However, the direct link between the

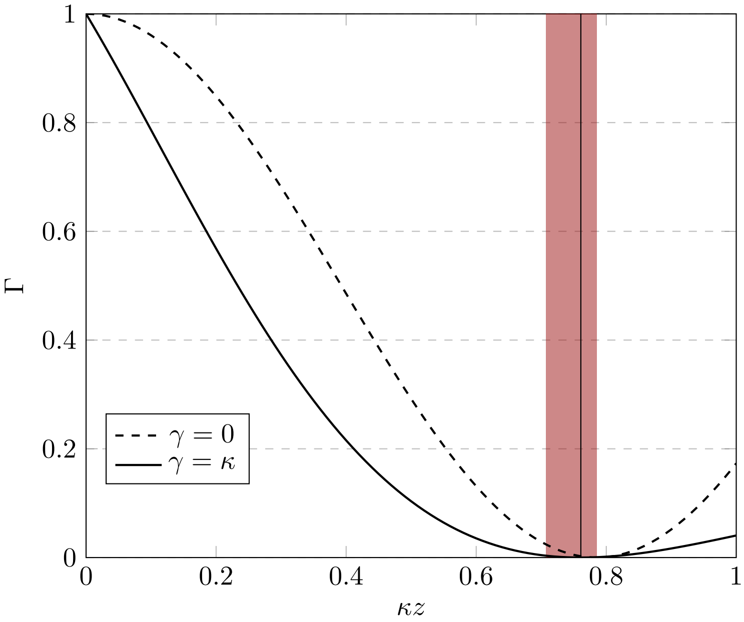

Fig. 5.2.: The coincidence function in Eq. (5.22) of the $\mathcal{PT}$ coupler with an initial state $\hat{\rho}(0) = |1,1\rangle\langle 1,1|$. In the Hermitian case ($\gamma = 0$, dashed) the bunching occurs at $\kappa z = \pi/4$. In the $\mathcal{PT}$-symmetric case with $\gamma = \kappa$ (solid line) the bunching is shifted to smaller $\kappa z$. The black vertical line indicates the position of the shifted bunching ($\Gamma = 0$). The red area shows the possible range of the shift for which the system is still $\mathcal{PT}$-symmetric, i.e. $\gamma < 2\kappa$.

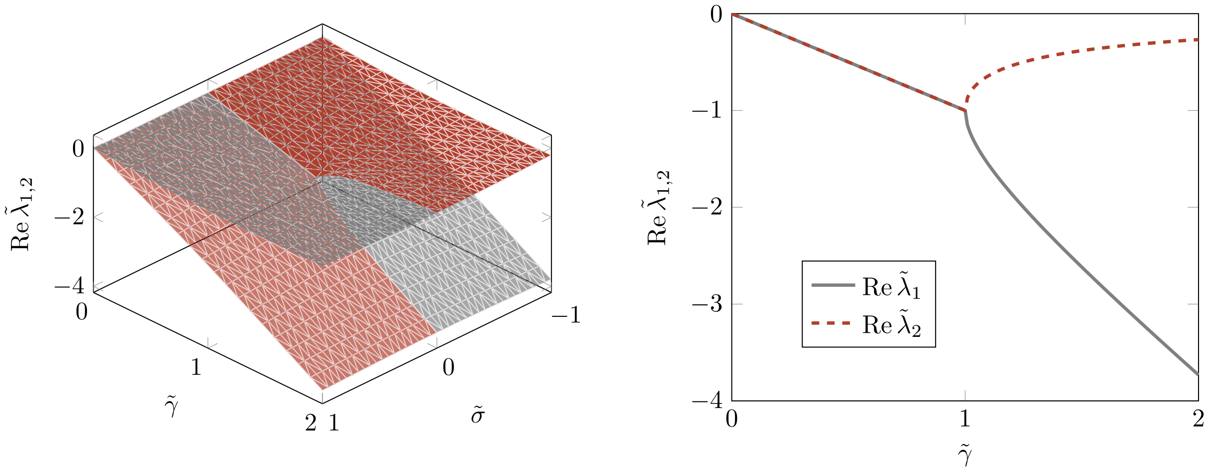

Fig. 5.3.: Real part of scaled eigenvalues $\tilde{\lambda}_1$ (grey) and $\tilde{\lambda}_2$ (red). Left as 3D surface with variable $\tilde{\sigma}$ and $\tilde{\gamma}$, right the curves for $\tilde{\sigma} = 0$. The EP, where the eigenvectors coalesce, occurs when $\tilde{\sigma} = 0$ and $\tilde{\gamma} = 1$.

eigensystems of $\boldsymbol{H}_{\text{eff}}$ and $\mathcal{R}'(\mathcal{L})$ is broken as the simple eigenequations (4.47) and (4.48) no longer hold for the generalised eigenvectors. Therefore, the generalised eigenvectors of $\mathcal{R}'(\mathcal{L})$ can no longer be calculated from those of $\boldsymbol{H}_{\text{eff}}$. Consequently, one has to find the Jordan normal form of $\mathcal{R}'(\mathcal{L})$ directly without the shortcut of constructing it from the eigensystem of $\boldsymbol{H}_{\text{eff}}$. However, finding the Jordan normal form with its generalised eigenvectors is generally possible. A simple Hilbert-space example of how to find the Jordan normal form of a regular representation and use it to formulate solutions for the two-photon coincidence $\Gamma$ at the EP is presented in Appendix D.

Another interesting aspect of the solution (4.82), which was shortly discussed in a general sense in the Section 4.3, is that the eigendecomposition allows to analyse the transport properties in a similar fashion as for Hermitian systems in Hilbert space. The key point was that depending on the multiindices $\boldsymbol{\alpha}$ and $\boldsymbol{\beta}$ the eigenvectors $|\boldsymbol{\alpha}, \boldsymbol{\beta}\rangle\rangle$ have different losses, i.e. real parts of their eigenvalues $\mu_{\boldsymbol{\alpha},\boldsymbol{\beta}} = \boldsymbol{\alpha} \cdot \boldsymbol{\lambda} + \boldsymbol{\beta} \cdot \boldsymbol{\lambda}^*$. Hence, a close examination of the fundamental eigenvalues $\lambda_i$ allows to estimate the propagation of a given input state. This can now be explicitly seen at the example of the $\mathcal{PT}$ coupler. In order to widen the scope we also add a detuning $\sigma_1 = \sigma$ to the first waveguide. This amounts to a replacement $\gamma + \mathrm{i}\sigma$ in all the above equations, e.g. for the eigenvalues in Eqs. (5.5) and (5.6) as well as for the coefficients $\epsilon_i$ and $\tau_i$. In this case, with the added detuning and additional normalisation by the coupling $\kappa$, the two fundamental eigenvalues are

$$\tilde{\lambda}_1 = -\tilde{\gamma} - \mathrm{i}\,\tilde{\sigma} + \mathrm{i}\,\sqrt{1 - (\tilde{\gamma} + \mathrm{i}\tilde{\sigma})^2}, \tag{5.24}$$

$$\tilde{\lambda}_2 = -\tilde{\gamma} - \mathrm{i}\,\tilde{\sigma} - \mathrm{i}\,\sqrt{1 - (\tilde{\gamma} + \mathrm{i}\tilde{\sigma})^2} \tag{5.25}$$

where we defined the scaled quantities $\tilde{\gamma} = \gamma/(2\kappa)$ and $\tilde{\sigma} = \sigma/(2\kappa)$.

In Fig. 5.3 we plotted the real parts of the scaled eigenvalues $\tilde{\lambda}_{1,2}$ that are responsible for the loss of the system. The left panel of Fig. 5.3 shows the 3D plot for $\tilde{\gamma}$ and $\tilde{\sigma}$ whereas the right panel shows specifically the case $\tilde{\sigma} = 0$. The latter is the usual spectrum of a two-mode classical $\mathcal{PT}$ system as shown for example in Refs. [151; 75; 72]. However, here the spectrum is tilted by the linear term $-\tilde{\gamma}$ which is the mean loss of the passive $\mathcal{PT}$ system. Nevertheless, the main features are the same and that is a degeneracy of the real parts for $\tilde{\gamma} < 1$, the $\mathcal{PT}$ phase, and a splitting for $\tilde{\gamma} > 1$, the $\mathcal{PT}$-broken phase.

In the $\mathcal{PT}$-broken phase, where $|\mathrm{Re}\,\tilde{\lambda}_2| < |\mathrm{Re}\,\tilde{\lambda}_1|$, this means that eigenvectors $|\boldsymbol{\alpha}, \boldsymbol{\beta}\rangle\rangle$ with $\alpha_2 > \alpha_1$ and $\beta_2 > \beta_1$ are not as strongly damped as eigenvectors with $\alpha_2 < \alpha_1$ and $\beta_2 < \beta_1$. Therefore, input states that have larger overlaps with the eigenvectors where $\alpha_2 > \alpha_1$ and $\beta_2 > \beta_1$ are less susceptible to loss. In the left panel of Fig. 5.3 the general picture with varying $\tilde{\sigma}$ is shown where for $\tilde{\sigma} \neq 0$ one eigenvalue always has a lower loss and subsequently is more favourable for transmission than the other. However, as we have seen by now, the Liouville space solution is similar to the familiar Hilbert space treatment yet not exactly identical. Most importantly the eigenvectors $|\boldsymbol{\alpha}, \boldsymbol{\beta}\rangle\rangle$ are not physical modes themselves, cf. Eq. (4.86). Consequently, the physical modes, or states, first have to be constructed from the $|\boldsymbol{\alpha}, \boldsymbol{\beta}\rangle\rangle$ and thus the eigenmode analysis to find perfect transmission is not as straightforward.

In order to show how to deal with these differences, we consider the two-mode case with one photon, for which the multiindices are restricted by $\alpha_1 + \alpha_2 \leq 1$ and $\beta_1 + \beta_2 \leq 1$. We suppose that the eigenvalues fulfil $|\mathrm{Re}\,\tilde{\lambda}_1| < |\mathrm{Re}\,\tilde{\lambda}_2|$, which is achieved by setting $\tilde{\sigma} < 0$. For an ideal transport with lowest losses we thus have to construct a quantum state from only those Liouvillian eigenvectors with $\alpha_1, \beta_1 \leq 1$ and $\alpha_2 = \beta_2 = 0$. The most general initial state in Liouville space is then

$$|\hat{\rho}(0)\rangle\rangle = h_1|(1,0),(1,0)\rangle\rangle + h_2|(1,0),(0,0)\rangle\rangle + h_3|(0,0),(1,0)\rangle\rangle + h_4|(0,0),(0,0)\rangle\rangle\,. \tag{5.26}$$

The coefficients $h_k$ are the overlaps $\langle\langle\boldsymbol{\alpha}, \boldsymbol{\beta}|\hat{\rho}(0)\rangle\rangle$ and parametrise all quantum states that experience lowest losses.

However, the coefficients $h_k$ cannot be chosen arbitrarily but have to obey a set of constraints for $\hat{\rho}(0)$ to be a proper density operator. First, we have the conservation of probability $\mathrm{Tr}\,\hat{\rho}(0) = 1$ which results in $h_4 = 1$. This was expected because the vacuum eigenstate $|0\rangle\rangle$ is the only Liouville space eigenvector with trace 1, cf. Eq. (4.86). Second, we demand that $\hat{\rho}(0)$ is Hermitian and thus we need $h_2 = h_3^*$ and $h_1 \in \mathbb{R}$. Third, the density operator has to be positive definite. In order to translate this into a condition on the coefficients $h_k$, we first calculate the matrix representation of $\hat{\rho}(0)$. For this we use the Hilbert space basis $|0,0\rangle$, $|1,0\rangle$, and $|0,1\rangle$. One example for the eigenvector $|(1,0),(1,0)\rangle\rangle$ can be found in Eq. (5.21) with all other eigenvectors being similarly calculated, see Eq. (C.3) in Appendix C. Note that the parameters $\epsilon_1$ and $\tau_1$ from Eq. (5.17) are changed with the aforementioned replacement $\gamma \to \gamma + \mathrm{i}\sigma$ in order to add the detuning. With the translation to the Hilbert space at hand, the density matrix is given by

$$\hat{\rho}(0) = \begin{pmatrix} 1 - h_1\left(|\epsilon_1|^2 + |\tau_1|^2\right) & h_2^*\,\epsilon_1^* & h_2^*\,\tau_1^* \\ h_2\,\epsilon_1 & h_1\,|\epsilon_1|^2 & h_1\,\epsilon_1\,\tau_1^* \\ h_2\,\tau_1 & h_1\,\epsilon_1^*\,\tau_1 & h_1\,|\tau_1|^2 \end{pmatrix}. \tag{5.27}$$

This matrix is positive definite if all its eigenvalues are positive definite. After calculating the eigenvalues of the above matrix, it is straightforward that the condition on the coefficients $h_k$ for $\hat{\rho}(0)$ to be positive definite is

$$h_1 - h_1^2 \left( |\epsilon_1|^2 + |\tau_1|^2 \right) \geq |h_2|^2. \tag{5.28}$$

This inequality yields all allowed values $h_1$ and $h_2$ to construct physical states that are transported with the least damping in the lossy waveguide system. One special case is $h_1 = (|\epsilon_1|^2 + |\tau_1|^2)^{-1}$ for which the one-photon subspace decouples from the zero-photon subspace ($h_2 = 0$). The initial state is then $|\psi\rangle = \sqrt{h_1}(\epsilon_1|1,0\rangle + \tau_1|0,1\rangle)$, which is in fact the eigenstate of the effective non-Hermitian Hamiltonian to the eigenvalue $\tilde{\lambda}_1$ that has the lower loss. This is of no suprise as we have already discussed in the last chapter that the eigenstates of $\hat{H}_{\text{eff}}$ resurface from the general eigenvectors when the dynamic is restricted to the highest-photon-number subspace, cf. Eq. (4.96). The same considerations can be made for more photons and an example for $N_{\text{p}} = 2$ is shown in the Appendix E.

In conclusion, the eigendecomposition solution (4.82) is a helpful tool in calculating the dynamics of small open waveguide systems. It provides a clear and straightforward way to calculate analytical expressions for the complete quantum state and thus for any observable. Because of the simple superoperator actions at its core, it could also be turned into numerical algorithms to handle larger numbers of modes or photons. In addition, the eigendecomposition can be used to analyse the propagation behaviour allowing the deliberate use of initial states that show slower decay. This idea can in principle be extended to other problems, e.g. designing specific outputs.

The main drawback of this technique is its requirement of $z$-independence. In order to overcome this obstacle, one could discretise a system of varying parameters and use the eigendecomposition solution for each incremental step, especially in conjunction with a numerical implementation of Eq. (4.82). However, this might require even for small systems a larger computational effort as compared to the inherently $z$-dependent Wei-Norman expansion, which we will showcase in the following section.

## 5.2. Wei-Norman solution for the lossy waveguide coupler

The Wei-Norman method is especially potent to investigate the two-waveguide $\mathcal{PT}$ coupler as it generally allows varying system parameters. The method is based on the algebraic structure analysis of the Lie algebra induced by the Liouvillian $\mathcal{L}$ as discussed in Section 4.4. Here, we showcase the Wei-Norman method for a lossy two-waveguide system. However, in order to be more general we consider not only the specific $\mathcal{PT}$ coupler as in the last section but a lossy two-waveguide system in general, for which the Liouvillian reads

$$\begin{aligned}\mathcal{L} = \sum_{k=1}^{2} \Big[ & (\mathrm{i}\sigma_k - \gamma_k)\, R_k^+ R_k^- - (\mathrm{i}\sigma_k + \gamma_k)\, L_k^+ L_k^- + 2\gamma_k\, L_k^- R_k^- \Big] \\ & - \mathrm{i}\kappa \left( L_k^+ L_{k+1}^- + L_{k+1}^+ L_k^- - R_{k+1}^+ R_k^- - R_k^+ R_{k+1}^- \right), \end{aligned} \tag{5.29}$$

taken from the expression in Eq. (4.21) for the $M$ waveguide system. The $\mathcal{PT}$ coupler is then the special case where $\sigma_k = 0$ and $\gamma_2 = 0$.

Following the outline of the Wei-Norman method in Section 4.4, the first step is to separate the Liouvillian in Eq. (5.29) as $\mathcal{L} = \mathcal{L}_\mathrm{R}+\mathcal{L}_\mathrm{S}$, i.e. into its solvable (radical) part $\mathcal{L}_\mathrm{R}$ and its semisimple part $\mathcal{L}_\mathrm{S}$. Both define their own evolution superoperators $\mathcal{U}_\mathrm{R}$ and $\mathcal{L}_\mathrm{S}$ with differential equations (4.102) and (4.103), respectively. Using the decomposition (4.104), we find for the solvable (radical) part of the Liouvillian

$$\begin{aligned}\mathcal{L}_\mathrm{R}(z) = &\frac{1}{2}\left(-\mathrm{i}(\sigma_1+\sigma_2) - (\gamma_1+\gamma_2)\right)\left(L_1^+L_1^- + L_2^+L_2^-\right)\\ &+ \frac{1}{2}\left(\mathrm{i}(\sigma_1+\sigma_2) - (\gamma_1+\gamma_2)\right)\left(R_1^+R_1^- + R_2^+R_2^-\right)\\ &+ 2\gamma_1\, L_1^-R_1^- + 2\gamma_2\, L_2^-R_2^- \end{aligned} \tag{5.30}$$

where one can clearly observe the emergence of mean values for the propagation constants $\sigma_k$ and the losses $\gamma_k$ as discussed earlier. Note that only the removing superoperators $L_1^-R_1^-$ and $L_2^-R_2^-$ of the total algebra occur because the mixed superoperators $L_1^-R_2^-$ and $L_2^-R_1^-$ do not span the original Liouvillian, cf. Eq. (5.29).

As for the semisimple part, we know that it is comprised of two isomorphic simple parts for the left and right superoperators. Hence, we can split this part as $\mathcal{L}_\mathrm{S}(z) = \mathcal{L}_{\mathrm{S}_1}(z) + \mathcal{L}_{\mathrm{S}_2}(z)$ with

$$\mathcal{L}_{\mathrm{S}_1}(z) = \frac{1}{2}\left(-\mathrm{i}(\sigma_1-\sigma_2) - (\gamma_1-\gamma_2)\right)\left(L_1^+L_1^- - L_2^+L_2^-\right) - \mathrm{i}\kappa\left(L_1^+L_2^- + L_2^+L_1^-\right), \tag{5.31}$$

$$\mathcal{L}_{\mathrm{S}_2}(z) = \frac{1}{2}\left(\mathrm{i}(\sigma_1-\sigma_2) - (\gamma_1-\gamma_2)\right)\left(R_1^+R_1^- - R_2^+R_2^-\right) + \mathrm{i}\kappa\left(R_1^+R_2^- + R_2^+R_1^-\right). \tag{5.32}$$

Note that $\mathcal{L}_{\mathrm{S}_1}$ and $\mathcal{L}_{\mathrm{S}_2}$ transform into one another under exchange of left and right actions, $L \leftrightarrow R$, and a complex conjugation of the possibly $z$-dependent prefactors.

Because the two algebras of left and right superoperators commutate with each other, they solve their own respective differential equations

$$\partial_z \mathcal{U}_{\mathrm{S}_j} = \mathcal{L}_{\mathrm{S}_j}\mathcal{U}_{\mathrm{S}_j}\,. \tag{5.33}$$

These sets are isomorphic such that we can solve both using one operator representation. In the present two-waveguide case, this is the special linear algebra $\mathfrak{sl}(2,\mathbb{C})$ of operators

$$\mathcal{K}_0 = L_1^+L_1^- - L_2^+L_2^- \vee R_1^+R_1^- - R_2^+R_2^-\,, \tag{5.34}$$

$$\mathcal{K}_+ = L_1^+L_2^- \vee R_1^+R_2^-\,, \tag{5.35}$$

$$\mathcal{K}_- = L_2^+L_1^- \vee R_2^+R_1^-\,, \tag{5.36}$$

with commutators

$$[\mathcal{K}_0,\mathcal{K}_\pm] = \pm 2\mathcal{K}_\pm, \quad [\mathcal{K}_+,\mathcal{K}_-] = \mathcal{K}_0\,. \tag{5.37}$$

This is the same algebra as it occurred in the Hilbert space example of the Levi decomposition in Section 4.2. Using the shared representation of $\mathfrak{sl}(2,\mathbb{C})$, the ansatz for the Wei-Norman expansion of the simple parts is chosen as

$$\mathcal{U}_{\mathrm{S}_1}(z) = \mathrm{e}^{f_+(z)\,\mathcal{K}_+}\mathrm{e}^{f_0(z)\,\mathcal{K}_0}\mathrm{e}^{f_-(z)\,\mathcal{K}_-} \tag{5.38}$$

and analogously for $\mathcal{U}_{\mathrm{S}_2}$ using the respective complex conjugate functions $f_i^*(z)$. This is because the prefactors in Eqs. (5.31) and (5.32) for $\mathcal{L}_{\mathrm{S}_1}$ and $\mathcal{L}_{\mathrm{S}_2}$ are complex conjugates of each other.

When inserting this ansatz into the differential equation (5.33) the result is a sum of superoperator products as shown for the general case in Eq. (4.100). For example, a term like

$$\mathrm{e}^{f_+ \mathcal{K}_+} \left(\partial_z f_0\right) \mathcal{K}_0 \mathrm{e}^{f_0 \mathcal{K}_0} \mathrm{e}^{f_- \mathcal{K}_-} \tag{5.39}$$

does occur where we dropped the $z$-argument for brevity. All these terms need to be rewritten in a form where the full evolution superoperator $\mathcal{U}_{\mathrm{S}_j}$ stands to the right in order to enable a comparison with the right-hand side of Eq. (5.33). For this, one has to carefully calculate the required commutator relations using the exponential operator expression (4.78). In case of the above example term, this results in

$$\begin{aligned}\left(\partial_z f_0\right) \mathrm{e}^{f_+ \mathcal{K}_+} \mathcal{K}_0 \mathrm{e}^{-f_+ \mathcal{K}_+} \mathcal{U}_{\mathrm{S}_1} &= \left(\partial_z f_0\right) \left(\mathrm{e}^{f_+ \,\mathrm{ad}_{\mathcal{K}_+}} \mathcal{K}_0\right) \mathcal{U}_{\mathrm{S}_1} \\ &= \left(\partial_z f_0\right) \left(\mathcal{K}_0 - 2 f_+ \mathcal{K}_+\right) \mathcal{U}_{\mathrm{S}_1} \,,\end{aligned} \tag{5.40}$$

which then has to be done for all terms that occur after differentiation of the ansatz (5.38). Comparing the result of that calculation with the right-hand side of Eq. (5.33), we derive the set of nonlinear differential equations for the functions $f_i(z)$ as

$$\partial_z f_- \, \mathrm{e}^{-2f_0} = -\mathrm{i}\kappa \,, \tag{5.41}$$

$$\partial_z f_0 + \partial_z f_- \, f_+ \, \mathrm{e}^{-2f_0} = -\mathrm{i}\Delta \,, \tag{5.42}$$

$$\partial_z f_+ - 2\partial_z f_0 \, f_+ - \partial_z f_- \, f_+^2 \, \mathrm{e}^{-2f_0} = -\mathrm{i}\kappa \,, \tag{5.43}$$

with initial conditions $f_i(0) = 0$ and where we defined $\Delta = -\frac{1}{2}\left[(\sigma_1 - \sigma_2) + \mathrm{i}\,(\gamma_1 - \gamma_2)\right]$.

In this special case the set of nonlinear equations allows us to rewrite the equation for $f_+$ as a Riccati differential equation,

$$\partial_z f_+ + \mathrm{i}2\Delta f_+ - \mathrm{i}\kappa f_+^2 + \mathrm{i}\kappa = 0 \,. \tag{5.44}$$

For more modes this can be generalised as a vector-valued Riccati equation, e.g. Ref. [152]. With the reformulation (5.44) the Eqs. (5.41) and (5.42) for $f_-$ and $f_0$ can be cast into

$$\partial_z f_0 = -\mathrm{i}\Delta + \mathrm{i}\kappa f_+, \tag{5.45}$$

$$\partial_z f_- = -\mathrm{i}\kappa \, \mathrm{e}^{2f_0}. \tag{5.46}$$

The Riccati equation (5.44) can be transformed into a linear ordinary differential equation of second order for a function $\phi(z)$ when defining

$$f_+ = \frac{\mathrm{i}}{\kappa} \frac{\partial_z \phi}{\phi}. \tag{5.47}$$

As long as $\kappa \neq 0$, this results in the differential equation

$$0 = \partial_z^2 \phi + \left(2\mathrm{i}\Delta - \frac{\partial_z \kappa}{\kappa}\right) \partial_z \phi + \kappa^2 \phi \tag{5.48}$$

with initial conditions $\partial_z\phi(0) = 0$ and $\phi(0) = 1$. Note that the first initial condition is necessary to ensure that $f_+(0) = 0$ whereas the second one is arbitrary, as long as it is not zero, and only chosen for convenience. The Eq. (5.48) can be numerically solved and leads to well defined, smooth functions $\phi(z)$ whose roots signify singularities of $f_+$. With the knowledge of $\phi(z)$ these singularities can often be avoided or lifted.

Furthermore, the functions $f_0$ and $f_-$ can also be defined with the help of the auxiliary function $\phi(z)$. For example, the differential equation for $f_0$, Eq. (5.45), is easily integrated, resulting in

$$f_0(z) = -\mathrm{i}\int_0^z \Delta(z')\,\mathrm{d}z' - \ln(\phi(z)). \tag{5.49}$$

Apparently, $f_0$ has also a singularity when $\phi(z) = 0$. In case of $f_-$, its Eq. (5.46) is not directly integrable. However, a similar ansatz as for $f_+$ can be made and reads

$$f_- = \frac{\mathrm{i}}{\kappa}\frac{\zeta}{\phi}. \tag{5.50}$$

The rationale is that, judging from Eq. (5.46), the function $f_-$ has also singularities whenever $\phi(z) = 0$. For the new auxiliary function $\zeta(z)$ a new first-order ordinary differential equation is readily derived as

$$0 = \partial_z\zeta - \zeta\left(\frac{\partial_z\phi}{\phi} + \frac{\partial_z\kappa}{\kappa}\right) + \frac{\kappa^2}{\phi}\mathrm{e}^{-2\mathrm{i}\int\Delta\,\mathrm{d}z}\,. \tag{5.51}$$

Although the singularities at $\phi(z) = 0$ still occur in this differential equation, they are not as severe as in the original nonlinear differential equation for $f_+(z)$ because this is now a linear differential equation and the function $\phi(z)$ is known. As a result, Eq. (5.51) is usually integrable by standard numerical procedures. In case these methods fail, however, one can still lift the singularity because the position of the singularity is known and even the finite value of the function $\zeta$ is given via Eq. (5.51) as

$$\zeta(z(\phi = 0)) = \frac{\kappa^2}{\partial_z\phi}\mathrm{e}^{-2\mathrm{i}\int\Delta\,\mathrm{d}z}. \tag{5.52}$$

With the above considerations the functions $f_i$ are readily calculated and thus the fundamental $\mathfrak{sl}(2,\mathbb{C})$-problem of the Wei-Norman expansion is determined. The total solution of the semisimple part is then given by the combined evolution superoperator $\mathcal{U}_\mathrm{S} = \mathcal{U}_{\mathrm{S}_1}\mathcal{U}_{\mathrm{S}_2}$ with

$$\mathcal{U}_{\mathrm{S}_1} = \mathrm{e}^{f_+\,L_1^+L_2^-}\,\mathrm{e}^{f_0\,\left(L_1^+L_1^- - L_2^+L_2^-\right)}\mathrm{e}^{f_-\,L_2^+L_1^-}, \tag{5.53}$$

$$\mathcal{U}_{\mathrm{S}_2} = \mathrm{e}^{f_+^*\,R_1^+R_2^-}\,\mathrm{e}^{f_0^*\,\left(R_1^+R_1^- - R_2^+R_2^-\right)}\mathrm{e}^{f_-^*\,R_2^+R_1^-}\,. \tag{5.54}$$

This structure is not surprising because the right action of the superoperators simply results in the evolution $\mathcal{U}_\mathrm{S}\,|\hat{\rho}\rangle\rangle = \hat{U}\,\hat{\rho}\,\hat{U}^\dagger$, where $\hat{U}$ is the evolution operator in the Wei-Norman expansion of a generic two-mode system that follows the $\mathfrak{sl}(2,\mathbb{C})$ algebra, cf. the example at the beginning of Section 4.2. Here, this two-mode system is described by the effective non-Hermitian Hamiltonian $\hat{H}_{\text{gain-loss}}$ of the active gain-loss system that results from the passive system once the mean loss is removed.

With the solution of the semisimple part of the algebra at hand, we now focus on the solvable (radical) part. The differential equation of interest is Eq. (4.103), for which the right-hand side $\left(\mathcal{U}_{\mathrm{S}}^{-1}\mathcal{L}_{\mathrm{R}}\mathcal{U}_{\mathrm{S}}\right)\mathcal{U}_{\mathrm{R}}$ has to be calculated first. Again, this can be done using the exponential operator expression (4.78) in conjunction with $\mathcal{L}_{\mathrm{R}}$ from Eq. (5.30) and $\mathcal{U}_{\mathrm{S}} = \mathcal{U}_{\mathrm{S}_1}\mathcal{U}_{\mathrm{S}_2}$ given by Eqs. (5.53) and (5.54), respectively. For example, the term with superoperators $L_2^- R_2^-$ in Eq. (5.30) can be reformulated as

$$\mathcal{U}_{\mathrm{S}}^{-1} L_2^- R_2^- \mathcal{U}_{\mathrm{S}} = \left(\mathcal{U}_{\mathrm{S}_1}^{-1} L_2^- \mathcal{U}_{\mathrm{S}_1}\right)\left(\mathcal{U}_{\mathrm{S}_2}^{-1} R_2^- \mathcal{U}_{\mathrm{S}_2}\right) , \tag{5.55}$$

when using the fact that superoperators $L_i^{\pm}$ and $R_i^{\pm}$ commutate with each other. Now one can use the exponential adjoint action (4.78) to calculate each individual term, e.g.

$$\begin{aligned}
\mathcal{U}_{\mathrm{S}_1}^{-1}\, L_2^-\, \mathcal{U}_{\mathrm{S}_1} &= \mathrm{e}^{-f_-\, L_2^+ L_1^-}\, \mathrm{e}^{-f_0\left(L_1^+ L_1^- - L_2^+ L_2^-\right)}\, \mathrm{e}^{-f_+\, L_1^+ L_2^-}\, L_2^-\, \mathrm{e}^{f_+\, L_1^+ L_2^-}\, \mathrm{e}^{f_0\left(L_1^+ L_1^- - L_2^+ L_2^-\right)}\, \mathrm{e}^{f_-\, L_2^+ L_1^-} \\
&= \mathrm{e}^{-f_-\, L_2^+ L_1^-}\, \mathrm{e}^{-f_0\left(L_1^+ L_1^- - L_2^+ L_2^-\right)}\, L_2^-\, \mathrm{e}^{f_0\left(L_1^+ L_1^- - L_2^+ L_2^-\right)}\, \mathrm{e}^{f_-\, L_2^+ L_1^-} \\
&= \mathrm{e}^{-f_-\, L_2^+ L_1^-}\, \mathrm{e}^{-f_0}\, L_2^-\, \mathrm{e}^{f_-\, L_2^+ L_1^-} \\
&= \mathrm{e}^{-f_0}\left(L_2^- + f_-\, L_1^-\right) .
\end{aligned} \tag{5.56}$$

Performing this for all terms in Eq. (5.30), the explicit result for $\mathcal{U}_{\mathrm{S}}^{-1}\mathcal{L}_{\mathrm{R}}\mathcal{U}_{\mathrm{S}}$ is

$$\begin{aligned}
\mathcal{U}_{\mathrm{S}}^{-1}\mathcal{L}_{\mathrm{R}}\mathcal{U}_{\mathrm{S}} = {} & \frac{1}{2}\left(-\mathrm{i}(\sigma_1+\sigma_2)-(\gamma_1+\gamma_2)\right)\left(L_1^+ L_1^- + L_2^+ L_2^-\right) \\
& + \frac{1}{2}\left(\mathrm{i}(\sigma_1+\sigma_2)-(\gamma_1+\gamma_2)\right)\left(R_1^+ R_1^- + R_2^+ R_2^-\right) \\
& + 2\gamma_1\Big(L_1^- R_1^- \left|\mathrm{e}^{f_0}+\mathrm{e}^{-f_0} f_+ f_-\right|^2 + L_1^- R_2^- \left(\mathrm{e}^{f_0}+\mathrm{e}^{-f_0} f_+ f_-\right)\mathrm{e}^{-f_0^*} f_+^* \\
& \qquad + L_2^- R_1^- \left(\mathrm{e}^{f_0^*}+\mathrm{e}^{-f_0^*} f_+^* f_-^*\right)\mathrm{e}^{-f_0} f_+ + L_2^- R_2^- \left|\mathrm{e}^{-f_0}\right|^2 |f_+|^2\Big) \\
& + 2\gamma_2\Big(L_1^- R_1^- \left|\mathrm{e}^{-f_0}\right|^2 |f_-|^2 + L_1^- R_2^- \left|\mathrm{e}^{-f_0}\right|^2 f_- \\
& \qquad + L_2^- R_1^- \left|\mathrm{e}^{-f_0}\right|^2 f_-^* + L_2^- R_2^- \left|\mathrm{e}^{-f_0}\right|^2\Big) ,
\end{aligned} \tag{5.57}$$

which yields the right-hand side of Eq. (4.103).

For the left-hand side we choose the ansatz

$$\begin{aligned}
\mathcal{U}_{\mathrm{R}} = {} & \mathrm{e}^{a_1(z)\left(L_1^+ L_1^- + L_2^+ L_2^-\right)}\, \mathrm{e}^{a_2(z)\left(R_1^+ R_1^- + R_2^+ R_2^-\right)} \\
& \times \mathrm{e}^{a_3(z)\, L_1^- R_1^-}\, \mathrm{e}^{a_4(z)\, L_2^- R_2^-}\, \mathrm{e}^{a_5(z)\, L_2^- R_1^-}\, \mathrm{e}^{a_6(z)\, L_1^- R_2^-} ,
\end{aligned} \tag{5.58}$$

for the evolution superoperator of the solvable (radical) part, from which the derivative $\partial_z \mathcal{U}_{\mathrm{R}}$ can be calculated resulting in a form similar to Eq. (4.100). Performing the necessary commutations, as was done for the simple parts, cf. Eqs. (5.39) and (5.40), the left-hand side can be brought into a form where $\mathcal{U}_{\mathrm{R}}$ stands to the right. Comparing that result to the right-hand side of Eq. (5.57) one can then read off the set of differential equations for the functions $a_i(z)$ from Eq. (4.103), which read

$$\partial_z a_1 = \frac{1}{2}\left[-\mathrm{i}\left(\sigma_1+\sigma_2\right)-\left(\gamma_1+\gamma_2\right)\right], \tag{5.59}$$

$$\partial_z a_2 = \frac{1}{2}\left[\mathrm{i}(\sigma_1+\sigma_2)-(\gamma_1+\gamma_2)\right], \tag{5.60}$$

$$\partial_z a_3 = 2\mathrm{e}^{a_1+a_2}\left(\gamma_1\left|\mathrm{e}^{f_0}+\mathrm{e}^{-f_0}f_+f_-\right|^2+\gamma_2\left|\mathrm{e}^{-f_0}\right|^2|f_-|^2\right), \tag{5.61}$$

$$\partial_z a_4 = 2\mathrm{e}^{a_1+a_2}\left(\gamma_1\left|\mathrm{e}^{-f_0}\right|^2|f_+|^2+\gamma_2\left|\mathrm{e}^{-f_0}\right|^2\right), \tag{5.62}$$

$$\partial_z a_5 = 2\mathrm{e}^{a_1+a_2}\left[\gamma_1\left(\mathrm{e}^{f_0^*}+\mathrm{e}^{-f_0^*}f_+^*f_-^*\right)\mathrm{e}^{-f_0}f_++\gamma_2\left|\mathrm{e}^{-f_0}\right|^2f_-^*\right], \tag{5.63}$$

$$\partial_z a_6 = 2\mathrm{e}^{a_1+a_2}\left[\gamma_1\left(\mathrm{e}^{f_0}+\mathrm{e}^{-f_0}f_+f_-\right)\mathrm{e}^{-f_0^*}f_+^*+\gamma_2\left|\mathrm{e}^{-f_0}\right|^2f_-\right]. \tag{5.64}$$

with the initial conditions $a_i(0) = 0$. As expected from the solvable algebra, this set is uncoupled and thus directly integrable. The functions $a_1(z)$ and $a_2(z)$ determine the Abelian contribution and are given by integrals of the (generally $z$-dependent) mean propagation constants and and mean losses. All other functions $a_i(z)$ with $i = 3, \ldots, 6$ determine the excitation-removing operations. Note that the singularities of the functions $f_i$ are removed in most terms of the equations for the $a_i$ functions because of the occurring combinations of $f_+$, $f_-$, and $\exp(f_0)$. Terms with remaining $\phi^{-1}$ are often integrable by standard numerical procedures or can be lifted.

With known solutions for the semisimple and solvable part the total evolution is $\mathcal{U} = \mathcal{U}_\mathrm{S}\mathcal{U}_\mathrm{R}$. Due to the separate exponential form of these operations it is possible to find analytical expressions by hand for the evolution of an input state in Fock basis. Such a state would generally be written as

$$|\hat{\rho}(0)\rangle\rangle = \sum_{\boldsymbol{n},\boldsymbol{m}} h_{\boldsymbol{n},\boldsymbol{m}}\,|\,(\boldsymbol{n},\boldsymbol{m})\rangle\rangle = \sum_{\boldsymbol{n},\boldsymbol{m}} h_{\boldsymbol{n},\boldsymbol{m}}\,|\boldsymbol{n}\rangle\langle\boldsymbol{m}| \tag{5.65}$$

where $\boldsymbol{n} = (n_1, n_2)$ and $\boldsymbol{m} = (m_1, m_2)$ and with the $h_{\boldsymbol{n},\boldsymbol{m}}$ as $z$-independent expansion coefficients which ensure that $|\hat{\rho}(0)\rangle\rangle$ is a physical state. Note that the multiindices $\boldsymbol{n}$ and $\boldsymbol{m}$ label physical Fock states in contrast to the Greek multiindices $\boldsymbol{\alpha}$, $\boldsymbol{\beta}$ of the Liouville space eigenvectors of $\mathcal{L}$. For one of the Fock dyads the evolution $\mathcal{U}|\,(\boldsymbol{n},\boldsymbol{m})\rangle\rangle$ reads

$$\begin{aligned}\mathcal{U}\,|\,(\boldsymbol{n},\boldsymbol{m})\rangle\rangle = &\sum_{k=0}^{\min(n_1,m_2)}\ \sum_{s=0}^{\min(n_2,m_1)}\ \sum_{v=0}^{\min(n_2-s,m_2-k)}\ \sum_{w=0}^{\min(n_1-k,m_1-s)}\\ &\sum_{p=0}^{n_1-k-w}\ \sum_{q=0}^{n_2-s-v+p}\ \sum_{l=0}^{m_1-s-w}\ \sum_{r=0}^{m_2-k-v+l} \frac{a_6^k\,a_5^s\,a_4^v\,a_3^w}{k!\,s!\,v!\,w!}\,\frac{f_-^p\,f_+^q\,f_-^{*\,l}\,f_+^{*\,r}}{p!\,q!\,l!\,r!}\\ &\times\exp(a_1\,(n_1+n_2-k-s-v-w))\\ &\times\exp(a_2\,(m_1+m_2-k-s-v-w))\\ &\times\exp(f_0\,(n_1-n_2-k-w+s+v-2p))\\ &\times\exp(f_0^*\,(m_1-m_2-s-w+k+v-2l))\\ &\times\sqrt{\frac{n_1!\,n_2!\,m_1!\,m_2!\,(n_1-k-w-p+q)!\,(m_1-s-w-l+r)!}{(n_2-s-v+p-q)!\,(m_2-k-v+l-r)!}}\\ &\times\frac{(n_2-s-v+p)!\,(m_2-k-v+l)!}{(n_2-s-v)!\,(m_2-k-v)!\,(m_1-s-w-l)!\,(n_1-k-w-p)!}\\ &\times|n_1-k-w-p+q,n_2-s-v+p-q\rangle\langle m_1-s-w-l+r,m_2-k-v+l-r|\,.\end{aligned}\tag{5.66}$$

With this expression any quantum state $|\hat{\rho}(z)\rangle\rangle$ can be calculated, given that the differential equations for the Wei-Norman expansion functions $f_i$ and $a_i$ can be solved. This in turn allows the calculation of any observable of interest.

As an example and sanity check we again calculate the coincidence rate $\Gamma$, but now with potentially $z$-dependent system parameters including nonzero propagation constants $\sigma_k$. The input state is thus again $\hat{\rho}(0)=|1,1\rangle\langle 1,1|$, meaning we only have to apply the general evolution of a Fock dyad in Eq. (5.66) once. For the two-photon coincidence rate we only need the summand with the $|1,1\rangle\langle 1,1|$-term in Eq. (5.66), which considerably simplifies the summation. Straightforward calculation of the sum yields

$$\Gamma = \mathrm{e}^{2\,(a_1+a_2)}\left|1+2f_+f_-\,\mathrm{e}^{-2f_0}\right|^2. \tag{5.67}$$

Note that only the functions $f_\pm$, $f_0$, and $a_{1,2}$ occur because the measurement is restricted to the highest-photon-number subspace $\mathcal{H}_{N_\mathrm{p}=2}$, Hence, the excitation-removing operators of $\mathcal{U}_\mathrm{R}$ in Eq. (5.58) do not contribute. When inserting the auxiliary functions from the Eqs. (5.47) and (5.50), the result reads

$$\Gamma = \mathrm{e}^{2\,(a_1+a_2)}\left|1-2\frac{\zeta\,\partial_z\phi}{\kappa^2}\,\mathrm{e}^{2\mathrm{i}\int\Delta\,\mathrm{d}z}\right|^2. \tag{5.68}$$

showing that although the functions $f_i$ do have singularities, the derived observable is indeed always bounded as expected.

The general solution in Eq. (5.67) is as of yet undetermined because we have not specified any system parameters and thus have not solved for the functions $f_i$ and $a_i$. For $z$-dependent parameters these have to be numerically integrated, e.g. by using the auxiliary functions $\phi(z)$ and $\zeta(z)$. However, in case of constant parameters, analytical solutions for the functions $f_i$ can be found and read

$$f_{\pm}(z) = \frac{\kappa \sin(\Theta z)}{\mathrm{i}\Theta \cos(\Theta z) - \Delta \sin(\Theta z)}, \tag{5.69}$$

$$f_0(z) = \frac{1}{2} \ln \left( \frac{\Theta \cos(\Theta z) - \mathrm{i}\Delta \sin(\Theta z)}{\Theta \cos(\Theta z) + \mathrm{i}\Delta \sin(\Theta z)} \frac{\Theta^2}{\Delta^2 + \kappa^2 \cos^2(\Theta z)} \right), \tag{5.70}$$

where $\Theta^2 = \kappa^2 + \Delta^2$. Based on these expressions, the Eqs. (5.59)-(5.64) for the functions $a_i$ can easily be integrated by numerical means.

For the $\mathcal{PT}$ coupler we have specifically $\Delta = -\mathrm{i}\gamma/2$ and $\Theta = \Omega/2$, which leads to

$$f_+ f_- \,\mathrm{e}^{-2f_0} = -\frac{4\kappa^2 \sin^2\left(\frac{1}{2}\Omega z\right)}{\Omega^2}. \tag{5.71}$$

Using $\sin^2(x/2) = (1 - \cos(x))/2$ and $a_1 = a_2 = -1/2\gamma z$, cf. Eqs. (5.59) and (5.60), it then follows that

$$\Gamma = \mathrm{e}^{-2\gamma z} \left( \frac{4\kappa^2 \cos(\Omega z) - \gamma^2}{\Omega^2} \right)^2, \tag{5.72}$$

which is the same result as given in Eq. (5.22), showing the consistency of both approaches.

The above example showcases how the Wei-Norman method allows to find solutions to the quantum master equation. However, the coincidence rate $\Gamma$ is restricted to the highest-photon-number subspace via postselection and could therefore be calculated directly from the effective non-Hermitian Hamiltonian using the Schrödinger equation. An interesting observable that, in contrast, needs the full quantum evolution over all photon-number subspaces, is the logarithmic negativity $LN(\hat{\rho})$. It is an entanglement monotone allowing to quantify the entanglement for states of a bipartite system AB that consists of subsystems A and B [153; 154; 155]. It is defined as

$$LN(\hat{\rho}) = \ln ||\hat{\rho}^{\mathrm{T_A}}||_1 \,, \tag{5.73}$$

where $\mathrm{T_A}$ denotes the partial transpose with respect to the subsystem A and $||M||_1 = \mathrm{Tr}|M| = \mathrm{Tr}\sqrt{M^\dagger M}$ is the trace norm. For $LN(\hat{\rho}) = 0$ the state $\hat{\rho}$ is separable under the bipartition and for $LN(\hat{\rho}) > 0$ the subsystems A and B are entangled.

In case of the $\mathcal{PT}$ coupler, we can partition the lossy two-waveguide system into A for the first, lossy waveguide and B for the second, lossless waveguide. As an example, we calculate the evolution of the initial state

$$\hat{\rho}(0) = \frac{1}{2}\Big( |2,0\rangle\langle 2,0| + |2,0\rangle\langle 0,2| + |0,2\rangle\langle 2,0| + |0,2\rangle\langle 0,2| \Big) \tag{5.74}$$

by using Eq. (5.66) four times for all combinations of the Fock multiindices $\boldsymbol{n}, \boldsymbol{m} \in \{(2,0),(0,2)\}$. The resulting density matrix is then partially transposed by interchanging the Fock indices of the dyads in Eq. (5.66), i.e.

$$\Big( |i_1, j_1\rangle\langle i_2, j_2| \Big)^{\mathrm{T_A}} = |i_2, j_1\rangle\langle i_1, j_2| \,. \tag{5.75}$$

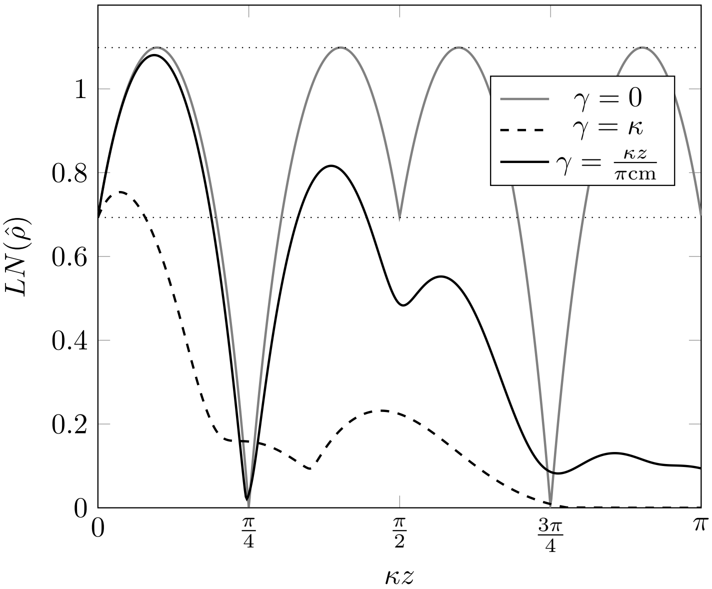

Fig. 5.4.: Logarithmic negativity $LN(\hat\rho)$ of the $\mathcal{PT}$ coupler. Calculated for no loss, constant loss $\gamma = \kappa$, and $z$-dependent loss $\gamma = \kappa z/(\pi\,\mathrm{cm})$. The values ln(2) and ln(3) are marked by horizontal, dotted lines and correspond to the states in Eqs. (5.74) and (5.76), respectively.

Note that the logarithmic negativity remains the same when using the partial transpose $\mathrm{T_B}$ with respect to subsystem B [155].

After calculating $\hat\rho^{\mathrm{T_A}}$, its trace norm can be computed via standard functions and in Fig. 5.4 some example cases are given for different losses. We included the case of no loss ($\gamma = 0$), constant loss ($\gamma = \kappa$), and linearly increasing loss $\gamma = \kappa z/\pi\mathrm{cm}$). Without losses, the initial state (5.74) first evolves into a maximally entangled state

$$\hat\rho\left(\frac{\pi}{8}\right) = \frac{1}{3}\Big(|2,0\rangle + |1,1\rangle + |0,2\rangle\Big)\Big(\langle 2,0| + \langle 1,1| + \langle 0,2|\Big), \tag{5.76}$$

i.e. the equal superposition of all two-photon states, followed by the separable state

$$\hat\rho\left(\frac{\pi}{4}\right) = |1,1\rangle\langle 1,1|\,. \tag{5.77}$$

This evolution then repeats itself. The horizontal, dotted lines in Fig. 5.4 mark the values $LN(\hat\rho) = \ln 2$ and $LN(\hat\rho) = \ln 3$ for the entangled states $\hat\rho(0)$ and $\hat\rho(\pi/8)$. When losses are included these oscillations become damped and slightly shifted, showing the entanglement degradation. The case of linearly increasing loss explicitly shows this transition as it initially has a similar behaviour as the lossless case and transitions to a damped case.

The above example calculation shows how our solution of the quantum master equation with the Wei-Norman method allows to compute any observable of the lossy waveguide coupler even for $z$-dependent system parameters. After implementation of the general solution of Eq. (5.66) any problem is reduced to finding the specific solutions for the expansion functions $f_i$ and $a_i$, which often are easily integrated via standard numerical procedures.

### 5.2.1. Exceptional points of arbitrary order in the $\mathcal{PT}$ coupler

An especially interesting case, for which even analytical solutions can be found, is the EP, i.e. $\gamma_1 = \gamma = 2\kappa$, $\gamma_2 = 0$, and $\sigma_i = 0$. Recall that in the eigendecomposition solution one has to find the Jordan decomposition of the regular representation of the Liouvillian and thus compute the eigendecomposition from scratch. With the Wei-Norman expansion, however, one still only has to solve the differential equations (5.42)-(5.43) for the functions $f_i$ and use those to integrate the Eqs. (5.59)-(5.64) for the functions $a_i$. As all parameters are $z$-independent when staying at the EP one can find analytical solutions for the functions $f_i$. More precisely, at the EP it holds that $\Delta = -\mathrm{i}\kappa$ in the differential equations (5.42)-(5.43). The corresponding solutions then read as

$$f_\pm(z) = -\frac{\mathrm{i}\kappa z}{1+\kappa z}\,, \tag{5.78}$$

$$f_0(z) = -\ln(1+\kappa z)\,. \tag{5.79}$$

Based on these closed form solutions, any observable of interest can be calculated at the EP. For example, using Eq. (5.67) the two-photon coincidence $\Gamma$ in the HOM experiment becomes

$$\Gamma_{\mathrm{EP}} = \mathrm{e}^{-4\kappa z}\left(1 - 2\,\kappa^2 z^2\right)^2. \tag{5.80}$$

However, up to this point, we omitted a crucial part in the discussion of the EP because we did not allude to the fact that the EP can be of different order depending on how many eigenstates coalesce. The discussion at the beginning of this chapter focussed on the diagonalisation of the matrix representation $\boldsymbol{H}_{\mathrm{eff}}$ of the underlying non-Hermitian Hamiltonian. In case of the two-mode coupler, this is a 2×2-dimensional matrix and thus only two eigenvectors are present and able to coalesce. This is the algebraic basis on which the actual eigenvectors of the system are later computed. Therefore, depending on the number of photons the system dimension is different. In Hilbert space for example, when only one-photon states are considered, the basis is $|(1,0)\rangle = (1,0)^{\mathrm{T}}$ and $|(0,1)\rangle = (0,1)^{\mathrm{T}}$. The effective non-Hermitian Hamiltonian in this basis is a $2\times2$-dimensional matrix and identical to $\boldsymbol{H}_{\mathrm{eff}}$. For more photons, the number of basis states increases linearly, e.g. $|(2,0)\rangle$, $|(1,1)\rangle$, and $|(0,2)\rangle$ for two photons and so on for larger photon numbers. Hence, the number of coalescing modes of the effective non-Hermitian Hamiltonian also increases linearly. This means that when states with $N_{\mathrm{p}}$ photons are initiated in the $\mathcal{PT}$ coupler, configured at the EP, this EP is of order $N_{\mathrm{p}}+1$.

Additionally, we note that the number of modes for the Liouvillian is even larger, i.e. an $M\times M$-dimensional $\boldsymbol{H}_{\mathrm{eff}}$ results in a $4M\times 4M$-dimensional regular representation $\mathcal{R}'(\mathcal{L})$ of the Liouvillian from which more ladder states are calculated. As a result, the order of the EP of $\mathcal{L}$ is technically larger. However, the coalescing eigenvectors $|\boldsymbol{\alpha},\boldsymbol{\beta}\rangle\rangle$ of $\mathcal{L}$ are not physical states themselves, cf. Eq. (4.86). In fact, we have seen that the physical eigenmodes of the Hamiltonian are constructed from the $|\boldsymbol{\alpha},\boldsymbol{\beta}\rangle\rangle$ and explicitly emerge when postselected to the highest-photon-number subspace, cf. Eq. (4.95). An investigation that distinguishes the unphysical eigenvectors of the Liouvillian of a linear chain of bosonic modes was recently done in Ref. [156]. However, the system in Ref. [156]

was coupled to a thermal bath and relied on higher-order coherence functions of the steady state. Such an approach is not viable here because the steady state is the vacuum state for our lossy waveguides. For this reason, and because the EP of the Hamiltonian and the Liouvillian always appear at the same positions, do we still talk of an EP of order $N_\mathrm{p}+1$.

The fact that $N_\mathrm{p}$ photon states allow the investigation of EPs of up to order $N_\mathrm{p}+1$ was already shown in Ref. [88]. There, the authors also calculated the dynamics of $N_\mathrm{p}$-photon states in the $\mathcal{PT}$ coupler using a Wei-Norman expansion. However, in contrast to our full quantum calculation in Liouville space, they used the effective non-Hermitian Hamiltonian $\hat{H}_\mathrm{eff}$ in Hilbert space. Their results are thus restricted to the highest-photon-number subspace. Nonetheless, they could theoretically show the coalescence of the $N_\mathrm{p}+1$ states at the EP and also resulting qualitative changes in the dynamics of an observable like the occupation

$$P(n,h,z) = \langle n-h,h|\hat{\rho}(z)|n-h,h\rangle \tag{5.81}$$

of states $|n-h,h\rangle$. Therefore, the work in Ref. [88] proposed a clear path to investigate EPs of order $N_\mathrm{p}+1$ in a small-sized optical system utilising $N_\mathrm{p}$-photon states and subsequent photon-number resolved detection. The last part, i.e. the postselection to the $N_\mathrm{p}$-photon subspace, is the crucial ingredient because the calculations using $\hat{H}_\mathrm{eff}$ instead of a full quantum treatment are only then valid. However, this means that all measurements with less photons are discarded. In addition, the $N_\mathrm{p}$-photon subspace has the major drawback that any observable also has a decay of $\exp(-N_\mathrm{p}\gamma z)$ from the mean loss. The resulting low count rates means lower visibilities and longer measurements.

We propose to overcome this issue by applying our Liouville space solution, which allows to potentially utilise all photon-number subspaces simultaneously. As an example, we show results for the occupation $P(n,h,z)$ over the different subspaces with photon numbers $n \leq N_\mathrm{p}$. For this we also assume a $z$-independent $\mathcal{PT}$ coupler meaning the starting point are the (analytical) solutions for $f_i(z)$, see Eq. (5.69), with which the other functions $a_j(z)$ can be numerically integrated according to Eqs. (5.59)-(5.64). Together they form the total solution for the evolution superoperator $\mathcal{U}$ of the open system.

In Fig. 5.5a we plotted the result in case of the input state $|\psi\rangle = (|0,5\rangle + |5,0\rangle)/\sqrt{2}$ and loss rates $\gamma = 0.5\kappa$, i.e. in the $\mathcal{PT}$ phase. The six plots show the occupation in the six photon-number subspaces along $\kappa z \in (0,5)$. The results in each subspace are scaled by the respective factor $\exp(n\gamma z)$ $(n = 0,1,\ldots,5)$ to offset the mean loss of the passive system. For the subspace with highest photon number ($n = N_\mathrm{p} = 5$), we obtain the same result as in Ref. [88] with visible oscillations. Similar oscillations occur in the lower lying Fock layers, albeit shifted because they are initially not populated. The gradual increase in these subspaces with photon numbers $0 < n < N_\mathrm{p}$ is due to the additional scale factor that offsets the mean loss. Without this rescaling these subspaces are only transiently filled as they themselves lose photons to their respective lower lying subspace. The only exception is the vacuum subspace ($n = 0$), which is gradually filled following a logistic increase.

The observed oscillations between the different states $|n-h,h\rangle$ in Fig. 5.5a are a clear indicator that the system is in the $\mathcal{PT}$-symmetric phase. In contrast, when going above the EP ($\gamma > 2\kappa$), the system undergoes a phase transition where some states show

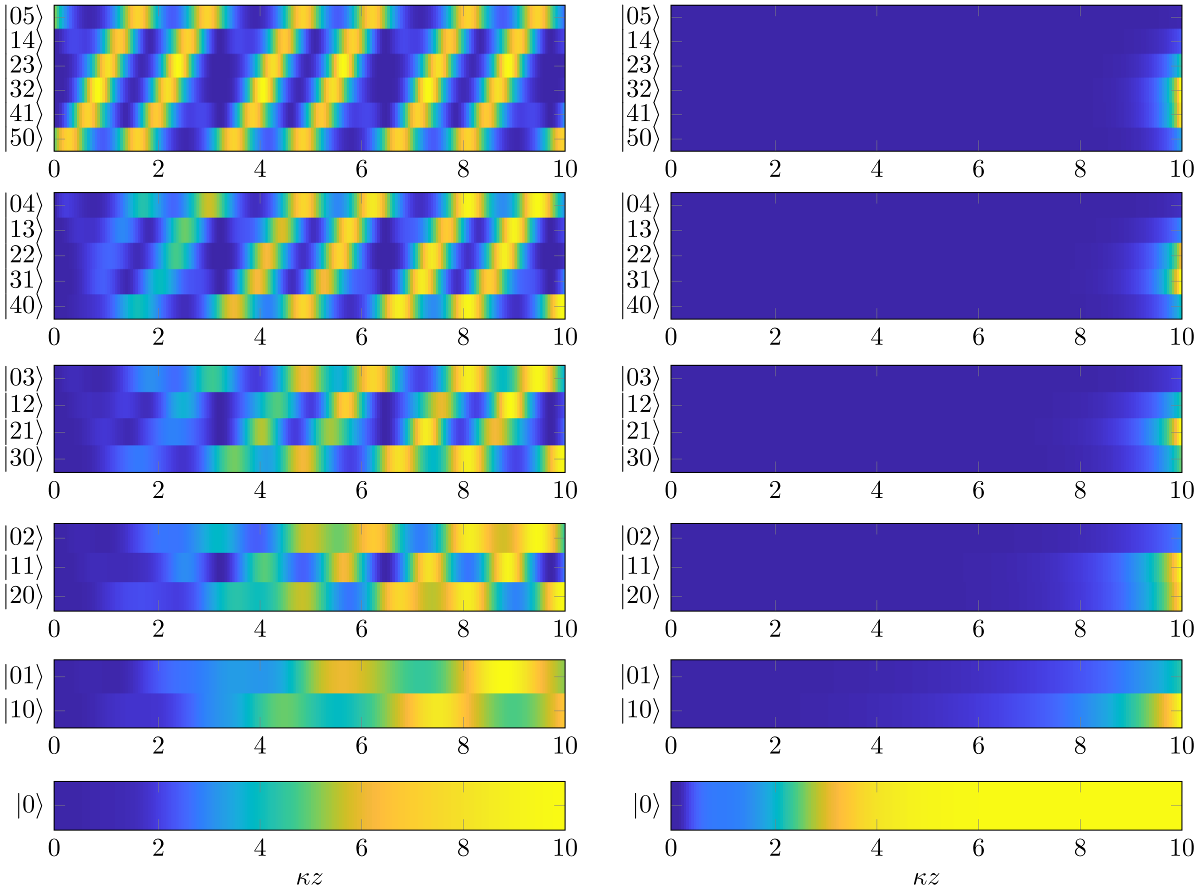

(a) $\mathcal{PT}$-symmetric phase (b) $\mathcal{PT}$-broken phase

Fig. 5.5.: Occupations $P(n, h, z)$ of the different states $|n - h, h\rangle$ for the input state $|\psi\rangle = (|0, 5\rangle + |5, 0\rangle)/\sqrt{2}$ and over all photon-number subspaces. (a) The system is in the $\mathcal{PT}$-symmetric phase ($\gamma = 0.5\kappa$). (b) The system is in the $\mathcal{PT}$-broken phase ($\gamma = 2.1\kappa$). In both cases, a normalisation factor $\exp(n\gamma z)$ is multiplied in each subspace with $n$ photons to offset the mean loss. In the $\mathcal{PT}$-broken phase this results in exponential growth that obscures the dynamics.

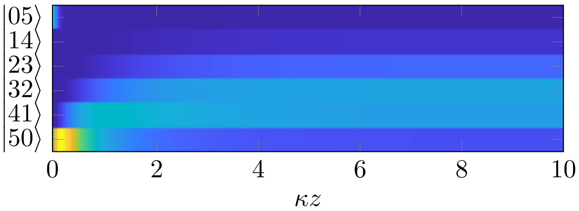

Fig. 5.6.: Normalised occupation $P(n, h, z)$ of the different states $|n-h, h\rangle$ in the $\mathcal{PT}$-broken phase ($\gamma = 2.1\kappa$). This is the normalised result from the highest panel in Fig. 5.5b and coincides with the result in Ref. [88].

exponential growth and others an exponential decay in addition to the mean loss of the passive system. In Fig. 5.5b the occupations are plotted for a loss rate of $\gamma = 2.1\kappa$ and with the same scaling to remove the overall loss in all subspaces. The result shows an exponential growth for states with more photons in the waveguide without loss ($h \lesssim n/2$). This qualitative change of the dynamics indicates that the system has to be in the $\mathcal{PT}$-broken phase. Note that this phase transition happens for all subspaces simultaneously. The reason for this is that the EP for the Hamiltonian and the Liouvillian appear at the same point in parameter space.

Unfortunately, the specific dynamics at or after the $\mathcal{PT}$-symmetry breaking cannot easily be studied due to the exponential growth, which concentrates the results for the occupations at the very end of the plotted domain of Fig. 5.5b. With the normalisation $\exp(n\gamma z)$, the occupations simply grow exponentially and without any normalisation the loss rates are too high, resulting in near zero occupations for any meaningful $z$, i.e. concentrating the resulting occupation at small $\kappa z$. One could rescale the result in the subspace with the highest photon number using the norm of the state that follows the non-Hermitian Hamiltonian, as was done in the original work [88]. This amounts to a normalisation where

$$\sum_{h=0}^{n} P(n, h, z) = 1\,, \; \forall z\,. \tag{5.82}$$

The result can be seen in Fig. 5.6, which replicates the normalised result from Ref. [88] and shows the concentration of population in states with more photons in the waveguide without loss ($h \lesssim n/2$). However, this normalisation does not work for the transiently populated subspaces with lower photon numbers because there exist no suitable references for them. For example, at $z = 0$ all occupations in the lower photon-number subspaces are zero which cannot be used for a normalisation.

Nonetheless, the phase transition from Fig. 5.5a to Fig. 5.5b is still noticeable. This shows that we can, in principle, use the derived Liouville space solution to study the full quantum evolution without discarding most of the experimental measurements via postselection. Consequently, the EP of order up to $N_{\mathrm{p}} + 1$ could be simultaneously investigated in all subspaces. For example, experimental measurements of the sensitivity, i.e. response under small perturbations, can thus utilise all outputs regardless of the number of photons reaching the detectors. However, we have seen that the needed loss to reach the EP already obscures the theoretical investigation because the exponential decay is so strong for higher photon numbers. An actual experiment might then be unreasonable without a drastic reduction in the threshold value for $\gamma$ to increase the visibilities our count rates. One possible route to overcome this problem of loss rates that are too high to see any detailed evolution could be a periodic modulation. Such periodic systems are best described in the framework of Floquet theory, which will be the focus of the next chapter where we investigate the $\mathcal{PT}$-symmetric Floquet coupler.

## Summary

In this chapter, the solutions for the quantum master equation of the lossy waveguide system were explicitly given for the two-waveguide case. Analytical calculations of the eigendecomposition solution from the previous chapter were performed. These were used to compute closed-form solutions of a two-photon coincidence rate of a HOM experiment, see Eq. (5.22). Furthermore, they allowed the construction of a general one-photon state, cf. Eq. (5.27), that experiences the least losses, i.e. is ideally propagated in the lossy waveguide coupler.

Application of the Wei-Norman method culminated in the general formula (5.66) for the evolution of Fock dyads $|\boldsymbol{n}\rangle\langle\boldsymbol{m}|$. Based on this, the generalisation of the two-photon coincidence rate for $z$-dependent system parameters was derived, see Eq. (5.67). Additionally, the logarithmic negativity for the evolution of an entangled two-photon input state was calculated. This required the full quantum evolution in contrast to the postselected two-photon coincidence rate and was done for constant as well as $z$-dependent losses.

Finally, the $\mathcal{PT}$ phase transition at higher-order EPs was investigated by calculation of the Fock-state occupation in all photon-number subspaces with a five-photon input state. The result showed the $\mathcal{PT}$ phase transition but also predicts prohibitively large losses for the higher-photon-number states. In the following chapter, this problem will be solved by using a periodically modulated loss rate.

# 6. The $\mathcal{PT}$-symmetric Floquet coupler

A major problem in observing any effects associated with exceptional points (EPs) is that they usually require strong losses to reach. For example, in the static passive $\mathcal{PT}$ coupler in Chapter 5 the $\mathcal{PT}$-breaking threshold is $\gamma = 2\kappa$. Observables, like the occupation $P(n, h, z)$ in Eq. (5.81), that rely on photon-number resolved measurements or any kind of postselection become increasingly difficult to measure because high losses translate to low count rates and thus long measurement times. However, any experiment faces a difficult challenge to measure heavily damped signals without considerable efforts to achieve the necessary signal-to-noise ratio.

Fortunately, the $\mathcal{PT}$-breaking threshold can be significantly reduced when some kind of periodic modulation is introduced to the coupler. This important result was already shown for dynamics under an effective non-Hermitian Hamiltonian [157; 158]. Here, we discuss the extension to the full quantum dynamics under the Liouvillian using the Wei-Norman solution for the lossy two-waveguide system with periodically modulated loss. The tool to describe periodic systems is the Floquet theory whose necessary basic elements are reviewed first and then applied to our Liouville formulation of the lossy waveguide system. We will see that a periodic $\mathcal{PT}$ coupler could then be brought to its EP under lower losses, bringing experimental implementations within reach.

## 6.1. Elements of Floquet theory

Floquet theory provides solutions to first-order differential equations, like the Schrödinger or paraxial Helmholz equations, that have periodic coefficients [159]. It formulates the evolution of a state with the help of Floquet eigenvalues and eigenvectors [160], i.e. in a similar manner to $z$-independent systems. The Floquet eigensystem then allows to analyse the general behaviour of the evolution, which we will use to determine the $\mathcal{PT}$-symmetric and $\mathcal{PT}$-broken phases. Note that the following introduction to Floquet theory is done for a general first-order differential equation with linear operators. However, we already use the Liouville space notation for consistency with the rest of the thesis. Afterwards, we discuss the specific applicability to the lossy waveguide systems considered in this thesis.

We start out with the differential equation

$$\partial_z |\hat{\rho}(z)\rangle\rangle = \mathcal{L}(z)\, |\hat{\rho}(z)\rangle\rangle\,, \tag{6.1}$$

with a $T$-periodic, linear operator $\mathcal{L}$. Solutions for the evolved vector are written as usual as

$$|\hat{\rho}(z)\rangle\rangle = \mathcal{U}(z)\, |\hat{\rho}(0)\rangle\rangle \,, \tag{6.2}$$

where the evolution operator $\mathcal{U}$ is also $T$-periodic. Although $z$-dependent systems generally only lead to $\mathcal{U}$ being divisible, cf. Eq. (4.12), the periodicity of $\mathcal{L}(z)$ leads to a special form of the semigroup property [160].

$$\mathcal{U}(z+T) = \mathcal{U}(z)\, \mathcal{U}(T) \,. \tag{6.3}$$

This relation implies that knowledge of $\mathcal{U}$ over one period $T$ allows the reconstruction of the evolution for arbitrary $z$, e.g. $\mathcal{U}(z+nT) = \mathcal{U}(z)\,\mathcal{U}^n(T)$.

The one-cycle evolution operator $\mathcal{U}(T)$ is the so-called *monodromy* of the evolution and is of central importance. Diagonalisation of the monodromy yields a complete basis $|n\rangle\rangle$ and eigenvalues, which are usually written in exponential form, leading to

$$\mathcal{U}(T) = \sum_n \mathrm{e}^{\mu_n T} |n\rangle\rangle\langle\langle n| \tag{6.4}$$

The values $\mu_n$ are the so-called Floquet exponents which give insight into the propagation behaviour. Their real parts are the Lyapunov exponents that indicate growth or decay and thus are vital for stability analyses of periodic systems.

In line with the exponential form of the eigenvalues of $\mathcal{U}(T)$, it is helpful to write the monodromy as

$$\mathcal{U}(T) = \exp(\mathcal{G}T) \,, \tag{6.5}$$

with a linear operator $\mathcal{G}$ whose eigenvalues are the Floquet exponents itself. However, due to the periodicity, these eigenvalues are not unique because

$$\mathrm{e}^{\mu_n T} = \mathrm{e}^{(\mu_n + \mathrm{i}k\frac{2\pi}{T})T} \,, \tag{6.6}$$

with some integer $k$, yields the same eigenvalues of $\mathcal{U}(T)$. Nonetheless, the eigenvalues $\mu_n$ are a helpful tool in analysing the propagation. When applied to the Schrödinger equation, these eigenvalues are proportional (by i) to the so-called quasienergies that are a mainstay of Floquet engineering [160].

For $z \neq T$, a useful representation of the evolution operator is

$$\mathcal{U}(z) = \mathcal{P}(z) \exp(\mathcal{G}z) \,. \tag{6.7}$$

with a $T$-periodic operator $\mathcal{P}$. A general initial state

$$|\hat{\rho}(0)\rangle\rangle = \sum_n c_n |n\rangle\rangle \tag{6.8}$$

then evolves like

$$\begin{aligned} |\hat{\rho}(z)\rangle\rangle &= \sum_n c_n\, \mathcal{P}(z)\, \mathrm{e}^{\mathcal{G}z} |n\rangle\rangle \\ &= \sum_n c_n\, \mathrm{e}^{\mu_n z} |u_n(z)\rangle\rangle \,, \end{aligned} \tag{6.9}$$

where

$$|u_n(z)\rangle\rangle = \mathcal{P}(z)|n\rangle\rangle \tag{6.10}$$

are the Floquet functions. In the Eq. (6.9), the expansion coefficients $c_n$ are constant and only the Floquet basis $\mathrm{e}^{\mu_n z}|u_n(z)\rangle\rangle$ is $z$-dependent. Therefore, this form is equivalent to a $z$-independent system only written with a $z$-dependent basis. Note that the Floquet functions $|u_n(z)\rangle\rangle$ are periodic because the operator $\mathcal{P}$ is periodic. As a result, the only amplitude altering influence can come from the Floquet or, more specifically, the Lyapunov exponents. Therefore, one has to look at the Lyapunov exponents when analysing whether a system, be it passive or active, is in the $\mathcal{PT}$-symmetric or $\mathcal{PT}$-broken phase.

For example a static, two-mode active $\mathcal{PT}$ system transitions from oscillations in the $\mathcal{PT}$ phase to one growing and one decaying mode in the $\mathcal{PT}$-broken phase. In a passive system this gets superseded by a mean loss in the $\mathcal{PT}$ phase, which leads to one reduced-loss mode and one increased-loss mode in the $\mathcal{PT}$-broken phase, cf. discussion of eigenvalues at the end of Sec. 5.1. Hence, the qualitative difference in the loss rates is a clear indication of whether a system is in the $\mathcal{PT}$-symmetric or $\mathcal{PT}$-broken phase. For periodic systems this behaviour can be deduced from the Lyapunov exponents once the monodromy matrix $\mathcal{U}(T)$ is diagonalised.

### Floquet theory in open systems

Because the Floquet theory holds for general first-order differential equations with linear operators, Hermiticity is not a requirement. Therefore, it is applicable to non-Hermitian operators $\mathcal{L}$ and thus, in principle, to open systems having a periodic Liouvillian. However, one has to carefully check whether the chosen form of $\mathcal{L}$ is a valid generator of a completely-positive, trace-preserving dynamical map. This can be fulfilled if one uses the dissipator of the accompanying $z$-independent system and replaces the occurring parameters with periodic functions. As the operators remain constant the Liouvillian remains a valid generator.

This approach was already discussed in Section 4.1.2 for general $z$-dependence. The key point was that the changes of the parameters happen on a coarse-grained scale, i.e. are slow compared to the loss mechanism. Because the photons are scattered from small modulations in the micrometer scale, a coarse-graining is already achieved when the changes happen on a centimetre scale. Under this condition, the system is approximated as having constant parameters on the micrometer scale and is well described by a Markovian system-bath interaction. As a result, the modulation frequency has to be in the range of inverse centimetres.

In the following example, we will use a periodic loss rate and we will see that the desired value for the modulation frequency is $\omega = 2\,\kappa$. The coupling strength $\kappa$ has to be weak for the coupled-mode description to be valid and is thus already of the order of $\mathrm{cm}^{-1}$. Consequently, the requirement of a slow modulation is fulfilled in our case. Therefore, we can again use the fundamental Liouvillian in Eq. (4.21) with a $z$-dependent loss rate.

As a final note, we add that there exist methods to formulate a Floquet Liouvillian in case that fast modulations change the operational form of $\mathcal{L}$ [161]. However, it might be the case that the paraxial approximation, with its assumption of a slowly-varying amplitude, breaks down first. This would require its own dedicated investigation.

## 6.2. The $\mathcal{PT}$-symmetric coupler with periodic loss

In order to make the previously considered $\mathcal{PT}$ coupler periodic, we consider the case of a periodically modulated loss in the first waveguide, i.e.

$$\gamma_1(z) = \frac{\gamma}{2}(1+\cos(\omega z))\,, \tag{6.11}$$

with period $T = 2\pi/\omega$. Apart from the $z$-independent coupling strength $\kappa$, all other parameters $(\sigma_i, \gamma_2)$ are zero.

With these preliminaries, the parameters $\gamma_1$ and $\kappa$ can be plugged into the set of nonlinear differential equations (5.41)-(5.43) and (5.59)-(5.64) to numerically solve for the functions $f_i(z)$ and $a_i(z)$, respectively. The resulting Wei-Norman expansion of the evolution superoperator $\mathcal{U}(z)$ can then be evaluated at $z = T$ to yield the monodromy of the process. In order to determine the eigenvalues of $\mathcal{U}(T)$, we first need to calculate its matrix representation. For this, we choose again the Fock basis $|\,(\boldsymbol{n},\boldsymbol{m})\rangle\rangle = |\boldsymbol{n}\rangle\langle\boldsymbol{m}|$ as already used in Eqs. (5.65) and (5.66). Note that this basis uses the Hilbert-Schmidt inner product (4.14), e.g.

$$\begin{aligned}\langle\langle(\boldsymbol{p},\boldsymbol{q})|(\boldsymbol{n},\boldsymbol{m})\rangle\rangle &= \mathrm{Tr}\left((|\boldsymbol{p}\rangle\langle\boldsymbol{q}|)^\dagger\,|\boldsymbol{n}\rangle\langle\boldsymbol{m}|\right)\\ &= \langle\boldsymbol{p}|\boldsymbol{n}\rangle\langle\boldsymbol{m}|\boldsymbol{q}\rangle.\end{aligned} \tag{6.12}$$

Additionally, one has to fix a certain order of the basis states such that a sensible index labelling can be performed. With a chosen basis, the monodromy matrix components

$$\langle\langle(\boldsymbol{p},\boldsymbol{q})|\,\mathcal{U}\,|(\boldsymbol{n},\boldsymbol{m})\rangle\rangle \tag{6.13}$$

can then be calculated using the solution of the evolved state from the previous chapter, Eq. (5.66). After diagonalisation, its eigenvalues provide the Lyapunov exponents which allow to probe the $\mathcal{PT}$ phase of the system.

### 6.2.1. Breaking of $\mathcal{PT}$ symmetry in the periodic coupler and the $\mathcal{PT}$ phase diagram

As an example we consider the case of a single photon in the two-mode waveguide system for which the Liouville space is spanned by nine states in total, e.g. $|0,0\rangle\langle 0,0|$, $|0,0\rangle\langle 1,0|$, $|0,0\rangle\langle 0,1|$, etc. The Lyapunov exponents for a loss amplitude $\gamma = 0.25\,\kappa$ and the two frequencies $\omega = 1.5\,\kappa$ and $\omega = 2\,\kappa$ are shown in Fig. 6.1a, respectively.

In the first case ($\omega = 1.5\,\kappa$, blue circles), it can be seen that the nine Lyapunov exponents occur in three sets at values $\mathrm{Re}(\mu) = 0, -\gamma/(4\kappa), -\gamma/(2\kappa)$. The first one, $\mathrm{Re}(\mu) = 0$, corresponds to the vacuum state $|0,0\rangle\langle 0,0|$ that does not show any loss. The other two

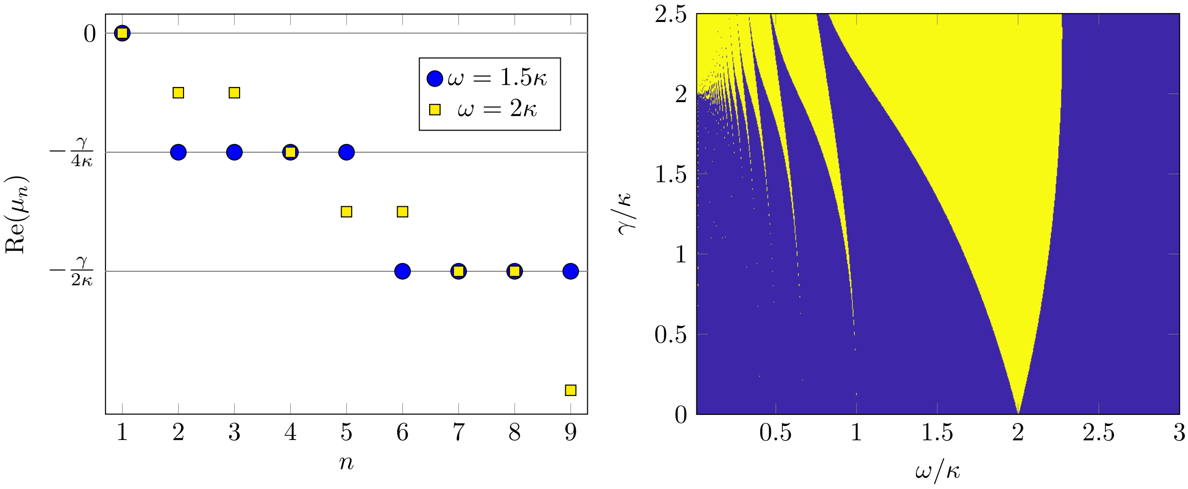

(a) Lyapunov exponents

(b) $\mathcal{PT}$phase diagram

Fig. 6.1.: (a) Lyapunov exponents for a modulated loss of amplitude $\gamma = 0.25\,\kappa$ and frequencies $\omega = 1.5\,\kappa$ and $\omega = 2\,\kappa$ corresponding to the $\mathcal{PT}$-symmetric and $\mathcal{PT}$-broken phases. The $\mathcal{PT}$ breaking is indicated by a split of the Lyapunov exponents around the mean loss values of the evolution (grey lines). (b) Full $\mathcal{PT}$ phase diagram based on the Lyapunov exponents with the $\mathcal{PT}$ phase in blue and the $\mathcal{PT}$-broken phase in yellow. At the resonance frequency of the lossless coupler, $\omega = 2\,\kappa$, the $\mathcal{PT}$-breaking threshold is greatly reduced.

sets show the mean losses for the single photon but equally distributed over the values $\gamma/(4\kappa)$ and $\gamma/(2\kappa)$, highlighted by grey lines. This two-fold structure is due to the fact that for the Liouville space we use dyads comprised of kets and bras from the underlying Hilbert space. In this case this means we get the first set from the four Liouville vectors $|0,1\rangle\langle 0,0|$, $|1,0\rangle\langle 0,0|$, $|0,0\rangle\langle 1,0|$, and $|0,0\rangle\langle 0,1|$ that contribute the one physical photon only once. For the modulated loss, see Eq. (6.11), mean value of the loss is $\gamma/4$. The second set then represents the four basis states $|0,1\rangle\langle 1,0|$, $|1,0\rangle\langle 1,0|$, $|1,0\rangle\langle 1,0|$, $|1,0\rangle\langle 0,1|$ that contribute the one physical photon twice, once from their kets and once from their bras and thus a total mean loss of $\gamma/2$ results. This structure holds also for larger photon numbers that in Hilbert space create their own ladder structure on top of this. Because the Lyapunov exponents clearly show that the system only experiences mean losses the system is in the $\mathcal{PT}$-symmetric phase.

In contrast, the Lyapunov exponents seen for the second case ($\omega = 2\kappa$, yellow squares in Fig. 6.1a, show a clear splitting from the mean values. This splitting is the signature of the $\mathcal{PT}$-broken phase. Based upon this criteria a $\mathcal{PT}$ phase diagram was calculated, which is seen in Fig. 6.1b with $\omega$-$\gamma$-axes scaled by $\kappa$. Here, the $\mathcal{PT}$ phase is coloured blue and the $\mathcal{PT}$-broken phase is yellow. The phase diagram shows that a $\mathcal{PT}$-phase transition can occur for different loss rate amplitudes $\gamma$ depending on the modulation frequency $\omega$. Most importantly, the static $\mathcal{PT}$-breaking threshold $\gamma = 2\,\kappa$ can be reduced considerably for certain frequencies. This is most prominent at the resonance frequency of the bare coupler, $\omega = 2\,\kappa$, for which the $\mathcal{PT}$ symmetry is broken for arbitrarily small loss rate amplitudes $\gamma$. For fractions of this resonance frequency, i.e. $\omega = \kappa, \kappa/2, \kappa/3, \dots$, similar features appear in the phase diagram. However, these cannot be seen to reach $\gamma \approx 0$ because of their small width along the $\omega$-axis. This behaviour of the $\mathcal{PT}$ phase diagram was also recorded in Ref. [157; 158] in case of the Rabi model, thus confirming our results.

We note that the phase diagram in Fig. 6.1b was calculated for a single photon but it stays the same regardless of the chosen number of photons. In fact, the phase diagram is the same as if we directly used the underlying effective non-Hermitian Hamiltonian and calculated a monodromy matrix in Hilbert space. This is to be expected because the effective non-Hermitian Hamiltonian governs the dynamics in the subspace of highest-photon number regardless of the system being periodic or not. In conjunction with the observation that all subspaces simultaneously cross the EP, as seen from Figs. 5.5 and 5.5b, it is obvious that this direct link of the $\mathcal{PT}$ phase to $\boldsymbol{H}_{\text{eff}}$ should also exist in the Floquet case. This reiterates the connection of the eigensystems and EPs of $\boldsymbol{H}_{\text{eff}}$ and $\mathcal{L}$ already made in Chapter 4.

Although this might simplify the calculation of the $\mathcal{PT}$phase diagram, this does not mean that the Floquet calculation of the monodromy $\mathcal{U}(T)$ in Liouville space was in vain. This is because we still need the full quantum calculation when calculating observables in all subspaces. In addition, the full solution provides all the Floquet exponents and functions for the decomposition (6.9). This allows a propagation analysis similar to the analysis based on the eigendecomposition in the $z$-independent case, cf. Eq. (4.82). This opens the door to Floquet engineering as in closed systems, cf. Ref. [160].

### 6.2.2. Exceptional points with reduced threshold

The key feature of the phase diagram in Fig. 6.1b was that it showed a strongly reduced $\mathcal{PT}$-breaking threshold for the loss rate amplitude $\gamma$ at and around the resonance frequency $\omega = 2\,\kappa$. In the static case this threshold was $\gamma = 2\,\kappa$, resulting in a strong overall loss. This overall loss can now be reduced considerably with the Floquet coupler at resonance, thus paving the way to efficiently probing the $\mathcal{PT}$ phase transition.

An example of how a modulated loss rate reduces the EP threshold can be seen by returning to the occupation $P(n, h, z)$ of states $|n - h, h\rangle$ as introduced in Eq. (5.81). With the monodromy matrix already computed to obtain the $\mathcal{PT}$ phase diagram, the evolution can be calculated at any given value of $z$ using Eq. (6.3). For values $z \gg T$ this greatly reduces the numerical effort as it allows to decompose the total evolutions into repeated applications of the monodromy followed by one application of the fractional evolution $\mathcal{U}(z)$. The occupation itself can then be calculated by similar steps as for the $z$-independent case using Eq. (5.66).

In Fig. 6.2 two results are shown for the input state $|\psi\rangle = (|0, 5\rangle + |5, 0\rangle)/\sqrt{2}$ as was used in Fig. 5.5. However, this five-photon state is now in both cases subject to the same loss amplitude $\gamma = 0.25\,\kappa$ but with different modulation frequencies. In Fig. 6.2a the frequency is $\omega = 1.5\,\kappa$ and in Fig. 6.2b it is $\omega = 2\,\kappa$. Judging from the $\mathcal{PT}$ phase diagram in Fig. 6.1b, the system is for $\omega = 1.5\kappa$ in the $\mathcal{PT}$-symmetric phase, whereas for $\omega = 2\,\kappa$ it is in the $\mathcal{PT}$-broken phase.

The occupation in Fig. 6.2a shows the case of $\mathcal{PT}$ symmetry with two oscillating strands that are overlaid by an overall loss. These two oscillating strands are the Floquet versions of the oscillations of the $z$-independent case. They occur with decreased losses in all subspaces except, of course, the vacuum subspace. In contrast, the $\mathcal{PT}$-broken case in Fig. 6.2b shows one of the strands being strongly damped and the other surviving for far longer, even compared to the $\mathcal{PT}$-symmetric case. The physical explanation for this is that a $z$-dependent mode (a strand) is strongly damped if it is predominantly concentrated in states $|n-h,h\rangle$ with more photons in the lossy waveguide when $\gamma_1(z)$ is large. The complement is the mode that undulates in just such a way that it is concentrated in the low-loss states, i.e. more photons in the loss-less waveguide, when $\gamma_1(z)$ is large. This mode then only occupies states with more photons in the lossy waveguide when $\gamma_1(z)$ is low. We note that this is simply the Floquet analogue of the usual signature of broken $\mathcal{PT}$ symmetry of one mode being amplified and the other suppressed.

The two results in Fig. 6.2 are interesting because they have the same loss amplitude $\gamma$ and differ only in the modulation frequency $\omega$. Yet, they show qualitatively different evolutions depending on whether or not they are in the $\mathcal{PT}$-symmetric or $\mathcal{PT}$-broken phase. Most notably, however, is that the used loss rate amplitude is only an eighth of the value needed to reach the EP in the unmodulated case. The $\mathcal{PT}$ phase transition can therefore easily be observed without any specific rescaling or normalisation, which was necessary in the $z$-independent case and a potentially major problem for any experimental test. As seen in the $\mathcal{PT}$ phase diagram, one could go to even lower loss amplitudes $\gamma$ as long as one stays at the resonance frequency $\omega = 2\,\kappa$. However, for smaller values of $\gamma$ the width of the $\mathcal{PT}$-broken phase becomes progressively narrower. This puts an increasingly high demand on the experimental precision. Nonetheless, the demonstrated Floquet $\mathcal{PT}$ coupler shows symmetry breaking at attainable losses which might prove to be the fitting platform to probe $\mathcal{PT}$ phase transitions in experiments.

## Summary

In this chapter we solved the problem of a prohibitively high loss required to reach the EP for the static $\mathcal{PT}$ coupler, i.e. $\gamma = 2\kappa$. This threshold was considerably reduced by using a periodically modulated loss rate, which we described in the framework of Floquet theory. Key point was the calculation of the monodromy matrix of the evolution using the two-waveguide Wei-Norman expansion from the previous chapter. The Lyapunov exponents of this monodromy matrix then showed a splitting whenever the system is in the $\mathcal{PT}$-broken phase and otherwise followed the mean loss when in the $\mathcal{PT}$-symmetric phase. Based on this criterion, a $\mathcal{PT}$ phase diagram was calculated that showed a reduced EP threshold at the resonance frequency of the bare, lossless coupler. This was confirmed by a calculation of the Fock-state occupation in all photon-number subspaces of a five-photon input state, as used in the previous chapter. Now, the $\mathcal{PT}$ phase transition was observed at $\gamma = 0.25\kappa$ with the potential of even lower values. This paves the way to realistic implementations to investigate the phase transition with multiple photons.

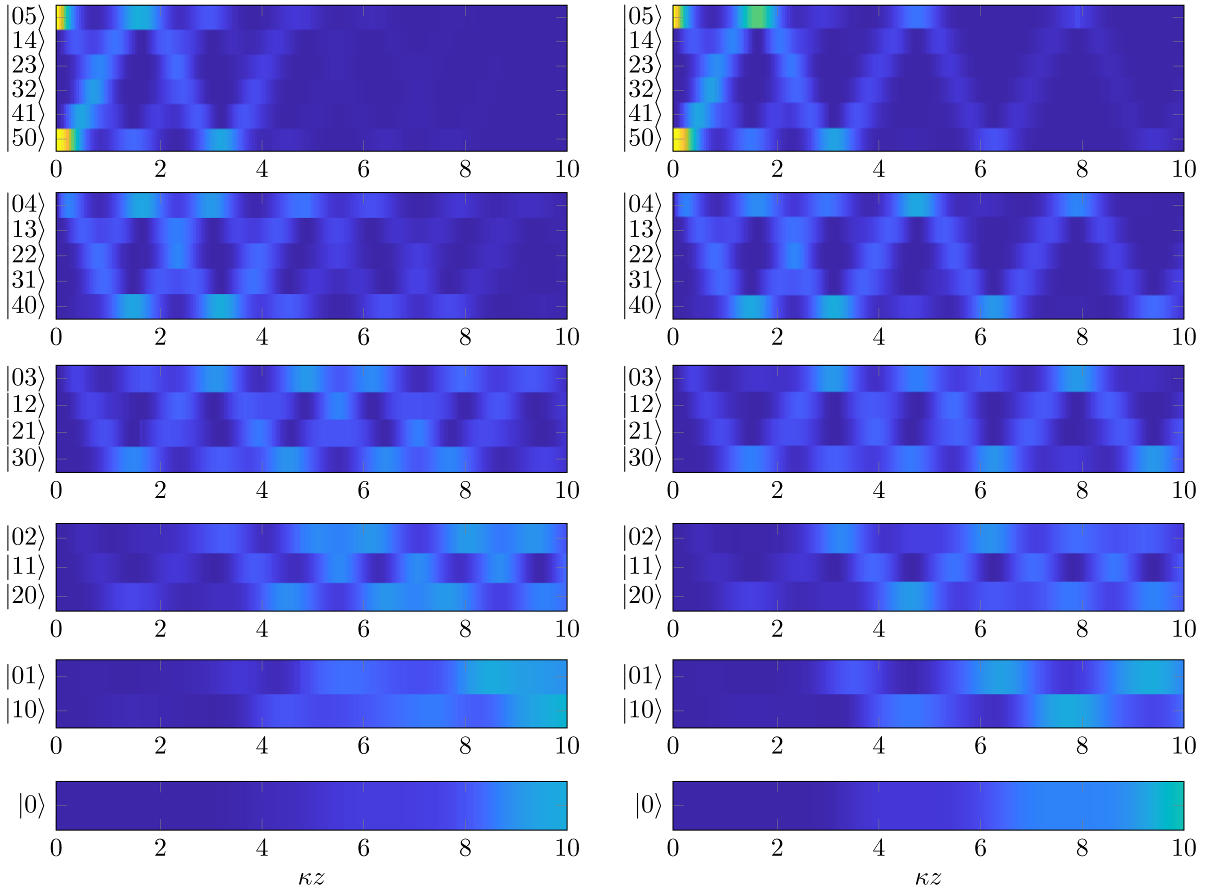

(a) Floquet $\mathcal{PT}$-symmetric phase

(b) Floquet $\mathcal{PT}$-broken phase

Fig. 6.2.: Occupations in the Floquet $\mathcal{PT}$ coupler for the input state $|\psi\rangle = (|5,0\rangle + |0,5\rangle)/\sqrt{2}$ over all subspaces with photon numbers $n \in \{0,1,2,3,4,5\}$. (a) $\mathcal{PT}$-symmetric case for $\gamma = 0.25\,\kappa$ and $\omega = 1.5\,\kappa$ where the system experiences oscillations with a common mean loss. (b) $\mathcal{PT}$-broken case for $\gamma = 0.25\,\kappa$ and $\omega = 2\,\kappa$ where instead the system has one growing and one decaying Floquet mode with mean loss on top.

# 7. Conclusion

This thesis revolves around theoretical descriptions of integrated photonic waveguides for the implementation of holonomic quantum gates and $\mathcal{PT}$ symmetries. The employed methods range from differential geometry, at the core of the holonomic computation, to Lie algebraic techniques for solving a quantum master equation of lossy waveguide systems. For both, the basis is a coupled-mode description originating from the paraxial Helmholtz equation that models the light propagation along the propagation direction $z$ (Chapter 2). This allows to test first-quantisation features within classical optics due to the mathematical equivalence to the Schrödinger equation. A proper quantisation then yielded equations of motions for the bosonic mode operators of the coupled single-mode waveguides.

This coupled-mode equation was employed to design a tripod waveguide system that implements a unitary gate, i.e. a holonomy, inside a degenerate subspace after cyclic adiabatic parameter variations. Key requirement was the adiabaticity of the variations, which was assured by an optimisation scheme based on the quantum metric. This optimisation enabled the design of a waveguide tripod that was experimentally tested in a collaboration with the group of Professor Alexander Szameit (Chapter 3). In an extension of the basic theory of holonomic quantum computation, we showed how the dimension of the holonomic gate can be increased by using multi-photon Fock states that nonlinearly increase the dimension of the degenerate subspace. Furthermore, an extension of the Hermitian theory to non-Hermitian Hamiltonians, and thus nonunitary holonomies, was discussed. This lead to an increase in the number of degrees-of-freedom by virtue of having more system parameters, e.g. loss rates. Such non-Hermitian Hamiltonians are frequently used in semiclassical approaches to open quantum systems but do not describe a true quantum evolution because they do not constitute a completely-positive, trace-preserving transformation. The question was thus raised, how such non-Hermitian Hamiltonians might correctly be implemented in an open system.

This question was answered in Chapter 4, where we demonstrated how a lossy waveguide system can be described in a full-quantum treatment based on a Markovian quantum master equation and under what conditions it suffices to use a non-Hermitian Hamiltonian. For this, we utilised two Lie algebraic approaches that analytically solve the quantum master equation in Liouville space, i.e. in which a Liouvillian takes on the role of the Hamiltonian of conventional quantum physics. First, we constructed ladder operators by diagonalising the regular representation of the Liouvillian. This allowed to construct a basis of eigenvectors which, in the $z$-independent case, can be used in conjunction with the Liouvillian's eigenvalues to calculate the evolution operator in Liouville space. The evolved quantum state can then be given as a decomposition in these Fock-like eigenstates. This opens the way to analyse the propagation behaviour of an input state based on the overlap with the eigenvectors and the respective eigenvalues. However, because the eigenvectors in Liouville space are not physical states of the underlying Hilbert space themselves, we showcased how to construct physical states from these eigenvectors. This discussion also showed that the eigenvectors of the Liouvillian actually included the eigenvectors of the related non-Hermitian Hamiltonian in Hilbert space once a postselection to the highest-photon subspace was made. This is due to the block structure of the regular representation of the Liouvillian, which contained the non-Hermitian Hamiltonian as one of its blocks.

The second approach was a Wei-Norman expansion of the evolution operator. This method is generally applicable to $z$-dependent systems and hinges on a structure analysis of the Lie algebra induced by the Liouvillian. The algebraic structure and the resulting decomposition of the Wei-Norman expansion confirmed the observation of the "hidden" non-Hermitian Hamiltonian under postselection. Under certain restrictions the evolution of the full quantum master equation was found to be equivalent to the dynamics under a non-Hermitian Hamiltonian with gain and loss plus an overall mean loss. These restriction were that the input state is only element of the highest-photon-number subspace and that all measurements are postselected to this subspace. Consequently, a passive, i.e. all-loss, waveguide system can be used to implement an active non-Hermitian Hamiltonian once postselected to the highest-photon-number space and corrected for the overall mean loss.

The eigendecomposition based on the regular representation as well as the Wei-Norman expansion were both applied to the instructive example of a passive $\mathcal{PT}$ coupler where one waveguide experiences loss (Chapter 5). Based on the eigendecomposition, analytical solutions for the two-photon correlation of a HOM experiment were calculated. Additionally, an ideally transported input state was constructed for a general lossy waveguide coupler after careful examination of the system's eigenvectors and eigenvalues in Liouville space.

The Wei-Norman method not only confirmed the analytical $z$-independent solution for the two-photon correlation but also generalised it to the $z$-dependent case. However, because the two-photon correlation is measured via postselection to the highest-photon-number subspace, it could already be computed directly with an effective non-Hermitian Hamiltonian. In order to show the full capability of our Liouville space solution, we also used the Wei-Norman method to calculate the logarithmic negativity of a two-photon input state, for which all photon-number subspaces are needed. This showed the degradation of entanglement with constant as well as $z$-dependent losses. Furthermore, the expansion was used to calculate the occupation of multiphoton states over the two waveguide modes. The calculation replicated earlier results in the highest-photon-number subspace, where the non-Hermitian Hamiltonian is sufficient, but gave solutions in all photon-number subspaces. This occupation was used to indicated a phase transition from the $\mathcal{PT}$-symmetric to the $\mathcal{PT}$-broken phase. However, this phase transition at the EP needed a high loss rate, which obscured the evolution and is thus not well suited for experimental implementation.

The problem of a prohibitively high loss rate to reach the EP was solved by introducing modulations into the system (Chapter 6). A calculation based on Floquet theory lead to a $\mathcal{PT}$ phase diagram that showed a significant decrease of the EP threshold when the modulation frequency is tuned to the resonance frequency of the lossless coupler.

Calculations of the occupation of multiphoton states for the modulated system confirmed that phase transitions can take place at much lower losses.

## Outlook

The developed techniques establish a theoretical basis that can be used not only for intricate implementations of optical holonomic quantum computing but also allow to test new frontiers of quantum $\mathcal{PT}$-symmetric effects.

The emergence of artificial non-Abelian gauge fields and holonomies together with the quantum metric-based optimisation already enabled a proof-of-principle experiment. The present theoretical work allows to build upon this in order to construct higher-dimensional gauge fields and holonomies using multiple photons. However, this might require a thorough investigation into the completeness of the constructed unitary groups. Using the discussed nonunitary holonomies for a larger parameter space, e.g. by inclusion of loss rates, could be enough to obtain the number of required closed curves but it its unknown where the limits for this approach lie. Also, for the simulation of nontrivial gauge field theories one would need some kind of interaction between the field and particles or other gauge fields. This could possibly be achieved by coupling multiple waveguide tripods but has not yet been completely conceptualised.

Quantum $\mathcal{PT}$-symmetric systems still pose many interesting questions and the present contribution might prove to be pivotal in the design and description of future experiments. For example, the distinction between the full quantum treatment and the (semi)classical approach might be tested by taking a closer look at the subtle differences of the higher order EPs of the Liouvillian and its respective effective non-Hermitian Hamiltonian. In addition, the correct quantum description of the lossy waveguides allows to use arbitrary nonclassical states such as entangled or squeezed states. The dynamics of such states at or near the EP are especially interesting as they might be used to counteract the quantum noise and thus lead the way to quantum $\mathcal{PT}$ sensors.

# A. Geometric interpretation of adiabatic transport in degenerate subspaces

In this appendix we try to give the reader a better understanding of the geometric interpretations as used in Chapter 3. The mentioned parts in the main text can be thought of as the tips of icebergs and in this appendix we take a look at the first metre below water that shows that these tips indeed belong to the same iceberg. This below-water-level approach to the geometric interpretation is based on [162; 108; 114; 117]. Readers not suffering from thalassophobia[1] might start their investigation at [105].

We start with a family of Hamiltonians $\{\hat{H}(\boldsymbol{x})\}$ that are parametrised by $N_{\mathcal{M}}$ classical system parameters $x^\nu, \nu = 1, \ldots, N_{\mathcal{M}}$ that define a point in the parameter manifold $\mathcal{M}$. The Hamiltonians act on a Hilbert space $\mathbb{C}^N$ with a $N_{\mathcal{D}}$-fold degenerate ground-state with zero energy, i.e. the *dark subspace* on which we want to implement our non-Abelian gauge fields or holonomies. The $N_{\mathcal{D}}$ dark states $|\mathcal{D}_a(\boldsymbol{x})\rangle$, $(a = 1, \ldots, N_{\mathcal{D}})$ form an $N$-dimensional, orthonormal basis at each point $\boldsymbol{x} \in \mathcal{M}$. When adiabatically traversing a curve $\mathcal{C}$ in $\mathcal{M}$ the dark subspace is kept well separated from the excited states and the dynamic of a state initially prepared in the dark state is exclusively restricted to it. This can be interpreted as equipping each point $\mathcal{M}$ with a $N_{\mathcal{D}}$*-frame* of the dark states.

We now order the $N$-dimensional dark states in a $N \times N_{\mathcal{D}}$ matrix $\boldsymbol{V}(\boldsymbol{x})$, i.e. in case of the tripod in the main text with the two dark states from Eqs. (3.35) and (3.36)

$$\boldsymbol{V} = \begin{pmatrix} \sin(\theta) & \sin(\phi)\cos(\theta) \\ -\cos(\theta) & \sin(\phi)\sin(\theta) \\ 0 & -\cos(\phi) \\ 0 & 0 \end{pmatrix}. \tag{A.1}$$

The matrix $\boldsymbol{V}$ represents the $N_{\mathcal{D}}$-frame and it constitutes a so-called Stiefel manifold

$$S_{N,N_{\mathcal{D}}}(\mathbb{C}) \cong \{\boldsymbol{V} \in \mathbb{C}^{N\times N_{\mathcal{D}}} | \boldsymbol{V}^\dagger \boldsymbol{V} = \mathbf{1}_{N_{\mathcal{D}}}\}. \tag{A.2}$$

When traversing the curve $\mathcal{C}$ in the parameter manifold, each $N_{\mathcal{D}}$-frame is connected to its infinitesimal neighbour in a nontrivial way since the basis vectors are $\boldsymbol{x}$-dependent. The canonical connection $\mathcal{A} = \boldsymbol{A}_\mu \mathrm{d}x^\mu$ on $S_{N,N_{\mathcal{D}}}(\mathbb{C})$ is a $\mathfrak{u}(N_{\mathcal{D}})$-valued one-form where $\mathfrak{u}(N_{\mathcal{D}})$ is the unitary algebra of dimension $N_{\mathcal{D}}$ The connection contains the information of how to *glue* the different $N_{\mathcal{D}}$-frames together and it is defined by

$$\mathcal{A} = V^\dagger \mathrm{d}V. \tag{A.3}$$

---

[1] The intense fear or dread of deep bodies of water.

Explicitly writing down this one-form for variation in the coordinates $x^\mu$, we find our gauge field

$$(\mathcal{A})_{ij} = (A_\mu)_{ij}\,\mathrm{d}x^\mu\,, \tag{A.4}$$

with

$$(A_\mu)_{ij} = \langle \mathcal{D}_i|\partial_\mu|\mathcal{D}_i\rangle. \tag{A.5}$$

As mentioned above, the connection $\mathcal{A}$ defines how to compare different $N_\mathcal{D}$-frames when travelling along $\mathcal{C}$ in $\mathcal{M}$ and with that also a notion of parallel transport. From the main text we also know that this connection is a gauge field connection with the unitary group $\mathrm{U}(N_\mathcal{D})$ as gauge symmetry. Additionally, we also showed in the main text that when the state is parallel transported it is always projected unto the dark subspace and thus undergoes an adiabatic evolution [114]. This marks the projection operator $\hat{P}$ onto the dark subspaces as an especially interesting quantity connected to the adiabaticity of the evolution. The projector $\hat{P}$ is formally defined in terms of Grassmann manifolds [108; 117]

$$G_{N,N_\mathcal{D}}(\mathbb{C}) = \{\hat{P}\in\mathbb{C}^{N\times N}|\hat{P}^2=\hat{P},\hat{P}^\dagger=\hat{P},\mathrm{Tr}\,\hat{P}=N_\mathcal{D}\}. \tag{A.6}$$

The importance of the projector for the adiabaticity of the evolution of a quantum state following the frames $\boldsymbol{V}$ is by no means accidentally. In fact, the Stiefel and Grassmann manifolds are intricately linked as they together form a principal $U(N_\mathcal{D})$-fibre bundle $(S_{N,N_\mathcal{D}}, G_{N,N_\mathcal{D}}, \pi, U(N_\mathcal{D}))$ under right-action of unitary matrices $U(N_\mathcal{D})$ on $S_{N,N_\mathcal{D}}$ and the map

$$\pi: S_{N,N_\mathcal{D}} \to G_{N,N_\mathcal{D}}, \qquad \pi(V) = VV^\dagger. \tag{A.7}$$

A simpler explanation as to why the Grassmann manifolds is so important for the evolution of a degenerate Hamiltonian is found when using the alternative definitions

$$G_{N,N_\mathcal{D}}(\mathbb{C}) \cong \frac{\mathrm{U}(N)}{\mathrm{U}(N_\mathcal{D})\times\mathrm{U}(N-N_\mathcal{D})}. \tag{A.8}$$

Informally speaking, the Grassmann manifold $G_{N,N_\mathcal{D}}(\mathbb{C})$ is the manifold of all unitary evolutions $\mathrm{U}(N)$, i.e. all physical evolution of the $N\times N$ Hamiltonian, which show a clear separation into a $\mathrm{U}(N_\mathcal{D})$ and $\mathrm{U}(N-N_\mathcal{D})$ submanifold, i.e. the $N_\mathcal{D}$-degenerate subspace and the rest of the total Hilbert space.

The parallel or adiabatic transport that is exactly defined as such a separate evolution is therefore best described with the Grassmann manifold. On the other hand, the gauge field connection (A.3) lives in the Stiefel manifold and both manifolds are connected via the principal bundle structure (A.7). This bundle is perhaps ideally identified with the simple fibre drawn in Fig. 3.1b of the main text. The parameter manifold is still underlying all these manifolds, but as we have seen the exact fibre structure is more complicated.

With the importance of the Grassmann manifold for the adiabaticity established we can justify the emergence of the quantum metric in Eq. (3.32) in the main text as it is simply the metric on $G_{N,N_\mathcal{D}}(\mathbb{C})$,

$$||\mathrm{d}P||^2 = \mathrm{Tr}\,(\mathrm{d}P\mathrm{d}P)\,, \tag{A.9}$$

where for a given parametrisation $\{x^\nu\}$ we have

$$\mathrm{Tr}\,(\mathrm{d}P\mathrm{d}P) = \mathrm{Tr}\,(\partial_\mu P \partial_\nu P)\,\mathrm{d}x^\mu \mathrm{d}x^\nu = g_{\mu\nu}\mathrm{d}x^\mu \mathrm{d}x^\nu, \tag{A.10}$$

with the quantum metric

$$g_{\mu\nu} = \mathrm{Tr}\,(\partial_\mu P \partial_\nu P)\,. \tag{A.11}$$

For the tripod case, i.e. using (A.1) and the map (A.7), we find

$$\boldsymbol{g} = 2\mathrm{diag}\left(1, \cos^2(\phi)\right). \tag{A.12}$$

As discussed in the main text, we can theoretically look for the geodesics that minimise the path traversed in the Grassmann manifold and thus create the most adiabatic evolution. The geodesic equations derived from the quantum metric are

$$\mathrm{d}_z^2\phi + \cos\phi\sin\phi(\mathrm{d}_z\theta)^2 = 0, \tag{A.13}$$

$$\mathrm{d}_z^2\theta - 2\tan\phi\mathrm{d}_z\theta\mathrm{d}_z\phi = 0 \tag{A.14}$$

and the boundary conditions can be drawn from the initial and final states as listed in Eq. (3.48) for which we set $P(z_\mathrm{i})/S(z_\mathrm{i}) \approx 0$ and $S(z_\mathrm{f})/P(z_\mathrm{f}) \approx 0$. These translate into boundary conditions $\phi(z_\mathrm{i}) = \phi(z_\mathrm{f}) = \pi/2$ and $\theta(z_\mathrm{i}) = 0$, $\theta(z_\mathrm{f}) = \pi/2$. This yields $\phi(z) = \pi/2$ and $\theta(z) = \pi/2z$ for the geodesic which coincides with the result found in [163] using the Dykhne-Davis-Pechukas (DDP) method to minimize nonadiabatic transitions. However, as discusses in the main text, this geodesic is not feasible in a realistic experiment that puts additional constraints on the parameter variations, e.g. coupling strength, which is why this geodesic is not used in the optimisation.

We close this appendix with two final points. First, we mentioned in the main text that the Christoffel symbol $\Gamma^\nu_{\mu\epsilon}$ and the gauge field $(A_\mu)_{ij}$ are both connections but are not identical. This manifested itself in the different nature of the Latin and Greek indices in $(A_\mu)_{ij}$ and $\Gamma^\nu_{\mu\epsilon}$. We already alluded to the fact that this is due to the different "nature" of the fibres and now we have seen the detailed fibre bundle structure of the gauge field connection. The Christoffel symbol is then identified with tangent fibre spaces comprised of the tangent planes (or frames) defined at each point of a coordinate manifold via derivatives along the coordinate lines. In a more general picture this is connected to the symmetry group or transformation operations under consideration. For the gauge field connection $(A_\mu)_{ij}$ this is $U(N_\mathcal{D})$, i.e. rotations in the dark subspace, whereas for the Christoffel symbol these are the Jacobi matrices, i.e. coordinate transformations.

This difference leads to the fact that one cannot use the metric tensor $\tilde{g}_{\mu\varepsilon}$ from differential geometry which is directly connected to the Christoffel symbol via

$$\Gamma^\nu_{\mu\epsilon} = \frac{1}{2}\tilde{g}^{\nu\gamma}\left(\partial_\varepsilon\tilde{g}_{\gamma\mu} + \partial_\mu\tilde{g}_{\gamma\varepsilon} - \partial_\gamma\tilde{g}_{\mu\varepsilon}\right). \tag{A.15}$$

Geodesics are often only known from this geometric standpoint, e.g. the shortest flight paths on the globe from the metric $\tilde{g}_{\mu\varepsilon}$ for spherical coordinates. For the gauge field connection there is no such relation to the quantum metric which needs the more complicated approach via the Grassmann manifolds and fibre bundles. Indeed, the actually compatible metric to the gauge field connection is the trivial metric $\delta_{ij}$. It correctly gives the scalar products of the dark states $\langle\mathcal{D}_i(z)|\mathcal{D}_j(z)\rangle = \delta_{ij}\,\forall z$ and it fulfils the requirement of vanishing covariant derivative [164], i.e.

$$\mathrm{D}\delta_{ij} = \partial\delta_{ij} - A_i^k\,\delta_{kj} - A_j^k\,\delta_{ik} = 0. \tag{A.16}$$

The fact that the metric for the Latin indices is the trivial metric, is also the reason why we did not chose to use the covariant representation with upper and lower indices as there is no distinction with the trivial metric $\delta_{ij}$. The Eq. (A.16) also is important because it ensures that $\boldsymbol{A}_\nu^\dagger = -\boldsymbol{A}_\nu$, i.e. the correct condition of anti-Hermiticity that leads to a unitary operator $\boldsymbol{\mathcal{U}} = \mathcal{P}\exp\left(-\oint A_\nu \mathrm{d}x^\nu\right) \in U(N_{\mathcal{D}})$.

The second and last point concerns the quantum geometric tensor (QGT) mentioned in the main text, whose trace of its real part is the quantum metric $g_{\mu\nu}$ and imaginary part is the field strength tensor $\boldsymbol{F}_{\mu\nu}$. Due to these connections, the QGT is vital in any geometric or topological investigation of physical systems and recently the QGT was measured by itself [165; 166]. Here, we show for completeness that the above claimed connections hold true.

The components of the QGT $\boldsymbol{Q}_{\mu\nu}$ in an $N$-fold degenerate system with basis states $|\psi_i\rangle$ $(i = 1, N)$ are defined as [114]

$$(\boldsymbol{Q}_{\mu\nu})_{ij} = \langle\partial_\mu\psi_i|(1-\hat{P})|\partial_\nu\psi_j\rangle\,, \tag{A.17}$$

with $\hat{P} = \sum_k |\psi_k\rangle\langle\psi_k|$. The imaginary part of $\boldsymbol{Q}_{\mu\nu}$ has the components

$$\begin{aligned}(\boldsymbol{Q}_{\mu\nu} - \boldsymbol{Q}_{\mu\nu}^\dagger)_{ij} =& \langle\partial_\mu\psi_i|\partial_\nu\psi_j\rangle - \langle\partial_\nu\psi_i|\partial_\mu\psi_j\rangle \\ &- \sum_k \langle\partial_\mu\psi_i|\psi_k\rangle\langle\psi_k|\partial_\nu\psi_j\rangle \\ &- \sum_k \langle\partial_\mu\psi_k|\psi_j\rangle\langle\psi_i|\partial_\nu\psi_k\rangle\,,\end{aligned} \tag{A.18}$$

when using the relations $(\boldsymbol{Q}_{\mu\nu}^\dagger)_{ij} = (\boldsymbol{Q}_{\mu\nu})_{ji}^*$, $\langle\psi|\phi\rangle^* = \langle\phi|\psi\rangle$, and $\langle\partial_\mu\psi_i|\psi_j\rangle = -\langle\psi_i|\partial_\mu\psi_j\rangle$ $(\forall i, j)$. The later results from the orthogonality of the basis, i.e. $\partial_\mu\langle\psi_i|\psi_j\rangle = \partial_\mu\delta_{ij} = 0$.

In comparison, when using the definition of the gauge field connection (A.5) the field strength tensor is

$$\begin{aligned}\boldsymbol{F}_{\mu\nu} &= \partial_\mu\boldsymbol{A}_\nu - \partial_\nu\boldsymbol{A}_\mu + [\boldsymbol{A}_\mu, \boldsymbol{A}_\nu] \\ &= \sum_{ij}\partial_\mu(\boldsymbol{A}_\nu)_{ij}|\psi_i\rangle\langle\psi_j| - \sum_{ij}\partial_\nu(\boldsymbol{A}_\mu)_{ij}|\psi_i\rangle\langle\psi_j| + \sum_{ijmn}(\boldsymbol{A}_\mu)_{ij}(\boldsymbol{A}_\nu)_{mn}\Big[|\psi_i\rangle\langle\psi_j|, |\psi_m\rangle\langle\psi_n|\Big] \\ &= \sum_{ij}\Big(\langle\partial_\mu\psi_i|\partial_\nu\psi_j\rangle - \langle\partial_\nu\psi_i|\partial_\mu\psi_j\rangle \\ &\qquad - \sum_k\langle\partial_\mu\psi_i|\psi_k\rangle\langle\psi_k|\partial_\nu\psi_j\rangle - \sum_k\langle\partial_\mu\psi_k|\psi_j\rangle\langle\psi_i|\partial_\nu\psi_k\rangle\Big)|\psi_i\rangle\langle\psi_j|\,,\end{aligned} \tag{A.19}$$

where we used the same relations as above as well as the fact that $|\partial_\mu\partial_\nu\psi\rangle = |\partial_\nu\partial_\mu\psi\rangle$ and

$$\Big[|\psi_i\rangle\langle\psi_j|, |\psi_m\rangle\langle\psi_n|\Big] = \delta_{jm}|\psi_i\rangle\langle\psi_n| - \delta_{ni}|\psi_m\rangle\langle\psi_j|. \tag{A.20}$$

The components of $\boldsymbol{F}_{\mu\nu}$ then coincide with $(\boldsymbol{Q}_{\mu\nu} - \boldsymbol{Q}^\dagger_{\mu\nu})_{ij}$ from Eq. (A.18).

Likewise, the trace of the real part of $\boldsymbol{Q}_{\mu\nu}$ is

$$\begin{aligned}\mathrm{Tr}(\boldsymbol{Q}_{\mu\nu} + \boldsymbol{Q}^\dagger_{\mu\nu}) =& \sum_i \Big( \langle \partial_\mu \psi_i | \partial_\nu \psi_i \rangle + \langle \partial_\nu \psi_i | \partial_\mu \psi_i \rangle \\ & - \sum_k \left( \langle \partial_\mu \psi_i | \psi_k \rangle \langle \psi_k | \partial_\nu \psi_i \rangle + \langle \partial_\nu \psi_i | \psi_k \rangle \langle \psi_k | \partial_\mu \psi_i \rangle \right) \Big) \end{aligned} \tag{A.21}$$

which equals

$$\begin{aligned} g_{\mu\nu} = \mathrm{Tr}\left(\partial_\mu \hat{P}\, \partial_\nu \hat{P}\right) =& \sum_{ik} \langle \psi_k | \partial_\mu \psi_i \rangle \langle \psi_i | \partial_\nu \psi_k \rangle + \langle \partial_\nu \psi_k | \psi_i \rangle \langle \partial_\mu \psi_i | \psi_k \rangle \\ & \quad + \langle \partial_\nu \psi_k | \partial_\mu \psi_i \rangle\, \delta_{ik} + \langle \partial_\mu \psi_i | \partial_\nu \psi_k \rangle\, \delta_{ik} \\ =& \sum_i \Big( \langle \partial_\mu \psi_i | \partial_\nu \psi_i \rangle + \langle \partial_\nu \psi_i | \partial_\mu \psi_i \rangle \\ & \quad - \sum_k \left( \langle \partial_\mu \psi_i | \psi_k \rangle \langle \psi_k | \partial_\nu \psi_i \rangle + \langle \partial_\nu \psi_i | \psi_k \rangle \langle \psi_k | \partial_\mu \psi_i \rangle \right) \Big), \end{aligned} \tag{A.22}$$

when we use the relation $\langle \partial_\mu \psi_i | \psi_j \rangle = -\langle \psi_i | \partial_\mu \psi_j \rangle$ again. The quantum geometric tensor thus captures elegantly all the geometric properties of the evolution in a united formulation.

# B. Non-Abelian gauge fields from a detuned waveguide tripod

We consider a system of four waveguides where three waveguides $L$, $R$, $U$ are placed around a central waveguide $C$, cf. Fig. 3.3c. The outer waveguides are sufficiently far apart from each other such that they do not couple. However, they couple indirectly via the central waveguide. In addition, the upper waveguide has a detuning $\Delta\beta$ of its propagation constant with respect to the other waveguides.

Using the tight-binding approximation, the following equations of motion for the amplitudes in the respective waveguides result

$$\mathrm{i}\,\partial_z \begin{pmatrix} a_L \\ a_R \\ \tilde{a}_U \\ a_C \end{pmatrix} = \begin{pmatrix} 0 & 0 & 0 & S \\ 0 & 0 & 0 & P \\ 0 & 0 & \Delta\beta & Q \\ S & P & Q & 0 \end{pmatrix} \cdot \begin{pmatrix} a_L \\ a_R \\ \tilde{a}_U \\ a_C \end{pmatrix} . \tag{B.1}$$

With the transformation $\tilde{a}_U \to \mathrm{e}^{\mathrm{i}\varphi} a_U$ with $\partial_z \varphi = -\Delta\beta$ the system of equations changes to

$$\mathrm{i}\,\partial_z \begin{pmatrix} a_L \\ a_R \\ a_U \\ a_C \end{pmatrix} = \begin{pmatrix} 0 & 0 & 0 & S \\ 0 & 0 & 0 & P \\ 0 & 0 & 0 & Q\mathrm{e}^{-\mathrm{i}\varphi} \\ S & P & Q\mathrm{e}^{\mathrm{i}\varphi} & 0 \end{pmatrix} \cdot \begin{pmatrix} a_L \\ a_R \\ a_U \\ a_C \end{pmatrix} . \tag{B.2}$$

The above system has two degenerate eigenstates with zero eigenvalue called *dark states*. Written with the eigenmodes of the individual waveguides as basis, these are

$$|\Phi_1\rangle = \frac{P}{\sqrt{S^2+P^2}} \mathrm{e}^{\mathrm{i}\varphi} |w_L\rangle - \frac{S}{\sqrt{S^2+P^2}} \mathrm{e}^{\mathrm{i}\varphi} |w_R\rangle \, , \tag{B.3}$$

$$\begin{aligned} |\Phi_2\rangle = {} & \frac{Q}{\sqrt{S^2+P^2+Q^2}} \frac{S}{\sqrt{S^2+P^2}} \mathrm{e}^{\mathrm{i}\varphi} |w_L\rangle \\ & + \frac{Q}{\sqrt{S^2+P^2+Q^2}} \frac{P}{\sqrt{S^2+P^2}} \mathrm{e}^{\mathrm{i}\varphi} |w_R\rangle \\ & - \frac{\sqrt{S^2+P^2}}{\sqrt{S^2+P^2+Q^2}} |w_U\rangle \, . \end{aligned} \tag{B.4}$$

Calculating the $\boldsymbol{A}_\nu$ using the definition (3.25) together with the darkstates from Eqs. (B.3) and (B.4) yields

$$\boldsymbol{A}_S = \mathrm{i}\,\frac{P}{S^2+P^2}\frac{Q}{\sqrt{S^2+P^2+Q^2}}\,\boldsymbol{\sigma}_y\,, \tag{B.5}$$

$$\boldsymbol{A}_P = -\mathrm{i}\,\frac{S}{S^2+P^2}\frac{Q}{\sqrt{S^2+P^2+Q^2}}\,\boldsymbol{\sigma}_y\,, \tag{B.6}$$

$$\boldsymbol{A}_\varphi = \frac{\mathrm{i}}{2}\left(\left(-1+\frac{Q^2}{S^2+P^2+Q^2}\right)\mathbb{1}+\frac{S^2+P^2}{S^2+P^2+Q^2}\,\boldsymbol{\sigma}_z\right). \tag{B.7}$$

The components $\boldsymbol{A}_S$ and $\boldsymbol{A}_P$ are the same components as for the tripod without detuning, see Eqs. (3.40) and (3.41). However, now we have the additional component $\boldsymbol{A}_\varphi$ along the detuning parameter. Because $\boldsymbol{A}_\varphi$ includes the $2\times 2$ identity matrix, we do have a general $U(2)$ gauge field instead of a simpler $SU(2)$ gauge field where only the Pauli matrices $\boldsymbol{\sigma}_j$ act as generators.

Because the gauge field connection now features noncommuting Pauli matrices, the holonomy $\boldsymbol{U}$ is not straightforwardly calculated due to the required path-ordering. However, when integrating along the coordinate lines $S$, $P$ and $\varphi$, we can simply integrate. Therefore, we choose a rectangular path, a so-called plaquette, for our curve along these lines, allowing to calculate a specific Wilson loop using Eq. (3.31).

We let $Q$ be constant and sequentially vary $\varphi$ or $S$ together with $P$. Starting with a variation of $\varphi$, for this simple rectangular path the time evolution $\boldsymbol{U}$ of the four sequential *hops* are

$$\begin{aligned}
\boldsymbol{U} =& \boldsymbol{U}_4\boldsymbol{U}_3\boldsymbol{U}_2\boldsymbol{U}_1\\
=&\exp\left(\mathrm{i}\,\boldsymbol{\sigma}_y\,Q\int\limits_{z_3}^{z_4}\mathrm{d}z\,\frac{S\dot{P}-\dot{S}P}{(S^2+P^2)\sqrt{S^2+P^2+Q^2}}\right)\\
&\times\exp\left(-\frac{\mathrm{i}}{2}\int\limits_{z_2}^{z_3}\mathrm{d}z\,\dot{\varphi}\left(\left(1+\frac{Q^2}{S^2+P^2+Q^2}\right)\mathbf{1}+\frac{S^2+P^2}{S^2+P^2+Q^2}\boldsymbol{\sigma}_z\right)\right)\\
&\times\exp\left(\mathrm{i}\,\boldsymbol{\sigma}_y\,Q\int\limits_{z_1}^{z_2}\mathrm{d}z\,\frac{S\dot{P}-\dot{S}P}{(S^2+P^2)\sqrt{S^2+P^2+Q^2}}\right)\\
&\times\exp\left(-\frac{\mathrm{i}}{2}\int\limits_{z_0}^{z_1}\mathrm{d}z\,\dot{\varphi}\left(\left(1+\frac{Q^2}{S^2+P^2+Q^2}\right)\mathbf{1}+\frac{S^2+P^2}{S^2+P^2+Q^2}\boldsymbol{\sigma}_z\right)\right),
\end{aligned} \tag{B.8}$$

where the dot notation indicate derivatives with respect to $z$. Note that the integrals range totally from $z_0$, the beginning of the waveguide structure, to $z_4$, the end of the structure. In order to have a closed curve in parameter space, it is required that the couplings $S$, $P$ and phase $\varphi$ return to their initial values, e.g. $S(z_0) = S(z_4)$. The occurrence of the identity matrix in $\boldsymbol{U_1}$ and $\boldsymbol{U_3}$ as a generator makes $\boldsymbol{U}$ an element of the unitary group $U(2)$ instead of the special unitary group $SU(2)$ where only the Pauli matrices are the generators. Defining

$$\begin{aligned}
\gamma_j &= \frac{Q^2}{S_j^2 + P^2 + Q^2}\,, && \text{(B.9)}\\
\Delta\varphi &= \varphi_1 - \varphi_0\,, && \text{(B.10)}\\
\eta_0 &= Q\int\limits_{z_2}^{z_3} \mathrm{d}z\, \frac{S\dot{P} - \dot{S}P}{(S^2+P^2)\sqrt{S^2+P^2+Q^2}}\,, && \text{(B.11)}\\
\eta_1 &= Q\int\limits_{z_4}^{z_1} \mathrm{d}z\, \frac{S\dot{P} - \dot{S}P}{(S^2+P^2)\sqrt{S^2+P^2+Q^2}}\,, && \text{(B.12)}
\end{aligned}$$

the calculation of $\boldsymbol{U}$ is straightforward and yields for the link variables along the plaquette

$$\begin{aligned}
\boldsymbol{U}_1 &= \exp\left(-\mathrm{i}\Delta\varphi \begin{pmatrix} 1 & 0 \\ 0 & \gamma_0 \end{pmatrix}\right) = \begin{pmatrix} \mathrm{e}^{-\mathrm{i}\Delta\varphi} & 0 \\ 0 & \mathrm{e}^{-\mathrm{i}\Delta\varphi\gamma_0} \end{pmatrix} && \text{(B.13)}\\
\boldsymbol{U}_2 &= \exp\left(\mathrm{i}\eta_0\boldsymbol{\sigma}_y\right) = \mathbf{1}\cos(\eta_0) - \mathrm{i}\,\boldsymbol{\sigma}_y\sin(\eta_0) && \text{(B.14)}\\
\boldsymbol{U}_3 &= \exp\left(\mathrm{i}\Delta\varphi \begin{pmatrix} 1 & 0 \\ 0 & \gamma_1 \end{pmatrix}\right) = \begin{pmatrix} \mathrm{e}^{\mathrm{i}\Delta\varphi} & 0 \\ 0 & \mathrm{e}^{\mathrm{i}\Delta\varphi\gamma_1} \end{pmatrix} && \text{(B.15)}\\
\boldsymbol{U}_4 &= \exp\left(\mathrm{i}\eta_1\boldsymbol{\sigma}_y\right) = \mathbf{1}\cos(\eta_1) - \mathrm{i}\,\boldsymbol{\sigma}_y\sin(\eta_1) && \text{(B.16)}
\end{aligned}$$

The resulting unitary transformation for one plaquette is

$$\boldsymbol{U} = \begin{pmatrix} \cos(\eta_0)\cos(\eta_1) - \sin(\eta_0)\sin(\eta_1)\mathrm{e}^{\mathrm{i}\Delta\varphi(1-\gamma_1)} & \cos(\eta_0)\sin(\eta_1)\mathrm{e}^{\mathrm{i}\Delta\varphi(\gamma_0-\gamma_1)} + \cos(\eta_1)\sin(\eta_0)\mathrm{e}^{-\mathrm{i}\Delta\varphi(1-\gamma_0)} \\ -\cos(\eta_0)\sin(\eta_1) - \cos(\eta_1)\sin(\eta_0)\mathrm{e}^{\mathrm{i}\Delta\varphi(1-\gamma_1)} & \cos(\eta_0)\cos(\eta_1)\mathrm{e}^{\mathrm{i}\Delta\varphi(\gamma_0-\gamma_1)} - \sin(\eta_0)\sin(\eta_1)\mathrm{e}^{-\mathrm{i}\Delta\varphi(1-\gamma_0)} \end{pmatrix}. \tag{B.17}$$

The trace of this behemoth gives the gauge-invariant Wilson loop

$$\begin{aligned}
W_{\mathcal{C}} = &\cos(\eta_0)\cos(\eta_1)\left(1 + \mathrm{e}^{\mathrm{i}\Delta\varphi(\gamma_0-\gamma_1)}\right)\\
&- \sin(\eta_0)\sin(\eta_1)\left(\mathrm{e}^{\mathrm{i}\Delta\varphi(1-\gamma_1)} + \mathrm{e}^{-\mathrm{i}\Delta\varphi(1-\gamma_0)}\right). \qquad \text{(B.18)}
\end{aligned}$$

Because $\boldsymbol{A}_\varphi$ includes the identity matrix $\mathbb{1}$, the resulting holonomy $\boldsymbol{U}$ is an element of U(2). Consequently, the Wilson loop is a complex number in contrast to the case of gauge fields from the special unitary group $SU(2)$ from Section 3.5 where the Wilson loop is always real. Consequently, one has to make interferometric measurements instead of the simpler intensity measurements conducted in [116] but which are equally possible with additional waveguides for reference.

# C. Detailed eigendecomposition of the $|1,1\rangle\langle 1,1|$-state in Liouville space

Based on the general eigendecomposition solution (4.82) one can technically compute the evolution of any input state $|\hat{\rho}(0)\rangle\rangle$ for constant system parameters. However, the involved eigenvectors $|\boldsymbol{\alpha},\boldsymbol{\beta}\rangle\rangle$, see Eq. (4.67), and overlaps $\langle\langle\boldsymbol{\alpha},\boldsymbol{\beta}|\hat{\rho}(0)\rangle\rangle$, see Eq. (4.83) or (5.18), need to be calculated with the rather unfamiliar left and right actions of the superoperators, cf. Eq. (4.16), as well as the Hilbert-Schmidt inner product (4.14). Therefore, we showcase here the example of the $|1,1\rangle\langle 1,1|$-state for the HOM experiment with its coincidence function $\Gamma(z)$ as appearing in Eq. (5.22).

As discussed in the main text, the summation in the eigendecomposition solution (4.82) is restricted to multiindices $|\boldsymbol{\alpha}|, |\boldsymbol{\beta}| \leq N_\mathrm{p}$ with the maximal input state photon number $N_\mathrm{p} = 2$ for the HOM experiment. The right eigenvectors we need to calculate are thus $|(0,0),(0,0)\rangle\rangle$, $|(1,0),(0,0)\rangle\rangle$, $|(1,0),(1,0)\rangle\rangle$, $\ldots$, $|(2,0),(2,0)\rangle\rangle$, etc. Fortunately, due to the symmetry of the input state, $|\hat{\rho}(0)\rangle\rangle = |1,1\rangle\langle 1,1|$ the overlaps for most of these eigenvectors are zero. Using the definitions (5.13) and (5.13) for the annihilation superoperators $P_i^-$ and $Q_m^-$, the only nonzero overlaps are proportional to

$$\mathrm{Tr}\left(P_i^-\, Q_m^- |11\rangle\langle 11|\right) = \epsilon_i\, \epsilon_m^* + \tau_i\, \tau_m^*, \tag{C.1}$$

$$\mathrm{Tr}\left(P_i^-\, P_j^-\, Q_m^-\, Q_n^- |11\rangle\langle 11|\right) = \left(\epsilon_i\, \tau_j + \tau_i\, \epsilon_j\right)\left(\epsilon_m^*\, \tau_n^* + \tau_m^*\, \epsilon_n^*\right). \tag{C.2}$$

All other have an unbalanced number of annihilation operators acting from the left and right and thus evaluate to zero under the trace. Note that the overlaps are simply the above results with the appropriate $(\boldsymbol{\alpha}!\boldsymbol{\beta}!)^{-1/2}$ weights, cf. (4.83).

This symmetry of the input state now reduces the number of relevant right eigenvectors to 14. One for all indices zero, $|(0,0),(0,0)\rangle\rangle$, four with indices totalling one , e.g. $|(1,0),(1,0)\rangle\rangle$, $|(1,0),(0,1)\rangle\rangle$, and nine with indices totalling two, e.g. $\ldots$, $|(2,0),(2,0)\rangle\rangle$, $|(1,1),(2,0)\rangle\rangle$, $|(0,2),(2,0)\rangle\rangle$. The four eigenvectors with multiindices $|\boldsymbol{\alpha}|, |\boldsymbol{\beta}| = 1$ have the form

$$\begin{aligned} P_i^+\, Q_m^+ |0\rangle\rangle &= \left(\epsilon_i\left(L_1^+ - R_1^-\right) + \tau_i\left(L_2^+ - R_2^-\right)\right)\left(\epsilon_m^*\left(R_1^+ - L_1^-\right) + \tau_m^*\left(R_2^+ - L_2^-\right)\right)|0,0\rangle\langle 0,0| \\ &= \epsilon_i\, \epsilon_m^* \Big(|10\rangle\langle 10| - |00\rangle\langle 00|\Big) + \epsilon_i\, \tau_m^* |10\rangle\langle 01| \\ &+ \epsilon_m^*\, \tau_i |01\rangle\langle 10| + \tau_i\, \tau_m^* \Big(|01\rangle\langle 01| - |00\rangle\langle 00|\Big), \end{aligned} \tag{C.3}$$

and the nine eigenvectors with multiindices $|\boldsymbol{\alpha}|, |\boldsymbol{\beta}| = 2$ have the form

$$
\begin{aligned}
P_i^+\, P_j^+\, Q_m^+\, Q_n^+ |0\rangle\rangle = {} & |20\rangle\langle 20|\, (2\,\epsilon_i\,\epsilon_j\,\epsilon_m^*\,\epsilon_n^*) + |20\rangle\langle 02|\, (2\epsilon_i\,\epsilon_j\,\tau_m^*\,\tau_n^*) \\
& + |02\rangle\langle 20|\, (2\,\tau_i\,\tau_j\,\epsilon_m^*\,\epsilon_n^*) + |02\rangle\langle 02|\, (2\tau_i\,\tau_j\,\tau_m^*\,\tau_n^*) \\
& + |11\rangle\langle 11|\, (\epsilon_i\,\tau_j + \tau_i\,\epsilon_j)\, (\epsilon_m^*\,\tau_n^* + \tau_m^*\,\epsilon_n^*) \\
& + |11\rangle\langle 20| \sqrt{2}\,\epsilon_m^*\,\epsilon_n^*\, (\epsilon_i\,\tau_j + \tau_i\,\epsilon_j) \\
& + |11\rangle\langle 02| \sqrt{2}\,\tau_m^*\,\tau_n^*\, (\epsilon_i\,\tau_j + \tau_i\,\epsilon_j) \\
& + |20\rangle\langle 11| \sqrt{2}\,\epsilon_i\,\epsilon_j\, (\epsilon_m^*\,\tau_n^* + \tau_m^*\,\epsilon_n^*) \\
& + |02\rangle\langle 11| \sqrt{2}\,\tau_i\,\tau_j\, (\epsilon_m^*\,\tau_n^* + \tau_m^*\,\epsilon_n^*) \\
& - |10\rangle\langle 10|\, (4\,\epsilon_i\,\epsilon_j\epsilon_m^*\,\epsilon_n^* + (\epsilon_i\,\tau_j + \tau_i\,\epsilon_j)\, (\epsilon_m^*\,\tau_n^* + \tau_m^*\,\epsilon_n^*)) \\
& - |10\rangle\langle 01|\, (2\,\epsilon_i\,\epsilon_j\, (\epsilon_m^*\,\tau_n^* + \tau_m^*\,\epsilon_n^*) + 2\,\tau_m^*\,\tau_n^*\, (\epsilon_i\,\tau_j + \tau_i\,\epsilon_j)) \\
& - |01\rangle\langle 10|\, (2\,\tau_i\,\tau_j\, (\epsilon_m^*\,\tau_n^* + \tau_m^*\,\epsilon_n^*) + 2\epsilon_m^*\,\epsilon_n^*\, (\epsilon_i\,\tau_j + \tau_i\,\epsilon_j)) \\
& - |01\rangle\langle 01|\, (4\,\tau_i\,\tau_j\,\tau_m^*\,\tau_n^* + (\epsilon_i\,\tau_j + \tau_i\,\epsilon_j)\, (\epsilon_m^*\,\tau_n^* + \tau_m^*\,\epsilon_n^*)) \\
& + |00\rangle\langle 00|\, (2\,\tau_i\,\tau_j\,\tau_m^*\,\tau_n^* + (\epsilon_i\,\tau_j + \tau_i\,\epsilon_j)\, (\epsilon_m^*\,\tau_n^* + \tau_m^*\,\epsilon_n^*) + 2\,\epsilon_i\,\epsilon_j\,\epsilon_m^*\,\epsilon_n^*)\,,
\end{aligned}
\tag{C.4}
$$

Now that the overlaps and eigenvectors are known, the only thing missing for the eigendecomposition are the exponential prefactors with eigenvalues $\mu_{\boldsymbol{\alpha},\boldsymbol{\beta}} = \boldsymbol{\alpha}\cdot\boldsymbol{\lambda} + \boldsymbol{\alpha}\cdot\boldsymbol{\lambda}^*$ from (4.76) where $\lambda_\pm = -\gamma/2 \pm \mathrm{i}\sqrt{\kappa^2 - (\gamma/2)^2} = -\gamma/2 \pm \mathrm{i}\Omega/2$. These are easily calculated and read

$$\mathrm{e}^{\mu_{(2,0),(2,0)} z} = \mathrm{e}^{(2\lambda_1 + 2\lambda_1^*) z} = \mathrm{e}^{-2\gamma z}, \tag{C.5}$$

$$\mathrm{e}^{\mu_{(1,1),(2,0)} z} = \mathrm{e}^{-2\gamma z}\mathrm{e}^{-\mathrm{i}\Omega z}, \tag{C.6}$$

$$\mathrm{e}^{\mu_{(0,2),(2,0)} z} = \mathrm{e}^{-2\gamma z}\mathrm{e}^{-2\mathrm{i}\Omega z}, \tag{C.7}$$

$$\vdots \tag{C.8}$$

With the overlaps, eigenvectors, and prefactors one can, in principle, calculate the quantum state at any given value of $z$. For specific observables, the effort can be significantly reduced by selecting the relevant contributions. When calculating the coincidence function $\Gamma = \langle \hat{a}_1^\dagger \hat{a}_2^\dagger \hat{a}_1 \hat{a}_2 \rangle$ for example, we see that the only contributing right eigenvectors are those with $|\boldsymbol{\alpha}|, |\boldsymbol{\beta}| = 2$ and specificially only their $|11\rangle\langle 11|$-terms, cf. (C.4). Collecting all these terms for all index combinations $i, j, m, n = 0, 1, 2$ from the general solution (C.4) with overlaps, (C.2), respective weights $(\boldsymbol{\alpha}!\boldsymbol{\beta}!)^{-1/2}$, and exponential prefactors, leads to

$$
\begin{aligned}
\Gamma(z) = {} & \frac{1}{2!2!}(4|\epsilon_1|^2|\tau_1|^2)^2 \mathrm{e}^{-2\gamma z} \\
& + \frac{1}{2!}(2\epsilon_1^*\tau_1^*\left(\epsilon_1\tau_2 + \tau_1\epsilon_2\right))^2 \mathrm{e}^{-2\gamma z}\mathrm{e}^{-\mathrm{i}\Omega z} \\
& + \frac{1}{2!2!}(4\epsilon_1^*\tau_1^*\epsilon_2\tau_2)^2 \mathrm{e}^{-2\gamma z}\mathrm{e}^{-\mathrm{i}2\Omega z} \\
& + \frac{1}{2!}(2\epsilon_1\tau_1\left(\epsilon_1^*\tau_2^* + \tau_1^*\epsilon_2^*\right))^2 \mathrm{e}^{-2\gamma z}\mathrm{e}^{\mathrm{i}\Omega z} \\
& + (\left(\epsilon_1\tau_2 + \tau_1\epsilon_2\right)\left(\epsilon_1^*\tau_2^* + \tau_1^*\epsilon_2^*\right))^2 \mathrm{e}^{-2\gamma z} \\
& + \frac{1}{2!}(2\epsilon_2\tau_2\left(\epsilon_1^*\tau_2^* + \tau_1^*\epsilon_2^*\right))^2 \mathrm{e}^{-2\gamma z}\mathrm{e}^{-\mathrm{i}\Omega z} \\
& + \frac{1}{2!2!}(4\epsilon_2^*\tau_2^*\epsilon_1\tau_1)^2 \mathrm{e}^{-2\gamma z}\mathrm{e}^{\mathrm{i}2\Omega z} \\
& + \frac{1}{2!}(2\epsilon_2^*\tau_2^*\left(\epsilon_1\tau_2 + \tau_1\epsilon_2\right))^2 \mathrm{e}^{-2\gamma z}\mathrm{e}^{\mathrm{i}\Omega z} \\
& + \frac{1}{2!2!}(4|\epsilon_2|^2|\tau_2|^2)^2 \mathrm{e}^{-2\gamma z}.
\end{aligned}
\tag{C.9}
$$

Inserting the expressions in (5.17) for the $\epsilon_i$ and $\tau_i$ then yields the Fourier series components of the result in Eq. (5.22).

# D. Regular representations at the exceptional point

In this appendix we show how our approach with regular representations can be used to calculate solutions at the EP, i.e. where the system is no longer diagonalisable and one needs the general Jordan decomposition. As an example, we illustrate the key points using the effective non-Hermitian Hamiltonian in Hilbert space instead of the original Liouvillian $\mathcal{L}$. This is just for brevity as the approach is identical with the only difference being that the Liouville space $\mathfrak{L}$ dimensions are double the Hilbert space dimensions. The following results are thus clearer and still easily applicable to any calculations at the EP with the full Liouvillian.

We start with the Schrödinger equation

$$\partial_z|\psi\rangle = -\mathrm{i}\hat{H}|\psi\rangle \tag{D.1}$$

for a two-waveguide system where one waveguide expierences loss. This setting is described by the effective $\mathcal{PT}$-symmetric Hamiltonian

$$\hat{H} = -\mathrm{i}\gamma\hat{a}^\dagger\hat{a} + \kappa\left(\hat{a}^\dagger\hat{b} + \hat{b}^\dagger\hat{a}\right), \tag{D.2}$$

with the bosonic mode operators $\hat{a}$ and $\hat{b}$ for waveguide 1 and 2, respectively. The general solution of the Schrödinger equation is of course given by

$$|\psi(z)\rangle = \mathrm{e}^{-\mathrm{i}\hat{H}z}|\psi(0)\rangle \tag{D.3}$$

and thus we look for a eigendecomposition of the Hamiltonian as basis which we construct in a similar manner as for the Liouvillian discussed in Chapter 4 and 5.

The regular representation $\mathcal{R}(-\mathrm{i}\hat{H})$ in the basis $\{\hat{a}^\dagger, \hat{b}^\dagger, \hat{a}, \hat{b}\}$ reads

$$\mathcal{R}(-\mathrm{i}\hat{H}) = \begin{pmatrix} -\gamma & -\mathrm{i}\kappa & 0 & 0 \\ -\mathrm{i}\kappa & 0 & 0 & 0 \\ 0 & 0 & \gamma & \mathrm{i}\kappa \\ 0 & 0 & \mathrm{i}\kappa & 0 \end{pmatrix}, \tag{D.4}$$

with already absorbed prefactor $-\mathrm{i}$. At the EP ($\gamma = 2\kappa$), this matrix is no longer diagonalisable and we instead need to find the Jordan decomposition $R(-\mathrm{i}\hat{H}) = SJS^{-1}$. For the above parameters we find for the Jordan decomposition

$$S = \begin{pmatrix} -\mathrm{i} & \frac{\mathrm{i}}{\kappa} & 0 & 0 \\ 1 & 0 & 0 & 0 \\ 0 & 0 & -\mathrm{i} & -\frac{\mathrm{i}}{\kappa} \\ 0 & 0 & 1 & 0 \end{pmatrix}, \qquad J = \begin{pmatrix} -\kappa & 1 & 0 & 0 \\ 0 & -\kappa & 0 & 0 \\ 0 & 0 & \kappa & 1 \\ 0 & 0 & 0 & \kappa \end{pmatrix}, \qquad S^{-1} = \begin{pmatrix} 0 & 1 & 0 & 0 \\ -\mathrm{i}\kappa & \kappa & 0 & 0 \\ 0 & 0 & 0 & 1 \\ 0 & 0 & \mathrm{i}\kappa & -\kappa \end{pmatrix}. \tag{D.5}$$

The new creation and annihilation operators, i.e. eigenvectors of the regular representation, are then easily calculated by

$$S^{-1} \cdot \begin{pmatrix} \hat{a}^\dagger \\ \hat{b}^\dagger \\ \hat{a} \\ \hat{b} \end{pmatrix} = \begin{pmatrix} \hat{c}^+ \\ \hat{d}^+ \\ \hat{d}^- \\ \hat{c}^- \end{pmatrix} = \begin{pmatrix} \hat{b}^\dagger \\ -\mathrm{i}\kappa\, \hat{a}^\dagger + \kappa\, \hat{b}^\dagger \\ \hat{b} \\ \mathrm{i}\kappa\hat{a} - \kappa\hat{b} \end{pmatrix}. \tag{D.6}$$

Notice that due to the non-Hermiticity the new creation operators are no longer necessarily the Hermitian conjugate of the annihilation operators. Additionally, what is special for this solution at the EP is that apparently without normalisation $\hat{d}^+$ and $\hat{d}^-$ are not dimensionless. What is even more striking is that we have the following commutators

$$\left[\hat{d}^-, \hat{d}^+\right] = \kappa, \quad \left[\hat{c}^-, \hat{c}^+\right] = -\kappa, \tag{D.7}$$

$$\left[\hat{d}^-, \hat{c}^+\right] = 1, \quad \left[\hat{c}^-, \hat{d}^+\right] = 0, \tag{D.8}$$

showing that the modes are no longer separated into two orthogonal spaces.

If we look especially at the creation operators, which we will need shortly for calculating the state evolution, we have

$$\hat{c}^+ = \hat{b}^\dagger, \tag{D.9}$$

$$\hat{d}^+ = -\mathrm{i}\kappa\, \hat{a}^\dagger + \kappa\, \hat{b}^\dagger \tag{D.10}$$

which have the following commutators with the Hamiltonian:

$$\left[-\mathrm{i}\hat{H}, \hat{c}^+\right] = -\kappa\, \hat{c}^+ + \hat{d}^+, \tag{D.11}$$

$$\left[-\mathrm{i}\hat{H}, \hat{d}^+\right] = -\kappa\, \hat{d}^+. \tag{D.12}$$

Apparently, the new operators do no longer have a simple interpretation as ladder operators that create or annihilate excitations. Nonetheless, they permit the construction of a (generalised) basis as per their construction from the Jordan decomposition.

The procedure would therefore be to first construct the input state $|\psi(0)\rangle$ in terms of the original, physical mode operators $\hat{a}$ and $\hat{b}$ acting on the vacuum and then transform them to the new abstract operators $\hat{c}^\pm$ and $\hat{d}^\pm$. Because the action of the evolution on the vacuum is known, i.e. $\exp -\mathrm{i}\hat{H}z|0\rangle = 0$, we then only have to commute the new abstract operators with the evolution operator $\exp -\mathrm{i}\hat{H}z$. For this we calculate the left-right application, i.e. evolution, of these operators as

$$\mathrm{e}^{-\mathrm{i}\hat{H}z}\hat{c}^{+}\mathrm{e}^{\mathrm{i}\hat{H}z} = \mathrm{e}^{-\kappa z}\left(\hat{c}^{+} + z\,\hat{d}^{+}\right), \tag{D.13}$$

$$\mathrm{e}^{-\mathrm{i}\hat{H}z}\hat{d}^{+}\mathrm{e}^{\mathrm{i}\hat{H}z} = \mathrm{e}^{-\kappa z}\hat{d}^{+} \tag{D.14}$$

by applying the adjoint action $\mathrm{e}^{X}Y\mathrm{e}^{-X} = Y + [X,Y] + [X,[X,Y]]/2 + ...$ This can of course be applied to powers of the new operators, i.e.

$$\mathrm{e}^{-\mathrm{i}\hat{H}z}\left(\hat{c}^{+}\right)^{n}\mathrm{e}^{\mathrm{i}\hat{H}z} = \mathrm{e}^{-\mathrm{i}\hat{H}z}\hat{c}^{+}\mathrm{e}^{\mathrm{i}\hat{H}z}\mathrm{e}^{-\mathrm{i}\hat{H}z}\hat{c}^{+}\mathrm{e}^{\mathrm{i}\hat{H}z}\cdots\mathrm{e}^{-\mathrm{i}\hat{H}z}\hat{c}^{+}\mathrm{e}^{-\mathrm{i}\hat{H}z} = \mathrm{e}^{-n\kappa z}\left(\hat{c}^{+} + z\,\hat{d}^{+}\right)^{n}, \tag{D.15}$$

$$\mathrm{e}^{-\mathrm{i}\hat{H}z}\left(\hat{d}^{+}\right)^{n}\mathrm{e}^{\mathrm{i}\hat{H}z} = \mathrm{e}^{-n\kappa z}\left(\hat{d}^{+}\right)^{n}. \tag{D.16}$$

Based on these equations we can compute the evolution of arbitrary input states and use them to calculate any desired observable. As an example, we again consider a HOM experiment with the input state $|\psi_{\mathrm{in}}\rangle = |1_a, 1_b\rangle$. We now replace the creation operators of the physical modes with the new operators using the Jordan decomposition in Eq. (D.6):

$$\begin{aligned} |\psi(z)\rangle &= \mathrm{e}^{-\mathrm{i}\hat{H}z}|1_a, 1_b\rangle \\ &= \mathrm{e}^{-\mathrm{i}\hat{H}z}\hat{a}^{\dagger}\hat{b}^{\dagger}|0,0\rangle = \mathrm{e}^{-\mathrm{i}\hat{H}z}\left(-\mathrm{i}\left(\hat{c}^{\dagger}\right)^{2} + \frac{\mathrm{i}}{\kappa}\hat{d}^{+}\hat{c}^{+}\right)|0,0\rangle\,. \end{aligned} \tag{D.17}$$

With the help of Eqs. (D.15) and (D.16), we can then apply the evolution operator resulting in the evolved state

$$|\psi(z)\rangle = \mathrm{i}\,\mathrm{e}^{-2\kappa z}\left(-\left(\hat{c}^{+}\right)^{2} + \hat{d}^{+}\hat{c}^{+}\left(\frac{1}{\kappa} - 2z\right) + \left(\hat{d}^{\dagger}\right)^{2}\left(\frac{z}{\kappa} - z^{2}\right)\right)|0,0\rangle. \tag{D.18}$$

If we transform back to the physical modes, we obtain

$$|\psi(z)\rangle = \mathrm{e}^{-2\kappa z}\Big(-\mathrm{i}\kappa z(1+\kappa z)|0,2\rangle + (1-2\kappa^{2}z^{2})|1,1\rangle - \mathrm{i}\kappa z(1-\kappa z)|2,0\rangle\Big). \tag{D.19}$$

Because we are only interested in the two-photon coincidence rate $\Gamma = \langle\hat{a}_1^{\dagger}\hat{a}_2^{\dagger}\hat{a}_1\hat{a}_2\rangle$ we find

$$\Gamma_{\mathrm{EP}} = \mathrm{e}^{-4\kappa z}\left(1 - 2\kappa^{2}z^{2}\right)^{2}, \tag{D.20}$$

which is indeed the same compared to the original solution (5.22) in the limit $\gamma \to 2\kappa$.

# E. Ideal propagation in lossy waveguides for two-photon states

In Chapter 5 we showed for the two-mode and one-photon case how to construct input states that experience the lowest loss based on the eigendecomposition solution (4.82). Here, we add another example with a two-photon state in order to provide further understanding.

We again assume that $\tilde{\sigma} < 0$ meaning the eigenvalues from Eqs. (5.24) and (5.25) fulfil the relation $|\mathrm{Re}\tilde{\lambda}_1| < |\mathrm{Re}\tilde{\lambda}_2|$. As a result, those eigenvectors $|\boldsymbol{\alpha}, \boldsymbol{\beta}\rangle\rangle$ with indices $\alpha_2, \beta_2 = 0$ should generally result in a propagation with lower losses. Because we now have $N_\mathrm{p} = 2$ photons, the multiindices are restricted by $|\boldsymbol{\alpha}|, |\boldsymbol{\beta}| \leq 2$ meaning we have to construct our ideal input states with eigenvectors having multiindices $\boldsymbol{\alpha}, \boldsymbol{\beta} = (2,0), (1,0), (0,0)$, i.e.

$$\begin{aligned}|\hat{\rho}_0\rangle\rangle = {} & h_1|(2,0),(2,0)\rangle\rangle + h_2|(2,0),(1,0)\rangle\rangle + h_3|(1,0),(2,0)\rangle\rangle + h_4|(2,0),(0,0)\rangle\rangle \\ & + h_5|(0,0),(2,0)\rangle\rangle + h_6|(1,0),(1,0)\rangle\rangle + h_7|(1,0),(0,0)\rangle\rangle + h_8|(0,0),(1,0)\rangle\rangle \\ & + h_9|(0,0),(0,0)\rangle\rangle\,. \end{aligned} \tag{E.1}$$

As for the one-photon case, the coefficients $h_k$ are the overlap $\langle\langle \boldsymbol{\alpha}, \boldsymbol{\beta}|\rho(0)\rangle\rangle$ which are as of yet undetermined. Demanding $|\hat{\rho}(0)\rangle\rangle$ to be a physical state, i.e. positive definite, Hermitian, and with $\mathrm{Tr}\hat{\rho}_0 = 1$, leads to a range of permissible weights $h_k$. The condition $\mathrm{Tr}\hat{\rho}_0 = 1$ is easily satisfied by setting $h_9 = 1$, because $\mathrm{Tr}(|(0,0),(0,0)\rangle\rangle) = 1$ and all other Liouvillian eigenvectors have trace zero. Furthermore, the Hermiticity is ensured by setting $h_7 = h_8^*$, $h_4 = h_5^*$, and $h_2 = h_3^*$.

Now, for the positivity constraint we again need to calculate the matrix form of $|\hat{\rho}(0)\rangle\rangle$ in Hilbert space by explicitly calculating the eigenvectors $|\boldsymbol{\alpha}, \boldsymbol{\beta}\rangle\rangle$. Note, again, that the parameters $\epsilon_1$ and $\tau_1$ from Eq. (5.17) are changed with the replacement $\gamma \to \gamma + \mathrm{i}\sigma$ in order to add the detuning. The result in the basis $\{|00\rangle, |10\rangle, |01\rangle, |20\rangle, |11\rangle, |02\rangle\}$ is

$$\hat{\rho} = \begin{pmatrix} 1 - h_1 2r^4 - h_6 r^2 & h_8\epsilon_1^* - h_3 2\epsilon_1^* r^2 & h_8\tau_1^* - h_3 2\tau_1^* r^2 & h_5 {\epsilon_1^*}^2\sqrt{2} & h_5\epsilon_1^*\tau_1^* 2 & h_5{\tau_1^*}^2\sqrt{2} \\ & |\epsilon_1|^2(h_6 - 4h_1 r^2) & \epsilon_1\tau_1^*(h_6 - 4h_1 r^2) & h_3|\epsilon_1|^2\epsilon_1^*\sqrt{2} & h_3 2|\epsilon_1|^2\tau_1^* & h_3\epsilon_1{\tau_1^*}^2\sqrt{2} \\ & & |\tau_1|^2(h_6 - h_1 r^2) & h_3{\epsilon_1^*}^2\tau_1\sqrt{2} & h_3 2|\tau_1|^2\epsilon_1^* & h_3|\tau_1|^2\tau_1^*\sqrt{2} \\ & & & 2h_1|\epsilon_1|^4 & h_1\sqrt{8}|\epsilon_1|^2\epsilon_1\tau_1^* & h_1 2\epsilon_1^2{\tau_1^*}^2 \\ & & & & 4h_1|\epsilon_1|^2|\tau_1|^2 & h_1\sqrt{8}|\tau_1|^2\epsilon_1\tau_1^* \\ & & & & & 2h_1|\tau_1|^4 \end{pmatrix}, \tag{E.2}$$

with $r^2 = |\epsilon_1|^2 + |\tau_1|^2$ and the complex conjugate parts in the lower off-diagonals not shown. Due to its size, the eigenvalues of this matrix cannot be given as closed analytic forms meaning we cannot derive a concise conditions for the remaining $h_k$ as we could in the one-photon case, see Eq. (5.28). Nonetheless, one can find permissible ranges for the weights $h_k$ via numerical means and still construct states with lowest losses. The approach remains the same for more photons.

# Bibliography

[1] M. Planck, “Über das Gesetz der Energieverteilung im Normalspektrum,” Ann. Phys. **309**, 553 (1901).

[2] A. Einstein, “Über einen die Erzeugung und Verwandlung des Lichtes betreffenden heuristischen Gesichtspunkt,” Ann. Phys. **17**, 132 (1905).

[3] M. Riedel, M. Kovacs, P. Zoller, J. Mlynek, and T. Calarco, “Europe's quantum flagship initiative,” Quantum Sci. Technol. **4**, 020501 (2019).

[4] M. G. Basset, F. Setzpfandt, F. Steinlechner, E. Beckert, T. Pertsch, and M. Gräfe, “Perspectives for applications of quantum imaging,” Laser Photonics Rev. **13**, 1900097 (2019).

[5] C. L. Degen, F. Reinhard, and P. Cappellaro, “Quantum sensing,” Rev. Mod. Phys. **89**, 035002 (2017).

[6] M. A. Nielsen and I. L. Chuang, *Quantum Computation and Quantum Information* (Cambridge University Press, 2000).

[7] W. Vogel and D.-G. Welsch, *Quantum Optics*, 3rd ed. (Wiley (Weinheim), 2006).

[8] B. Huttner and S. M. Barnett, “Quantization of the electromagnetic field in dielectrics,” Phys. Rev. A **46**, 4306 (1992).

[9] S. Scheel, L. Knöll, and D.-G. Welsch, “QED commutation relations for inhomogeneous Kramers-Kronig dielectrics,” Phys. Rev. A **58**, 700 (1998).

[10] B. E. A. Saleh and M. C. Teich, *Grundlagen der Photonik*, 2nd ed. (Wiley (Weinheim), 2008).

[11] S. P. Walborn, C. H. Monken, S. Pádua, and P. H. Souto Ribeiro, “Spatial correlations in parametric down-conversion,” Phys. Rep. **495**, 87 (2010).

[12] J. S. Bell, “On the Einstein Podolsky Rosen paradox,” Physics Physique Fizika **1**, 195 (1964).

[13] N. Brunner, D. Cavalcanti, S. Pironio, V. Scarani, and S. Wehner, “Bell nonlocality,” Rev. Mod. Phys. **86**, 419 (2014).

[14] E. Knill, R. Laflamme, and G. J. Milburn, “A scheme for efficient quantum computation with linear optics,” Nature **409**, 46 (2001).

[15] J. L. O'Brien, "Optical quantum computing," Science **318**, 1567 (2007).

[16] L. Thylén and L. Wosinski, "Integrated photonics in the 21st century," Photonics Res. **2**, 75 (2014).

[17] S. Nolte, M. Will, J. Burghoff, and A. Tünnermann, "Femtosecond waveguide writing: a new avenue to three-dimensional integrated optics," Appl. Phys. A **77**, 109 (2003).

[18] A. Szameit and S. Nolte, "Discrete optics in femtosecond-laser-written photonic structure," J. Phys. B: At. Mol. Opt. Phys. **43**, 163001 (2010).

[19] L. Sansoni, F. Sciarrino, G. Vallone, P. Mataloni, A. Crespi, R. Ramponi, and R. Osellame, "Polarization entangled state measurement on a chip," Phys. Rev. Lett. **105**, 200503 (2010).

[20] R. Heilmann, M. Gräfe, S. Nolte, and A. Szameit, "Arbitrary photonic wave plate operations on chip: Realizing Hadamard, Pauli-X, and rotation gates for polarisation qubits," Sci. Rep. **4**, 4118 (2014).

[21] O. Alibart, V. D'Auria, M. Micheli, F. Doutre, F. Kaiser, L. Labonté, T. Lunghi, É. Picholle, and S. Tanzilli, "Quantum photonics at telecom wavelengths based on lithium niobate waveguides," J. Opt. **18**, 104001 (2016).

[22] A. Politi, M. J. Cryan, J. G. Rarity, S. Yu, and J. L. O'Brien, "Silica-on-silicon waveguide quantum circuits," Science **320**, 646 (2008).

[23] T. Meany, M. Gräfe, R. Heilmann, A. Perez-Leija, S. Gross, M. J. Steel, M. J. Withford, and A. Szameit, "Laser written circuits for quantum photonics," Laser Photonics Rev. **9**, 363 (2015).

[24] S. Longhi, "Quantum-optical analogies using photonic structures," Laser Photonics Rev. **3**, 243 (2009).

[25] M. C. Rechtsman, J. M. Zeuner, Y. Plotnik, Y. Lumer, D. Podolsky, F. Dreisow, S. Nolte, M. Segev, and A. Szameit, "Photonic Floquet topological insulators," Nature **496**, 196 (2013).

[26] S. Weimann, M. Kremer, Y. Plotnik, Y. Lumer, S. Nolte, K. G. Makris, M. Segev, M. C. Rechtsman, and A. Szameit, "Topologically protected bound states in photonic parity-time-symmetric crystals," Nat. Mater. **16**, 433 (2017).

[27] M. Tillmann, B. Dakić, R. Heilmann, S. Nolte, A. Szameit, and P. Walther, "Experimental boson sampling," Nat. Photonics **7**, 540 (2013).

[28] M. Gräfe, R. Heilmann, A. Perez-Leija, R. Keil, F. Dreisow, M. Heinrich, H. Moya-Cessa, S. Nolte, D. N. Christodoulides, and A. Szameit, "On-chip generation of high-order single photon W-states," Nat. Photonics **8**, 791 (2014).

[29] M. Lebugle, M. Gräfe, R. Heilmann, A. Perez-Leija, S. Nolte, and A. Szameit, "Experimental observation of N00N state Bloch oscillations," Nat. Commun **6**, 8273 (2015).

[30] K. Itoh, W. Watanabe, S. Nolte, and C. B. Schaffer, "Ultrafast processes for bulk modification of transparent materials," MRS Bull. **31**, 620 (2006).

[31] A. Crespi, R. Ramponi, R. Osellame, L. Sansoni, I. Bongioanni, F. Sciarrino, G. Vallone, and P. Mataloni, "Integrated photonic quantum gates for polarization qubits," Nat. Commun. **2**, 566 (2011).

[32] S. Weimann, A. Perez-Leija, M. Lebugle, R. Keil, M. Tichy, M. Gräfe, R. Heilmann, S. Nolte, H. Moya-Cessa, G. Weihs, D. N. Christodoulides, and A. Szameit, "Implementation of quantum and classical discrete fractional Fourier transforms," Nat. Commun. **7**, 11027 (2015).

[33] L. Sansoni, F. Sciarrino, G. Vallone, P. Mataloni, A. Crespi, R. Ramponi, and R. Osellame, "Two-particle bosonic-fermionic quantum walk via integrated photonics," Phys. Rev. Lett **108**, 010502 (2012).

[34] A. Crespi, R. Osellame, R. Ramponi, V. Giovannetti, R. Fazio, L. Sansoni, F. De Nicola, F. Sciarrino, and P. Mataloni, "Anderson localization of entangled photons in an integrated quantum walk," Nat. Photonics **7**, 322 (2013).

[35] J. Carolan, J. D. A. Meinecke, P. J. Shadbolt, N. J. Russell, N. Ismail, K. Wörhoff, T. Rudolph, M. G. Thompson, J. L. O'Brien, J. C. F. Matthews, and A. Laing, "On the experimental verification of quantum complexity in linear optics," Nat. Photonics **8**, 621 (2014).

[36] K. Poulios, R. Keil, D. Fry, J. D. A. Meinecke, J. C. F. Matthews, A. Politi, M. Lobino, M. Gräfe, M. Heinrich, S. Nolte, A. Szameit, and J. L. O'Brien, "Quantum walks of correlated photon pairs in two-dimensional waveguide arrays," Phys. Rev. Lett. **112**, 143604 (2014).

[37] Y. Aharonov and D. Bohm, "Significance of electromagnetic potentials in the quantum theory," Phys. Rev. **115**, 485 (1959).

[38] K. G. Wilson, "Confinement of quarks," Phys. Rev. D **10**, 2445 (1974).

[39] T. Lancaster and S. J. Blundell, *Quantum Field Theory for the Gifted Amateur* (Oxford University Press, 2014).

[40] P. Zanardi and M. Rasetti, "Holonomic quantum computation," Phys. Lett. A **264**, 94 (1999).

[41] P. Solinas, P. Zanardi, and N. Zanghì, "Robustness of non-Abelian holonomic quantum gates against parametric noise," Phys. Rev. A **70**, 042316 (2004).

[42] S. Pancharatnam, “Generalized theory of interference and its applications,” Proc. Indian Acad. Sci. A. **44**, 247 (1956).

[43] M. V. Berry, “Quantal phase factors accompanying adiabatic changes,” Proc. Math. Phys. Eng. Sci. **392**, 45 (1984).

[44] F. Wilczek and A. Zee, “Appearance of gauge structure in simple dynamical systems,” Phys. Rev. Lett. **52**, 2111 (1984).

[45] J. Pachos and P. Zanardi, “Quantum holonomies for quantum computing,” Int. J. Mod. Phys. B **15**, 1257 (2001).

[46] J. K. Pachos, *Introduction to Topological Quantum Computation* (Cambridge University Press, 2012).

[47] N. Goldman, A. Kubasiak, P. Gaspard, and M. Lewenstein, “Ultracold atomic gases in non-Abelian gauge potentials: The case of constant Wilson loop,” Phys. Rev. A **79**, 023624 (2009).

[48] J. Dalibard, F. Gerbier, G. Juzeliŭnas, and P. Öhberg, “Colloquium: Artificial gauge potentials for neutral atoms,” Rev. Mod. Phys. **83**, 1523 (2011).

[49] N. Goldman, G. Juzeliŭnas, P. Öhberg, and I. B. Spielman, “Light-induced gauge fields for ultracold atoms,” Rep. Prog. Phys. **77**, 126401 (2014).

[50] A. Lemmer, A. Bermudez, and M. B. Plenio, “Driven geometric phase gates with trapped ions,” New J. Phys. **15**, 083001 (2013).

[51] L. B. Ma, S. L. Li, V. M. Fomin, M. Hentschel, J. B. Götte, Y. Yin, M. R. Jorgensen, and O. G. Schmidt, “Spin–orbit coupling of light in asymmetric microcavities,” Nat. Commun. **7**, 10983 (2016).

[52] M. Schlosshauer, “Quantum decoherence,” Phys. Rep. **831**, 1 (2019).

[53] H.-P. Breuer and F. Petruccione, *The Theory of Open Quantum Systems* (Oxford University Press, 2006).

[54] P. Zanardi and M. Rasetti, “Noiseless quantum codes,” Phys. Rev. Lett. **79**, 3306 (1997).

[55] D. A. Lidar, I. L. Chuang, and K. B. Whaley, “Decoherence-free subspaces for quantum computation,” Phys. Rev. Lett. **81**, 2594 (1998).

[56] J. Kempe, D. Bacon, D. A. Lidar, and K. B. Whaley, “Theory of decoherence-free fault-tolerant universal quantum computation,” Phys. Rev. A **63**, 042307 (2001).

[57] P. Zanardi, “Stabilizing quantum information,” Phys. Rev. A **63**, 012301 (2000).

[58] B. Kraus, H. P. Büchler, S. Diehl, A. Kantian, A. Micheli, and P. Zoller, "Preparation of entangled states by quantum Markov processes," Phys. Rev. A **78**, 042307 (2008).

[59] S. G. Schirmer and X. Wang, "Stabilizing open quantum systems by Markovian reservoir engineering," Phys. Rev. A **81**, 062306 (2010).

[60] N. Yamamoto, "Pure Gaussian state generation via dissipation: a quantum stochastic differential equation approach," Philos. Trans. Royal Soc. A **370**, 53324 (2012).

[61] C. M. Bender, D. C. Brody, and H. F. Jones, "Complex extension of quantum mechanics," Phys. Rev. Lett. **89**, 270401 (2002).

[62] D. C. Brody, "Biorthogonal quantum mechanics," J. Phys. A: Math. Theor. **47**, 035305 (2014).

[63] W. D. Heiss, "The physics of exceptional points," J. Phys. A: Math. Theor. **45**, 444016 (2012).

[64] W. D. Heiss and H. L. Harney, "The chirality of exceptional points," Eur. Phys. J. D **17**, 149 (2001).

[65] C. Dembowski, H.-D. Gräf, H. L. Harney, A. Heine, W. D. Heiss, H. Rehfeld, and A. Richter, "Experimental observation of the topological structure of exceptional points," Phys. Rev. Lett. **86**, 787 (2001).

[66] J. Doppler, A. A. Mailybaev, J. Böhm, U. Kuhl, A. Girschik, F. Libisch, T. J. Milburn, P. Rabl, and N. Moiseyev amd S. Rotter, "Dynamically encircling an exceptional point for asymmetric mode switching," Nature **537**, 76 (2016).

[67] S. Klaiman, U. Günther, and N. Moiseyev, "Visualisation of branch points in $\mathcal{PT}$-symmetric waveguides," Phys. Rev. Lett. **101**, 080402 (2008).

[68] B. Peng, Ş. K. Özdemir, S. Rotter, H. Yilmaz, M. Liertzer, F. Monifi, C. M. Bender, F. Nori, and L. Yang, "Loss-induced suppression and revival of lasing," Science **346**, 328 (2014).

[69] J. Wiersig, "Enhancing the sensitivity of frequency and energy splitting detection by using exceptional points: Application to microcavity sensors for single-particle detection," Phys. Rev. Lett. **112**, 203901 (2014).

[70] Z.P. Liu, J. Zhang, Ş. K. Özdemir, B. Peng, H. Jing, X.-Y. Lü, C.-W. Li, L. Yang, F. Nori, and Y. Liu, "Metrology with $\mathcal{PT}$-symmetric cavities: Enhanced sensitivity near the $\mathcal{PT}$-phase transition," Phys. Rev. Lett. **117**, 110802 (2016).

[71] W. Chen, Ş. K. Özdemir, G. Zhao, J. Wiersig, and L. Yang, "Exceptional points enhance sensing in an optical microcavity," Nature **548**, 192 (2017).

[72] M.-A. Miri and A. Alù, "Exceptional points in optics and photonics," Science **363**, 42 (2019).

[73] C. M. Bender and S. Boettcher, "Real spectra in non-Hermitian Hamiltonians having $\mathcal{PT}$ symmetry," Phys. Rev. Lett. **80**, 5243 (1998).

[74] D. Christodoulides and J. Yang, *Parity-time Symmetry and Its Applications* (Springer (Singapore), 2018).

[75] J. Schindler, A. Li, M. C. Zheng, F. M. Ellis, and T. Kottos, "Experimental study of active LRC circuits with $\mathcal{PT}$ symmetries," Phys. Rev. A **84**, 040101(R) (2011).

[76] C. M. Bender, B. K. Berntson, D. Parker, and E. Samuel, "Observation of $\mathcal{PT}$ phase transition in a simple mechanical system," Am. J. Phys. **81**, 173 (2013).

[77] C. E. Rüter, K. G. Makris, R. El-Ganainy, D. N. Christodoulides, M. Segev, and D. Kip, "Observation of parity–time symmetry in optics," Nat. Phys. **6**, 192 (2010).

[78] L. Xiao, X. Zhan, Z. H. Bian, K. K. Wang, X. Zhang, X. P. Wang, J. Li, K. Mochizuki, D. Kim, N. Kawakami, W. Yi, H. Obuse, B. C. Sanders, and P. Xue, "Observation of topological edge states in parity–time-symmetric quantum walks," Nat. Phys. **13**, 1117 (2017).

[79] J. Li, A. K. Harter, J. Liu, L. de Melo, Y. N. Joglekar, and L. Luo, "Observation of parity-time symmetry breaking transitions in a dissipative Floquet system of ultracold atoms," Nat. Commun. **10**, 855 (2019).

[80] Y. Wu, W. Liu, J. Geng, X. Song, X. Ye, C.-K. Duan, X. Rong, and J. Du, "Observation of parity-time symmetry breaking in a single-spin system," Science **346**, 878 (2019).

[81] M. Naghiloo, M. Abbasi, Y. N. Joglekar, and K. W. Murch, "Quantum state tomography across the exceptional point in a single dissipative qubit," Nat. Phys. **15**, 1232 (2019).

[82] F. Klauck, L. Teuber, M. Ornigotti, M. Heinrich, S. Scheel, and A. Szameit, "Observation of $\mathcal{PT}$-symmetric quantum interference," Nat. Photonics **13**, 883 (2019).

[83] J. Wiersig, "Review of exceptional point-based sensors," Photonics Res. **8**, 1457 (2020).

[84] S. Scheel and A. Szameit, "$\mathcal{PT}$-symmetric photonic quantum systems with gain and loss do not exist," EPL **122**, 34001 (2018).

[85] C. Chen, L. Jin, and R.-B. Liu, "Sensitivity of parameter estimation near the exceptional point of a non-Hermitian system," New. J. Phys. **21**, 083002 (2019).

[86] H. Wang, Y.-H. Lai, M.-G. Suh, and K. Vahala, "Petermann-factor sensitivity limit near an exceptional point in a Brillouin ring laser gyroscope," Nat. Commun. **11**, 1610 (2020).

[87] M. V. Berry, "Mode degeneracies and the Petermann excess-noise factor for unstable lasers," J. Mod. Opt. **50**, 63 (2003).

[88] M. A. Quiroz-Juárez, A. Perez-Leija, K. Tschernig, B. M. Rodríguez Lara, O. S. Magaña-Loaiza, K. Busch, Y. N. Joglekar, and R. J. León-Montiel, "Exceptional points of any order in a single, lossy waveguide beam splitter by photon-number-resolving detection," Photonics Res. **7**, 862 (2019).

[89] W. D. Heiss and W.-H. Steeb, "Avoided level crossings and Riemann sheet structure," J. Math. Phys. **32**, 3003 (1991).

[90] H. Hodaei, A. U. Hassan, S. Wittek, H. Garcia-Gracia, R. El-Ganainy, D. N. Christodoulides, and M. Khajavikhan, "Enhanced sensitivity at higher-order exceptional points," Nature **548**, 187 (2017).

[91] J. Pinske, L. Teuber, and S. Scheel, "Highly degenerate photonic waveguide structures for holonomic computation," Phys. Rev. A **101**, 062314 (2020).

[92] J. Pinske, L. Teuber, and S. Scheel, "Holonomic gates in pseudo-Hermitian quantum systems," Phys. Rev. A **100**, 042316 (2019).

[93] A. Szameit, F. Dreisow, T. Pertsch, S. Nolte, and A. Tünnermann, "Control of directional evanescent coupling in fs laser written waveguides," Opt. Express **15**, 1579 (2007).

[94] A. Yariv, "Coupled-mode theory for guided-wave optics," IEEE J. Quantum Electron. **9**, 919 (1973).

[95] A. Yariv, *Optical Electronics*, 4th ed. (Saunders College Publishing (New York), 1991).

[96] S. Weimann, *Complex Lattice Modes in Waveguide Networks and Photonic Solids*, Ph.D. thesis, University of Rostock (2018).

[97] S. Weinberg, *The Quantum Theory of Fields - Vol. 1: Foundations* (Cambridge University Press, 1995).

[98] I. Abram, "Quantum theory of light propagation: Linear medium," Phys. Rev. A **35**, 4661 (1987).

[99] B. Huttner, S. Serulnik, and Y. Ben-Aryeh, "Quantum analysis of light propagation in a parametric amplifier," Phys. Rev. A **42**, 5594 (1990).

[100] M. Toren and Y. Ben-Aryeh, “The problem of propagation in quantum optics, with applications to amplification, coupling of EM modes and distributed feedback lasers,” Quantum Opt.: J. Eur. Opt. Soc. **6**, 425 (1994).

[101] Y. Ben-Aryeh, A. Lukš, and V. Peřinová, “The concept of equal space commutators in quantum optics,” Phys. Lett. A **165**, 19 (1992).

[102] Y. Ben-Aryeh and S. Serulnik, “The quantum treatment of propagation in non-linear optical media by the use of temporal modes,” Phys. Lett. A **155**, 473 (1991).

[103] J. Liñares and M. C. Nistal, “Quantization of coupled modes propagation in integrated optical waveguides,” J. Mod. Opt. **50**, 781 (2003).

[104] U. Leonhardt and T. Philbin, *Geometry and Light - The Science of Invisibility* (Dover Publications, Inc. (New York), 2010).

[105] M. Nakahara, *Geometry, Topology and Physics*, 2nd ed. (CRC Press, 2003).

[106] A. P. Balachandran, G. Marmo, B.-S. Skagerstam, and A. Stern, *Gauge Theories and Fiber Bundles - Applications to Particle Dynamics (Lecture Notes in Physics)* (Springer (Berlin), 1983).

[107] D. Husemoller, *Fibre Bundles*, 3rd ed. (Springer (New York), 1994).

[108] S. Tanimura, M. Nakahara, and D. Hayashi, “Exact solutions of the isoholonomic problem and the optimal control problem in holonomic quantum computation,” J. Math. Phys. **46**, 022101 (2005).

[109] T. P. Cheng and L.-F. Li, *Gauge theory of elementary particle physics* (Oxford University Press, 1984).

[110] M. C. Bañuls and K. Cichy, “Review on novel methods for lattice gauge theories,” Rep. Prog. Phys. **83**, 024401 (2020).

[111] M. D. Schwartz, *Quantum Field Theory and the Standard Modell* (Cambridge University Press, 2014).

[112] N. Bourbaki, *Elements of Mathematics, Algebra I* (Springer (Berlin), 1989).

[113] S. Winitzki, *Linear Algebra via Exterior Products* (lulu.com, 2010).

[114] Y.-Q. Ma, S. Chen, H. Fan, and W.-M. Liu, “Abelian and non-Abelian quantum geometric tensor,” Phys. Rev. B **81**, 245129 (2010).

[115] R. Giles, “Reconstruction of gauge potentials from Wilson loops,” Phys. Rev. D **24**, 2160 (1981).

[116] M. Kremer, L. Teuber, A. Szameit, and S. Scheel, “Optimal design strategy for non-Abelian geometric phases using Abelian gauge fields based on quantum metric,” Phys. Rev. Research **1**, 033117 (2019).

[117] A. T. Rezakhani, D. F. Abasto, D. A. Lidar, and P. Zanardi, "Intrinsic geometry of quantum adiabatic evolution and quantum phase transitions," Phys. Rev. A **82**, 012321 (2010).

[118] J. P. Provost and G. Vallee, "Riemannian structure on manifolds of quantum states," Commun. Math. Phys. **76**, 289 (1980).

[119] K. Bergmann, H. Theuer, and B. W. Shore, "Coherent population transfer among quantum states of atoms and molecules," Rev. Mod. Phys. **70**, 1003 (1998).

[120] R. G. Unanyan, B. W. Shore, and K. Bergmann, "Laser-driven population transfer in four-level atoms: Consequences of non-Abelian geometrical adiabatic phase factors," Phys. Rev. A **59**, 2910 (1999).

[121] S. Longhi, G. Della Valle, M. Ornigotti, and P. Laporta, "Coherent tunneling by adiabatic passage in an optical waveguide system," Phys. Rev. B **76**, 201101 (2007).

[122] F. Dreisow, A. Szameit, M. Heinrich, R. Keil, S. Nolte, A. Tünnermann, and S. Longhi, "Adiabatic transfer of light via a continuum in optical waveguides," Opt. Lett. **34**, 2405 (2009).

[123] A. Mostafazadeh, "Pseudo-Hermitian representation of quantum mechanics," Int. J. Geom. Methods Mod. Phys. **7**, 1191 (2010).

[124] A. Mostafazadeh, "Energy observable for a quantum system with a dynamical Hilbert space and a global geometric extension of quantum theory," Phys. Rev. D **98**, 046022 (2018).

[125] C. M. Bender, D. C. Brody, and H. F. Jones, "Must a Hamiltonian be Hermitian?" Am. J. Phys. **71**, 1095 (2003).

[126] J. Gong and Q. H. Wang, "Time-dependent $\mathcal{PT}$-symmetric quantum mechanics," J. Phys. A: Math. Theor. **46**, 485302 (2013).

[127] L. Teuber and S. Scheel, "Solving the quantum master equation of coupled harmonic oscillators with Lie-algebra methods," Phys. Rev. A **101**, 042124 (2020).

[128] G. Lindblad, "On the generators of quantum dynamical semigroups," Commun. Math. Phys. **48**, 119 (1976).

[129] H.-P. Breuer, E.-M. Laine, and J. Piilo, "Measure for the degree of non-Markovian behavior of quantum processes in open systems," Phys. Rev. Lett. **103**, 210401 (2009).

[130] T. C. Guo and W. W. Guo, "A potential scattering formulation for mode couplings of electromagnetic waves in waveguides," J. Appl. Phys. **52**, 635 (1981).

[131] T. Eichelkraut, S. Weimann, S. Stützer, S. Nolte, and A. Szameit, "Radiation-loss management in modulated waveguides," Opt. Lett. **39**, 6831 (2014).

[132] M. Kremer, T. Biesenthal, L. J. Maczewsky, M. Heinrich, R. Thomale, and A. Szameit, "Demonstration of a two-dimensional $\mathcal{PT}$-symmetric crystal," Nat. Commun. **10**, 435 (2019).

[133] M. Ban, "Lie-algebra methods in quantum optics: The Liouville-space formulation," Phys. Rev. A **47**, 5093 (1993).

[134] I. M. Gel'fand and N. J. Vilenkin, *Generalized Functions, Volume 4: Applications of Harmonic Analysis* (Academic (New York), 1964).

[135] A. Bohm, J. D. Dollard, and M. Gadella, *Direc Kets, Gamow Vectors and Gel'fand Triplets* (Springer (Berlin), 1989).

[136] A. Bohm, S. Maxson, M. Loewe, and M. Gadella, "Quantum mechanical irreversibility," Physica A **236**, 485 (1997).

[137] R. Gilmore, *Lie Groups, Physics, and Geometry: An Introduction for Physicists, Engineers and Chemists* (Cambridge University Press, 2008).

[138] F. Minganti, A. Miranowicz, R. W. Chhajlany, and F. Nori, "Quantum exceptional points of non-Hermitian Hamiltonians and Liouvillians: The effects of quantum jumps," Phys. Rev. A **100**, 062131 (2019).

[139] D. Honda, H. Nakazato, and M. Yoshida, "Spectral resolution of the Liouvillian of the Lindblad master equation for a harmonic oscillator," J. Math. Phys. **51**, 072107 (2010).

[140] F. Wolf and H. J. Korsch, "Time-evolution operators for (coupled) time-dependent oscillators and Lie algebraic structure theory," Phys. Rev. A **37**, 1934 (1988).

[141] S. Scheel, "Permanents in linear optical networks," arXiv:quant-ph/0406127 (2004).

[142] S. Scheel and S. Y. Buhmann, "Macroscopic quantum electrodynamics — Concepts and Applications," Acta Phys. Slovaca **58**, 675 (2008).

[143] M. Marcus and H. Minc, "Permanents," Am. Math. Mon. **72**, 577 (1965).

[144] Caianiello, "On quantum field theory - i: Explicit solution of Dyson's equation in electrodynamics without use of Feynman graphs," Nuovo Cimento **10**, 1634 (1953).

[145] E. R. Caianiello, *Combinatorics and Renormalization in Quantum Field Theory* (Frontiers in Physics, Lecture Note Series (W. A. Benjamin, Reading, MA), 1973).

[146] J. Wei and E. Norman, "Lie algebraic solution of linear differential equations," J. Math. Phys. **4**, 575 (1963).

[147] W. Magnus, "On the exponential solution of differential equations for a linear operator," Comm. Pure Appl. Math. **7**, 649 (1954).

[148] J. Wei and E. Norman, "On global representation of the solutions of linear differential equations as a product of exponentials," Proc. Am. Math. Soc. **15**, 327 (1964).

[149] C. K. Hong amd Z. Y. Ou and L. Mandel, "Measurement of subpicosecond time intervals between two photons by interference," Phys. Rev. Lett. **59**, 2044 (1987).

[150] K. Hofmann, *Propagation von nichtklassischem Licht durch verlustbehaftete Wellenleiterstrukturen*, Master's thesis, University of Rostock (2019).

[151] A. Guo, G. J. Salamo, D. Duchesne, R. Morandotti, M. Volatier-Ravat, V. Aimez, G. A. Siviloglou, and D. N. Christodoulides, "Observation of $\mathcal{PT}$-symmetry breaking in complex optical potentials," Phys. Rev. Lett. **103**, 093902 (2009).

[152] S. Charzyński and M. Kuś, "Wei–Norman equations for a unitary evolution," J. Phys. A: Math. Theor. **46**, 265208 (2013).

[153] G. Vidal and R. F. Werner, "Computable measure of entanglement," Phys. Rev. A **65**, 032314 (2002).

[154] M. B. Plenio, "Logarithmic negativity: A full entanglement monotone that is not convex," Phys. Rev. Lett. **95**, 090503 (2005).

[155] R. Horodecki, P. Horodecki, M. Horodecki, and K. Horodecki, "Quantum entanglement," Rev. Mod. Phys. **81**, 865 (2009).

[156] I. I. Arkhipov, A. Miranowicz, F. Minganti, , and F. Nori, "Liouvillian exceptional points of any order in dissipative linear bosonic systems: Coherence functions and switching between $\mathcal{PT}$ and anti-$\mathcal{PT}$ symmetries," Phys. Rev. A **102**, 033715 (2020).

[157] Y. N. Joglekar, Rahul Marathe, P. Durganandini, and R. K. Pathak, "$\mathcal{PT}$ spectroscopy of the Rabi problem," Phys. Rev. A **90**, 040101 (2014).

[158] T. E. Lee and Y. N. Joglekar, "$\mathcal{PT}$-symmetric Rabi model: Perturbation theory," Phys. Rev. A **92**, 042103 (2015).

[159] G. Floquet, "Sur les équations différentielles linéaires à coefficients périodiques," Ann. Sci. École. Normal. Sup. **12**, 47 (1883).

[160] M. Holthaus, "Floquet engineering with quasienergy bands of periodically driven optical lattices," J. Phys. B: At. Mol. Opt. Phys. **49**, 013001 (2016).

[161] S. Kohler, T. Dittrich, and P. Hänggi, "Floquet-Markovian description of the parametrically driven, dissipative harmonic quantum oscillator," Phys. Rev. E **55**, 300 (1997).

[162] K. Fujii, "Note on coherent states and adiabatic connections, curvatures," J. Math. Phys. **41**, 4406 (2000).

[163] G. S. Vasilev, A. Kuhn, and N. V. Vitanov, "Optimum pulse shapes for stimulated Raman adiabatic passage," Phys. Rev. A **80**, 013417 (2009).

[164] J. Dell, J. L. deLyra, and L. Smolin, "Quantization of a gauge theory with independent metric and connection fields," Phys. Rev. D **34**, 3012 (1986).

[165] M. Yu, P. Yang, M. Gong, Q. Cao, Q. Lu, H. Liu, S. Zhang, M. B. Plenio, F. Jelezko, T. Ozawa, N. Goldman, and J. Cai, "Experimental measurement of the quantum geometric tensor using coupled qubits in diamond," Natl. Sci. Rev. **7**, 254 (2019).

[166] A. Gianfrate, O. Bleu, L. Dominici, V. Ardizzone, M. De Giorgi, G. Lerario D. Ballarini, K. W. West, L. N. Pfeiffer, D. D. Solnyshkov, D. Sanvitto, and G. Malpuech, "Measurement of the quantum geometric tensor and of the anomalous Hall drift," Nature **578**, 381 (2020).

# Selbstständigkeitserklärung

Ich gebe folgende Erklärung ab:

1. Die Gelegenheit zum vorliegenden Promotionsvorhaben ist mir nicht kommerziell vermittelt worden. Insbesondere habe ich keine Organisation eingeschaltet, die gegen Entgelt Betreuerinnen/Betreuer für die Anfertigung von Dissertationen sucht oder die mir obliegenden Pflichten hinsichtlich der Prüfungsleistungen für mich ganz oder teilweise erledigt.

2. Ich versichere hiermit an Eides statt, dass ich die vorliegende Arbeit selbstständig angefertigt und ohne fremde Hilfe verfasst habe. Dazu habe ich keine außer den von mir angegebenen Hilfsmitteln und Quellen verwendet und die den benutzten Werken inhaltlich und wörtlich entnommenen Stellen habe ich als solche kenntlich gemacht.

Rostock, den

# Danksagung

An dieser Stelle möchte ich denjenigen Danken, ohne deren Unterstützung diese Arbeit nicht möglich gewesen wäre. Der größte Dank gilt dabei meinem Betreuer Prof. Stefan Scheel. In seiner Arbeitsgruppe habe ich mich bereits zum Masterstudium wohl gefühlt und ich bin froh auch zu meinem Promotionsstudium Teil seiner Gruppe gewesen zu sein. Trotz vieler anderer Aufgaben und Verantwortungen hat er sich immer die Zeit für mich und meine Fragen genommen. Die Diskussionen über Physik, als auch seine Anekdoten aus aller Welt, werde ich sehr vermissen.

Ebenso möchte ich Prof. Alexander Szameit danken der mit seiner AG eine enge Verzahnung von Theorie und Experiment ermöglichte, die die Arbeit erst richtig spannend gemacht hat. Insbesondere danke ich seinen AG-Mitglieder Friedericke Klauck und Mark Kremer für die immer freundliche und erfolgreiche Zusammenarbeit.

Darüberhinaus danke ich auch allen Mitgliedern meiner AG, die ebenso stets offene Ohren bei Problem hatten sowie die Pausen besonders amüsant gemacht haben. Besonderer Dank gilt meinen Studienfreunden, allen voran Helge, Nis, Eric, Thomas und Tobi, die das Physikstudium in Rostock von Anfang bis Ende unvergesslich gemacht haben.

Neben all den Leuten vom Physikinstitut habe ich auch besonders meiner Verlobten Julia Rager zu danken. Mit ihr an meiner Seite waren selbst die anstrengensten Zeiten meines Studiums leicht zu überwinden und ich bin ihr unendlich dankbar für ihre Liebe und Fürsorge.

Zum Schluss danke ich noch meinen Eltern und meiner Schwester. Meinen Eltern, dass sie mir mit ihrer vollkommenen Unterstützung erst die Möglichkeit gegeben haben, Physik zu studieren und meiner Schwester, dass sie mich all die Jahre nicht nur ausgehalten, sondern auch immer zum Lachen gebracht hat.

Danke an euch alle!